

**A Thesis Submitted for the Degree of PhD at the University of Warwick**

**Permanent WRAP URL:**

<http://wrap.warwick.ac.uk/181404>

**Copyright and reuse:**

This thesis is made available online and is protected by original copyright.

Please scroll down to view the document itself.

Please refer to the repository record for this item for information to help you to cite it.

Our policy information is available from the repository home page.

For more information, please contact the WRAP Team at: [wrap@warwick.ac.uk](mailto:wrap@warwick.ac.uk)

**Investigation of the structural  
regulation of periplasmic  
amidases during cell division in  
*Escherichia coli***

**Tyler Charles Baverstock, Mbio**

A thesis presented for the partial fulfillment degree  
of  
Doctor of Philosophy in Life Sciences



Department Life Sciences, Structural Biology  
University of Warwick  
April 2023

# Contents

<b>1</b>	<b>Introduction</b>	<b>12</b>
1.1	Gram-Negative Bacterial cell wall . . . . .	12
1.1.1	Structure . . . . .	12
1.1.2	Cell wall synthesis . . . . .	14
1.2	<i>Escherichia coli</i> Bacterial cell division . . . . .	16
1.2.1	FtsZ polymerisation and Z-ring assembly . . . . .	18
1.2.2	Z-ring assembly and Polymerisation . . . . .	20
1.2.3	Formation of the proto Z-ring . . . . .	22
1.2.4	The transmembrane Divisome assembly . . . . .	27
1.2.5	Activating the assembled Divisome . . . . .	42
1.2.6	Final division stages . . . . .	44
1.3	FtsEX and EnvC pathway . . . . .	51
1.3.1	Type VII ABC transporters . . . . .	51
1.3.2	FtsEX . . . . .	60
1.3.3	EnvC, an amidase regulator . . . . .	67
1.4	Periplasmic amidases . . . . .	71
1.4.1	Bacterial peptidoglycan cleaving enzymes . . . . .	71
1.4.2	N-acetylmuramoyl-L-alanine type 3 <i>E. coli</i> periplasmic amidases . . . . .	74

1.5	Project Aims and Objectives . . . . .	88
<b>2</b>	<b>Materials and Methods</b>	<b>89</b>
2.1	Chemical and reagent suppliers . . . . .	89
2.2	Buffer solutions . . . . .	89
2.3	Bacterial Growth and manipulation . . . . .	89
2.3.1	Bacterial growth media . . . . .	89
2.3.2	Bacterial strains . . . . .	90
2.3.3	Bacterial vectors . . . . .	95
2.3.4	Preparation of <i>E. coli</i> competent cells for DNA transformation . . . . .	95
2.3.5	Bacterial heat shock transformation . . . . .	95
2.4	DNA manipulation techniques . . . . .	96
2.4.1	Primer and plasmid design for cloning . . . . .	96
2.4.2	Primer and plasmid design for mutagenesis . . . . .	96
2.4.3	Polymerase Chain Reaction . . . . .	96
2.4.4	Mutagenesis Polymerase Chain Reaction . . . . .	96
2.4.5	Agarose gel electrophoresis . . . . .	97
2.4.6	Purification of PCR products . . . . .	97
2.4.7	Restriction Cloning . . . . .	97
2.4.8	Preparation of plasmid DNA . . . . .	97
2.4.9	Quantifying DNA . . . . .	97
2.4.10	Sequencing plasmid constructs . . . . .	98

2.4.11	Generation of amidase genomic knockouts . . . . .	98
2.5	Microbiology Assays . . . . .	99
2.5.1	Bacterial two-hybrid . . . . .	99
2.5.2	Bacterial growth curves . . . . .	100
2.5.3	Cell wall stability spot plate assay . . . . .	100
2.5.4	Minimum inhibitory concentration . . . . .	100
2.5.5	Microscopy . . . . .	101
2.6	Protein Expression and Purification . . . . .	102
2.6.1	<i>E. coli</i> protein expression . . . . .	102
2.6.2	Preparation of crude cell lysates . . . . .	102
2.6.3	Immobilised Metal Affinity Chromatography . . . . .	102
2.6.4	Gel filtration . . . . .	103
2.6.5	Sodium dodecyl sulfate–polyacrylamide gel electrophoresis	103
2.7	X-ray Crystallography . . . . .	104
2.7.1	Setup of crystal trials . . . . .	104
2.7.2	Crystal collection and transit . . . . .	104
2.7.3	AmiA X-ray diffraction structure determination . . . . .	104
2.7.4	Data sharing and materials . . . . .	105
2.7.5	Structural modelling . . . . .	105
2.7.6	Genomic sequence alignments . . . . .	105
<b>3</b>	<b>Investigating interactions of EnvC in the divisome</b>	<b>106</b>

3.1	Abstract . . . . .	106
3.2	Introduction . . . . .	107
3.3	Results . . . . .	113
3.3.1	The X-lobe of FtsX is essential in the interaction with EnvC	113
3.3.2	EnvC self-inhibition prevents amidase interaction . . . . .	115
3.3.3	YibQ is not an EnvC interactor nor a component of the divisome . . . . .	125
3.3.4	NlpI is a potential scaffold protein for the divisome . . . . .	128
3.4	Discussion . . . . .	132
<b>4</b>	<b>Knockout characterisation of the FtsEX:EnvC:Amidase pathway</b>	<b>136</b>
4.1	Abstract . . . . .	136
4.2	Introduction . . . . .	137
4.3	Results . . . . .	138
4.3.1	Generating divisome <i>E. coli</i> double ( $\Delta amiab$ ) and triple ( $\Delta amiabc$ ) division-associated knockouts . . . . .	138
4.3.2	FtsEX:EnvC pathway is essential for survival under low osmolarity and detergent conditions . . . . .	141
4.3.3	Cell wall permeability is a symptom of knockouts in the FtsEX:EnvC pathway . . . . .	146
4.3.4	Proper cell separation is a key function of the FtsEX:EnvC pathway . . . . .	150
4.4	Discussion . . . . .	155
<b>5</b>	<b>Structure of <i>E. coli</i> amidase, AmiA</b>	<b>158</b>

5.1	Abstract . . . . .	158
5.2	Introduction . . . . .	159
5.3	Results . . . . .	160
5.3.1	Generating <i>E. coli</i> AmiA crystals and X-ray diffraction . .	160
5.3.2	AmiA is a typical N-acetylmuramoyl-L-alanine type 3 <i>E. coli</i> periplasmic amidase . . . . .	163
5.3.3	AmiA interaction helix is highly mobile . . . . .	167
5.3.4	AmiA contains high internal and active site conservation .	169
5.3.5	AmiA contains a Zinc ion, essential for function . . . . .	171
5.3.6	AmiA has a conserved catalytic domain found in other type 3 amidases in <i>E. coli</i> . . . . .	174
5.4	Discussion . . . . .	181
<b>6</b>	<b>Mutational analysis of the <i>E. coli</i> periplasmic amidase, AmiA</b>	<b>184</b>
6.1	Abstract . . . . .	184
6.2	Introduction . . . . .	185
6.3	Results . . . . .	188
6.3.1	AmiA is activated by direct interaction with EnvC . . . . .	188
6.3.2	AmiA interaction with EnvC is dependent on a set of hydrophobic residues in the interaction helix . . . . .	190
6.3.3	The blocking helix is essential to AmiA self-regulation . .	194
6.3.4	AmiA active site and Zinc-binding residues are essential for function . . . . .	199
6.4	Discussion . . . . .	201

<b>7 Final Discussion</b>	<b>204</b>
<b>8 Appendix</b>	<b>248</b>

## **Acknowledgements**

For providing training and funding for this PhD project, I would like to thank the Midlands Integrative Biosciences Training Project, under the Biotechnology and Biological Sciences Research Council. My primary supervisor, Dr Allister Crow, I would like to thank and appreciate his guidance, training and support through the good and difficult parts of the project. For his exceptional cloning abilities, maintaining the laboratory and all round guidance as a colleague and a friend, I would like to thank Dr Jonathan Cook. I would also like to thank Martin McAndrew for his help in my project and knowledge on structural modelling and computational biology. I like to thank Professor David Roper for being my secondary supervisor. I would like to thank my wife-to-be Magdalena Kay for her endless support through the tough stages of this PhD project and giving me the strength to finish this work. Lastly, I would like to appreciate the help and kindness of everyone of the Warwick university IBRB floor two.

### **Summary of the PhD experience:**

*”It is possible to commit no mistakes and still lose. That is not weakness; that is life.” - Captain Jean-Luc Picard*

*”The definition of insanity is doing the same thing over and over and expecting different results.” - Albert Einstein.*

*“Highly illogical.” – Spock*

## Declaration

This thesis is submitted to the University of Warwick in support of my application for the degree of Doctor of Philosophy in Life Sciences. It has been composed by myself and has not been submitted in any previous application for any degree.

There is data presented in this thesis which is presented or sourced from published work during the PhD including:

### Published, 2020

Insights into bacterial cell division from a structure of EnvC bound to the FtsX periplasmic domain. Cook J, Baverstock TC, McAndrew MBL, Stansfeld PJ, Roper DI, Crow A. Proc Natl Acad Sci U S A. 2020 Nov 10;117(45):28355-28365. doi: 10.1073/pnas.2017134117. Epub 2020 Oct 23. PMID: 33097670; PMCID: PMC7668044.

Work included: Bacterial two-hybrid figure in **Figure 23**, bacterial two-hybrid and co-purification in **Figure 24**

### Under review, 2023

Structures of peptidoglycan amidases in isolation and bound to a cognate activator Jonathan Cook<sup>†</sup>, Tyler Baverstock<sup>†</sup>, Martin McAndrew, David Roper, Phillip Stansfeld, Allister Crow. School of Life Sciences, University of Warwick, United Kingdom. (<sup>†</sup> = Joint first author)

Work included: Model presented in **Figure 48** used the in-review structure PDB = 8C0J as a template.

## Abstract

During bacterial cell division, amidases hydrolyse peptidoglycan to allow daughter cell separation. During the final stages of cell division, septal peptidoglycan between the two daughter cells prevents cell separation. Proteins called N-acetylmuramoyl-L-alanine type 3 amidases hydrolyse the amide bond between glycan strands. This allows successful daughter cell separation. This hydrolase activity is tightly regulated by a pathway of protein interactions to avoid uncontrolled peptidoglycan degradation. The exact structural mechanism of the protein interaction pathway involved in regulating the activity of such amidases is currently unknown. Here it is shown, the molecular regulatory mechanism by which, *Escherichia coli* amidase, AmiA, is activated by the interaction of EnvC. It was found that EnvC, an amidase regulator, is self-regulated by a restraining helix over the amidase binding LytM domain evidenced by bacterial-two-hybrid and co-purification analysis of EnvC truncated variants. By solving a 2.35 angstrom structure of *E. coli* and building an AmiA bound to EnvC LytM domain model, the molecular mechanism of the removal of a blocking helix over AmiA's active site by the interaction of an interaction helix in AmiA to EnvC. These results show a stringently structurally regulated amidase activation pathway, with no availability of the amidase active site without interaction with a regulator protein. This is a potentially conserved regulatory system that could be used to model amidase regulation in other bacterial species. As a part of fundamental biology in a model bacterial system, it is anticipated that the understanding found in this research could extend to understanding related cell division pathways in other bacterial species. As an application of this regulation mechanism, there is a potential antibiotic target to be found in cell division amidases, as without self-regulation, amidases may uncontrollably hydrolyse peptidoglycan, weakening the integrity of cells to make them more susceptible to other antibiotic treatments.

## Abbreviations

- MICs = Minimal inhibitory concentrations
- PG = Peptidoglycan
- GlcNAc = N-Acetylglucosamine
- MurNAc = N-Acetylmuramic acid
- UDP = Uridine diphosphate
- CTL = C-terminal linker
- CTP = C-terminal peptide
- CTV = C-terminal variable region
- Fts = Filamenting temperature-sensitive mutant
- PBP = Penicillin binding protein
- SDS = Sodium Dodecyl Sulfate
- MAL = Muramic- $\delta$ -lactam
- *dif* = Deletion induced filamentation
- SPOR = Sporulation related repeat
- Lol = Lipoprotein outer membrane localisation (pathway)

# 1 Introduction

## 1.1 Gram-Negative Bacterial cell wall

A significant proportion of bacteria are often classified into Gram-positive, Gram-negative and Mycobacterial which represent differences in their cell wall and membrane structures (Brown et al., 2020). Whether a bacterium is Gram-positive or Gram-negative or Mycobacterial determines the method of synthesis by which a bacteria maintains its outer layers to respond to the environment, other microorganisms and antibiotics. The architecture and synthesis of the bacterial outer layers have been under continual scientific investigation due to its importance in cell survival as well as a target for existing and potentially new antibiotic targets.

### 1.1.1 Structure

The structure of a Gram-negative cell wall differs significantly to that of Gram-positive bacteria (**Figure 1**). There is an outer and inner membrane present in Gram-negative bacteria encompassing a periplasmic space between them. A small layer of cross-linked glycan strands called peptidoglycan resides in this periplasmic space, anchored to both membranes by a series of lipoproteins (Silhavy et al., 2010).

The peptidoglycan layer consists of glycan chains of alternating units of *N*-acetylglucosamine (GlcNAc) and *N*-acetylmuramic acid (MurNAc) cross-linked by two short peptide chains of flexible peptides. This forms a hydrophilic lattice network, which combined with the outer membrane, is resistant to hydrophobic compounds such as bile salts, which are present in the human digestive system (May & Grabowicz, 2018). The outer membrane is a unique asset to Gram-negative bacteria as it provides structural integrity to confer resistance to harsh environments and prevents antibiotics reaching intracellular targets (May & Grabowicz, 2018).

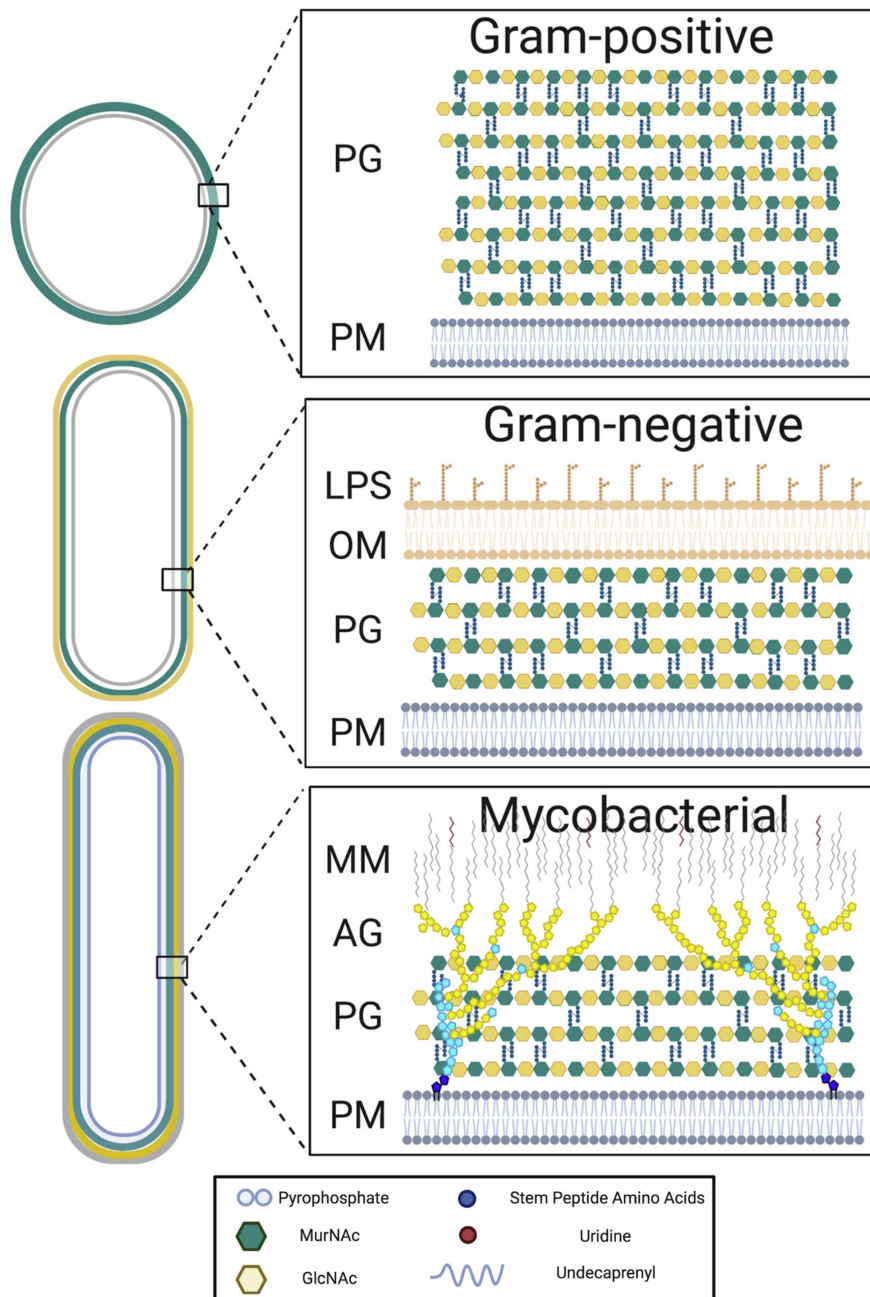


**Figure 1: Structural features of the cell wall of Gram-positives, Gram-negatives, and mycobacteria.** PG, peptidoglycan; PM, plasma membrane; LPS, lipopolysaccharide; MM, mycomembrane; OM, outer membrane; AG, arabinogalactan. Gram-positive exhibits a single plasma membrane with a large layer of peptidoglycan, Gram-negative exhibits outer and inner membranes with a smaller peptidoglycan layer compared to Gram-positive. Mycobacteria have an intermediate (compared to Gram-positive and negative) peptidoglycan layer with attached arabinogalactan which form a scaffold for mycolic acids. (Brown et al., 2020)  
 (A) Source: (Brown et al., 2020)

### 1.1.2 Cell wall synthesis

An essential process to build and maintain the peptidoglycan layer in bacteria, the cell wall synthesis pathway is a series of modifications of peptides and sugars in the cytoplasm which are transferred to the periplasm (**Figure 2**). The pathway starts with the formation of UDP-MurNAc-L-Ala-D-Glu-L-Lys-D-Ala-D-Ala, known as Park's nucleotide, in the cytoplasm, created from a series of precursors and modifications (Garde et al., 2021). The Park's nucleotide is transferred to a lipid carrier located on the cytosolic side of the inner membrane, forming lipid I. A GlcNAc molecule is added to the MurNAc of Lipid I to form Lipid II (Garde et al., 2021). After translocation via the flippase MurJ, Lipid II is transferred to the periplasm side of the inner membrane (Garde et al., 2021).

A series of transpeptidation and transglycosylation reactions performed by penicillin binding proteins (PBPs), RoadA, FtsW and MtgA, take place to integrate the precursor into the peptidoglycan chain. The terminal D-alanine of the pentapeptide is either removed by D-alanyl-D-alanine carboxypeptidase or substituted by cross-linking to other peptides. As a result, the GlcNAc-MurNAc chain is grown, cross-linked to other chains by pentapeptide cross-links (Garde et al., 2021). This essential process in bacteria must be strictly coordinated with processes such as spore formation, peptidoglycan elongation and cell division.

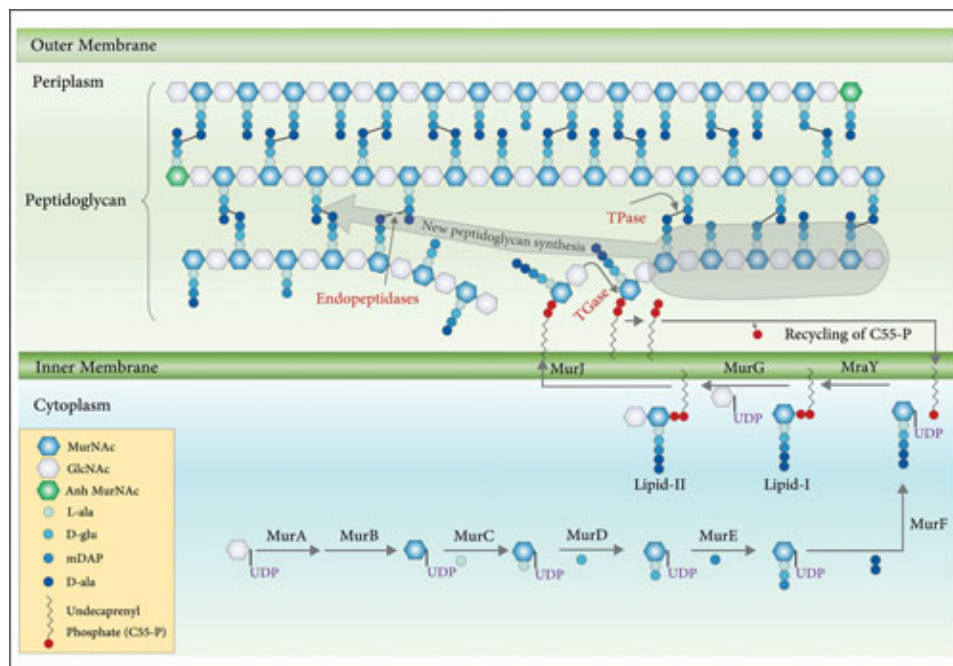


**Figure 2: Schematic depicting peptidoglycan biosynthetic pathway.** Peptidoglycan precursors are synthesized in the cytoplasm by a series of enzymes, MurA, B, C, D, E, and F, that convert UDP-GlcNAc to form UDP-MurNAc-pentapeptide (also referred to as Park's nucleotide), which is subsequently attached to the lipid transporter (undecaprenyl phosphate; C55P) by MraY to yield lipid-I that is converted to the final peptidoglycan precursor lipid-II, by addition of a GlcNAc moiety by MurG. A flippase MurJ transports lipid-II across the IM to the periplasm. Lipid-II is polymerized into the peptidoglycan by synthases, with C55P being recycled to the cytoplasm. Transglutaminase activity of RodA, FtsW, PBP1a, PBP1b, and MtgA catalyzes glycan polymerization, whereas transglycosylase activity of PBP2, PBP3, PBP1a, and PBP1b contributes to peptide cross-link formation (refer to Box 1). Hydrolysis mediated by d,d-endopeptidases, MepS, -M, and -H leads to cleavage of existing peptide cross-links to make space for the incorporation of nascent glycan strands. Anh-MurNAc (green hexagon) is the terminal residue in a glycan strand. The gray arrow indicates the direction of synthesis.

. Caption and image: (Garde et al., 2021)

## 1.2 *Escherichia coli* Bacterial cell division

Gram-negative bacterial cell division is an essential process to the life cycle of a bacterium, therefore, is a tightly regulated process. The process is achieved by a collection of interacting globular and transmembrane proteins called the 'divisome' (de Boer, 2010; Du & Lutkenhaus, 2019; Haeusser & Margolin, 2016; Nanninga, 1991; Söderström & Daley, 2017). The system begins with a tubulin-like protein called FtsZ, which localises to the mid-cell division site and forms a foundation for the recruitment of subsequent divisome proteins while maintaining an organised assembly of peptidoglycan (PG) cross wall via a protein distribution and coupling mechanism, FtsZ dynamic treadmilling (Levin & Janakiraman, 2021; McCausland et al., 2021).

FtsZ polymerises into a ring structure deemed 'z-ring' and associates with the inner membrane, mediated by the proteins FtsA, ZipA and ZapA (Du & Lutkenhaus, 2019). Later divisome proteins are recruited in a genetically determined order (**Figure 3**): FtsEX, FtsK, FtsQ, FtsL/B, FtsW, FtsI, FtsN, AmiC (Aarsman et al., 2005; Goehring & Beckwith, 2005). Although this order of proteins may not be representative of the complexities of the temporal concentrations or true recruitment of the divisome assembly *in vivo*, however, for clarity of explanation, this chapter will follow this order.

The divisome perform a set of regulatory and structural roles including; recruitment of downstream proteins, DNA-coupling, PG synthesis and PG hydrolysis . Once the concentrations of divisome proteins reach optimum during the cell cycle, cell wall septal PG hydrolysis and synthesis commences (via amidases and septal PG synthases respectively), likely activated by protein conformational changes (Du & Lutkenhaus, 2017; Levin & Janakiraman, 2021). Constriction of the membrane occurs, driven by FtsZ-treadmilling while maintaining uniformity with synthesis enzymes across the septum. The division process ends with the disassembly of the divisome during the invagination of the outer membrane to leading to daughter cell separation (Du & Lutkenhaus, 2017; Levin & Janakiraman, 2021).



### 1.2.1 FtsZ polymerisation and Z-ring assembly

The filamenting temperature sensitive mutant Z (FtsZ) is an essential cell division protein with a series of solved crystal structures from multiple species all which show a significant structural homology to the eukaryotic derived cytoskeleton protein tubulin, including the *Escherichia coli* FtsZ (**Figure 4**) (Schumacher et al., 2020).

FtsZ consists of two main domains (**Figure 4**), a protofilament-forming globular N-terminal GTP-binding domain; containing six  $\beta$ -sheets in parallel surrounded by six  $\alpha$ -helices then, connected by a long  $\alpha$ -helix, a C-terminal linker (CTL) which appears as an intrinsically disordered region (Levin & Janakiraman, 2021; Schumacher et al., 2020) which varies greatly in length and primary sequence between bacterial phylum (Gardner et al., 2013). Interestingly, the GTP binding activity of this tubulin-like GTP-binding core is crucial in the formation of straight protofilaments *in vitro* (Löwe & Amos, 1998; Schumacher et al., 2020). The protein concludes with a C-terminal peptide (CTP), which is a highly conserved region of 14 amino acids that are involved in the interactions with FtsA, ZipA and other accessory proteins, resulting in the association to the membrane (Gardner et al., 2013; Ortiz et al., 2016). This is possible due to the flexibility of the CTL to allow the CTP to interact with multiple different proteins of varied structures (Schumacher et al., 2017). Lastly, at the extreme C-terminus of FtsZ, there is a C-terminal variable region (CTV) which is a determinant of lateral interactions between FtsZ polymers (Buske & Levin, 2012) (Levin & Janakiraman, 2021).



### 1.2.2 Z-ring assembly and Polymerisation

The polymerisation of FtsZ is crucial to its function in the formation of the z-ring and recruitment of subsequent divisome proteins (**Figure 5**). The N-terminal core of FtsZ, GTP-binding *in vitro* is required for FtsZ assembly into protofilaments (like eukaryotic tubulin) and GTP-hydrolysis destabilises the polymer (Erickson et al., 2010; Romberg et al., 2001). This GTP binding and hydrolysis loop drives FtsZ treadmilling (Bisson-Filho et al., 2017; X. Yang et al., 2017)), which is the act by elongation of the FtsZ polymer at one end while the other end shortens on the same polymer, while subunits within the polymer are stationary as the positive end adds subunits and the negative end loses subunits (Loose & Mitchison, 2014). The Z ring *in vivo* is an arrangement of polymerised FtsZ protofilaments located at the midcell with pools of FtsZ molecules from cytoplasmic and membrane-bound pools dynamically interacting with it (Anderson et al., 2004; Y. Chen & Erickson, 2005).

The Z-ring formation and localisation in the cell is suggested to be regulated by a number of systems. Firstly, FtsZ concentration during different culturing conditions does not appear to have an effect on z-ring assembly (Rueda et al., 2003) as although under nutrient-poor and slow growing conditions, z-rings are still present in around 60 % of the cells (Männik et al., 2018). Richer medium indicate mostly unaltered FtsZ concentrations while 94 % of cells contain z-rings (Weart & Levin, 2003), understandably as a nutrient-rich medium promotes cell growth.

A pivotal Z-ring formation control is the localisation of high concentrations of FtsZ polymers to the midcell ready for division. Several protein systems work together to achieve this; the Min system inhibits FtsZ assembly at the cell poles (Boer et al., 1989; Lutkenhaus, 2009; Rowlett & Margolin, 2013), SlmA stop FtsZ assembling over unsegregated chromosomes (Bailey et al., 2014) (during nucleoid occlusion when DNA replication overlaps with cell division (W. R. Cook et al., 1989; Woldringh et al., 1991) and the Ter-MatP linkage system meet the FtsZ with the termination of DNA replication and is the only known positive positional regulator of FtsZ known in *E. coli* (Bailey et al., 2014; J. A. Buss et al., 2017). Lastly, these systems are supported by Zaps (FtsZ-associated proteins) which promote FtsZ polymerisation and stabilise the Z-ring (J. A. Buss et al., 2017; Huang et al., 2013).

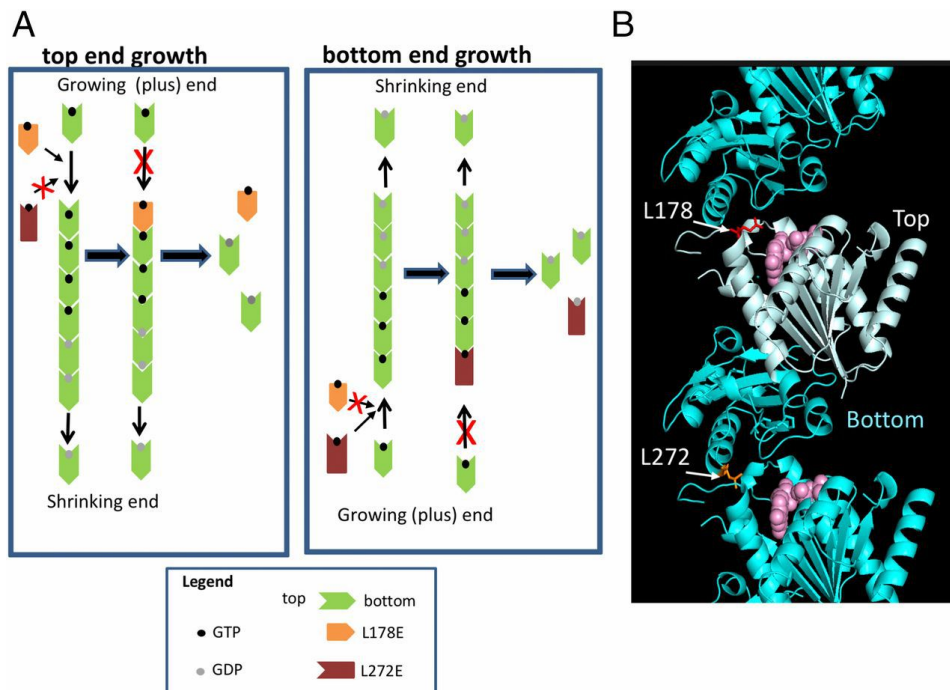


**Figure 5: FtsZ longitudinal interface mutants and the scheme used to determine FtsZ polymer polarity.** (A) Two possible scenarios for the growth of FtsZ polymers. In the first case (top-end growth), FtsZ polymerizes in the same direction as tubulin with the bottom surface of an incoming subunit interacting with the top surface (GTP end) of the subunit at the growing end of a polymer, called the plus (+) end in tubulin. Subunits at the shrinking end dissociate from the filament following GTP hydrolysis. In this case, the top-surface mutant (FtsZL178E) adds to a treadmilling filament blocking further subunit addition resulting in disassembly from the shrinking end, while the bottom-surface mutant (FtsZL272E) does not have an effect. In the second situation, FtsZ polymerizes in the opposite direction of tubulin. In this case, the bottom-surface mutant FtsZL272E adds to the growing end of the filament and would block further growth, while the top-surface mutant does not have an effect. (B) FtsZ interface mutants used in this study. The FtsZL178E monomer was superimposed on the FtsZ filament from *Staphylococcus aureus* (PDB::3VOB). The GTP-binding domain (N-terminal) is the top interface (light cyan), while the domain containing the T7 synergy loop (C-terminal) is the bottom interface (dark cyan). GDP is pink. Figure and caption sourced from (Du et al., 2018)

### **1.2.3 Formation of the proto Z-ring**

The formation of the proto z-ring is the recruitment and polymerisation of FtsZ polymers to the cytoplasmic membrane with the aid of essential divisome proteins; FtsA, ZipA and the Zap proteins. The assembly of the z-ring ring is beginning of the formation of the divisome. It begins with essential division proteins FtsA and ZipA (Pichoff & Lutkenhaus, 2002; RayChaudhuri, 1999) assisting FtsZ polymers to associate to the inner membrane, forming the core of the cytokinetic ring at the midcell (Hale & Boer, 1997; Pichoff et al., 2019). Division cannot occur without both FtsA and ZipA (Pichoff & Lutkenhaus, 2002; RayChaudhuri, 1999). A critical ratio of FtsA:FtsZ and ZipA:FtsZ concentrations are needed for division to occur and excess (compared to FtsZ concentration) of either FtsA or ZipA inhibit the process (Dai & Lutkenhaus, 1992; Hale & Boer, 1997). Both FtsA and ZipA are independently recruited and can either interact with FtsZ at the CTP and/or can anchor FtsZ polymers to the membrane and support FtsZ assembly (Hale & de Boer, 1999; Haney et al., 2001; Z. Liu et al., 1999; Ma & Margolin, 1999). Lastly, the Zap proteins; ZapAB, ZapC and ZapD all bind to FtsZ and promote FtsZ polymer interactions in the proto z-ring (Huang et al., 2013). This would appear to be in an individually redundant overlapping role (J. Buss et al., 2013; J. Durand-Heredia et al., 2012; J. M. Durand-Heredia et al., 2011; Hale et al., 2011) as cells only exhibit moderate filamentation in double or more Zap knockouts (J. Buss et al., 2013; J. Durand-Heredia et al., 2012; J. M. Durand-Heredia et al., 2011; Hale et al., 2011).

#### **1.2.3.1 FtsA**

FtsA is a peripheral membrane protein which aside from mediating FtsZ polymer interaction with the cytoplasmic membrane, will also interact and promote the recruitment of downstream divisome proteins, including FtsQ, FtsI, FtsN and FtsEX (Bernard et al., 2007; Corbin et al., 2004; Pichoff et al., 2012). FtsA is a generally conserved ATPase within the actin superfamily and forms actin-like protofilaments which if prevented by mutation, temperature-sensitive FtsA cells elongate, indicating the importance of FtsA filament formation (Fusinita van den Ent & Löwe, 2000; Szwedziak et al., 2012).

To mediate FtsZ polymer interactions, FtsA acts by exerting force on membranes and causing a redistribution of the membrane architecture and directly engaging FtsZ polymers in a reconstituted system (Conti et al., 2018) (**Figure 6**). FtsA also recruits FtsZ to phospholipid vesicles via direct FtsZ C-terminal interactions and regulation of FtsZ assembly kinetics (Conti et al., 2018). The ATP hydrolysis activity of FtsA lacks a clear function although mutations close to the ATP-binding site of FtsA cause cells to arrest during cell division (Herricks et al., 2014). This may indicate a similar polymer ATP-hydrolysis disassembly function found in FtsZ/tubulin/actin where other FtsA mutants which produce defective oligomerisation in FtsA, generally have reduced ATP hydrolysis rates (Conti et al., 2018; Herricks et al., 2014).

### 1.2.3.2 ZipA

ZipA is a type 1 inner membrane protein, present only in *Gammaproteobacteria* (Levin & Janakiraman, 2021) which anchors FtsZ polymers to the inner membrane (Hale & Boer, 1997) (**Figure 6**). Further functions include promoting the stability of the cytokinetic ring, possibly by bundling FtsZ polymers at the midcell by a potential ZipA ability to cross-link FtsZ polymers shown *in vitro* (Hale et al., 2000; RayChaudhuri, 1999). ZipA contains two main domains, firstly, a FtsZ binding domain which binds to the last 20 amino acids on the C-terminal end of FtsZ and is essential for ZipA function, where cells lacking ZipA are not rescued by mutated ZipA lacking the FtsZ binding domain (Hale et al., 2000).

Secondly, the N-terminal membrane anchor domain is also essential for function although a specific function of this domain is unknown (Hale et al., 2000). *FtsA* gain-of-function mutants (*ftsA\** (*ftsA-R286W*)) appear to bypass the requirement of ZipA suggesting ZipA is primarily a membrane anchor for FtsZ (Geissler & Margolin, 2005; Pichoff et al., 2012). Another function of ZipA does arise however in gain-of-function *FtsA* mutants regarding downstream protein interactions. *FtsA* in these strains generally form shorter oligomers, which appear to expose more sites of interactions in these diverse downstream proteins which can be obstructed by larger *FtsA* oligomers (Haney et al., 2001; Krupka et al., 2017; Schoenemann et al., 2018; Szwedziak et al., 2012). *FtsA* and ZipA also have been shown to directly interact (Vega & Margolin, 2019). This suggests ZipA is a modulator and an enhancer of *FtsA* by competing for the *FtsA*/ZipA binding site on the FtsZ CTP, disrupting the *FtsA* oligomers into shorter chains, promoting function (Levin & Janakiraman, 2021; Pichoff et al., 2012; Vega & Margolin, 2019).

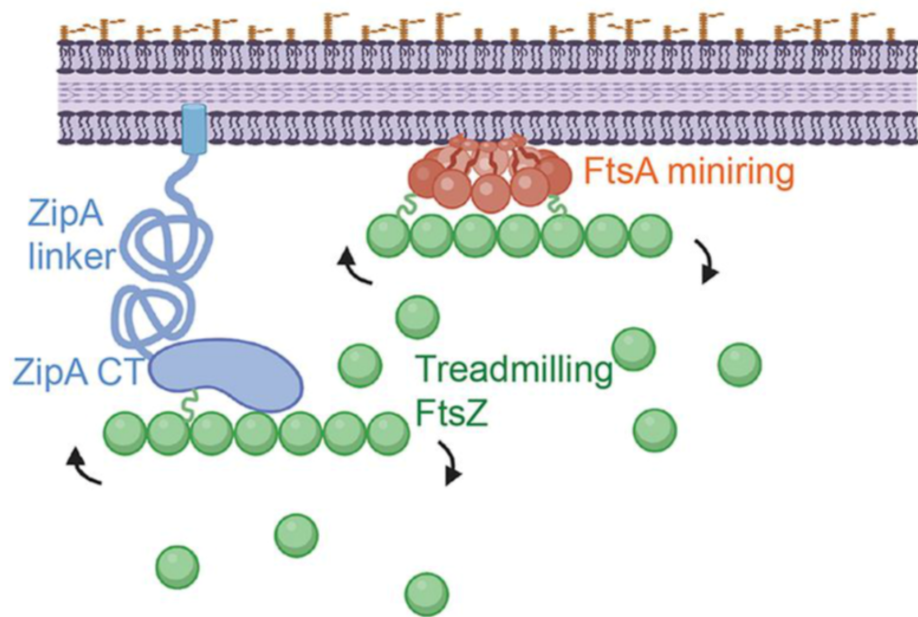


**Figure 6: Overview of potential protoring protein interactions.** (A) ZipA, with its N-terminal transmembrane domain, unstructured linker domain, and C-terminal (CT) FtsZ-binding domain, is shown attached to an FtsZ protofilament undergoing subunit treadmilling. FtsZ has its own unstructured linker, shown as a green squiggle. FtsA, tethered to the cytoplasmic membrane with its C-terminal amphipathic helix and a putative linker domain (shown as an orange squiggle), forms oligomeric minirings (shown here) that, like ZipA, bind to treadmilling FtsZ protofilaments. The figure was created with Biorender. Figure and caption sourced from (Schoenemann et al., 2020)

### 1.2.3.3 Zap proteins

The Zap (Z-associated protein) proteins are the last notable collection of proteins which modulate Z-ring formation by increasing lateral interactions between FtsZ protofilaments; ZapAB complex, ZapC and ZapD (Huang et al., 2013).

Each Zap protein is noted to have varying mechanisms of action. ZapA forms tetramers and cross-links FtsZ filaments via the FtsZ core domain (Hale et al., 2000; Roseboom et al., 2018) and ZapD performs a similar function while as a dimer forming cross-links via interactions with the FtsZ CTD (Huang et al., 2016; Schumacher et al., 2017). ZapC monomers bind to the large FtsZ globular core (instead of the CTD) to cross-link FtsZ polymers possibly by using two pockets eluding to a ZapC-mediated FtsZ bundling (J. M. Durand-Heredia et al., 2011; Hale et al., 2011). Interestingly, ZapA has an additional function to recruit ZapB which appears to sense the presence of nucleoids, perhaps aiding in the localisation of ZapA without FtsZ (Roseboom et al., 2018). This appears to be a semi-redundant system but non-essential, as cells lacking single Zap genes present moderate Z-ring diffuse phenotypes however cells lacking two or more Zaps, suffer typical division elongation phenotypes (J. Buss et al., 2013; J. Durand-Heredia et al., 2012; J. M. Durand-Heredia et al., 2011; Hale et al., 2011).

As the Z-ring is now anchored to the cytoplasmic membrane, its growth regulated by the accumulation of FtsZ polymers with aid of essential divisome proteins. Downstream divisome proteins are now recruited via FtsA and ZipA to form the termed, 'late' divisome.

#### 1.2.4 The transmembrane Divisome assembly

As division progresses, cross wall septal PG must be hydrolysed, new septal PG must be synthesised, cell constriction and separation must be directed, all of which is tightly regulated. This is the role of the transevelope divisome. As mentioned earlier, divisome proteins have been genetically-hierarchically determined to form a possible order of assembly (Goehring & Beckwith, 2005), although, multiple of these 'late' divisome proteins have unaffected concentrations during the cell cycle (Vischer et al., 2015; Weart & Levin, 2003). Perhaps a hypothesis closer to reality, that similar to FtsZ, the threshold concentrations of divisome proteins at the nascent septal site prompts PG synthesis at the midcell, and not just the recruitment of said proteins (Si et al., 2019).

##### 1.2.4.1 FtsEX

Aside from the cytoplasmic division proteins, FtsZ/FtsA/ZipA/Zaps, the first genetically-hierarchically determined protein complex of the 'late' divisome is FtsEX (Goehring & Beckwith, 2005). During the early stages of division, a type VII ABC transporter, FtsEX localises to the midcell via the interactions with FtsA and FtsZ at the cytokinetic ring (Corbin et al., 2007; Du et al., 2019; Reddy, 2007; Schmidt et al., 2004). FtsEX holds a dual role in the divisome, firstly, FtsEX appears to interact and antagonise FtsA polymerisation, promoting divisome assembly as un-polymerised FtsA favors cell division (Du et al., 2016). Secondly, FtsEX interacts with a murein amidase regulator, EnvC, which regulates septal peptidoglycan hydrolysis via periplasmic amidases (J. Cook et al., 2020). *E. coli* FtsEX knockouts suffer from the cell elongation and chaining phenotype and while *E. coli*  $\Delta$ *ftsEX* will grow in standard conditions, growth is significantly hindered under low osmolarity or detergent conditions (J. Cook et al., 2020; Du et al., 2016).

#### 1.2.4.2 FtsK, a DNA translocase

A DNA translocase, FtsK localises to the septum via the interactions with FtsZ and FtsA (Pichoff & Lutkenhaus, 2002; L. Wang & Lutkenhaus, 1998; X. C. Yu et al., 1998). FtsK corrects aberrant division due to unsegregated chromosomal material via a pumping mechanism, which removes DNA from the division septum (Jean et al., 2020). This multidomain membrane protein is composed of three main domains; FtsK<sub>N</sub>, FtsL, FtsC (Dubarry et al., 2010; Massey et al., 2006; L. Wang & Lutkenhaus, 1998; X.-C. Yu et al., 1998). The FtsK<sub>N</sub> domain contains four transmembrane helices localised and embedded into the inner membrane of the division septum and is essential for the cell to coordinate chromosome segregation with cell division (Barre et al., 2000; Massey et al., 2006; X. Wang et al., 2005). Although extremely variable in other strains in terms of length and composition, the FtsL linker domain is essential in *E. coli* for chromosomal *dif* (deletion induced filamentation) recombination and cell division (Bigot et al., 2004; Boyle et al., 2000). Lastly, the FtsC 512 residue C-terminal DNA-dependent ATPase domain is a member of the RecA-like family which form rings and create nucleotide binding pockets between subunits. The functions of this FtsC derivative were found to be both the translocation of dsDNA and the activation of *ZerCD* site-specific recombination at *dif* (Aussel et al., 2002; Massey et al., 2004; Pease et al., 2005; Saleh et al., 2004; X.-C. Yu et al., 1998). FtsK appears to have two key roles in cell division, one essential, which is the recruitment of downstream proteins, primarily the FtsQLB complex and the other function, a non-essential chromosome partitioning role, in which *E. coli* cells lacking FtsC, are defective in chromosomal segregation and septation (L. Wang & Lutkenhaus, 1998; X.-C. Yu et al., 1998).

#### 1.2.4.3 FtsQLBWI complex, a recruiting turned PG synthesis system

A trio of widely conserved bitopic membrane proteins, FtsQ, FtsL and FtsB hold a range of essential functions for the assembly of the divisome; initially as a protein scaffold, to a sensing mechanism for the subsequent cell wall remodeling processes (Begg et al., 1980; D'Ulisse et al., 2007; B. Liu et al., 2015; Park et al., 2020; Scheffers et al., 2007; Tsang & Bernhardt, 2015). As the first point of contact for the FtsQLB complex, FtsQ is dependent on FtsK for localisation to the cell division site, although prior to this, FtsL and FtsB (both containing a leucine zipper-like sequence) depend on each other and FtsQ for division site localisation, interact with FtsQ and perform a pre-assembly of the FtsQLB complex, likely before FtsQ interacts with FtsK, localising the whole complex together (Buddelmeijer & Beckwith, 2004; D'Ulisse et al., 2007; Ghigo et al., 1999).

FtsQ's main roles are localisation and recruitment due its significant interaction catalogue, FtsA, FtsK, FtsX, FtsL, FtsB, FtsW, FtsI, FtsN and YmgF (an inner transmembrane divisome interacting protein), where FtsA and FtsK interact at the FtsQ cytoplasmic tail, where other interactions all occur in the large periplasmic domain or transmembrane region (**Figure 7**) (Di Lallo et al., 2003; D'Ulisse et al., 2007; Karimova et al., 2005).

As mentioned, FtsL and FtsB interact which forms a scaffold basis for the recruitment of other divisome proteins to the division site, namely, FtsW, FtsI and FtsN (Gonzalez et al., 2010; Park et al., 2020). Interestingly, FtsL appears to have an essential role in the activation of septal peptidoglycan synthesis. Interacting with the cytoplasmic domain of FtsL, FtsWI complex is recruited to the division site which FtsN may interact with the FtsQLB complex and convert it from a recruitment complex into an an activator using FtsL to interact with FtsI to activate FtsW, promoting septal peptidoglycan synthesis (Gonzalez et al., 2010; Park et al., 2020).

Recently, the structure of the FtsQLBWI complex was solved in *Pseudomonas aeruginosa* (**Figure 7**), although with several regions of low resolution the overall structure supports previous mutational studies of the complex (Käshammer et al., 2022). The structures of the five proteins support their current function predictions; FtsQ transmembrane domain is not present in the FtsWIQBL complex but the  $\beta$  domain is further suggesting the recruitment role, FtsBL extend together into the periplasm interacting with FtsWI, ready for activation (Käshammer et al., 2022). The structure shows the inactive scaffold state of the complex with predictions of a active state extending FtsWI into the peptidoglycan for their PG remodelling functions (Käshammer et al., 2022).

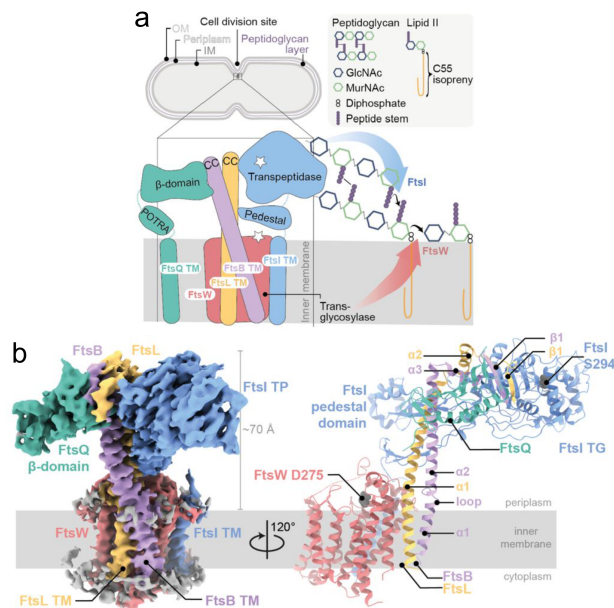


**Figure 7: Biochemical and structural characterisation of the core divisome complex FtsW IQBL from *P. aeruginosa*.** (A) Septal peptidoglycan synthesis by FtsW IQBL during Gram-negative bacterial cell division. The transglycosylase FtsW (red), and transpeptidase FtsI (blue) bind the non-enzymatic subcomplex FtsQBL (green, violet and yellow, respectively). The complex contains 14 transmembrane helices – ten from FtsW and one each from FtsIQLB. The transglycosylase FtsW catalyses the polymerisation of GlcNAc-MurNAc disaccharides from Lipid II. The transpeptidase FtsI crosslinks the peptides from the nascent chain to adjacent peptides in the peptidoglycan layer between residues three and four. OM: outer membrane, IM: inner membrane, GlcNAc: N-acetylglucosamine, MurNAc: N-acetylmuramic acid, CC: coiled coil, TM: transmembrane. (LEFT) side-view of the PaFtsW IQBL cryo-EM density at an overall resolution of 3.7 Å. Protein colours are the same as those in (A). Residual density from the detergent micelle is visible around the transmembrane domain in grey. Right panel: model of PaFtsW IQBL, rotated by 120° with respect to the density on the left-hand side. The putative FtsW active site residue D275 is indicated, as is the FtsI active site residue S294. The FtsW loop 219-233 and FtsI loop 45-50 are shown as a dotted line as they were too flexible to build. FtsQ<sup>TM</sup> and FtsQ<sup>β</sup> were not resolved and are not shown. Caption and figure adapted and sourced from (Käshammer et al., 2022)

#### 1.2.4.4 FtsWI

Another protein complex of the divisome, FtsW and FtsI are essential proteins which mediate the synthesis of septal peptidoglycan (Begg et al., 1980; Egan et al., 2020; Taguchi et al., 2019; L. Wang et al., 1998; Weiss et al., 1999). Both proteins recruited to the by the FtsQLB complex although FtsI appears to depend on its own membrane anchor and multiple division proteins; FtsZ, FtsA, FtsQ and FtsL (L. Wang et al., 1998; Weiss et al., 1999). FtsW is a 10-pass transmembrane monofunctional glycotransferase which polymerises lipid II into peptidoglycan, however, this activity only occurs when FtsW is in a complex with FtsI (Egan et al., 2020; Taguchi et al., 2019; L. Wang et al., 1998). FtsW may also have flippase activity to translocate lipid II across the inner membrane although this has not been shown *in vivo* and the flippase MurJ appears to be primary lipid II flippase in *E. coli* (Egan et al., 2020; Meeske et al., 2015; Ruiz, 2008; Sham et al., 2014; Taguchi et al., 2019). FtsI (also known as PBP3) is a class B penicillin-binding protein which has a monofunctional transpeptidase activity to crosslink peptidoglycan layers (Egan et al., 2020; Sauvage et al., 2014).

The divisome proteins described to this point (FtsZ, FtsA, ZipA, FtsEX, FtsK, FtsQLBWI) are assembled, although inactive, the last recruited protein, FtsN is essential in the activation and stabilisation of the assembled divisome.

#### 1.2.4.5 FtsN

Often termed as an activator and stabiliser of the divisome machinery, a small concentration of FtsN initially localises to the septum via a direct interaction with the 1C subdomain of FtsA, mediated by ZipA, before the onset of constriction (Addinall et al., 1997; Busiek et al., 2012; J. C. Chen & Beckwith, 2001; Dai et al., 1993; Weiss, 2015; Wissel & Weiss, 2004). Another bitopic transmembrane protein (J.-C. Yang et al., 2004), FtsN contains a short, N-terminal positively charged cytoplasmic domain, a 19 long residue periplasmic subdomain and a C-terminal SPOR (sporulation related repeat) domain (**Figure 8**) (Busiek et al., 2012; Duncan et al., 2013; Goehring et al., 2007; Yahashiri et al., 2015). For further accumulation of FtsN at the septum, FtsI and FtsQ must have been recruited (Addinall et al., 1997). The SPOR domain of FtsN activates a self-enhanced accumulation via the binding to denuded septal peptidoglycan that is only transiently available during the constriction process (Duncan et al., 2013; Gerding et al., 2009; Yahashiri et al., 2015).

FtsN holds a number of roles in the divisome machinery; the binding of FtsN to septal peptidoglycan appears to stabilise divisome machinery (Ursinus et al., 2004) leading to FtsN activating septal peptidoglycan synthesis by two pathways (Weiss, 2015). The interaction between FtsN and FtsA structurally alters FtsA into a form of 'ON' conformation while the short periplasmic subdomain of FtsN interacts with FtsQLB causing another conformational change to 'ON'. Both interactions lead to the allosteric activation of septal peptidoglycan synthesis while also directly interacting with its assembly partner FtsI (Addinall et al., 1997; Busiek et al., 2012; Goehring et al., 2007; Weiss, 2015). FtsN interacts with periplasmic, transmembrane and cytoplasmic components of the divisome, presumably aiding in the coordination of septal peptidoglycan synthesis.

In FtsN overexpressed cells, the protein can rescue multiple divisome mutants including; *ftsK*, *FtsQ*, *FtsI*, *FtsEX* by an enhanced direct interaction between FtsN and FtsA (Goehring et al., 2006; Pichoff et al., 2018) however, cells with gain-of-function mutations in *ftsA*, *FtsL*, *FtsB*, *FtsW*, *FtsI* can bypass FtsN function (Bernard et al., 2007; Du et al., 2016; B. Liu et al., 2015; Park et al., 2020; Tsang & Bernhardt, 2015; X. Yang et al., 2021). Although the function of FtsN can be overridden by overexpressions of other divisome proteins, under standard conditions, FtsN is required for the activation of septal peptidoglycan synthesis and the stabilisation of divisome complexes, connecting the deemed early and late divisome components, in a potential feedback regulation role.



**Table 1: Key components of the divisome.** C= Cytoplasm, P = Periplasm, IM = Inner membrane, OM = Outer membrane

Protein	Function	Location	Size (kDa)	Protein-protein interactions	References
FtsZ	Tubulin-like polymerising scaffold for the early divisome. Regulates septa PG synthesis	C	40.3	FtsZ, FtsA, ZipA, Zap proteins, FtsEX, FtsK and FtsI	(Anderson et al., 2004; Y. Chen & Erickson, 2005; Erickson et al., 2010; Romberg et al., 2001; Schumacher et al., 2020) PDB: 6UNX, 6UMK, 8GZX <i>Escherichia coli</i>
FtsA	Polymerising Actin-like primary membrane tether and mediator of FtsZ. Recruits multiple downstream division proteins.	C, IM	45.3	FtsZ, FtsA, FtsEX, FtsQ, FtsI and FtsN	(Bernard et al., 2007; Conti et al., 2018; Corbin et al., 2004; Pichoff et al., 2012) PDB: 7Q6F <i>Vibrio maritimus</i>
ZipA	A second membrane anchor of FtsZ and FtsZ polymer crosslinker. Modulator and enhancer of FtsA oligomers.	C, IM, P	36.5	FtsZ and FtsA	(Geissler & Margolin, 2005; Hale & Boer, 1997; Hale et al., 2000; Pichoff et al., 2012) PDB: 1F47 <i>Escherichia coli</i>
Zaps	Increase lateral interactions between FtsZ	C	ZapA (12.6), ZapB (9.6), ZapC (20.6), ZapD (28.3)	FtsZ, ZapABCD	(Hale et al., 2011; Huang et al., 2013; Huang et al., 2016) PDB: 5E1L (ZapC) <i>Escherichia coli</i>

<b>Protein</b>	<b>Function</b>	<b>Location</b>	<b>Size (kDa)</b>	<b>Protein-protein interactions</b>	<b>References and PDB</b>
FtsEX	Regulator of septal peptidoglycan amidases. Recruitment of downstream divisome proteins. Conditionally essential under low osmolarity conditions	C, IM, P	FtsX (38.5), FtsE (24.4)	FtsEX, FtsA, FtsZ, FtsQ, EnvC	(J. Cook et al., 2020; Corbin et al., 2007; Du & Lutkenhaus, 2019; Du et al., 2016; Reddy, 2007; Schmidt et al., 2004) PDB: 8I6O <i>Pseudomonas aeruginosa</i> , 6TPI <i>Escherichia coli</i>
FtsK	Coordination and correction of chromosome segregation, recruitment of other divisome proteins	C, IM	146.7	FtsZ, FtsK, FtsQ, FtsL and FtsI	(Dubarry et al., 2010; Jean et al., 2020; Massey et al., 2006; Pichoff & Lutkenhaus, 2002; L. Wang et al., 1998; X. C. Yu et al., 1998) PDB: 2IUS, 2J5P <i>Escherichia coli</i>
FtsQ	Recruits other divisome proteins. Activator and regulator of septal peptidoglycan synthesis.	IM, P	31.4	FtsA, FtsK, FtsQ, FtsL, FtsB, FtsW, FtsI and FtsN	(Buddelmeijer & Beckwith, 2004; Di Lallo et al., 2003; D'Ulisse et al., 2007; Ghigo et al., 1999; Karimova et al., 2005) PDB: 2VH1 <i>Escherichia coli</i> , 8BH1 <i>Pseudomonas aeruginosa</i> <i>PAOI</i>

<b>Protein</b>	<b>Function</b>	<b>Location</b>	<b>Size (kDa)</b>	<b>Protein-protein interactions</b>	<b>References and PDB</b>
FtsL	Recruits other divisome proteins. Activator and regulator of septal peptidoglycan synthesis.	IM, P	13.6	FtsK, FtsQ, FtsL, FtsB, FtsW, and FtsI	(Buddelmeijer & Beckwith, 2004; Di Lallo et al., 2003; D'Ulisse et al., 2007; Ghigo et al., 1999; Gonzalez et al., 2010; Karimova et al., 2005; Park et al., 2020) PDB: 8HHH <i>Escherichia coli</i> , 8BH1 <i>Pseudomonas aeruginosa PAO1</i>
FtsB	Recruits other divisome proteins. Activator and regulator of septal peptidoglycan synthesis.	IM, P	11.6	FtsQ, FtsL, FtsB, and FtsI	(Buddelmeijer & Beckwith, 2004; Di Lallo et al., 2003; D'Ulisse et al., 2007; Ghigo et al., 1999; Gonzalez et al., 2010; Karimova et al., 2005; Park et al., 2020) PDB: 4IFF <i>Escherichia coli</i> , 8BH1 <i>Pseudomonas aeruginosa PAO1</i>

<b>Protein</b>	<b>Function</b>	<b>Location</b>	<b>Size (kDa)</b>	<b>Protein-protein interactions</b>	<b>References and PDB</b>
FtsW	Septal transglycosylase	IM, P	46	FtsQ, FtsL, and FtsI	(Egan et al., 2020; Ruiz, 2008; Sham et al., 2014; Taguchi et al., 2019; L. Wang & Lutkenhaus, 1998) PDB: 8BH1 <i>Pseudomonas aeruginosa PAO1</i>
FtsI (PBP3)	Septal transpeptidase	IM, P	63.9	FtsA, FtsK, FtsQ, FtsL, FtsB, FtsW, and FtsI	(Egan et al., 2020; Sauvage et al., 2014) PDB: 7ONO, 7ONN, 7ONW <i>Escherichia coli</i> , 8BH1 <i>Pseudomonas aeruginosa PAO1</i>
FtsN	Activator and stabiliser of the assembled divisome. Regulator of septal peptidoglycan synthesis.	IM, P	35.8	FtsA, FtsQ, FtsI, and FtsN	(Addinall et al., 1997; Busiek et al., 2012; J. C. Chen & Beckwith, 2001; Dai et al., 1993; Weiss, 2015; Wissel & Weiss, 2004) PDB: 6YN0, 1UTA <i>Escherichia coli</i>

<b>Protein</b>	<b>Function</b>	<b>Location</b>	<b>Size (kDa)</b>	<b>Protein-protein interactions</b>	<b>References and PDB</b>
EnvC	Regulator of amidase activity	P	46.5	FtsX, AmiA and AmiB	(Heidrich et al., 2001; Peters et al., 2013b; Priyadarshini et al., 2007; Uehara et al., 2009; Uehara et al., 2010) PDB: 6TPI <i>Escherichia coli</i>
NlpD	Regulator of amidase activity	OM, P	40.1	YraP and AmiC	(Heidrich et al., 2001; Priyadarshini et al., 2007; Uehara et al., 2009; Uehara et al., 2010) PDB: N/A
AmiA	Hydrolysis of septal peptidoglycan	P	31.4	EnvC and ActS	(Crawford et al., 2011; Gurnani Serrano et al., 2021; Sham et al., 2011; Vermassen et al., 2019; D. C. Yang et al., 2011; D. C. Yang et al., 2012b) PDB: 8C2O <i>Escherichia coli</i>

<b>Protein</b>	<b>Function</b>	<b>Location</b>	<b>Size (kDa)</b>	<b>Protein-protein interactions</b>	<b>References and PDB</b>
AmiB	Hydrolysis of septal peptidoglycan	P	48	EnvC and ActS	(Crawford et al., 2011; Gurnani Serrano et al., 2021; Sham et al., 2011; Vermassen et al., 2019; D. C. Yang et al., 2011; D. C. Yang et al., 2012a, 2012b) PDB: 8C0J <i>Escherichia coli</i>
AmiC	Hydrolysis of septal peptidoglycan	P	45.6	NlpD and ActS	(Crawford et al., 2011; Gurnani Serrano et al., 2021; Rocaboy et al., 2013; Sham et al., 2011; Vermassen et al., 2019; D. C. Yang et al., 2011; D. C. Yang et al., 2012b) PDB: 4BIN <i>Escherichia coli</i>
End of Table					

### **1.2.5 Activating the assembled Divisome**

During the introduction of FtsN, the assembled divisome machinery begins to stabilise and activate. A set of process begin to couple together during the final stages of cell division; coordination of septal peptidoglycan synthesis and hydrolysis, distribution of divisome components across the septum and the constriction of the membranes.

#### **1.2.5.1 Coordination of division with DNA replication and cell growth**

The intricate interactions between cell growth, DNA replication, division and the temporal nature of each stage of division must be coordinated for successful production of viable daughter cells. DNA replication is coordinated with the divisome through a number of systems; the Min negative positional regulator system (which inhibits FtsZ assembly at the cell poles) (Boer et al., 1989; Lutkenhaus, 2009; Rowlett & Margolin, 2013), nucleoid occlusion which prevents Z-rings from constricting over unsegregated nucleotide (Rowlett & Margolin, 2015), Ter-MatP positive positional regulator linkage system which interacts with FtsZ at the termination of DNA replication (Bailey et al., 2014; J. A. Buss et al., 2017) and finally FtsK which pumps chromosome material away from the division septum (Jean et al., 2020).

Coordinating cell growth with division is a process that is currently not well understood. What is known is there are two main mechanisms in the divisome; division proteins must accumulate to a threshold amount at the division site and the subsequent changes of interactions within the divisome (Park et al., 2020; Si et al., 2019; Tsang & Bernhardt, 2015). These situations lead to the activation of septal peptidoglycan synthesis via FtsW and FtsI, however the mechanism on how septal peptidoglycan synthesis converts from elongation to cross wall formation is unknown (Egan et al., 2020; Levin & Janakiraman, 2021)

### 1.2.5.2 Activation of septal peptidoglycan remodelling

As mentioned in Section 1.2.4, FtsW and FtsI are localised and activated by interactions between FtsN, FtsQLB and FtsA throughout the division process. During the early cell cycle, the concentrations of transmembrane divisome proteins including FtsN and FtsQLB are low along with the levels of FtsZ polymers present at the division site (Si et al., 2019). As the cell grows, the concentrations of these divisome proteins increase as does the availability of FtsN binding sites of FtsA (Corbin et al., 2004; Goehring et al., 2006; Pichoff et al., 2018). During this period, further amounts of FtsQLB, FtsWI and FtsN are recruited and further enhanced by ZipA and FtsEX interactions with FtsN and FtsA which expose the FtsN binding site in FtsA (Corbin et al., 2007). As local concentrations of divisome proteins rise as the cell grows, FtsN interaction with FtsQLB is promoted to confer a conformational change in FtsQLB from a recruitment only 'OFF' state to an active 'ON' state while this is likely promoted by the interaction between FtsN N-terminal cytoplasmic domain and FtsA (Addinall et al., 1997; Busiek et al., 2012; Gerding et al., 2009; Goehring et al., 2007; Weiss, 2015). The combination of interactions from FtsQLB and FtsA onto FtsWI initiates septal peptidoglycan synthesis (B. Liu et al., 2015; Park et al., 2020; Tsang & Bernhardt, 2015).

As the synthesis of new septal peptidoglycan continues at the septum edge, periplasmic peptidoglycan hydrolases called amidases, hydrolyse the peptide side chains from the glycan chains near the outer membrane, which helps facilitate cell constriction and separation (Egan et al., 2020; Priyadarshini et al., 2007). In *E. coli*, there are three main amidases responsible for peptidoglycan hydrolysis during division; AmiA, AmiB, AmiC which are strictly regulated (Egan et al., 2020; Priyadarshini et al., 2007). AmiA and AmiB are regulated by the the cross-membrane EnvC-FtsEX complex in an ATP-dependent reaction which may cause a conformational change throughout FtsEX, transferred into EnvC which activates AmiA/AmiB (Bernhardt & De Boer, 2004; J. Cook et al., 2020; Egan et al., 2020; Priyadarshini et al., 2007; D. C. Yang et al., 2011). AmiC is regulated by the outer-membrane NlpD although this interaction is not well understood (Tsang et al., 2017). AmiB and AmiC appear to only localise to the septum after FtsN has been localised (Bernhardt & de Boer, 2003; Tsang et al., 2017), however AmiA is suggested to be distributed throughout the periplasm during the whole cell cycle (Bernhardt & de Boer, 2003). Only in triple mutant  $\Delta amiabc$  knockout cells does a clear

cell chaining phenotype occur where cells fail to separate properly (Heidrich et al., 2001; Uehara et al., 2010). This suggests a possible redundant system, where an essential process as PG hydrolysis could be affected by the external environment, thus function overlap is a survival mechanism (Mueller & Levin, 2020).

In a positive feedback loop, the products of amidase activity producing denuded glycans is bound by the FtsN SPOR domain, further enhancing recruitment of FtsN to the septum leading to further activation of FtsWI via FtsQLB (B. Liu et al., 2015). Related by the SPOR domains, other proteins localise to the septum including DedD which again interact with FtsQLB and up-regulate the activation of FtsWI (B. Liu et al., 2019) in-conjunction with FtsN. Interestingly, DedD can compensate for FtsN if the activity of FtsN is reduced by mutation (B. Liu et al., 2019).

Another addition to the septal peptidoglycan synthesis system, bi-functional class A penicillin-binding protein, PBP1b, has both glycotransferase and transpeptidase activities to assist in division (Bertsche et al., 2006; Egan et al., 2014). While PBP1b generally localises throughout the cell, it can accumulate at the division site (Bertsche et al., 2006; Egan et al., 2014). This PBP is regulated both by FtsWI and LpoB-CpoB lipoprotein-periplasmic linkage systems (Gray et al., 2015) along with SPOR domain proteins (like DedD) can up-regulate the function of PBP1b (Pazos et al., 2020).

## **1.2.6 Final division stages**

### **1.2.6.1 Constriction**

The final stages of division involves parallel septal peptidoglycan synthesis and cleavage leading to the invagination of the outer membrane reaching a point of constriction, disassembly and closing of the final pore between daughter cells (Levin & Janakiraman, 2021). The ending stages are coordinated by the pushing force of new septal PG synthesis, leading to inner membrane constriction, guided by FtsZ treadmilling, leading to the invagination of the outer membrane via the Tol system, ending in the disassembly of the divisome and closing of the pore to produce two daughter cells (Levin & Janakiraman, 2021).

### 1.2.6.2 Constriction; FtsZ treadmilling guiding PG synthesis

Septal PG synthesis is the most significant force in which constriction of the cytoplasmic membrane occurs and is guided by FtsZ treadmilling (Spratt, 1975). The rate of FtsZ treadmilling, while guides septal PG synthesis, appears to not be the rate limiting step of cytoplasmic membrane constriction, the rate of PG synthesis is. Key pieces of evidence of this includes quantitative super-resolution imaging of *E. coli* cells, showing strains of mutated FtsZ (including GTPase activity) did not affect constriction but was limited by PG synthesis enzymes and divisome chromosome coupling (Coltharp et al., 2016; Monteiro et al., 2018; Whitley et al., 2021). A second key piece of evidence indicates that FtsZ disassembles before the final pore is closed, suggesting it is not essential in these final division stages (Skoog et al., 2012; Söderström et al., 2014).

While not the limiting part of septation, FtsZ treadmilling is still key in the coordination of PG synthesis enzymes. As previously mentioned, FtsZ treadmilling is powered by GTP binding and hydrolysis, and treadmilling evenly directs PG synthesis enzymes circumferentially across the septum (**Figure 9**) (X. Yang et al., 2017). FtsZ distributes divisome proteins via a diffusion and capture mechanism (Baranova et al., 2020). Cytoplasmic tails of FtsN and FtsQ co-migrate directionally with treadmilling FtsZ-FtsA co-filaments however these cytosolic peptides showed random motion and transient confinement, suggesting moving zone of signalling activity at FtsZ-FtsA co-filaments but diffusion of proteins after transient FtsZ interactions (Baranova et al., 2020). In single-molecule analysis experiments, this dynamic appears also true for FtsWI and FtsN however, fluorescence recovery after photo-bleaching (FRAP) and super-resolution imaging indicates that FtsZ and FtsN have a spatial separation and form different macromolecular complexes instead of one large complex (Söderström et al., 2018).

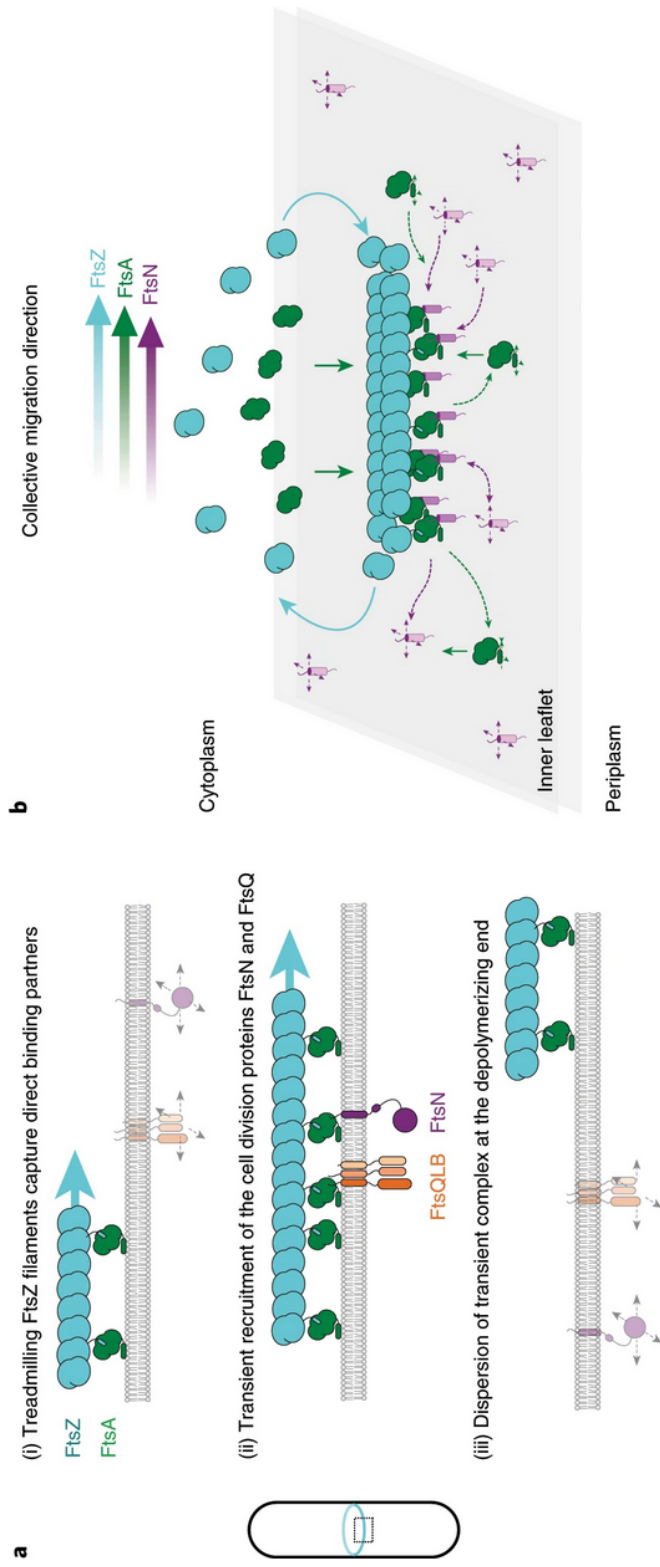


**Figure 9: Schematic of coupling between treadmilling FtsZ filaments and cell division proteins.** (A) At the early stages of cell division, treadmilling FtsZ filaments in the Z ring act as a dynamic scaffold to recruit transmembrane proteins freely diffusing in the membrane. Both FtsN and FtsQ directly bind to the FtsZ-FtsA coflament to form a transient, stationary complex, which can then recruit other division proteins to the division site via interactions in the membrane or periplasm. Due to the local increase in concentration, weak interactions between proteins can be sufficient to initiate assembly of the division machinery. (B) Schematic of the proposed mechanism of co-migration. Freely diffusing FtsN in the membrane binds to the treadmilling FtsZ-FtsA filament on the membrane surface. While proteins reversibly bind along the whole length of the filaments, there is a net accumulation of proteins at the growing end. In contrast, proteins rapidly disperse at the depolymerizing end. This dynamic coupling to the treadmilling filaments permits a collective co-migration at the ensemble level while individual proteins show uncorrelated behaviour. Figure and caption sourced from (Baranova et al., 2020)

### 1.2.6.3 FtsWI dynamics

The interactions of FtsZ-treadmilling and FtsW/FtsI complexes appear to differ to FtsN and FtsQ. FtsW and FtsI are dynamically in two states: a fast-track population coupled with FtsZ-treadmilling and a slow-moving population dependent on active PG synthesis (and independent on FtsZ-treadmilling activity) (X. Yang et al., 2021). The slow-moving population still exhibits a directional movement but is independent of FtsZ and is sensitive during the inhibition of transglycosylase and transpeptidase activities indicating this slow-track population is active in septal PG synthesis (X. Yang et al., 2021). This evidence produces a model of FtsZ-treadmilling distributing PG synthesis enzymes evenly circumferentially across the septum (Levin & Janakiraman, 2021). Similar to FtsQ and FtsN, FtsWI appears to end-track FtsZ polymers directionally across the septum while the positive and negative ends of FtsZ polymers grow and shrink respectively (X. Yang et al., 2017). This distributes PG synthesis enzymes evenly across the septum, in the case for FtsWI, FtsN and FtsQLB switch FtsWI into the active state. Interestingly this appears to occur when FtsWI dissociates from FtsZ polymers, into the slow-moving population state (X. Yang et al., 2021). This is further supported by *E. coli* FtsZ GTPase mutants have a reduced ability to evenly distributed PG synthesis enzymes while not significantly affecting the whole PG synthesis activity (X. Yang et al., 2017). The FtsZ treadmilling activity therefore regulates the directional movement of multiple divisome proteins, distributing them evenly across the division septum, while aiding in the control of PG synthesis enzyme activation coupled with FtsN and FtsQLB.

#### 1.2.6.4 Invagination of the outer membrane

The Tol-Pal complex couples outer membrane invagination with PG synthesis. This complex, which reaches across the whole cell envelope, is composed of five proteins, the TolA / TolQ / TolR complex in the cytoplasmic membrane and the TolB / Pal complex in the periplasm and outer membrane respectively (Szczepaniak, Press, et al., 2020). Leading up to division, the TolB-pal complex laterally diffuse across the outer membrane while TolA and the TolQ / TolR complex associate to the cytoplasmic membrane, where TolA binds to form the TolA / TolQ / TolR triple protein complex (Szczepaniak, Holmes, et al., 2020; Szczepaniak, Press, et al., 2020). During cell division, TolQAR accumulates at the septum while a proton motive force causes a conformational change in the complex which leads to the extension of TolR to bind to the cell wall and TolA to extend and bind to TolB at the outer membrane (Szczepaniak, Press, et al., 2020). This consequently causes Pal to dissociate from the outer membrane and TolB to bind septal PG. Interestingly, only in the presence of localised TolQAR complex will Pal dissociate from TolB and bind the septal PG, then leaving TolB to interact with non-septal Pal, anchoring it to the outer membrane, which appears as a regulatory mechanism for septal invagination (Gerding et al., 2007; Szczepaniak, Holmes, et al., 2020; Szczepaniak, Press, et al., 2020).

Once Pal is bound to septal PG, it stabilises the link between the outer membrane and the peptidoglycan layer in the daughter cells (Szczepaniak, Holmes, et al., 2020; Szczepaniak, Press, et al., 2020). The interactions between in the Pal / TolB complex and the Pal interactions with PG are essential for normal efficient outer membrane invagination (Petiti et al., 2019; Szczepaniak, Holmes, et al., 2020). Mutants lacking Tol-Pal proteins exhibit chaining, outer membrane vesiculation, membrane integrity defects and outer membrane invagination delay (Gerding et al., 2007).

The Tol-Pal system couples with PG synthesis and cleavage via indirect regulation, for example, TolA binds to PBP1B to reverse the inhibitory affects of CpoB (regulator of transpeptidase activity) or that it is theorised that Tol-Pal regulates amidase activity to an extent via NlpD, although no direct interactions have been found (Szczepaniak, Press, et al., 2020). This shows the Tol-Pal system as a driving force of outer membrane PG stabilisation, invagination and a potential indirect regulator

to couple PG synthesis and cleavage together with outer membrane invagination.

#### **1.2.6.5 Closing of the pore and the disassembly of the divisome**

The end steps of division involve the constriction, closing of the daughter cell's pore and disassembly of the divisome. These final steps are not well understood with only a hand-full of studies highlighting what is known so far. Firstly, as mentioned before, constriction is determined by the rate of PG synthesis and influenced by chromosome segregation, a hypothesis supported by mutants such as cells lacking matP (which interacts with DNA and promotes correct chromosome segregation), close the pore faster compared to wild-type (Coltharp et al., 2016). Prior to closure, the cytoplasm of both daughter cells is separated by cytoplasmic membrane fusion and/or the final synthesis of PG (Skoog et al., 2012). The outer membrane is then closed after the final stages of PG synthesis via periplasmic amidases (Skoog et al., 2012). How both of these membrane fusion events occur and their mechanisms are still unknown (Levin & Janakiraman, 2021).

Disassembly of the divisome machinery is again another mostly unknown process. The signal which drives disassembly is unclear, it could be biophysical (such as membrane curvature) and/or transient interactions during the closing septal pore with unknown protein factors (Levin & Janakiraman, 2021; Söderström et al., 2014) although ZapB and ZapE are suggested to be factors in the disassembly of the divisome (Marteyn et al., 2014; Pazos et al., 2013). What is known about the disassembly process is based upon super-resolution microscopy with fluorescent divisome fusion proteins which determined that disassembly occurs at a seemingly similar order to assembly; FtsZ:ZapA, ZipA:FtsA, FtsL:FtsQ, FtsL:FtsN, FtsN indicating a potential first in, first out mechanic (Söderström et al., 2016). The other divisome proteins however are only hypothesised to follow this order. As previously mentioned, FtsZ is not required for the constriction of the outer membrane and thus leaves the septum before the closure of the pore (Söderström et al., 2014). Curiously, a small population of FtsN molecules remain in a ring, the SPOR domain remains at the division site as it may be that the final FtsN molecules will disperse when all the denuded glycan strands are processed back into the peptidoglycan cell wall (Alcorlo et al., 2019; Söderström et al., 2018).

This divisome is a complex network of transiently interacting proteins all work-

ing to mediate and perform a successful cell division. While there is a wealth of information regarding the structures, interactions and localisation of proteins throughout the division process there is still much to research regarding the temporal localisation of all proteins present and their respective structural mechanisms, to the unknown of the final disassembly steps of division. There are still multiple protein networks of interactions which are still unclear to why *E. coli* and other bacterial species differ from one another, however understanding the *E. coli* is an essential model to understanding other divisome systems in other bacterial species and for potential antibiotic targets.

### 1.3 FtsEX and EnvC pathway

As described in the previous section, the FtsEX:EnvC:AmiA/AmiB pathway regulates the activities of two out of the three periplasmic amidases tasked with cleaving peptidoglycan during the late stages of cell division. Although not essential in cell division, this pathway is important to the survival and proper septation of the cell and the structural basis of amidase regulation maybe conserved which means a potentially worthwhile antibiotic target worth investigating.

#### 1.3.1 Type VII ABC transporters

FtsEX is an unusual member of a large family of ATP-binding cassette (ABC) transporter proteins. These are usually transmembrane proteins, present in all three domains of life, which use nucleotide binding and hydrolysis to transport substrates like drugs, sugars, ions, proteins and amino acids across membranes . ABC transporters generally exhibit four characteristic structural domains; two variable transmembrane domains (TMDs) and two core conserved nucleotide-binding domains (NBDs), located in the cytoplasm (Rees et al., 2009). These domains share a set of highly conserved motifs which are present in ABC transporters. Due to the variety of substrates, the sequences and structures of TMDs can differ along with the addition of other protein components such as a high affinity binding protein in the periplasm for example (Rees et al., 2009).

There are seven structurally distinct ABC transporter families which are further classed by their function. Type I/II/III ABC transporters are importers, type IV/V are exporters and type IV/VII are more unusual as mechanotransducers (**Figure 10**) (Greene et al., 2018).

Type VII ABC transporters such as MacB (Crow et al., 2017; Greene et al., 2018), LolCDE (Tang et al., 2021) and FtsEX (Crow et al., 2017) have been shown to have a general mechanism dependent on the binding and hydrolysis of ATP. This ATP-dependent activity causes conformational changes in the nucleotide binding domains leading to a switch between inward-open and outward-open states allowing substrates to pass through the membrane (Wilkens, 2015). During the inward state, the NBDs are separated allowing for substrate binding to the cytoplasmic side of the TMDs. When ATP binds to the NBDs, these domains associate closely

with each other leading to a conformational change in the TMDs in the conserved coupling helix (Wilkins, 2015). This produces the outward-open state which has a significantly lowered affinity for the bound substrate which allows the release of said substrate on the other side of the membrane. To reset the process, ATP hydrolysis changes the transporter conformation back to inward-open state (Wilkins, 2015). In other ABC transporter types and variations of this mechanism are known with states coupled by a proton motive force (e.g. MsbA) (H. Singh et al., 2016) but type VII transports can lack a substrate but instead a transfer of a signal in a signalling pathway (Crow et al., 2017).

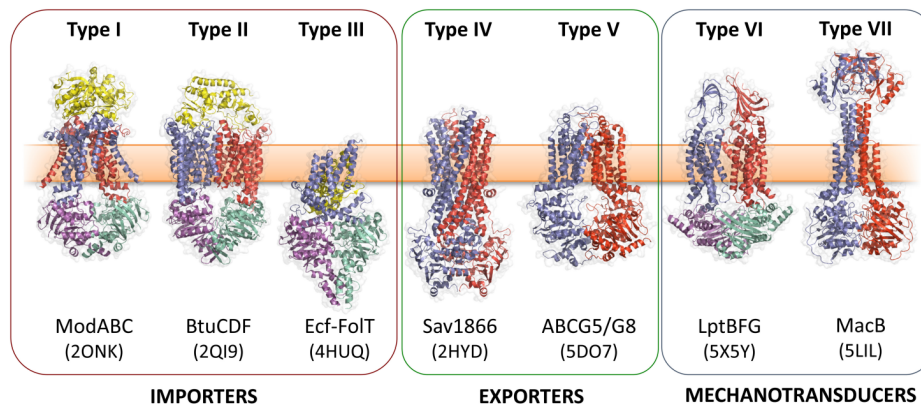


**Figure 10: Seven ABC transporter superfamilies.** A single representative from each superfamily is shown colored by protein chain. PDB identifiers are given in parentheses. The seven ABC folds are here further divided into three “classes” based on function. Families I-III are importers, Type IV and V are exporters and Types VI and VII are mechanotransducers. Note that the two ABC exporter families here termed Type IV and Type V are also sometimes referred to as type I and II ABC exporters. From left to right: the molybdate transporter (Hollenstein et al., 2007) (ModABC), vitamin B12 transporter (Korkhov et al., 2012) (BtuCDF), folate importer (Xu et al., 2013) (Ecf-FolT), multidrug exporter (Dawson & Locher, 2006) (Sav1866), the sterol transporter (J.-Y. Lee et al., 2016) (ABCG5/G8), the lipopolysaccharide extractor (Luo et al., 2017) (LptBFG) and the enterotoxin and macrolide transporter (Crow et al., 2017) (MacB). Folds are named by extension of a previously established convention (ter Beek et al., 2014). Figure and caption sourced from (Greene et al., 2018).

### 1.3.1.1 Type VII founder, MacB

As FtsEX is a type VII ABC transporter, it is important to outline why this type is unique in the superfamily. Firstly, it is key to note that ABC transporters in Gram-negative bacteria, instead of the classic exporter model of transporting substrates independently across a membrane, other ABC transporters can form as a part of larger structures called tripartite efflux pumps; this is the case for the founding member of the type VII ABC transporter family, MacB (Crow et al., 2017; Greene et al., 2018).

MacB is part of the MacAB-TolC tripartite efflux pump system which is suggested as an antibiotic resistance mechanism as by ejecting antibiotics out of the cell (Greene et al., 2018). The structure and mechanism defines the type VII transporter class (**Figure 11**), as there is no direct substrate but a transmembrane conformational change that transfers a signal to drive substrate through TolC-like exit ducts (Crow et al., 2017). MacB monomers consists of four transmembrane helices, an N-terminal NBD, a periplasmic domain between helices 1 and 2, short extracytoplasmic loops on helices 3 and 4 and finally a cytoplasmic N-terminus amphipathic helix connecting helix 1 to the NBD (Crow et al., 2017).

The MacB *in vivo* resides as a dimer with the mechanism beginning in a nucleotide-free state with NBDs parted and the periplasmic domains also parted (**Figure 11**) (Crow et al., 2017). This allows substrates to enter the pump system via the cavity between MacB and MacA. Upon ATP binding, a conformational change where the NBDs reversibly dimerise together causing the transmembrane stalk helices to associate together which lastly causes the MacB periplasmic domains to closely associate together (Crow et al., 2017). This creates a pressure system which pushes the substrate through the MecA channel. Substrates are prevented from back flow by a valve in MacA (Crow et al., 2017). ATP hydrolysis resets MacB with the periplasmic domains and stalk helices parting leading to the separation of the NBD dimer on the cytoplasmic side. This mechanism has been compared to a molecular bellows driven by mechanotransmission (Crow et al., 2017).

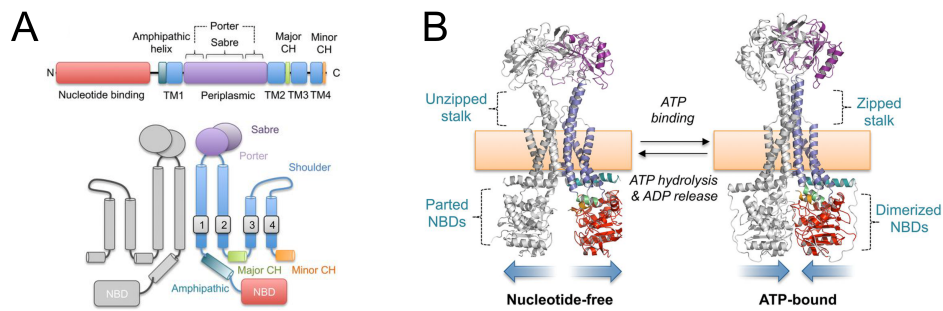


**Figure 11: Structure and Mechanotransmission mechanism of MacB.** (A, TOP) Linear domain organization of the MacB polypeptide. (A. BOTTOM) Topology of MacB. (B) Nucleotide-free (Left) and ATP-bound MacB (Right). Both models represent *E. coli* MacB; the nucleotide-free form is extracted from the cryo-EM structure of the MacAB-TolC complex (5NIL), and the ATP-bound form is a homology model generated from the crystal structure of the nucleotide-bound AaMacB (5LIL). Figures and captions adapted from (Crow et al., 2017)

### 1.3.1.2 The Lol system, confirmation of mechanotransmission

As the class of type VII ABC transporters became more understood, more recently, another ABC transporter system has been investigated, the LolCDE system.

Like many Gram-negative bacteria, the *E. coli* outer membrane contains lipoproteins as a key structural component which hold a variety of functions including; translocation / insertion of outer membrane proteins/lipids (e.g. phospholipids (Bishop et al., 2000; Malinverni & Silhavy, 2009; Raetz et al., 2007; Rowlett et al., 2017), and outer membrane lipoproteins (Knowles et al., 2009; Kovacs-Simon et al., 2011; S.-I. Narita et al., 2004)). The end result is to maintain the integrity and function of the outer membrane bilayer. In *E. coli*, around 90 outer membrane proteins are transported and sorted by the lipoprotein outer membrane localisation (Lol) pathway (S.-I. Narita & Tokuda, 2017; Yakushi et al., 2000) involving five proteins, LolCDEAB which are stationed between the inner and outer membranes (Tokuda & Matsuyama, 2004).

The lipoprotein transport Lol pathway begins with the synthesis and translocation of a pre-lipoprotein from the cytoplasm to the periplasmic side of the inner membrane by the translocase SecYEG (Mori & Ito, 2001; S.-I. Narita & Tokuda, 2017). The pre-lipoprotein is modified into a lipoprotein with the signal peptide cleaved and the conserved N-terminus cysteine N-acylated with a diacylglycerol added to the same cysteine (Hillmann et al., 2011; Mao et al., 2016; Vogeley et al., 2016). The ABC transporter complex LolCDE is located on the periplasmic side of the inner membrane and binds to mature lipoproteins to transfer them to the periplasmic chaperone protein LolA (Gennity & Inouye, 1991; Masuda et al., 2002; Seydel et al., 1999). This occurs via the ATP hydrolysis in the ATPase LolD coupled with the association of the periplasmic domain LolC to LolA (Kaplan et al., 2018; Okuda & Tokuda, 2009). LolA then transports the lipoprotein to the outer membrane lipoprotein LolB of which integrates the new lipoprotein into the outer membrane (Matsuyama et al., 1997; Nakada et al., 2009; Takeda et al., 2003; Tsukahara et al., 2009). The Lol system is conserved and deemed essential in Gram-negative bacteria (S.-i. Narita et al., 2002) and is known to be powered by a lipoprotein affinity gradient (Matsuyama et al., 1997; Takeda et al., 2003; Tsukahara et al., 2009). Due to the importance of this system, it is a prime target for antibiotic developments and LolCDE is known to bind to small-molecule

inhibitors producing an antibacterial effect (Lorenz et al., 2016; McLeod et al., 2015; Nayar et al., 2015; Nickerson et al., 2018).

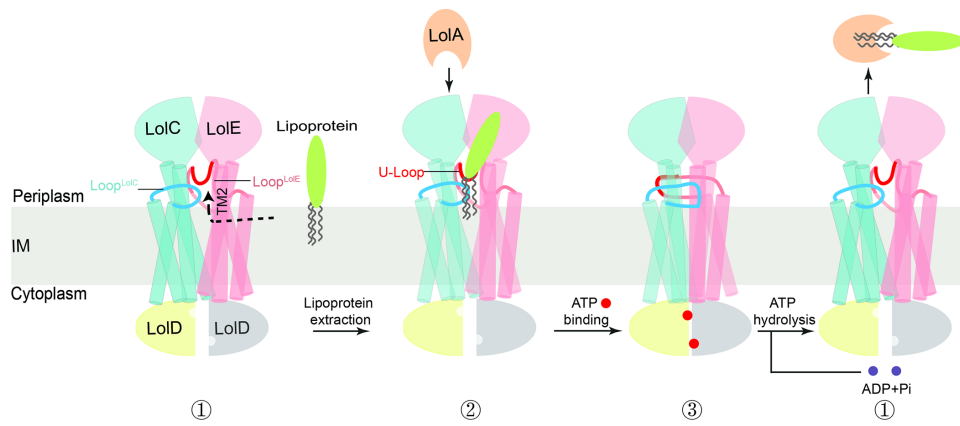


**Figure 12: Proposed model for lipoprotein extraction and transfer to LolA.** ATP and ADP are shown as balls in red and purple, respectively. The dashed arrow indicates the path for lipoproteins entry into the cavity. The apo-LolCDE, RcsF-LolCDE and AMPPNP-LolCDE structures represent structures in 1, 2, and 3, respectively. Figure and caption sourced from (Bei et al., 2022)

LolCDE ABC transporter crystal structure shows it is a heterodimer of transmembrane domains of LolC and LolE bound to a homodimer of LolD, nucleotide-binding domains (**Figure 12**) (Tang et al., 2021). The type VII ABC transporter, MacB has a similar configuration with the homo-dimerisation of a nucleotide-binding domain, transmembrane helices and a periplasmic domain (Crow et al., 2017). Unlike other ABC transporters there is a 'door bar' which is an extension of transmembrane helix 3 of LolE which protrudes into the periplasm and bends towards LolC until it runs parallel to the inner membrane (Tang et al., 2021). The nucleotide-binding domains of LolCDE contain RacA-like subdomains and structural folds which are typical for ABC transporters (Locher, 2016; Tang et al., 2019).

The mechanism of action of LolCDE appears mostly typical for a type VII ABC transporter using a mechanotransducing mechanism, like that of MacB (**Figure 12**) (Crow et al., 2017). LolCDE begins in a apo state in a relaxed conformation with NBDs far separated. During lipoprotein binding into the central transmembrane channel, the NBDs move closer together but insufficient for dimerisation. LolA binds to the periplasmic 'door bar' on LolC however does not affect the LolCDE conformation. When ATP binds however, the NBDs dimerise into a closed state causing a conformational change in the transmembrane domains, closing the central channel, moving the lipoprotein upwards towards LolA. The LolE periplasmic domain remains blocking access of the lipoprotein to LolA. Once ATP hydrolysis occurs, the NBDs draw apart causing a conformational change in the transmembrane domains rotating the periplasmic domain of LolC, creating a deformed transmembrane interface and allowing LolA to bind to the lipoprotein leading to the LolA bound lipoprotein dissociates from LolC into the periplasm. The cycle then begins anew in the apo state (Tang et al., 2021).

This structure was another piece of evidence of the type VII ABC transporter mechanotransmission mechanism to transfer substrates through or from a membrane.

## **1.3.2 FtsEX**

### **1.3.2.1 FtsEX of the past**

Originally thought to be only relevant for bacterial growth in different osmolality conditions (Ricard & Hirota, 1973) and a potential indirect division role with inserting division proteins with FtsY (a signal recognition particle receptor) into the membrane (Crickmore & Salmond, 1992; Gibbs et al., 1992; Gill et al., 1986; Salmond & Plakidou, 1984). It was later discovered that FtsEX forms a predicted ABC transporter complex and is essential to the stability of the divisome in low osmolarity conditions (Corbin et al., 2007; Karimova et al., 2005; Reddy, 2007; Schmidt et al., 2004), however it was only more recently the true functions and interactions of FtsEX were discovered (J. Cook et al., 2020; Pichoff et al., 2019).

### 1.3.2.2 FtsEX functions

As mentioned previously, FtsEX holds multiple roles in cell division and is conditionally essential in low osmolarity conditions (Leeuw et al., 1999; Reddy, 2007; Ricard & Hirota, 1973; Schmidt et al., 2004; Taschner et al., 1988). FtsEX localises to the septum with FtsE (once in a complex with FtsX), which is the main factor to localise the complex to the Z-ring based on the FtsX independent interaction of FtsE with only the C-terminal peptide of FtsZ (Du & Lutkenhaus, 2019). This is supported by the overexpression of FtsEX appears to displace FtsA and ZipA binding to the CTP on FtsZ (Du & Lutkenhaus, 2019).

The removal of FtsEX provides understanding on its function. In *E. coli*, mutants lacking FtsEX did not affect Z-ring formation, however, a filamentation phenotype occurred before slower growth along with the downstream division proteins prevented from localising; FtsK, FtsQ, FtsI and FtsN (Schmidt et al., 2004). These phenotypes can be suppressed however if FtsN is overexpressed or gain-of-function mutated FtsA can all rescue cells lacking FtsEX to a significant degree to produce only a mildly filamentation phenotype (Du et al., 2016; Pichoff et al., 2018; Reddy, 2007; Schmidt et al., 2004). This was later deduced to be the result of the upregulation of FtsN to interact with FtsA while FtsN is recruited to the septum early, thus recruiting FtsWI and FtsQLB earlier (Pichoff et al., 2018).

The proto z-ring protein, FtsA, requires the interaction with FtsX in order to recruit the late divisome proteins to the septum. Interestingly, mutations in FtsA (R63H or G366D) or FtsX ( $\Delta$ 4-69) prevent the recruitment of the downstream divisome proteins with no effect on FtsEX localisation (Du et al., 2019; Du et al., 2016), indicating if mutations promote FtsA interactions with FtsN and/or negatively affect FtsA self-interaction, remove the requirement for the FtsA:FtsEX interaction and bypass ZipA (which is also a requirement for downstream divisome protein recruitment by anchoring FtsZ polymers). This is thought to be FtsEX directly antagonising FtsA polymerisation which allows FtsA to interact and recruit downstream divisome proteins (Du & Lutkenhaus, 2017; Du et al., 2016; Pichoff et al., 2012).

### 1.3.2.3 FtsEX structure

FtsEX is a type VII ABC transporter where FtsE contains the cytoplasmic nucleotide binding domain and FtsX contains the transmembrane domains along with a periplasmic domain (Gibbs et al., 1992; Leeuw et al., 1999). The periplasmic loop between TM1 and TM2 present indicates it is unlikely to be a substrate channel (Arends et al., 2009; Daley et al., 2005). As an ABC transporter, ATP hydrolysis should cause a conformational change in FtsX moving the periplasmic domain further into the periplasm (Arends et al., 2009). This would be consistent with the type VII ABC transporter's mechanotransmission mechanism such as in MacB and LolCDE where the conformational change is crucial for their function (Crow et al., 2017; Greene et al., 2018). A structural model of FtsEX based on MacB supports this claim (**Figure 13**) (Du et al., 2019; Pichoff et al., 2019).

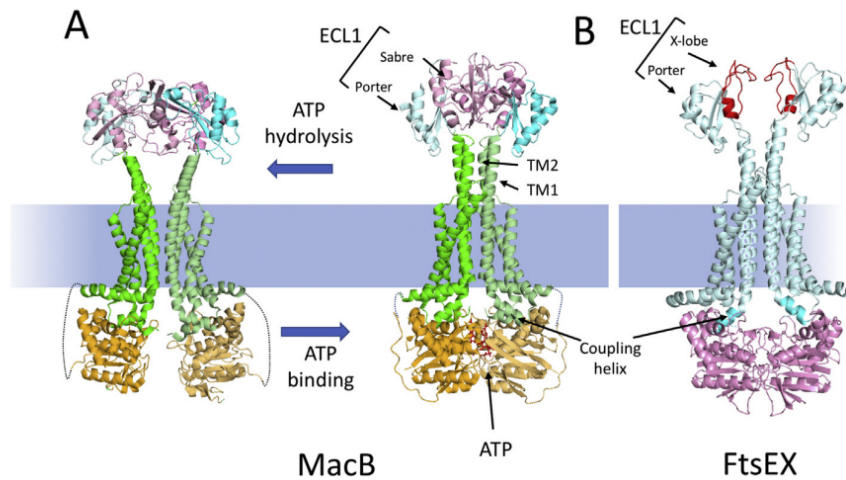


**Figure 13: MacB as a model for the Type VII subfamily of ABC transporters and comparison to a model of FtsEX.** (A) The structures of a MacB dimer in the nucleotide free form (5NIL) and the ATP bound form (5LJ7) are depicted. The NBD (light orange), the membrane component (green) and the large extracellular domain (ECL1) are depicted. ECL1 is split into two domains: porter (cyan) and sabre (pink). ATP binding brings the NBDs together causing the long TM1 and TM2 helices to form a tight helical bundle distal to the membrane causing conformational changes in the ECL1. The linkage between the NBD and the membrane component is not resolved in the structure and is indicated by a dotted line. (B) A model of the ATP form of FtsEX (Du et al., 2019); FtsE (pink) FtsX (cyan). The ECL1 of FtsX has a porter domain and a unique FtsX domain (called X-lobe [red]) instead of a sabre domain. This domain is responsible for interaction with the coiled coil region of its effector. The coupling helix of the TMD (FtsX) is inserted into a cleft of the NBD (FtsE). Figure and caption sourced from (Pichoff et al., 2019)

The FtsEX model (**Figure 13**) highlights the similarities between MacB and FtsEX within type VII ABC transporters. Each FtsX monomer has four transmembrane domains and a porter domain like MacB monomers (Crow et al., 2017). FtsEX periplasmic domain contains a X-lobe instead of a sabre (small alpha beta rich extracytoplasmic) domain (Mavrici et al., 2014; Rued et al., 2019). FtsE NBDs appear to dimerise when ATP binding (like that of MacB) which may lead to conformational changes in the transmembrane domains that in turn alters the conformation of the periplasmic domains assuming is important for function (Crow et al., 2017). The FtsEX ATP hydrolysis mechanism and its effect on function is explored later.

#### 1.3.2.4 FtsEX ATPase activity and PG hydrolysis

The function of the ATPase activity of FtsE has multiple implications for the recruitment of the divisome, constriction activation and PG hydrolysis. It was found that when mutating residues in the conserved Walker A and Walker B motifs of FtsE, FtsEX still localised to the Z-ring and recruited the downstream divisome proteins, however the assembled divisome was inactive (Arends et al., 2009). These ATP mutants produce a similar phenotype to inhibiting FtsI and FtsE mutant D162N indicating that without ATP binding and/or hydrolysis, this blocks FtsA from starting constriction (by FtsA interaction with FtsN) although an overexpression of FtsN will bypass this block and activate the divisome (Du et al., 2019; Du et al., 2016). Therefore FtsE ATPase activity regulates divisome activation but not assembly by modulating PG synthesis.

To separate daughter cells, the septal PG must be hydrolysed. As previously mentioned, in *E. coli*, there are three periplasmic amidases; AmiA, AmiB and AmiC, which cleave septal PG (Heidrich et al., 2002). These are regulated by EnvC (for AmiA and AmiB) and NlpD (AmiC) (Peters et al., 2011; Rocaboy et al., 2013). FtsEX has been found to be a regulator of PG hydrolysis in *E. coli* and in other species such as *Streptococcus pneumoniae* (Alcorlo et al., 2020) and *Mycobacterium tuberculosis* (Mavrici et al., 2014). In *E. coli* FtsEX is believed to interact with EnvC which in turn interacts with EnvC to activate AmiA/AmiB **Figure 14** (Pichoff et al., 2019).

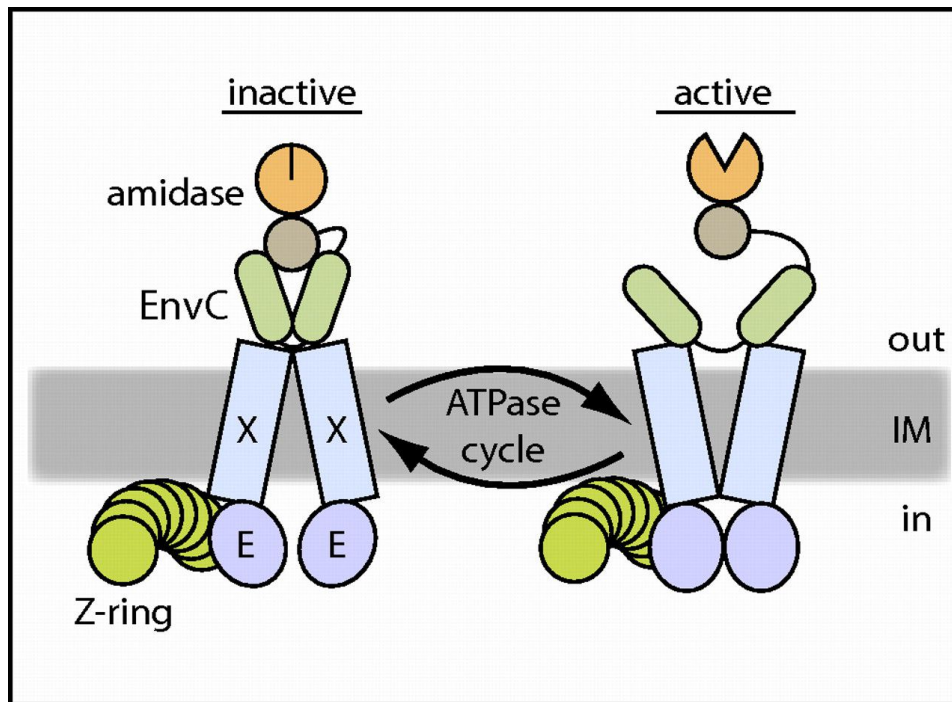


**Figure 14: Model for FtsEX function in regulating PG amidase activity at the division site.** Shown is a schematic diagram of a putative FtsEX-EnvC-amidase complex at the Z-ring. We propose that conformational changes in FtsEX induced by FtsE-mediated ATP hydrolysis are transmitted to EnvC to control its ability to activate the amidases so that they can cleave the septal PG (not drawn). The model is not meant to reflect actual interaction stoichiometries, because they have yet to be determined. In addition, it is not yet clear if the amidases remain in complex with EnvC as drawn or if this interaction is also regulated. Figure and caption sourced from (D. C. Yang et al., 2011)

As **Figure 14** indicates, FtsEX requires its ATPase activity to control PG hydrolysis as supported by; FtsEX mutants with defective ATPase activity do not rescue chained cells which lack NlpD and FtsEX (D. C. Yang et al., 2011), additionally, in *S.pneumoniae*, the ATPase function of FtsE is essential to activate PcsB and for in proper membrane constriction (Arends et al., 2009; Briggs et al., 2021; Sham et al., 2013). In another system, in *B.subtilis*, FtsEX interacts with a similar protein, CwlO, an endopeptidase, in with cannot be activated by FtsEX if FtsE cannot bind or hydrolyse ATP (Domínguez-Cuevas et al., 2013; Meisner et al., 2013). This system however is used in cell elongation not cell division, suggesting in potentially other roles of FtsEX outside of cell division in other systems (Pichoff et al., 2019).

**Figure 14** raises further questions however; Are amidases bound to EnvC throughout their activation or do they interact, become active and then dissociate in an active conformation? Why does EnvC need to bind to FtsEX in order to interact with AmiA/AmiB? How are the amidases structurally regulated? These questions are addressed in this section and in this thesis.

### 1.3.3 EnvC, an amidase regulator

Throughout bacterial genomics, there are a collection of PG hydrolases with a range of functions to hydrolyse specific bonds in peptidoglycan all for varying purposes (Firczuk & Bochtler, 2007; van Heijenoort, 2011; Vollmer et al., 2008). A number of these hydrolases contain LytM-domains which attribute to their function of PG hydrolysis, interestingly, there are some proteins which contain LytM-domains but lose their catalytic activity, in favor of other functions, such as the amidase regulator, EnvC (Uehara et al., 2010).

Proteins which contain LytM (Peptidase M23) domains (Finn et al., 2008) are named after lysostaphin (LytM) from *Staphylococcus aureus* which was the first thoroughly-characterised zinc metallo-endopeptidase that hydrolysed pentaglycine cross-links in the PG (Browder et al., 1965; Firczuk & Bochtler, 2007; Firczuk et al., 2005; Peters et al., 2013b). Of the structurally characterised proteins containing related LytM domains, most of them are also metallo-endopeptidases (Cohen et al., 2009; Lu et al., 2006; S. K. Singh et al., 2012), and can be found to have functions in systems such as cell division/elongation, sporulation and cell-shape formation (Bonis et al., 2010; Cohen et al., 2009; Goley et al., 2010; Meisner & Moran, 2011; Möll et al., 2010; Peters et al., 2013b; Poggio et al., 2010; S. K. Singh et al., 2012; Sycuro et al., 2010; Uehara et al., 2009). There are some unusual exceptions to these endopeptidases including SpollQ from *Bacillus subtilis* (J et al., 2012; Lev-dikov et al., 2012; Meisner & Moran, 2011) and EnvC / NlpD / ActS from *E. coli* (Peters et al., 2013a; Uehara et al., 2010), which do not appear to have hydrolytic activity.

EnvC and NlpD are LytM domain proteins which do not have metallopeptidase activity and appear to have regulatory roles on periplasmic PG amidases (Uehara et al., 2010). EnvC and NlpD are missing conserved metal-binding and catalytic residues, thus potentially missing a metal ion, which active metallopeptidases contain, essential for function (Uehara et al., 2010). As mentioned previously, the 3 PG amidases in *E. coli* are required to cleave the septal PG in order for daughter cells to separate at the end of cell division (Heidrich et al., 2001; Priyadarshini et al., 2007; Uehara et al., 2009). If all 3 amidases or both EnvC and NlpD are removed in *E. coli* knockout strains, it produces the classic chaining phenotype with cells connected with PG and partially constricted outer membranes (Heidrich et al., 2001;

Priyadarshini et al., 2007; Uehara et al., 2009). Amidases are currently hypothesised to be activated by the removal of the autoinhibitory alpha-helix which blocks the active site (D. C. Yang et al., 2012b). EnvC / NlpD do not appear to cleave this autoinhibitory helix as the molecular weight of amidases does not change upon LytM domain incubation with the conclusion that the helix is moved via structural rearrangement imposed by EnvC or NlpD (Uehara et al., 2010). More recently, ActS, is another LytM domain protein shown to lack activity but hold a regulatory role on *E. coli* periplasmic amidases although primarily under lipopolysaccharide depletion cellular stress (Gurnani Serrano et al., 2021). This collectively suggests a primary regulatory role of EnvC and NlpD on peptidoglycan periplasmic amidases during cell division.

As EnvC is not itself an active metallopeptidase, but a regulatory LytM factor, it is not unreasonable to suggest itself if being regulated. EnvC appears to activate AmiA and AmiB via the control of the aforementioned type VII ABC transporter, FtsEX (D. C. Yang et al., 2011). It is thought that through the ATP binding and hydrolysis powered conformational changes, FtsEX regulates EnvC to activate and cause the release of the inhibitory domain of AmiA and AmiB (Crawford et al., 2011; Sham et al., 2011; D. C. Yang et al., 2011). The structural mechanism of this regulation however is currently not well understood.

### 1.3.3.1 EnvC LytM structure

In support of EnvC as a regulatory LytM factor, a structure of only the LytM domain has been solved (Figure X) (Peters et al., 2013b). Unsurprisingly, this LytM domain is highly similar to other LytM proteins however lacks a metal ion, metal-binding residues and active site residues which are common in active metallopeptidases (Peters et al., 2013b). Therefore EnvC cannot cleave PG but further believed to regulate AmiA and AmiB in the periplasm that can (Peters et al., 2013b). By site directed mutagenesis in EnvC LytM domain, the key residues required in the interaction and activation of amidases have been deduced (**Figure 15**) (Peters et al., 2013b). Key residues found *in vivo* and *in vitro* for EnvC regulatory function reside in the degenerate active-site cleft including; K321, Y350, V353, Y401 and R405 (Peters et al., 2013b). EnvC constructs with mutations in these sites do still localise to the septum during cell division however have significantly reduced activation ability onto AmiB *in vitro* (Peters et al., 2013b). How these mutants affect the full length EnvC protein is still largely unknown at the molecular level. Although the molecular mechanism of how FtsEX interacts and regulates EnvC to regulate periplasmic amidases is still largely unknown. How EnvC alters the amidases conformation to produce an active amidase also remains to be elucidated.

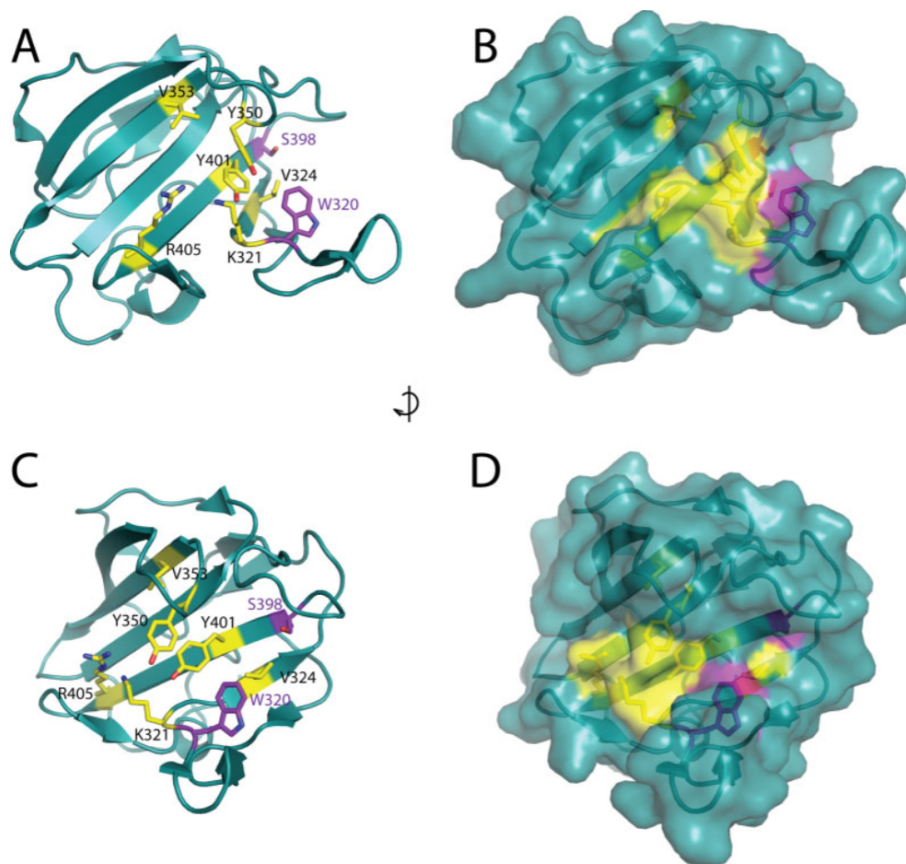


**Figure 15: EnvC residues important for function cluster in and around the degenerate active-site cleft.** Residues important for EnvC function are shown as yellow coloured sticks on the structure of LytEnvC including two corresponding to those required for metallo-endopeptidase activity in other LytM domains. The two remaining ‘degenerate’ active-site residues are shown as purple coloured sticks. Both ribbon (A, C) and surface (B, D) representations of the structures are shown. Side views (A, B) and front views (C, D) of the cleft are shown. Structures in (C) and (D) are rotated roughly 90 degrees clockwise relative to the structures in (A) and (B). Figures and captions sourced from (Peters et al., 2013b)

## 1.4 Periplasmic amidases

### 1.4.1 Bacterial peptidoglycan cleaving enzymes

In bacteria, there are a vast range of cell wall peptidoglycan cleaving enzymes which vary on the bond in peptidoglycan they cut, specifically there are 3 classes of these peptidoglycan cleaving enzymes; amidases, glycosidases and peptidases of which all hold differing functions ranging from cell division, cell wall rearrangement, recycling and cell lysis (Fenton et al., 2010; Rigden et al., 2003; Szveda et al., 2012; Vermassen et al., 2019). These differ in terms of their structure and function but have conserved catalytic domains within each class of peptidoglycan cleaving enzyme (Alcorlo et al., 2017). N-acetylmuramoyl-L-alanine amidases (PG amidases) are the focus of this section. Peptidoglycan amidases hydrolyse the amide bond linking the glycan strand with the stem peptide, specifically between the MurNAc and L-alanine residues (**Figure 16**) (Höltje, 1995; Vollmer et al., 2008). There are three types of N-acetylmuramoyl-L-alanine amidases in bacteria; type 2, type 3 and type 5, these differ in their catalytic domains (Vermassen et al., 2019).

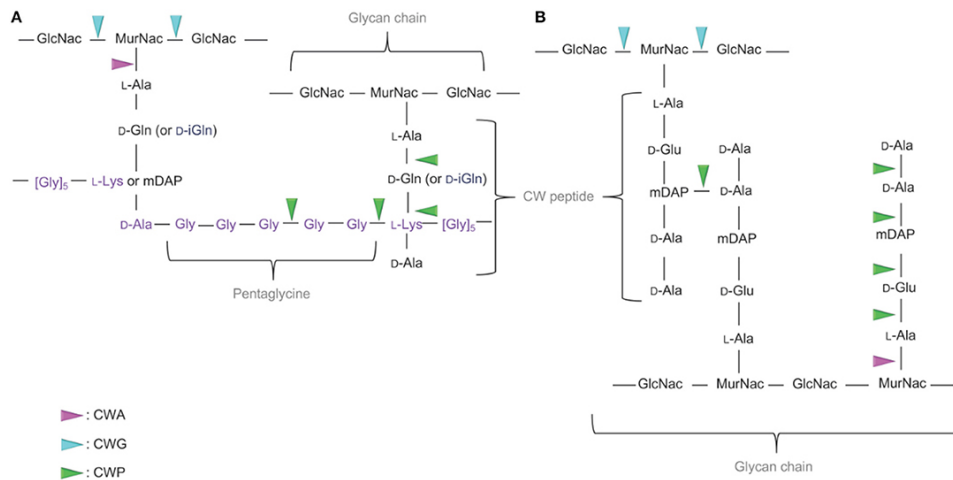


**Figure 16: Targets of the bacterial cell wall hydrolases (or peptidoglycan cleaving enzymes) (CWHs) in Cell wall-monoderm and LPS-diderm bacteria.** (A) In the Cell wall (CW) of CW-monoderm bacteria, the alternating subunits of N-acetylglucosamine (GlcNac) and N-acetylmuramic acid (MurNac) are amide linked to the alanine of the wall peptide alanine, glutamine or isoglutamine, meso-diaminopimelic acid (mDAP) or lysine and alanine. In *S. aureus*, the pentaglycine cross bridge is linked to the alanine of the CW peptide. (B) In the CW of LPS-diderm bacteria, the alternating subunits of N-acetylglucosamine (GlcNac) and N-acetylmuramic acid (MurNac) are amide linked to the alanine of tetrapeptide alanine, glutamine, mDAP and alanine. N-acetylglucosaminidase hydrolyses the glycan component of the cell wall on the reducing side of the GlcNac. N-acetylmuramidases cleave the same bond but form N-acetyl-1,6-anhydro-muramyl intermediates during cleavage. N-acetylmuramoyl-L-alanine amidase cleaves a critical amide bond between the glycan moiety (MurNac) and the peptide moiety (L-alanine) of the peptidoglycan. Peptidase cleaves an amide bond between two amino acids (depicted in green). CWA, CW amidase; CWG, CW glycosidase; CWP, CW peptidase. Figure and caption sourced from (Vermassen et al., 2019)

In *E. coli*, AmpD and AmiD are the most characterised type 2 amidases (Heijenoort, 2001; Höltje et al., 1994). AmpD quickly cleaves the 1,6-anhydro-MurNAc-L-Ala bonds present in MurNAc and tetrapeptides (Heijenoort, 2001; Höltje et al., 1994). The lipoprotein, AmiD cleaves 1,6-anhydro-MurNAc-L-Ala and MurNAc-L-Ala bonds as a broader specificity (Pennartz et al., 2009). Hydrolysis is a zinc-dependent reaction occurs in a L-shape cavity where a  $Zn^{2+}$  ion is present between the glycan and peptide stem binding sites (M. Lee et al., 2013; Martínez-Caballero et al., 2013). The type 2 amidase is regulated via an open and closed conformation system in which the substrate and peptide-stem binding sites become available upon a significant secondary structural rearrangements after activation (Carrasco-López et al., 2011; Liepinsh et al., 2003).

Another zinc-dependent amidase, type 3 amidases have a number of well characterised examples. AmiA, AmiB, AmiC are examples of periplasmic PG amidases in *E. coli* which have been shown to produce L-Ala-D-Gly-mDAP tripeptide and L-Ala-D-Glu-mDAP after cleaving the amide bond between the stem peptide L-Ala and MurNAc (Büttner et al., 2014; Rocaboy et al., 2013; Zoll et al., 2012). Again, similar to type 2, a solved *E. coli* AmiC structure suggests an open and close mechanism, changing the availability of the active site (Rocaboy et al., 2013).

Lastly, type 5 amidases is the least understood family. There is a type 5, cell wall hydrolyse present in Dp-1, a bacteriophage of *S. pneumoniae* in which was found to require choline for full activity (Garcia et al., 1983; Lopez, 1981). This family of amidases is generally still an unknown with no structural information available (Vermassen et al., 2019).

#### 1.4.2 N-acetylmuramoyl-L-alanine type 3 *E. coli* periplasmic amidases

As previously mentioned, the three N-acetylmuramoyl-L-alanine type 3 periplasmic amidases in *E. coli* are crucial for the end stages of cell division. As new peptidoglycan is synthesised at the division site, the old peptidoglycan must be hydrolysed for proper constriction and daughter cell separation to occur (Attaibi & den Blaauwen, 2022). Without these amidases, cells cannot properly separate, as exhibited by triple amidase mutants ( $\Delta amiabc$ ) in *E. coli* which show a long chained phenotype, and this phenotype is copied if their regulators, EnvC and NlpD are removed together (Heidrich et al., 2001; Priyadarshini et al., 2007; Uehara et al., 2009). In an apparently redundant amidase system, the three amidases do still present differences in terms of sequence, structure, localisation, regulation and potentially function.

#### 1.4.2.1 Localisation of *E. coli* cell-division associated amidases

During cell division *E. coli* amidases are directed to the periplasm of the gram-negative bacteria (Bernhardt & de Boer, 2003; Möll et al., 2014; Yakhnina et al., 2015). Beginning in the cytoplasm, the three amidases appear to transfer into the periplasm by different molecular systems. AmiA and AmiC are suggested to use the Tat system to transport folded AmiA and AmiC into the periplasm due to Tat-targeting motifs in their signal sequence and GFP fusions appear to remain in the cytoplasm when the Tat system is removed (Bernhardt & de Boer, 2003). Interestingly, AmiB lacks a Tat-targeting motif in the signal sequence and does appear to rescue the chaining phenotype of Tat<sup>-</sup> cells, suggesting that AmiB may use the Sec system instead to reach the periplasm (Bernhardt & de Boer, 2003), although Tat<sup>-</sup> cells still express all three amidases (including AmiB which does not appear to use this route), the chaining phenotype maybe caused by other issues in this pathway and/or limited AmiA and AmiC reaching the periplasm.

For cell division amidases to be effective, they localise to the division site to hydrolyse the septal peptidoglycan. Firstly, AmiC has been strongly suggested to localise to the septum in *E. coli* cells via GFP tagged amidase fusions with fluorescence microscopy (Bernhardt & de Boer, 2003). This GFP fusion consistently rescued *E. coli* cells lacking AmiA and AmiC (Bernhardt & de Boer, 2003). Although AmiB has not been directly shown to localise to the septum in *E. coli*, it is generally assumed to as other AmiB proteins in *Pseudomonas aeruginosa* and *Vibrio cholerae* have been clearly shown that the equivalent AmiB localises to the setpum (via fluorescence microscopy) and is required for cell division in these systems (Möll et al., 2014; Yakhnina et al., 2015). Interestingly, *E. coli* AmiA localisation is more conflicting. Again using fluorescence microscopy, AmiA does not solely localise to the septum but is reported to distribute throughout the periplasm (Bernhardt & de Boer, 2003), however on closer inspection of the microscopy , it appears that AmiA has a mild preference for the septum while still present throughout the periplasm although this is difficult to support without further evidence. AmiA is the smallest of the three *E. coli* type 3 amidases, lacking a targeting domain AmiB and AmiC have, which could theoretically contribute to the difference in localisation.

#### 1.4.2.2 Structure of *E. coli* cell-division associated amidases

##### AmiC

There is currently only one type 3 *E. coli* amidase solved structure, AmiC (**Figure 17**) (Rocaboy et al., 2013). The 2.5 angstrom structure highlights two main domains, the AMIN and the catalytic domains, connected by a linker. The AMIN domain is a superimposable four-stranded anti-parallel  $\beta$ -sheets with conserved outer surfaces (Rocaboy et al., 2013). The  $\beta$ -sheets are closed on one side by a small  $\alpha$  helix (Rocaboy et al., 2013). This is the first report of an AMIN domain fold. The function of this AMIN domain is reported to be essential for the proper localisation of AmiC to the active site (Bernhardt & de Boer, 2003) and has been shown via pull-down experiments that the domain binds to peptidoglycan (Rocaboy et al., 2013).

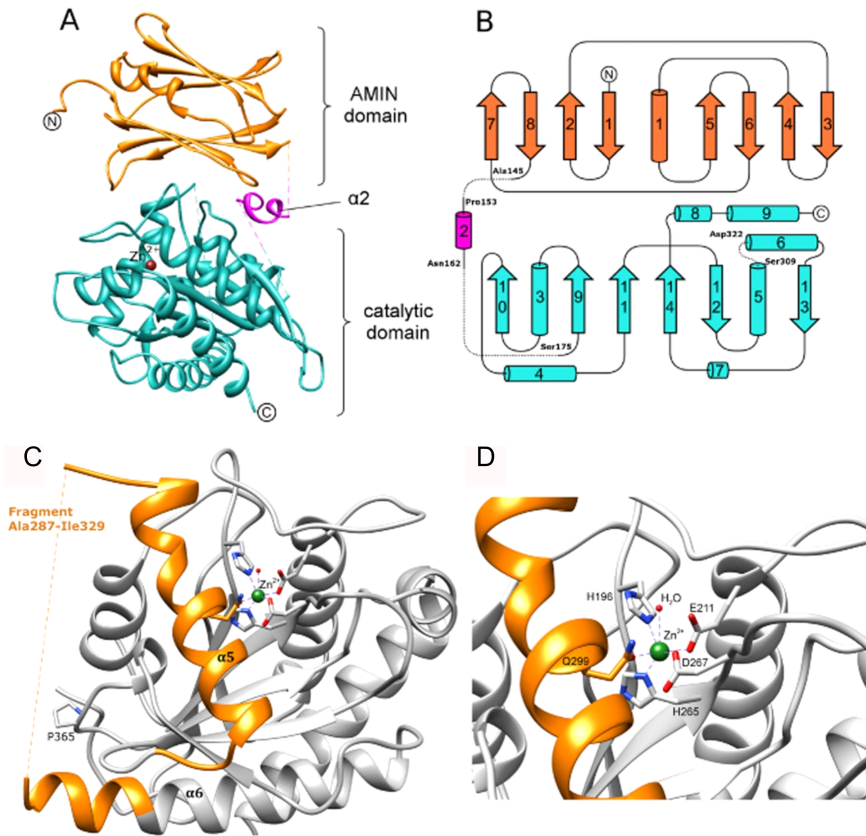


**Figure 17: Crystal structure and catalytic domain of AmiC.** (A) The AMIN domain, the linker and the catalytic domain are respectively shown in orange, violet and cyan. (B) Topology of AmiC. Stretches of missing residues are represented as dashed lines. Residues preceding and following the missing segments are labelled. (C) Cartoon representation of the catalytic domain. The fragment removed to produce the mutant  $\text{AmiC}\Delta\text{H5}$  (see in text) is depicted in orange. The catalytic zinc is shown in green. (D) Close-up on the catalytic site of AmiC. The catalytic zinc and the obstructing helix  $\alpha 5$  are shown in green and orange respectively. The chelating residues are represented as sticks (nitrogens and oxygens are shown in blue and red respectively). Figure and captions sourced from (Rocaboy et al., 2013)

The catalytic domain (**Figure 17**) is overall conserved in comparison with other amidase type 3 family proteins (Korndörfer et al., 2006; Mayer et al., 2011; D. C. Yang et al., 2011). The fold contains a strongly twisted 6-stranded  $\beta$ -sheet flanked by six  $\alpha$  helices (Rocaboy et al., 2013). There are four residues essential for catalytic activity which are stringently conserved; His196, His265 and Glu211 all chelate the key catalytic  $\text{Zn}^{2+}$  ion (Rocaboy et al., 2013). Lastly there is Glu373 which is suggested to be important in the proton transfer during catalysis in metalloproteases (Rocaboy et al., 2013). There is an  $\alpha$  helix which appears to obstruct the active site in AmiC which aligns with an AmiB structure in *Bartonella henselae*, where another inhibiting helix blocks the active site (D. C. Yang et al., 2012b). This is in contrast however to other amidase type 3 proteins which lack this regulatory helix such as the amidase from *Neisseria meningitidis* (Zhang et al., 2008). In this AmiC structure however, there is a missing region between helices 5 and 6 which is reported to be motile, thus resulting in reduced electron density in model building. This region could be important in the activation mechanism required for the movement of the blocking helix from the active site.

Unsurprisingly, the regulator to AmiC, NlpD was shown to directly interact (although only *in vitro*), believed to lead into a conformational change in AmiC to move the blocking helix away from the active site (Rocaboy et al., 2013). To support this claim, this paper removed the blocking helix and found this AmiC variant was consecutively active regardless of NlpD presence (Rocaboy et al., 2013). This structure paints a picture of an amidase with a regulatory system based on a self-inhibition mechanism controlled by another protein regulator which alters the amidase structural conformation, altering active site availability.

## AmiB

Currently there is no *E. coli* structure of the type 3 amidase, AmiB, there is however a solved catalytic domain of an AmiB orthologue from *Bartonella henselae* (**Figure 18**) (D. C. Yang et al., 2012b). Unsurprisingly, the overall fold of this amidase is very similar to that of the *E. coli* AmiC (Rocaboy et al., 2013) and another type 3 amidase in *Bacillus(Paenibacillus) polymyxa var.colistinus* (Yamane et al., 2001). There is again a clear regulatory  $\alpha$  helix which blocks the active site suggesting a conserved regulatory system across type 3 amidases (D. C. Yang et al., 2012b). The zinc binding residues which include; H188, E203, H257, D259 and E290 all appear conserved when compared to the *E. coli* AmiB sequence and *E. coli* AmiC structure (Rocaboy et al., 2013; D. C. Yang et al., 2012b). This model however does lack the additional assumed targeting domain present in this AmiB orthologue and in *E. coli* AmiB which this domain is still largely an unknown in terms of structure and function. The connecting residues between helices 3 and 4 in this structure were also missing, similar to that of the *E. coli* AmiC structure (Rocaboy et al., 2013; D. C. Yang et al., 2012b) perhaps due to high residue mobility or clipped to aid in crystallisation.

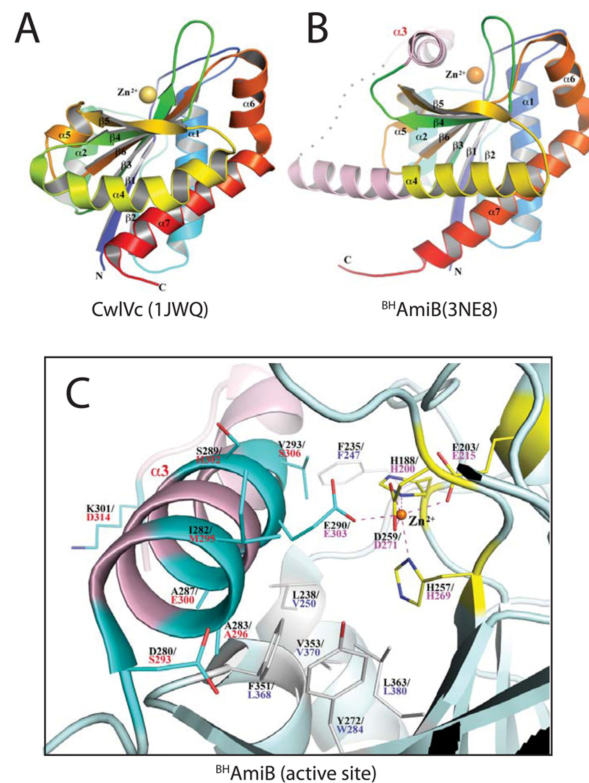


**Figure 18: Crystal structure of *Bartonella henselae* AmiB.** (A and B) Shown are rainbow-coloured cartoon diagrams of the CwlVc (A) and <sup>BH</sup>AmiB (B) structures with the N-termini in blue and the C-termini in red. The catalytic Zn<sup>2+</sup> ion is drawn as a sphere. All secondary structures are labelled. In numbering  $\alpha$ -helices,  $\alpha 3$  is omitted from the numbering of CwlVc so that all common elements are numbered identically for CwlVc and <sup>BH</sup>AmiB. The regulatory region unique to cell separation amidases is coloured pink in the <sup>BH</sup>AmiB structure with the structurally disordered loop region (E303-T308) represented by a dotted line. The unique  $\alpha 3$  helix is labelled in pink. (C) Close-up view of the <sup>BH</sup>AmiB active site and regulatory helix. All residues are drawn in stick format and the Zn<sup>2+</sup> ion is represented as an orange sphere. The Zn<sup>2+</sup> ion is co-ordinated by H188, E203, H257, D259 (bidentate) and E290 with their carbon atoms drawn in yellow. Residue numbers for *E. coli* AmiB are provided in red underneath those for <sup>BH</sup>AmiB. Positions in the structure corresponding to amino acid substitutions in the lytic AmiB variants are drawn with their carbon atoms in cyan. The residue corresponding to Q333 of *E. coli* AmiB (T315 of <sup>BH</sup>AmiB) is located in the N-terminal region of the  $\alpha 4$  helix and they are out of view in this figure. Hydrophobic residues on the floor of binding cleft are also displayed in white. Figure and captions sourced (D. C. Yang et al., 2012b).

As another support of the regulatory model in the type 3 amidases, lytic *E. coli* AmiB mutants were created of which the mutants which affected the predicted regulatory helix in the *E. coli* AmiB caused higher levels of cell lysis if over-expressed in *E. coli* cells. This suggested that the predicted regulatory helix prevents AmiB from performing its function and hydrolysing peptidoglycan uncontrollably. Interestingly as a continuation of the lytic experiment, *E. coli* AmiA mutants were created in the equivalent regulatory helix which caused lysis in wild-type cells when again over-expressed (D. C. Yang et al., 2012b), further evidencing potential conservation of self-regulation across all three division associated amidases in *E.coli*, and potentially other bacterial species..

## AmiA

Lastly, the *E. coli* type 3 amidase AmiA is also a mystery in terms of structural information. There is a structure of an AmiA from *Staphylococcus aureus* bound to a peptidoglycan-derived ligand (Büttner et al., 2014) however this is a type 2 amidase, more closely resembling AmiD from *E. coli* (Kerff et al., 2010).

From alpha-fold and sequence analysis, the overall fold appears similar to that of other type 3 amidase catalytic domains, including a blocking helix covering a potential active site (Jumper et al., 2021) with a potentially flexible helix region (of unknown function) unresolved in the AmiC structure (Rocaboy et al., 2013). The alpha-fold model prediction (**Figure 19A**) contains high confidence in the main amidase fold and internal residues however the blocking helix and deemed mobile helix have lower confidence indicating potential unique residues for a specific function present in AmiA. Unsurprisingly, alpha-fold struggles to predict the signal peptide and both termini of the structure as these regions are usually not modelled in crystallography. AmiA was aligned and overlaid with the *E. coli* AmiC structure (Rocaboy et al., 2013) to place an assumed zinc in the predicted active site covered by the blocking helix, although the model is not able to determine any zinc-binding active site residues accurately (**Figure 19B**). The *E. coli* AmiA does however lack the AMIN/targeting domain of AmiB and AmiC and only presents a catalytic domain which asks the question on the difference of AmiA localisation, function and regulation.

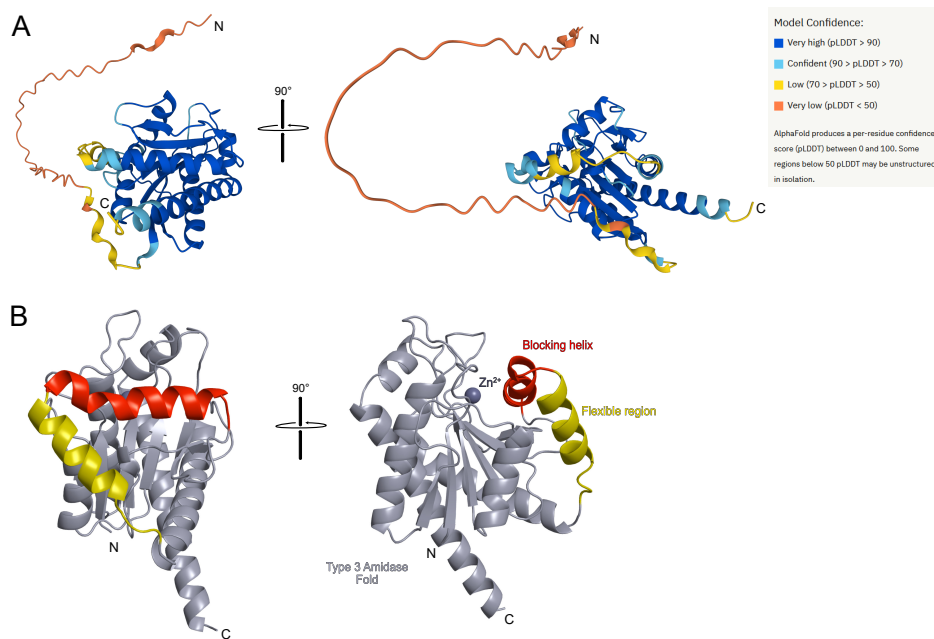


**Figure 19: Alphafold prediction of *E. coli* AmiA.** (A) Alphafold output of *E. coli* AmiA rotated along a vertical axis by 90 degrees with confidence grading legend from Alphafold. (B) Feature highlights of *E. coli* AmiA lacking the signal sequence for clarity rotated along a vertical axis by 90 degrees. From an alignment with *E. coli* AmiC 4BIN (Rocaboy et al., 2013), a zinc ion was added to the AmiA model with a prediction to be a zinc co-factor based amidase, like AmiC. A potential active site blocking helix was highlighted red with a similar flexible helix (which unsolved in *E. coli* AmiC 4BIN (Rocaboy et al., 2013)) shown in yellow.

### 1.4.2.3 Regulation and function of *E. coli* cell-division associated amidases

These *E. coli* cell-division associated type 3 amidases are responsible for the hydrolysis of septal peptidoglycan during cell division (Levin & Janakiraman, 2021). As indicated by the *E. coli* AmiC structure (and AmiC constitutively active construct), without a form of self-regulation, the amidases would be uncontrollably active, causing peptidoglycan damage to the cell (Rocaboy et al., 2013). It is known that the non-active LytM proteins EnvC and NlpD regulate AmiA/AmiB and AmiC respectively (Levin & Janakiraman, 2021; Vermassen et al., 2019). The reasons for different amidase regulators and three different amidases in *E. coli* nor the complete regulatory picture is however not well understood.

At the start of this PhD, in terms of EnvC regulating AmiA/AmiB activity, while it is known the key residues in the LytM domain of EnvC which interact with AmiA/AmiB to during activation, it is however the structural mechanism by which FtsEX interacts with EnvC which in turn interacts with AmiA/AmiB is unknown. To add to the complexity of the system, another regulator ActS has been shown to also contain an inactive LytM domain and activate AmiA, AmiB and AmiC with a preference to AmiC, perhaps only under lipopolysaccharide depletion stress although this requires further data to explore the direct protein-protein interactions (Gurnani Serrano et al., 2021).

NlpD is a further mystery with limited structural information available with only a potential interacting partner or activator, YraP identified (Tsang et al., 2017). NlpD is known to be anchored to the outer membrane suggesting AmiC acts at a different location in the periplasmic AmiA/AmiB EnvC FtsEX system which is localised to the inner membrane (Tsang et al., 2017). The variation in periplasmic positioning of amidase regulators may suggest subtle differences in AmiC functions to that of AmiA/AmiB in terms of temporal and peptidoglycan cleaving enzyme functions.

Although it has not been widely discussed, the roles of each of the three cell-division *E. coli* amidases while all work to conclude a successful daughter cell separation, the difference in localisation, periplasmic transport, varying extra domains (aside from the conserved catalytic domain) and the presence of different regulators. Answers to these unknown factors have been touched on with a potential staggered activity of AmiA/B/C towards the end cell division, where AmiC arrives later than EnvC suggesting a late acting AmiC is key for the final con-

striction and daughter cell separation, although AmiA and AmiB will perform the same function if AmiC is mutated out (Priyadarshini et al., 2007). The EnvC:AmiA/AmiB system is therefore suggested to initiate septal peptidoglycan hydrolysis and NlpD:AmiC concludes the process (Priyadarshini et al., 2007) although further evidence is required.

#### **1.4.2.4 Other amidase-regulator systems**

Recently, as a potential model for other type 3 amidases, there has been the first characterised type 3 amidase structurally solved bound to its respective regulator, CwlD:GerS complex from *Clostridioides difficile* (**Figure 20**) (Alves Feliciano et al., 2021). This complex is key to hydrolyse muramic- $\delta$ -lactam, a key component in the protective layer called the cortex in spore forming bacteria (Alves Feliciano et al., 2021).

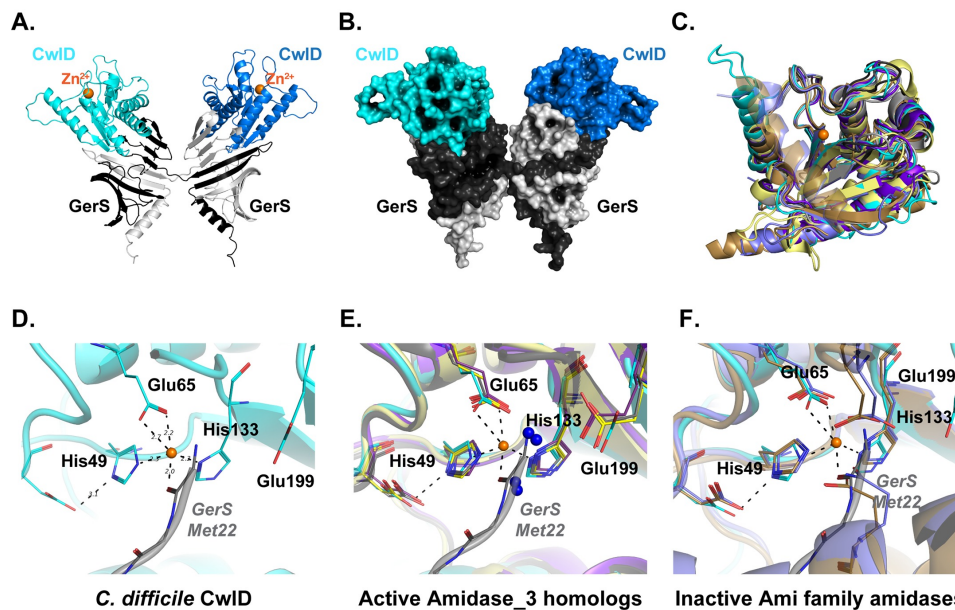


**Figure 20: Structure of the CwID:GerS complex.** (A) Shown is the cartoon representation of the CwID:GerS complex within the crystal with CwID in blue tones and GerS in grey. The crystallographic asymmetric unit contains a single protomer of each with the 2 GerS/2 CwID assembly formed by domain swapping of the GerS monomers. (B) The assembly is shown in space filling representation. (C) Least squares superposition of CwID (cyan throughout) and its homologs performed using Superpose (Winn et al., 2011) in CCP4. (D) Close-up view of the metal binding site for CwID with GerS from a fortuitous crystal packing (grey) providing coordination of the ion. (E) CwID homolog structures (CwID *Paenibacillus polymyxa* PDBID 1JWQ, unpublished; *C. difficile* CD2761 amidase 3 family member, 4RN7, unpublished; *Nostoc punctiforme*, AmiC2, 5EMI (Büttner et al., 2016); and *C. difficile* Cwp6, 5J72 (Usenik et al., 2017)) in the active form have the Zn<sup>2+</sup> atom accessible to the solvent. They also have water molecules serving as 1–2 ligands (blue spheres), one of which is coordinated by a conserved glutamate. (F) CwID homolog structures (*Bartonella henselae* AmiB PDBID 3NE8 (D. C. Yang et al., 2011) and *E. coli* AmiC 4BIN (Rocaboy et al., 2013)) in the inactive forms have residues from their respective inhibitory helices providing Zn<sup>2+</sup> ligands. Figure and caption sourced from (Alves Feliciano et al., 2021)

The solved structure reports a GerS homodimer bound to two CwID monomers which produces exposed active sites in CwID. While CwID appears to contain similar catalytic domain folds to the type 3 amidases already solved, there are some curious differences. Interestingly, while CwID can bind a  $Zn^{2+}$  co-factor, it can only stably do so while bound to GerS, otherwise the binding is unstable (Alves Feliciano et al., 2021). Curiously, the CwID amidase present in *Bacillus subtilis* is active without a regulator (Gilmore et al., 2004).

As a metallo-enzyme, without the zinc ion, CwID is inactive, therefore the stabilisation of the zinc ion binding is the self-regulatory mechanism of which is system uses (Alves Feliciano et al., 2021). Unsurprisingly, the active site where zinc binding residues are present, the residues are again conserved from CwID (His 49, Glu65, His133, Glu199) when compared to other type 3 amidases like AmiC (Alves Feliciano et al., 2021; Rocaboy et al., 2013).

This zinc stabilisation mechanism is an exciting contrast to the *E. coli* amidase self-inhibition blocking helix method suggesting different bacterial systems adapt to use different structural methods to regulate essential processes in their life cycle.

## 1.5 Project Aims and Objectives

The aim of this PhD thesis is to investigate the structural regulation of periplasmic type 3 amidases involved in bacterial cell division in *E. coli*.

### Objectives:

#### 1) To understand the interactions of EnvC:

- *What is the structural basis of the FtsEX:EnvC interaction?*
- *How is EnvC structurally regulated?*
- *Are there any other potential regulators, targets or competitors of EnvC?*

#### 2) Characterise the effect of divisome knockouts:

- *How essential are specific divisome components to cell growth, outer membrane stability, permeability and cell morphology?*
- *Characterise extent of the redundancy in the amidase system in bacterial cell division*

#### 3) To solve the structure of the *E. coli* amidase, AmiA:

- *How is AmiA activity regulated?*
- *What are the key residues required for interactions?*
- *What are the key residues in the active site?*

#### 4) To understand how AmiA is functionally regulated:

- *What are the key residues involved in EnvC interaction and amidase activity?*
- *How does AmiA interact with its regulator, EnvC?*
- *How does EnvC binding induce activation in AmiA?*

## **2 Materials and Methods**

### **2.1 Chemical and reagent suppliers**

All reagents used were obtained from the following suppliers if not stated otherwise; New England Biolabs (USA), Sigma-Aldrich (USA), Integrated DNA technologies (USA), Invitrogen (USA), Thermofisher scientific (USA), Fisher Scientific (UK), Merck (Germany), Promega (USA), Cleaver scientific (UK), VWR (USA), Sartorius stedim biotech (Germany), Nanotemper Technologies (Germany), Biotium (USA), GE Healthcare (USA), Roche (Switzerland). All chemical reagents used were analytical grade.

### **2.2 Buffer solutions**

All buffer solutions were prepared using purified water from a water purifier system. All buffers involved in microbiological work were either autoclaved or filtered using a 0.2  $\mu\text{m}$  syringe filter.

### **2.3 Bacterial Growth and manipulation**

#### **2.3.1 Bacterial growth media**

Luria-Bertani (LB) liquid medium (Bertani, 1951) was prepared by dissolving 10 g tryptone, 10 g sodium chloride, 5 g yeast extract in a final volume of one litre and autoclaved. The appropriate antibiotic was then added prior to any bacterial inoculation.

2YT liquid medium was prepared by dissolving 16 g tryptone, 5 g sodium chloride, 10 g yeast extract in a final volume of one litre and autoclaved. The appropriate antibiotic was then added prior to any bacterial inoculation.

Lbon50 medium was prepared by dissolving 10 g tryptone and 5 g yeast extract (Standard LB lacking NaCl) then 2-fold diluted with water in a final volume of one litre and autoclaved. The appropriate antibiotic was then added prior to any

bacterial inoculation.

LB agar plates were prepared by autoclaving LB media supplemented with 20 g of agar per litre. When cooled to 50°C, the appropriate antibiotics or compounds were added, and plates poured into sterile petri dishes and stored at 4°C for later use.

### **2.3.2 Bacterial strains**

The bacterial strains used in this report are presented in **Table 2**. DH5 alpha cells were used for all cloning and C43 (DE3) *E. coli* cells were used for all protein expression. As a base strain, all knockout mutational studies, parental strain BW25113 was used as a control. For all bacterial two-hybrid assays, the BTH101 strain was utilised.

**Table 2: Cell lines used in this thesis**

<b>Name</b>	<b>Species</b>	<b>Genotype</b>	<b>Notes</b>	<b>Figure</b>	<b>Source</b>
5-alpha Competent DH5 $\alpha$	<i>E. coli</i>	<i>fhuA2</i> $\Delta$ ( <i>argF-lacZ</i> ) <i>U169</i> <i>phoA</i> <i>glnV44</i> <i><math>\phi</math>80</i> $\Delta$ ( <i>lacZ</i> ) <i>M15</i> <i>gyrA96</i> <i>recA1</i> <i>relA1</i> <i>endA1</i> <i>thi-1</i> <i>hsdR17</i>	Exclusively used for cloning	-	New England Biolabs
C43 (DE3)	<i>E. coli</i>	<i>F</i> – <i>ompT</i> <i>hsdSB</i> ( <i>rB-</i> <i>mB-</i> ) <i>gal dcm</i> ( <i>DE3</i> )	Used for expression and purification of proteins	<b>Figures 39, 50, 52 and 53</b>	Sigma-Aldrich
BTH101	<i>E. coli</i>	<i>F-</i> , <i>cya-99</i> , <i>araD139</i> , <i>galE15</i> , <i>galK16</i> , <i>rpsL1</i> ( <i>Str r</i> ), <i>hsdR2</i> , <i>mcrA1</i> , <i>mcrB1</i> .	Used for all Bacterial two-hybrid experiments	<b>Figures 23, 24, 26, 31 and 49</b>	Euromedex
BW25113	<i>E. coli</i>	$\Delta$ ( <i>araD-araB</i> ) <i>567</i> $\Delta$ <i>lacZ4787</i> (:: <i>rrnB-3</i> ) $\lambda$ - <i>rph-1</i> $\Delta$ ( <i>rhaD-rhaB</i> ) <i>568</i> <i>hsdR514</i>	Used for as a control strain for all divisome knockout experiments	<b>Figures 33, 34 and 36, Section 4.3.3, and ??</b>	(Baba et al., 2006; Datsenko & Wanner, 2000)
JW2428-1	<i>E. coli</i>	$\Delta$ ( <i>araD-araB</i> ) <i>567</i> $\Delta$ <i>lacZ4787</i> (:: <i>rrnB-3</i> ) $\lambda$ - $\Delta$ <i>amiA764</i> :: <i>kan</i> <i>rph-1</i> $\Delta$ ( <i>rhaD-rhaB</i> ) <i>568</i> <i>hsdR514</i>	Used as a strain lacking AmiA for complementation experiments	<b>Figures 33, 34 and 36, Section 4.3.3, and ??</b>	(Baba et al., 2006; Datsenko & Wanner, 2000)

<b>Name</b>	<b>Species</b>	<b>Genotype</b>	<b>Notes</b>	<b>Figure</b>	<b>Source</b>
JW4127-1	<i>E. coli</i>	$\Delta(\text{araD-araB})567$ $\Delta\text{lacZ4787}>::\text{rrnB-3}$ $\lambda$ - <i>rph-1</i> $\Delta(\text{rhaD-rhaB})568$ $\Delta\text{amiB790}>::\text{kan}$ <i>hsdR514</i>	Used as a strain lacking AmiB for complementation experiments	<b>Figures 33, 34 and 36, Section 4.3.3, and ??</b>	(Baba et al., 2006; Datsenko & Wanner, 2000)
JW5449-1	<i>E. coli</i>	$\Delta(\text{araD-araB})567$ $\Delta\text{lacZ4787}>::\text{rrnB-3}$ $\lambda$ - $\Delta\text{amiC742}>::\text{kan}$ <i>rph-1</i> $\Delta(\text{rhaD-rhaB})568$ <i>hsdR514</i>	Used as a strain lacking AmiC for complementation experiments	<b>Figures 33, 34 and 36, Section 4.3.3, and ??</b>	(Baba et al., 2006; Datsenko & Wanner, 2000)
JW5646-3	<i>E. coli</i>	$\Delta(\text{araD-araB})567$ $\Delta\text{lacZ4787}>::\text{rrnB-3}$ $\lambda$ - $\Delta\text{envC725}>::\text{kan}$ <i>rph-1</i> $\Delta(\text{rhaD-rhaB})568$ <i>hsdR514</i>	Used as a strain lacking EnvC for complementation experiments	<b>Figures 33, 34 and 36, Section 4.3.3, and ??</b>	(Baba et al., 2006; Datsenko & Wanner, 2000)
JW2712-2	<i>E. coli</i>	$\Delta(\text{araD-araB})567$ $\Delta\text{lacZ4787}>::\text{rrnB-3}$ $\lambda$ - $\Delta\text{nlpD747}>::\text{kan}$ <i>rph-1</i> $\Delta(\text{rhaD-rhaB})568$ <i>hsdR514</i>	Used as a strain lacking NlpD for complementation experiments	<b>Figures 33, 34 and 36, Section 4.3.3, and ??</b>	(Baba et al., 2006; Datsenko & Wanner, 2000)
JC7	<i>E. coli</i>	$\Delta(\text{araD-araB})567$ $\Delta\text{lacZ4787}>::\text{rrnB-3}$ $\lambda$ - $\Delta\text{FtsEX}>::\text{kan}$ <i>rph-1</i> $\Delta(\text{rhaD-rhaB})568$ <i>hsdR514</i>	Used as a strain lacking FtsEX for complementation experiments	<b>Figures 33, 34 and 36, Section 4.3.3, and ??</b>	Dr Jonathan Cook, this project

<b>Name</b>	<b>Species</b>	<b>Genotype</b>	<b>Notes</b>	<b>Figure</b>	<b>Source</b>
TB1	<i>E. coli</i>	$\Delta(araD-araB)567$ $\Delta lacZ4787(::rrnB-3)$ $\lambda$ - $\Delta amiA764$ <i>rph-1</i> $\Delta(rhaD-rhaB)568$ $\Delta amiB790::kan$ <i>hsdR514</i>	Used as a strain lacking AmiA with no kanomycin cassette during the creation of the double amidase knockout ( $\Delta AmiAB$ )	<b>Figure 32</b>	Tyler Baverstock, this project and (Baba et al., 2006; Datsenko & Wanner, 2000)
TB2	<i>E. coli</i>	$\Delta(araD-araB)567$ $\Delta lacZ4787(::rrnB-3)$ $\lambda$ - $\Delta amiA764::kan$ <i>rph-1</i> $\Delta(rhaD-rhaB)568$ $\Delta amiB790::kan$ <i>hsdR514</i>	Used as a strain lacking AmiA and AmiB for complementation experiments	<b>Figures 32 to 34 and 36, Section 4.3.3, and ??</b>	Tyler Baverstock, this project and (Baba et al., 2006; Datsenko & Wanner, 2000)
TB3	<i>E. coli</i>	$\Delta(araD-araB)567$ $\Delta lacZ4787(::rrnB-3)$ $\lambda$ - $\Delta amiA764$ <i>rph-1</i> $\Delta(rhaD-rhaB)568$ $\Delta amiB790$ <i>hsdR514</i>	Used as a strain lacking AmiA and AmiB with no kanomycin cassette during the creation of the triple amidase knockout ( $\Delta AmiABC$ )	<b>Figure 32</b>	Tyler Baverstock, this project and (Baba et al., 2006; Datsenko & Wanner, 2000)

<b>Name</b>	<b>Species</b>	<b>Genotype</b>	<b>Notes</b>	<b>Figure</b>	<b>Source</b>
TB4	<i>E. coli</i>	$\Delta(araD-araB)567$ $\Delta lacZ4787(::rrnB-3)$ $\lambda$ - $\Delta amiC742::kan$ $\Delta amiA764::kan$ <i>rph-1</i> $\Delta(rhaD-rhaB)568$ $\Delta amiB790::kan$ <i>hsdR514</i>	Used as a strain lacking AmiA, AmiB and AmiC for complementation experiments	<b>Figures 32 to 34 and 36, Section 4.3.3, and ??</b>	Tyler Baverstock, this project and (Baba et al., 2006; Datsenko & Wanner, 2000)
End of Table					

### **2.3.3 Bacterial vectors**

All plasmid and mutation constructs used or created in this project are listed in **Table 5** (appendix).

### **2.3.4 Preparation of *E. coli* competent cells for DNA transformation**

A method adapted from (Hanahan, 1983) was used. A 5 ml overnight culture of a single colony was inoculated and incubated overnight at 37 °C, shaking at 180 RPM. This was used to inoculate a larger 50 ml culture in a 1 L flask and incubated at 37 °C, shaking at 180 RPM to OD<sub>600</sub> 0.48-0.5. Cells were cooled on ice for 10 minutes and subsequently centrifuged at 4, 500 x g for 15 minutes at 4 °C. Cell pellets were gently re-suspended in a third of the final growth volume in cold (4 °C) RF1 buffer (100 mM RbCl, 50 mM MnCl<sub>2</sub>·4H<sub>2</sub>O, 30 mM CH<sub>3</sub>COOK, 10 mM CaCl<sub>2</sub>, 15 % glycerol, pH 5.8) and stored on ice for 15 minutes. Cells were again pelleted at 4, 500 x g for 15 minutes at 4 °C. Final re-suspension in 1 in 12.5 growth volume in cold (4 °C) RF1 buffer (10 mM MOPS, 10 mM RbCl, 75 mM CaCl<sub>2</sub>, 15 % glycerol, pH 5.8). Competent cells were transferred into 100-200 µl aliquots in dry-ice chilled Eppendorf tubes and frozen at -80°C for later use. Competency checked using the transformation with a standard plasmid such as pET21a.

### **2.3.5 Bacterial heat shock transformation**

The transformation protocol was derived from the New England Biolabs protocol (Biolabs, 2022). Add 1-2 ng of plasmid DNA to 50 µl of thawed cryo-stored chemically competent cells. Cells were incubated on ice for 45 minutes, heat shocked at 42 °C for 40 seconds then cooled on ice for 5 minutes. For recovery, 450 µl of LB media was added and cells were incubated for 1 hour at 37 °C with shaking at 180 RPM. Transformed cells were plated on the appropriate selection agar plate antibiotic and incubated at 37 °C overnight.

## **2.4 DNA manipulation techniques**

### **2.4.1 Primer and plasmid design for cloning**

Primer oligonucleotides were designed based on available restriction cloning sites and using the Benchling software (Benchling, 2022). Primers were designed to be at least 20 nucleotide of complementary sequence with the desired restriction site and an extra five nucleotides adjacent to the restriction site for enzyme binding. All primers were ordered from either Sigma/Merck or Integrated DNA technologies. All whole plasmid synthesis was performed and purchased from Genetech. All cloned or synthesised constructs can be found in **Table 5** (appendix).

### **2.4.2 Primer and plasmid design for mutagenesis**

Mutagenesis primer oligonucleotides were designed using the QuikChange Primer Design online software available from Aligent . All primers were ordered from either Sigma/Merck or Integrated DNA technologies. All constructs containing mutated genes are listed in **Table 5** (appendix).

### **2.4.3 Polymerase Chain Reaction**

Polymerase Chain Reactions (PCR) were performed with temperatures and conditions optimised using the online NEB Tm calculator tool (NEB). PCR reaction mixtures followed the manufacturers protocol for Q5 polymerase (NEB).

### **2.4.4 Mutagenesis Polymerase Chain Reaction**

Mutagenesis PCRs were performed on with temperatures and conditions sourced from the Aligent QuikChange protocol (Aligent). PCR reaction mixtures followed the manufacturers protocol for pfu DNA polymerase (Aligent).

#### **2.4.5 Agarose gel electrophoresis**

Agarose gels were made between 1-2 % and prepared with 1 x TAE buffer (1 mM EDTA disodium salt, 40 mM Tris, 20 mM acetic acid) and Gel Red (Biotium). DNA samples were prepared with 6 x DNA loading buffer (NEB) and run for 1 hour at 120 V for optimal band separation. Gels were imaged using a UV transilluminator.

#### **2.4.6 Purification of PCR products**

All PCR products were purified using Monarch DNA Gel Extraction Kit (NEB) following the manufacturers protocol.

#### **2.4.7 Restriction Cloning**

All cloning was performed using the traditional restriction cloning method adapted from NEB. Alterations include extending all restriction digests to a minimum of 2 hours up to 3 hours at 37 °C. In the ligation of cut vector and insert, all incubations were performed at room temperature for minimum of 3 hours, up to overnight.

#### **2.4.8 Preparation of plasmid DNA**

All preparation of bacterial plasmid DNA was performed using a QIAprep Spin Miniprep Kit (QIAGEN) following the manufacturer's protocol.

#### **2.4.9 Quantifying DNA**

All DNA samples were quantified using a Multiskan SkyHigh Microplate reader  $\mu$ drop plate (Thermofisher) by measuring the absorbance at 260 and 280 nm. DNA purity was calculated using the ratio of absorbance between 260/280 nm. Sufficient purity DNA has a ratio between 1.6 to 2.0.

#### 2.4.10 Sequencing plasmid constructs

To validate constructs, plasmid or fragment DNA was checked using Sanger sequencing. Sequencing was performed by (Genewiz) and samples prepared as per the manufacturer's protocols.

#### 2.4.11 Generation of amidase genomic knockouts

The single single knockout amidase strains (JW2428-1 and JW4127-1) lacking *amiA* or *amiB* respectively were sourced from the keio collection (**Table 2**) which contain a kanamycin cassette in place in the chromosome of the gene encoding the amidase. These strains are derivatives of the parent strain *E. coli* BW25113 and their genotypes can be found in **Table 2**. To create TB2 (**Table 2**), the *E. coli* strain lacking both *amiA* or *amiB* in the chromosome, first JW2428-1 had the kanamycin cassette removed via FLP-FRT recombination (creating TB1, **Table 2**) and then using lambda red recombination (both processes using Gene Bridges gene deletion kit), to add a kanamycin cassette into the *amib* gene. For the triple amidase knockout strain (TB4, **Table 2**,  $\Delta amiabc$ ), the same process occurred with the TB2 strain having the kanamycin cassette removed via FLP-FRT recombination from the *amib* site (creating TB3, **Table 2**) and the using lambda red recombination, to add a kanamycin cassette into the *amib* gene, creating TB4 (**Table 2**). All four strains were checked for kanamycin resistance and verified using PCR amplification and Sanger sequencing (Genewiz) of the three gene locations using primers on either side of each genetic locus. All three amidase sites were checked in all four of the strains created to ensure no misguided or deletions occurred.

## 2.5 Microbiology Assays

### 2.5.1 Bacterial two-hybrid

The Euromedex BACTH system kit (Euromedex, 2022) was used for all Bacterial two-hybrid experiments to test *in vivo* protein-protein interactions. All stock plasmids and created plasmids are presented in **Table 5** (appendix). A modified version of the BACTH system kit was used.

As a brief explanation of the experimental system, the kit uses the interaction-mediated reconstitution of the catalytic domain adenylate cyclase (CyaA) from *Bordetella pertussis*. It exploits that complementary fragments T25 (first 224 amino acids of CyaA) and T18 (amino acids 225-399 of CyaA) are inactive when physically separated. When heterodimerisation occurs between the fragments occurs, causes cyclic AMP synthesis to occur. The cyclic AMP binds to catabolite activator protein, CAP which as a complex, cAMP/CAP activates gene expression for a reporter gene, such as the *lac* operon for blue white colony screening using x-galactose. Therefore proteins can be fused to T25 and T18 fragments and this system can be used to detect protein-protein interactions with blue colonies showing interaction and white showing no detected interaction when grown on x-galactose agar plates. (Euromedex, 2022)

The gene of interest was cloned (using the methods outlined in **Section 2.4**) into the four stock T25 or T18 plasmids (**Table 5**, appendix) to result in either N- or C- terminus orientation T18 or T25 fragments added to the gene of interest. A co-transformation of all orientations T18 and T25 constructs to be tested into BTH101 cells was performed and plated on ampicillin (100  $\mu\text{g}/\text{ml}$ ) and kanamycin (50  $\mu\text{g}/\text{ml}$ ) plates then glycerol stocks created. To setup the bacterial two-hybrid plate, all transformed BTH101 cells with desired constructs are spotted onto ampicillin (100  $\mu\text{g}/\text{ml}$ ) and kanamycin (50  $\mu\text{g}/\text{ml}$ ) IPTG (0.5 mM) X-GAL (40  $\mu\text{g}/\text{ml}$ ) plates (in triplicate) and incubated at room temperature for 3 days. Plates are scanned after 2 and then 3 day incubation using a standard document scanner. Colour change of colonies is observed in comparison with positive (blue) and negative (white) controls.

### **2.5.2 Bacterial growth curves**

Bacteria to be tested had overnight cultures setup before the experiment. Three growth medias were prepared with the appropriate antibiotic; LB only, Lbon50 and LB supplemented with 0.1 % Sodium dodecyl sulfate. Overnight cultures were serially diluted from OD<sub>600</sub> 1 to 0.001. All three medias were added to a sterile 96 well plate in triplicate and the diluted cultures to the plate added by a dilution of 1 in 10, culture to media. The plate was incubated at 37°C with periodic shaking in a Multiskan Skyhigh Microplate Spectrophotometer (Thermofisher) with whole plate spectrophotometer readings at OD<sub>600</sub> every 15 minutes for 24 hours.

### **2.5.3 Cell wall stability spot plate assay**

Bacteria to be tested had day cultures setup on the day of the experiments. Three agar plates were prepared with the appropriate antibiotic; LB IPTG (1 mM), Lbon50 IPTG (1mM) and LB IPTG (1 mM) supplemented with 0.1 % Sodium dodecyl sulfate. Sterile 96-well plates were prepared with the appropriate antibiotics; LB IPTG (1 mM) or Lbon50 IPTG (1 mM). Day cultures were diluted from OD<sub>600</sub> 1 down to ten, 10-fold serial dilutions in the pre-prepared 96-well plates with the respective growth medias. Each dilution was spotted onto the three different agar plates in triplicate, left to dry and incubated overnight at 37°C. Plates were scanned and imaged by a flatbed scanner the next day.

### **2.5.4 Minimum inhibitory concentration**

Bacteria to be tested had day cultures setup on the day of the experiments. The growth media used was LB IPTG (1 mM) supplemented with AMP (50 µg/ml). Growth media was inoculated with a glycerol stock of the desired bacterial strain to be tested. This day culture was growth until the OD<sub>600</sub> was 1.0.

For the vancomycin MICs, vancomycin dissolved in DMSO (Thermofisher) was directly added to the growth media (containing 25 µg/ml Ampicillin and 1 mM IPTG) to 1024 µg/ml (as the highest concentration used in the experiment) and filter sterilised (2 µm filter). To maintain consistently across each set of repeats, a set of falcon tubes containing growth media (containing 25 µg/ml Ampicillin and

1 mM IPTG) was used to create a 2-fold serial dilution using a 20 ml glass pipette, from 1024  $\mu\text{g/ml}$  down to 1  $\mu\text{g/ml}$ . The vancomycin serial dilution was transferred by multi-channel pipette into sterile 96-well plates for 200  $\mu\text{l}$  in each well with a control well lacking vancomycin. The day cultures at  $\text{OD}_{600} = 1$  were serially diluted in another sterile 96-well plate down to  $\text{OD}_{600} = 0.001$ . Finally 5  $\mu\text{l}$  of the diluted bacterial culture was added to each well in the 96-well plates containing vancomycin. Each plate contain 8 technical repeats.

For the SDS MICs, SDS was dissolved directly into the growth media (containing 25  $\mu\text{g/ml}$  Ampicillin and 1 mM IPTG) to 1024  $\mu\text{g/ml}$  (as the highest concentration used in the experiment) to 5.12 % w/v and filter sterilised (2  $\mu\text{m}$  filter). To maintain consistently across each set of repeats, a set of falcon tubes containing growth media (containing 25  $\mu\text{g/ml}$  Ampicillin and 1 mM IPTG) was used to create a 2-fold serial dilution using a 20 ml glass pipette, from 5.12 % w/v down to 0.05 % w/v. The SDS serial dilution was transferred by multi-channel pipette into sterile 96-well plates for 200  $\mu\text{l}$  in each well with a control well lacking SDS. The day cultures at  $\text{OD}_{600} = 1$  were serially diluted in another sterile 96-well plate down to  $\text{OD}_{600} = 0.001$ . Finally 5  $\mu\text{l}$  of the diluted bacterial culture was added to each well in the 96-well plates containing SDS. Each plate contain 8 technical repeats.

All plates were incubated for 18 hours static at 37<sup>o</sup>C overnight. Plates were cooled at RT for 30 minutes the next day and read at  $\text{OD}_{600}$  by a plate spectrophotometer.

### **2.5.5 Microscopy**

Bacteria to be tested had overnight cultures setup before the experiment using LB IPTG (1 mM) and ampicillin (100  $\mu\text{g/ml}$ ) supplemented with glycerol stocks and incubated at 37<sup>o</sup>C overnight with shaking. Cells were directly added to an agarose covered glass microscope slide for immediate observation. Images were taken using a Leica DMI8 inverted microscope under phase contrast conditions.

## **2.6 Protein Expression and Purification**

### **2.6.1 *E. coli* protein expression**

All protein expression was performed with 2YT media with appropriate antibiotic, inoculated with overnight cultures. Protein expression was performed in 1 L flasks and grown at 30°C with 180 RPM shaking, up to OD<sub>600</sub> 0.6 before inducing with 1 mM IPTG. Cultures were incubated overnight at 30°C with 180 RPM shaking. Cells were collected by centrifugation at 7,000 x g for 15 minutes, collated and frozen at -80°C.

### **2.6.2 Preparation of crude cell lysates**

Cell pellets were thawed at room temperature and gently re-suspended in binding buffer (50 mM HEPES, 300 mM NaCl, 35 mM Imidazole, 5 % glycerol, pH 7.2). All protein purification buffers are altered depending on the protein, which will be highlighted in the respective results sections. Re-suspended pellets were sonicated at 70 % power for 30 10-15 30 second bursts with a 30 second cool down on ice between each burst. Cell lysates were spun at 30, 000 x g for 25 minutes at 4 °C. The protein crude extract supernatant was collected and all further purification steps were performed at 4 °C.

### **2.6.3 Immobilised Metal Affinity Chromatography**

PD-10 empty disposable gravity columns (SLS) were used in conjunction with Profinity™ IMAC Ni-charged resin (BIORAD). The crude cell lysate was incubated with Ni-charged resin (750 µl per 50 ml lysate) for 1 hour with gentle tumbling at 4°C. The empty PD-10 column was equilibrated with binding buffer and 500 µl Ni-charged resin. The resin lysate mixture was run down the equilibrated PD-10 column to collect the protein bound resin. The resin was washed with binding buffer for 5-10 column volumes. To elute protein bound to the Ni-charged resin, two 10 minute incubations of 1.3 ml elution buffer (50 mM HEPES, 300 mM NaCl, 250 mM Imidazole, 5 % glycerol, pH 7.2) were performed, eluting the liquid after each incubation. Further elution incubations were done if further

protein could be eluted.

#### **2.6.4 Gel filtration**

To remove imidazole from the protein elution, PD-10 desalting columns (Cytiva) were used according to the manufacturers protocol. The buffer used in the protocol was storage buffer (20 mM HEPES, 350 mM NaCl, 5 % glycerol, pH 7.2).

#### **2.6.5 Sodium dodecyl sulfate–polyacrylamide gel electrophoresis**

Protein samples were analysed using sodium dodecyl sulfate–polyacrylamide gel electrophoresis (SDS-PAGE) was performed using a Mini-PROTEAN tetra system (BIORAD) using manufacturers protocol with 12 % acrylamide gels. To visualise proteins, gels were incubated with instant blue (Expedeon) and then washed in water. Gels were imaged using a Chemidoc gel documentation system (BIORAD).

## **2.7 X-ray Crystallography**

### **2.7.1 Setup of crystal trials**

Protein crystallisation trials were performed using the sitting drop method in 96-well SWISSCI MRC 2 Lens Crystallisation plates. Proteins were concentrated to > 10 mg/ml in storage buffer (**Section 2.6.4**). Pre-prepared crystallisation conditions were used to setup crystal plates (Molecular Dimensions, Hampton Research). A Formulatrix NT8 machine was used to dispense buffer and protein drops in a 2 to 1, 1 to 2 ratio per 2 drops respectively. Plates were sealed and incubated at RT or 4 °C.

### **2.7.2 Crystal collection and transit**

Protein crystals were observed under light microscopy for potential diffraction candidates. Selected crystals were collected by loop, immersed in 20 % glycerol and stored in liquid nitrogen. Under these conditions, crystals were transported by courier to Diamond Light Source, Oxford.

### **2.7.3 AmiA X-ray diffraction structure determination**

AmiA was used for crystallisation trials immediately after successful purification but centrifuged for 10 min at 15, 000 x g at 4 °C to remove any debris or precipitate proteins. Crystallisation trials used the sitting drop vapour diffusion method at RT. Diffraction quality crystals were obtained in the structure screen 1+2 screen (Molecular dimensions) in condition A7/C5/C6 in a 96-well plate: A7 = 2 M Ammonium acetate, 0.1 M sodium citrate, 30 % PEG 4000, pH 5.6, C5 = 1.4 M Sodium citrate tribasic dihydrate, 0.1 M sodium HEPES, pH 7.5 and C6 = 2 M Ammonium sulphate, 0.1 M sodium HEPES, 2 % PEG 400, pH 7.5. Crystals appeared after 2 weeks and grew to diffraction size after another 2 weeks. Dr Allister Crow harvested crystals in litholoops and plunge-frozen in liquid nitrogen ready for data collection at Diamond synchrotron (UK). Data was collected remotely for several crystals by Dr Allister Crow, the best diffracting to 2.35 angstrom resolution.

Initial processing including space group determination, scaling and merging were performed on the Diamond synchrotron server. Phases were determined by molecular displacement using a similar structure, PDB:5emi by using Phaser (McCoy et al., 2007). Phases were improved using solvent flattening and histogram matching using Parrot (Thain & Livny, 2005). Automated model building was performed in Buccaneer (Winn et al., 2011) to improve residue refinement. Models were completed using alternating rounds of model re-building via Coot (Emsley et al., 2010) and refinement via Refmac (Murshudov et al., 1997). Tools in Coot (Emsley et al., 2010) were used to assess geometry and Rampage (Lovell et al., 2003) to assess the distribution of backbone angles in the Ramachandran plot. Coordinates and structure factors have been deposited at the protein data bank. Further analysis of the structure used Pymol (LLC, 2023).

#### **2.7.4 Data sharing and materials**

Coordinates and structure factors of AmiA have been deposited with the Protein Data Bank - (PDB entry **8C2O**).

#### **2.7.5 Structural modelling**

All modelling was performed using SWISS model online software (A. Waterhouse et al., 2018) or AlphaFold (Jumper et al., 2021) and models visualised using Pymol (LLC, 2023).

#### **2.7.6 Genomic sequence alignments**

All sequence alignments were performed using Clustal Omega online tool (Sievers et al., 2011) and alignment files were visualised using Jalview (A. M. Waterhouse et al., 2009).

## 3 Investigating interactions of EnvC in the divisome

### 3.1 Abstract

During the final stages of bacterial cell division, periplasmic amidases cleave septal peptidoglycan to allow daughter cells to separate. These amidases are regulated by amidase regulators, in *E. coli* one such regulator is EnvC which regulates the activity of amidases AmiA and AmiB. EnvC is however itself regulated by a type VII ABC transporter called FtsEX. In this chapter the structural interactions between FtsX and EnvC are explored, with the key residues in the FtsX:EnvC interaction identified in FtsX. EnvC is shown to contain a self-regulation mechanism at the amidase binding site which is thought to be regulated by FtsEX, to prevent unregulated activation of AmiA or AmiB amidases. Lastly, other interactors of EnvC are explored finding YibQ, a genetic neighbour, confirmed not as an interactor and NlpI further confirmed as a scaffold protein in the periplasm interacting with multiple proteins, including EnvC. This is a step forward in understanding the structural regulation of the essential cell division amidase regulation pathway FtsEX:EnvC:AmiA/B which is believed to be present in multiple other bacterial species.

## 3.2 Introduction

This chapter focuses on the interactions of EnvC within the FtsEX:EnvC:AmiA/AmiB pathway and the wider divisome. The work performed in this chapter is either included or a follow-on off a paper published during this PhD: 'Insights into bacterial cell division from a structure of EnvC bound to the FtsX periplasmic domain' as mentioned in the declaration. For background on this chapter, and the PhD project contributions to the paper, a key relevant information overview of the paper will be provided below.

By X-ray crystallography, a 2.1 angstrom structure of one EnvC molecule bound to two FtsX periplasmic domains was solved (**Figure 21**). EnvC contains three key domains, a LytM domain (as previously solved by (Peters et al., 2013b)) with a restraining arm blocking over an amidase binding groove in LytM and lastly, a couple of  $\alpha$ -helices extended coiled coils which both bind the LytM domain towards the N-terminus with both coils interacting asymmetrically with the two FtsX periplasmic domains at the relative opposite end. The FtsX periplasmic domains contain a porter domain which is homologous to those found in MacB and LolC (Crow et al., 2017; Greene et al., 2018; Tang et al., 2021), which is a conserved motif in type VII ABC transporters. Lastly, there are two protruding helices called the X-lobe which appear important in EnvC binding (Du et al., 2016; Rued et al., 2019; D. C. Yang et al., 2011) and not found in other type VII ABC transporters. A model of EnvC binding to FtsEX (**Figure 21D**) represents the current hypothesis of how EnvC interacts with FtsX within the periplasm. The model highlights that a conformational change in FtsEX would change the interaction with EnvC, proposedly causing a conformational change in EnvC to allow amidase binding, further details of this mechanism are outlined later.

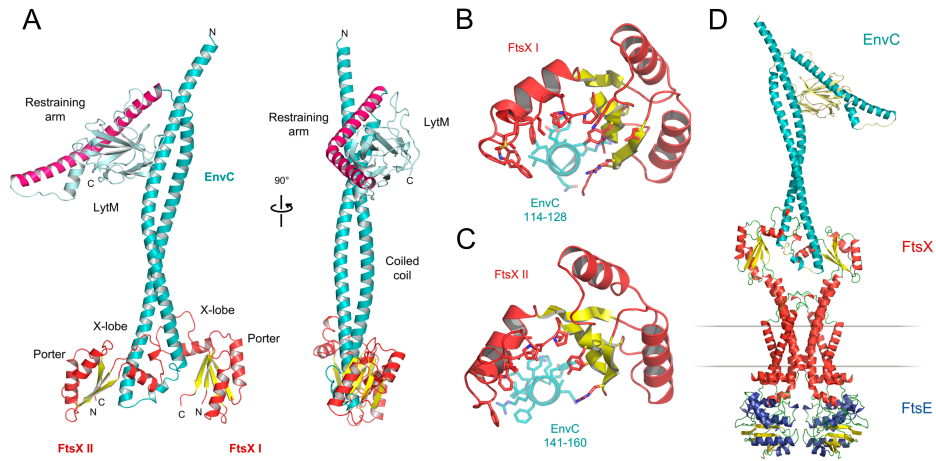


**Figure 21: Structure of EnvC bound to the FtsX periplasmic domains.** (A) Complete structure of mature *E. coli* EnvC bound to two molecules of the FtsX periplasmic domain. The two orientations shown are related by a 90° rotation about the vertical axis. (B) Close-up view of the interaction between the FtsX periplasmic domain and the first helix of the EnvC coiled coil domain. (C) An equivalent view of the second FtsX monomer bound to the second coiled coil helix. Interacting sidechains are shown with stick representation, and the bound helical elements of EnvC are partially transparent. (D) Proposed structure of the FtsEX-EnvC complex. Homology model for FtsEX-EnvC based on the crystal structure of EnvC bound to the FtsX periplasmic domain presented here and the MacB ABC transporter from *Acinetobacter baumannii* (Okada et al., 2017). PDB: 6TPI. Figures and captions sourced and adapted from (J. Cook et al., 2020)

Upon inspection of the EnvC:FtsX structure, an activation mechanism of EnvC by FtsEX interaction was theorised. Firstly, the full EnvC protein contains a restraining arm over the LytM domain (**Figure 21A**) which when previously determined AmiB binding residues found in (Peters et al., 2013b) are placed onto the LytM domain, the restraining arm visibly blocks these residues from binding AmiA or AmiB (J. Cook et al., 2020).

Based upon bacterial two-hybrid (**Figure 22C**), and other supporting evidences in (J. Cook et al., 2020) co-purification and periplasmic overexpression experiments, AmiB binding and activation by EnvC is confirmed to be prevented by the restraining arm and only successfully interact with the LytM domain of EnvC in the absence of this restraining arm. The experiment in **Figure 22C**, is the test whether EnvC truncated variants interact with AmiB. Bacterial-two-hybrid analysis as explained in 2.5.1, uses CyaA heterodimerisation to test protein-protein interaction between fusion proteins bound to T25 and T18 fragments. Using the *lac* operon and x-galactose, bacterial colonies that are blue show interaction and white colonies suggest no interaction detected. In the assay shown in (**Figure 22C**), the three EnvC variants mirror those shown in (**Figure 22B**), with only EnvC (278-419) lacking a restraining helix and is the only variant to interact with AmiB, showing this restraining arm blocks amidase interaction. The EnvC (216-247) - T25 construct (N-termini end facing of the restraining arm) interacting with all the EnvC variants containing the T18 fragment is a confirmation of self interaction and a control for proper protein folding. This experiment highlights a potential structural function of FtsEX to cause a conformational change in EnvC to move the restraining arm via the ATPase activity of FtsE, the ABC transporter ATPase domain.

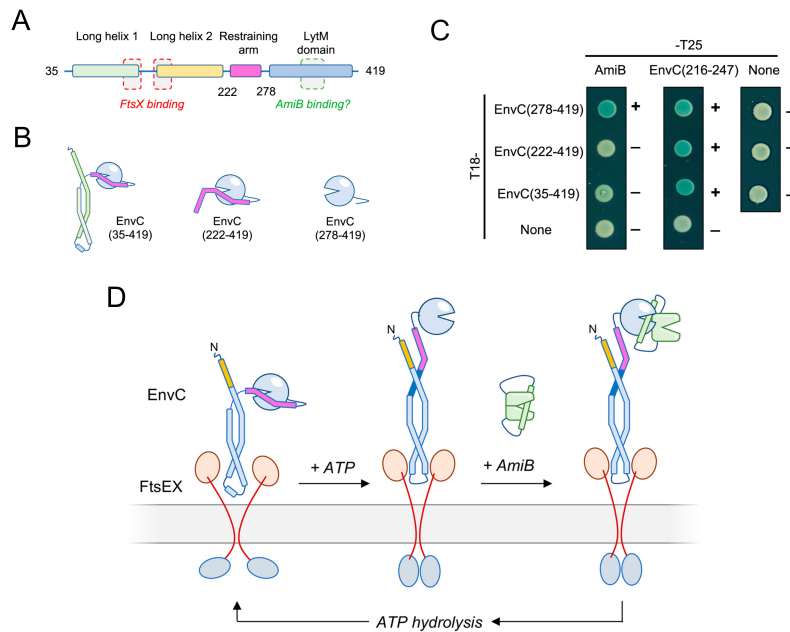


**Figure 22: Evidence for an autoinhibitory element in EnvC.** (A) Linear domain arrangement for mature EnvC. (B) Cartoon representations for three EnvC constructs used to probe AmiB binding and amidase activation. (C) Bacterial two-hybrid experiments showing interaction between EnvC variants and either AmiB or a fragment representing part of the restraining arm. (D) Overview of proposed conformational changes in FtsEX-EnvC during the ATP binding and hydrolysis cycle. Figure and caption adapted from (J. Cook et al., 2020).

Based on Gremlin analysis of co-evolving residues, heptad repeats were identified between the coiled coil and the restraining arm, leading to an EnvC activation hypothesis in which the restraining arm residues move to interact with their respective heptad and create an extended coiled coil (**Figure 22D**). Gremlin is an online tool which creates a statistical model of a protein family that measures both conservation and co-evolution patterns within the protein family (Balakrishnan et al., 2011; Kamisetty et al., 2013; Ovchinnikov et al., 2014). The strength of co-evolution is a strong prediction of residue-residue contacts in a 3D structure of a protein (Balakrishnan et al., 2011; Kamisetty et al., 2013; Ovchinnikov et al., 2014).

Based on MacB activation as a homology model for *E. coli* FtsEX, a mechanism of FtsEX mediated EnvC activation was modelled (**Figure 22D**). FtsEX begins with the ATPase domains of FtsE separated, FtsX periplasmic domains loosely interacting with EnvC and the EnvC molecule keeping the restraining arm covering the amidase binding groove in the LytM domain. Upon ATP binding, the FtsE molecules dimerise causing a conformational change in FtsEX and in turn, EnvC which moves the restraining arm into an extended coiled coil and allow the binding of AmiA/AmiB while the amidase binding groove in LytM is available. Once the activity of the amidases is complete, ATP is hydrolysed, FtsE ATPase domains separate, causing another conformational change through FtsX into EnvC, causing the amidase to dissociate, the restraining arm to return to the LytM domain, again, blocking the amidase binding site and interactions between EnvC and the FtsX periplasmic domains relax.

Further evidence is required to confirm this model of FtsEX-EnvC mediated amidase activation. A solved structure of an activated FtsEX:EnvC or EnvC bound to an amidase would provide a greater understanding into this ABC transporter mediated structural mechanism. This model does however further show a structural regulation system present in bacteria for amidase activity during bacterial cell division and that similar mechanisms could be found in other species and systems. The overall result of this paper provides a structural model of FtsEX mediated amidase regulation through EnvC.

In this chapter, the interaction between EnvC and FtsX is described using site-directed mutagenesis and using the bacterial two-hybrid technique, the interactions of EnvC with other division-associated proteins are explored. The proposed auto-inhibition mechanism of EnvC is tested using co-purification of EnvC variants with

AmiA combined with site-directed mutagenesis experiment of the LytM amidase binding residues in EnvC.

### 3.3 Results

#### 3.3.1 The X-lobe of FtsX is essential in the interaction with EnvC

The interface between the two FtsX periplasmic domains and the one bound EnvC molecule is part of the key to understanding how FtsEX structurally regulates EnvC and could be applied to other ABC transporter systems. The FtsX:EnvC interaction is uniquely challenging to investigate due to the presence of two FtsX molecules bound to only one EnvC molecule to form an asymmetrical interaction site. By point mutating one residue, in FtsX, it will affect interactions with EnvC on two opposite interfaces. Regardless of this however, using the crystal structure shown in **Figure 21**, key residues and regions of FtsX were chosen based on their apparent proximity to EnvC and potential important hydrogen bonding with EnvC residues. The mutations chosen to take place were in the hope to break or strongly hinder the FtsX and EnvC interaction.

The removal of the X-lobe appears to completely break the FtsX:EnvC interaction in the bacterial-two-hybrid (**Figure 23A/C**) and, as a control, X-lobe mutant has been shown to express properly in microscopy complementation experiments (J. Cook et al., 2020). The single residue mutations however appear to either have no effect or hinder the interaction to varying degrees (**Figure 23A/C**). Although, there were two single mutations, Y114E and F152E which significantly affected the FtsX:EnvC interactions to produce a delayed weakly blue phenotype in bacterial two-hybrid experiments (**Figure 23A/C**). Unsurprisingly, F152 is present in the EnvC interacting X-lobe but Y114 resides in the porter domain, potentially away from the main interacting residues of EnvC (**Figure 23A/C**), perhaps it is a residue with a more stabilising role of FtsX periplasmic domain. The blue colouration of these experiments is qualitative however and is open for interpretation and did require further exploration via follow on experiments in (J. Cook et al., 2020). As clearly outlined in 2.5.1 and in **Figure 23** caption, the experiment is controlled by incubation of empty vectors with FtsX and EnvC bacterial-two-hybrid constructs to check there are no false positive interactions. So, it is clear though that the X-lobe is further confirmed to be essential for the FtsX interaction with EnvC although the role of the significant residues in FtsX which can break EnvC interaction is up to speculation.

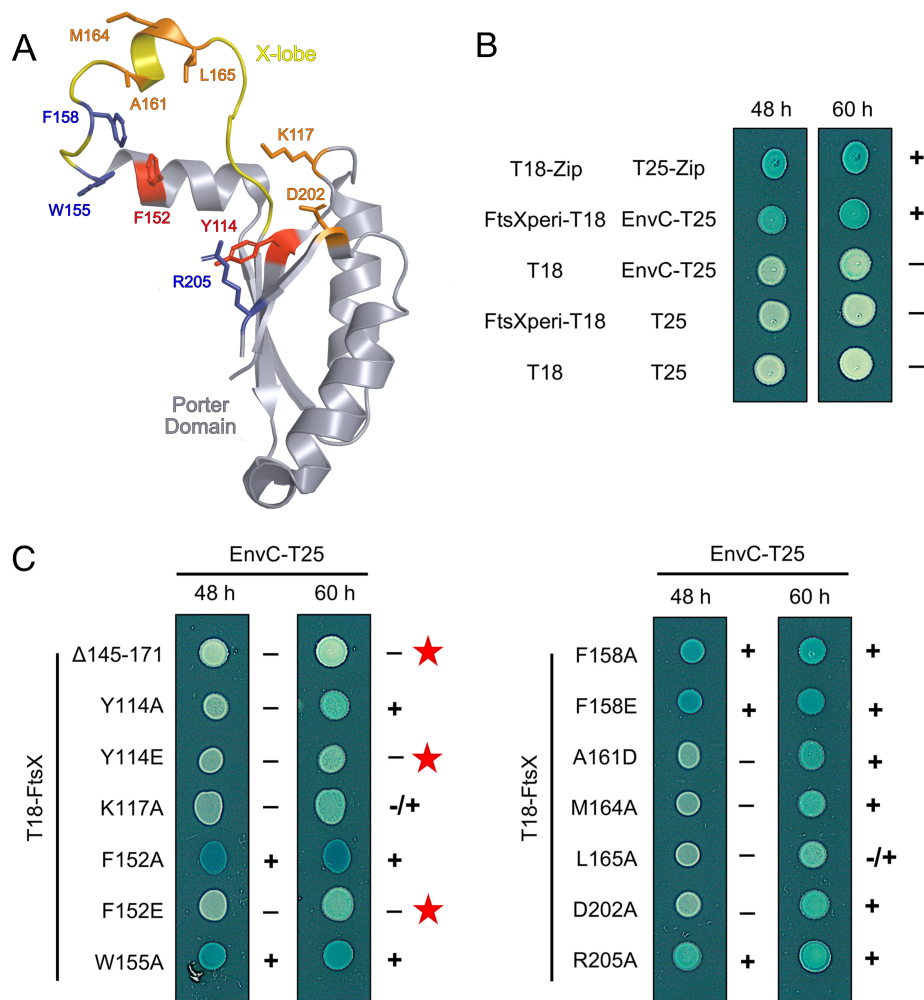


**Figure 23: Site Mutagenesis indicates key residues involved in FtsX:EnvC interactions**(A) FtsX periplasmic domain highlights the X-lobe (yellow) with the porter domain (grey) with residues labelled according to their ability to break the EnvC:FtsX interaction based on bacterial two-hybrid experiments (Red = Strongly, Orange = weakly, Blue = None) (B) As a positive control, the bacterial two-hybrid of FtsX periplasmic domain (residues 110-209) interaction with EnvC (residues 35-419) show a positive wild type interaction between the two proteins. As a technical positive control, the Leucine-zip is standard for bacterial two-hybrid experiments to confirm the a positive result produces a blue colony colour (B). As a negative control, empty T18 and T25 vectors were incubated with each other and other couple combinations respective FtsX and EnvC wild type constructs to show no unwanted interaction (B). Bacterial two-hybrid analysis for FtsX single residue mutants vs EnvC (residue 35-419) (C). The  $\Delta$ 145-171 mutant has a removed X-lobe. The red stars indicate the mutants which turned blue the slowest if at all. The positive and negative symbols indicate positive protein-protein interaction or no protein-protein interaction respectively. Bacterial two-hybrid was performed together on the same plate in repeat. NOTE: Residue numbering is based on the full length of all proteins. Creation of FtsX mutants and preliminary bacterial two-hybrid experiments performed by Tyler Baverstock, final paper spotting performed by Dr Jonathan Cook and Tyler Baverstock. Figure A is an adaptation of a diagram found in (J. Cook et al., 2020). Figure B/C sourced from (J. Cook et al., 2020)

### 3.3.2 EnvC self-inhibition prevents amidase interaction

As per the model proposed in (J. Cook et al., 2020), EnvC has a restraining helix blocking the amidase interaction site of the LytM domain, leading to the theory of a self-inhibition mechanism which is only lifted by the interaction and ATP binding of FtsEX. Further evidence is required to solidify this theory using bacterial two-hybrid screening, co-purifications (**Figure 24**), EnvC variants co-purifications combined with the investigation of the key residues involved in LytM responsible for amidase binding.

As the current literature suggests, and confirmed by the the bacterial two-hybrid assay (**Figure 24A**) only EnvC has direct protein-protein interactions with AmiA and AmiB then NlpD only interacts with AmiC. Both interactions however are only successful when both regulators are truncated into the LytM domain only (lacking any restraining helices), full length regulators do not interact with their respective amidases alone. This suggests that both EnvC and NlpD have a form of blocked LytM domains that require interactions from other proteins or specific conditions to allow amidases to interact. This is further supported by successful co-expression and purification of EnvC LytM his-tagged protein with untagged AmiA or AmiB (**Figure 24B**).

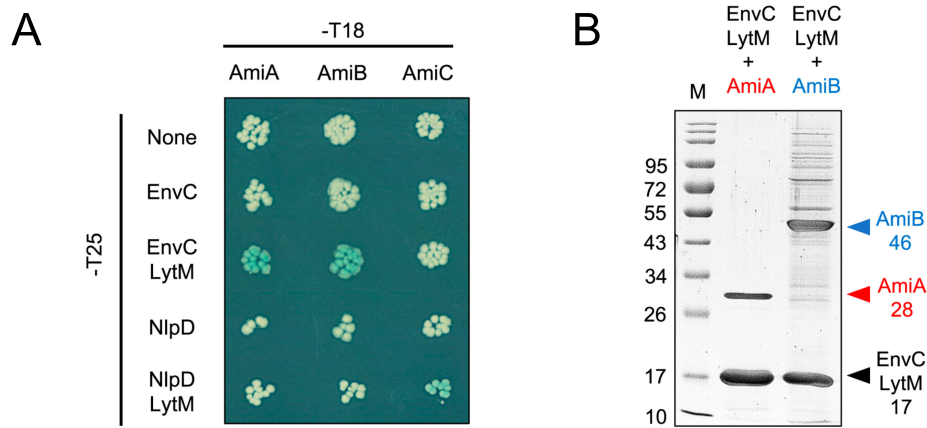


**Figure 24: The LytM domain only the EnvC interacts with amidases** (A) Bacterial two-hybrid assay probing interactions between the three *E. coli* amidases (AmiA, AmiB, and AmiC) and two peptidoglycan cleaving enzyme activators (EnvC or NlpD) as either full-length proteins or truncated LytM domains. Controls using empty T25 vector incubated with the amidase T18 constructs show a negative control with no false positives. For further controls, please see (J. Cook et al., 2020). (B) Co-purification of AmiA (lane 1) or AmiB (lane 2) with the EnvC LytM domain. All experiments were performed by Tyler Baverstock, figures sourced from (J. Cook et al., 2020). For further controls related to this experiment, please see (J. Cook et al., 2020)

To further evidence the self-inhibition mechanism in EnvC from (J. Cook et al., 2020), a series of co-purifications were performed with AmiA and his-tagged EnvC variants (**Figure 25**) with protein IDs confirmed using mass spectrometry analysis. Unsurprisingly, the LytM only of EnvC purifies with AmiA but both the full variant of EnvC and the EnvC LytM variant with the restraining arm both do not bind to AmiA and leave it in the flow-through after nickel affinity chromatography. EnvC and possibly NlpD therefore appear self-inhibited by a blocking helix over the LytM domain amidase interaction site which prevents unregulated amidase interaction and activation. This limits the amidase regulator's interaction with amidases to only when bound and activated by their own regulators, for EnvC, this would be FtsEX. The mechanism however how FtsEX causes a conformational change throughout EnvC and re-positions LytM blocking restraining arm is hypothesised in (J. Cook et al., 2020). The hypothesis is outlined in **22**, where the conformational changes in EnvC are caused by ATP binding and ATP hydrolysis of FtsEX, causing the removal and reinstatement of the EnvC restraining arm respectively. Only when the restraining arm of EnvC is not blocking the amidase binding site in EnvC LytM domain can AmiA or AmiB bind and become activated. This hypothesis however requires further structural evidence, especially in the area of interaction between EnvC and AmiA or AmiB.

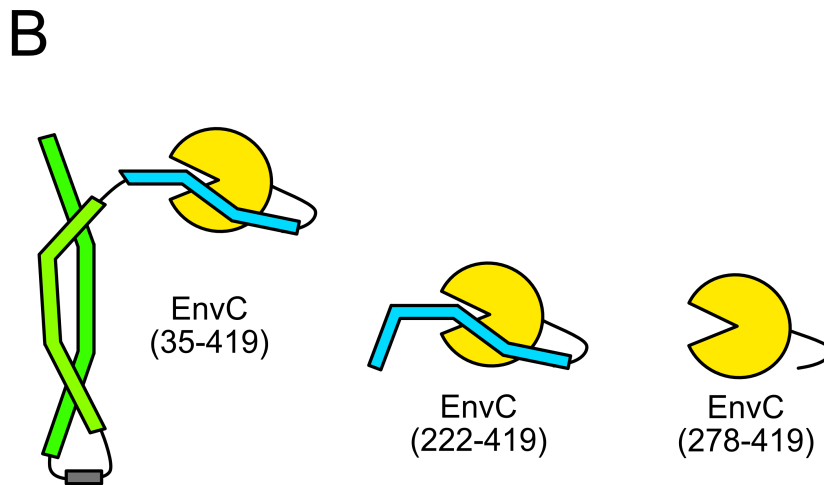
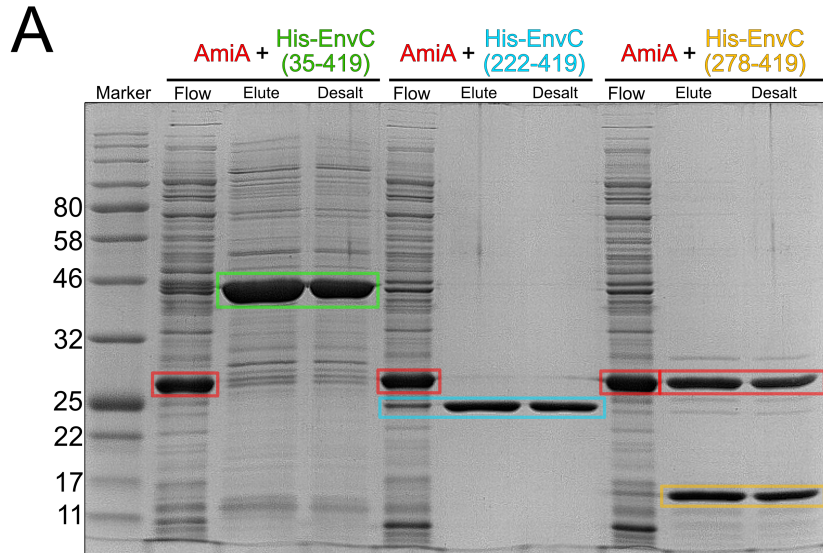


**Figure 25: EnvC restraining arm blocks amidase interaction *in vitro*** (A) Co-purifications of AmiA with EnvC constructs containing flow-through for unbound proteins. An SDS PAGE analysis imaged with a plain light gel imager.(Flow: Flowthrough after IMAC, Elute: Post immobilised metal affinity chromatography and Desalt: Post buffer equilibrated gel filtration. Protein IDs were confirmed using Mass spectrometry analysis.(B) EnvC variants blocking LytM amidase binding groove, inspired by (J. Cook et al., 2020). Colours match the rest of the figure.

To further investigate the interactions with EnvC and the amidases, mutations were performed in the LytM domain (lacking the restraining arm) to test the direct protein-protein interactions from some previously measured LytM residue mutations from (Peters et al., 2013a) that investigate the effect of LytM only mutations on the interaction with AmiB. Here, a preliminary bacterial two-hybrid experiment was used to measure the effect of these LytM mutations on the interaction with AmiB, along with new mutations based on the (J. Cook et al., 2020) EnvC:FtsX structure (**Figure 26**). As an idea for a control, the restraining helix (as a fragment) from EnvC was proposed to determine if there was proper folding of the LytM amidase binding mutants by binding to the LytM amidase binding groove if AmiB could not. However perhaps due to a caveat in this system that the protein being tested has a T25/T18 fragment added to the N- or C- terminus of the protein, resulting in the fusion protein and the fragment may cause molecular hindrance and could interfere with the desired protein interaction with the tested target protein. This effect could be stronger in a smaller desired protein such as the restraining helix, therefore the helix did not interact with the unaltered EnvC LytM, unfortunately rendering this specific control unusable.

The incubation of the LytM mutants with AmiB however indicated a surprising result that all LytM amidase binding mutants broke the interaction with AmiB, or rendered the interaction weak enough to not be detected by as the assay in the accurately measurable time-frame of the technique. The LytM mutations suggest the following residues and interacting loop to be essential in the LytM:AmiB interaction: K321, V324, Y350, V353, E403, R405, loop 312-320). This may suggest the importance of all chosen residues in the LytM to be essential to stabilise the the interaction with AmiB however, it may also show the importance of these residues in the proper folding of the LytM domain. A further control experiment however would be useful to confirm proper protein folding in the bacterial two-hybrid, an expression SDS-PAGE gel would hopefully show the proper folding and expression of the LytM binding mutants to further validate the experiment. By expressing these fusion proteins, lysing the cells and collecting the soluble protein fractions and loading this onto an SDS-PAGE analysis, if the fusion protein is present (and perhaps confirmed by mass spectrometry), then the construct is properly folded, and should be functional for the bacterial-two-hybrid assay. Further modification of the blocking helix B2H construct would also be worth an investigation.

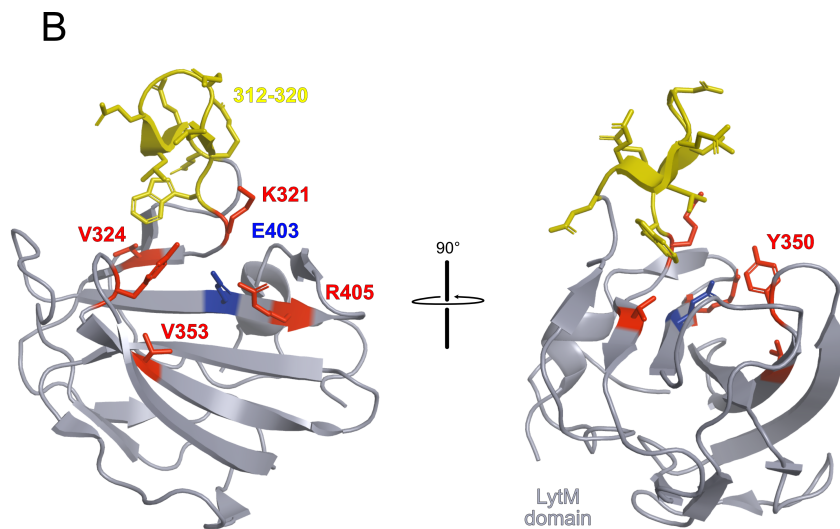
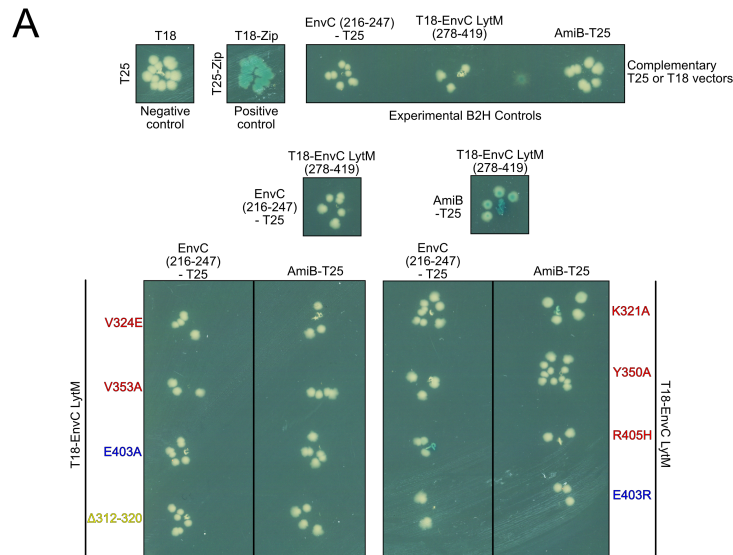


**Figure 26: EnvC LytM domain contains essential AmiB binding residues.** (A) Bacterial two-hybrid assay probing the key residues in EnvC LytM domain involved in amidase binding. The top band shows positive and negative controls of the experiment to check there are no false positives or negatives. The second set is the EnvC LytM domain interaction testing with the restraining arm of EnvC, this should interact by the crystal structure **21** and its purpose is a proper folding control for the EnvC mutants. The right colony on the second row is the wild type positive interaction with EnvC LytM domain and AmiB. The third set is the EnvC amidase binding point mutants in EnvC LytM domain vs AmiB or EnvC restraining arm. The idea is that if properly folded, the EnvC mutants will interact with the restraining arm but if AmiB binding is broken or significantly hindered, AmiB will not interact. EnvC LytM Mutants in red are based on previous studies (Peters et al., 2013a), Blue: This study, Yellow: Interaction loop, this study. Bacterial two-hybrid spots all present on the same plate. (B) EnvC LytM domain highlighting amidase binding residues. Structure rotated 90 degrees along a vertical axis (Red: (Peters et al., 2013b), Blue: This study, Yellow: Interaction loop, this study). Image created in Pymol from PDB = 6TPI from (J. Cook et al., 2020).

As potential co-crystallisation targets, other LytM:amidase systems were investigated and co-expression constructs were made of regulators and amidases to one, test if they also interact with other bacterial species and secondly, a hope for a crystal structure of an amidase bound to its regulator.

Firstly, ActS was reported to interact with all three amidases during cellular stress, with a preference to AmiC, interestingly, when AmiA is co-purified with his-tagged ActS LytM domain only, they interact in a similar fashion to EnvC LytM (**Figure 27 A**). Although reported by (Gurnani Serrano et al., 2021) to prefer interaction with AmiC, it is not unsurprising that ActS can interact with other amidases, it would be curious to investigate this further via bacterial two-hybrid analysis against other components of the divisome could be useful to investigate other potential regulatory partners of ActS. Furthermore, the ActS LytM domain contains more sequence similarity with NlpD LytM domain in comparison with the EnvC LytM domain (**Figure 28**), which is understandable as ActS apparently prefers AmiC, with NlpD having a determined strict preference to AmiC where EnvC only interacts with AmiA and AmiC. The similarity between all three regulators focuses onto the C-terminus containing the LytM domains.

Secondly, four homologs of EnvC and AmiA in *E. coli* were cloned and successfully co-purified from four species (**Figure 27 B**); *Enterobacter chengduensis*, *Edwardsiella tarda*, *Klebsiella pneumoniae* and *Serratia marcescens*. The EnvC LytM domain interacts with AmiA similar to the system in *E. coli*, suggesting a similar amidase regulation pathway is present in these species, however more evidence and a wider divisome investigation would be required to support this claim. The sequence alignment of the EnvC homologs with *E. coli* EnvC (**Figure 28**) however highlights significant similarity in the LytM domains in all homologs along with moderate similarity throughout the whole sequence excluding the initial N-terminus.

In terms of crystal trials, all four homolog purifications, *E. coli* AmiA and AmiB co-purifications with EnvC LytM domain were all expressed and purified successfully, enough to setup at least 5-10 crystal trials of each pair using different crystallisation screens from Molecular Dimensions. This was performed at room temperature and left for a year.

The homologs were chosen based on core conservation of interaction grooves and

active sites in the EnvC LytM and amidases receptively. It was also noted to have different sequence similarities to for variation for the best chance of crystallisation. The sequence similarity of both the Amidase and regulator pairs compared to *E. coli* are as follows; *Serratia marcescens*: AmiA = 65 % / EnvC = 65%, *Klebsiella pneumoniae*: AmiA = 89 %, EnvC = 85 %, *Enterobacter chengduensis*: AmiA = 89 % / EnvC = 89 %, *Edwardsiella tarda*: AmiA = 60 %, EnvC = 60 %.

Unfortunately no crystals were obtained from this endeavour, although micro crystals were obtained from *Edwardsiella tarda* EnvC and AmiA complex in 4M of Citrate (no pH specified in Molecular Dimensions). Ultimately this co-crystallisation experimental route was abandoned due to unsuccessful crystal trials and time constraints.

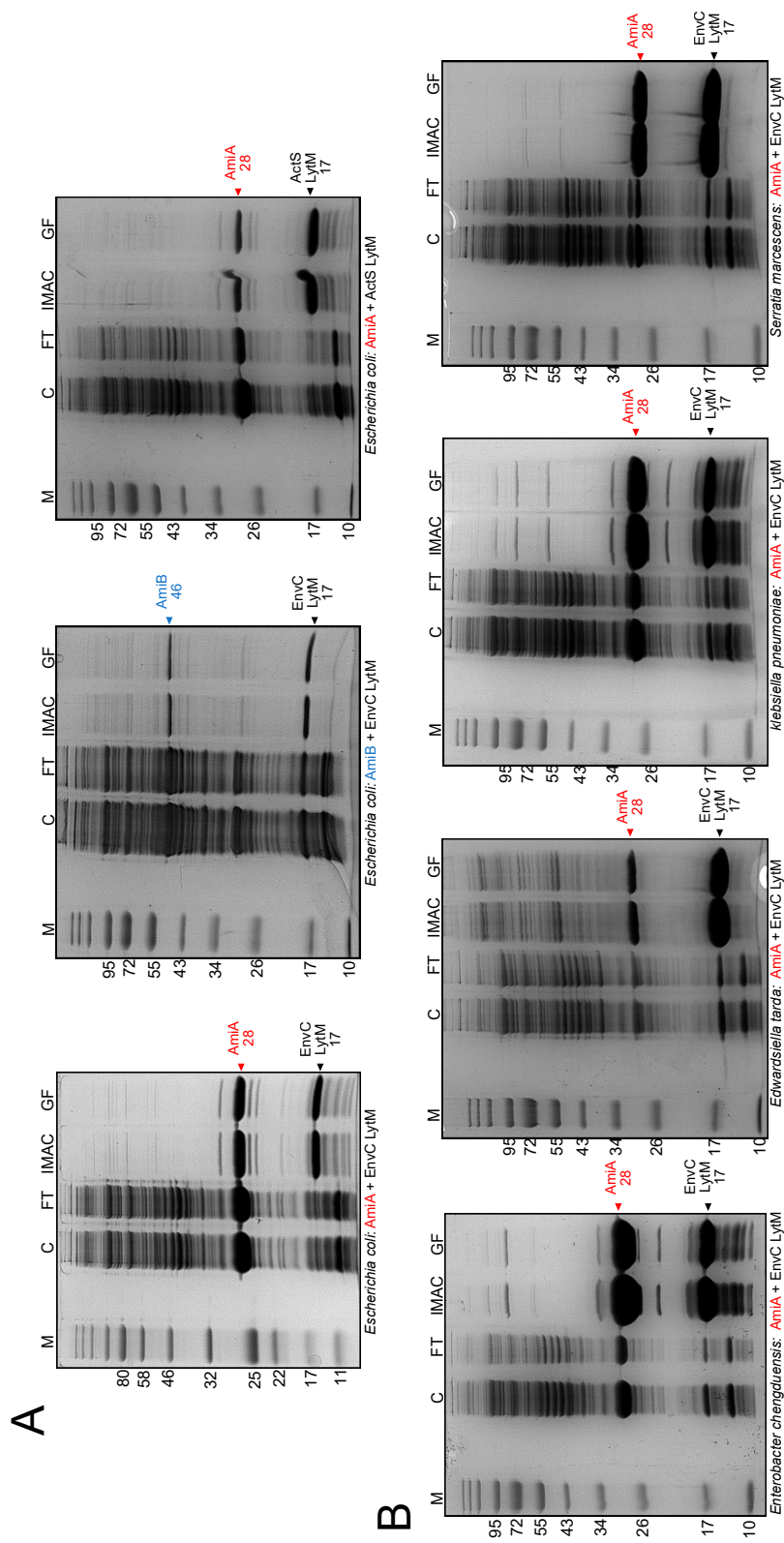


**Figure 27: Successful co-purification of amidase and regulator pairs from numerous species.** (A) Summary of the co-purifications of EnvC LytM with both AmiA and AmiB, along with the co-purification of ActS LytM domain with AmiA. (B) Co-purifications of different *E. coli* EnvC LytM and AmiA homologs. All constructs were co-expressed and co-purified by immobilised metal affinity chromatography and analysed by SDS PAGE. All successful purifications were setup into crystallisation trials.



### **3.3.3 YibQ is not an EnvC interactor nor a component of the divisome**

EnvC is part of a greater divisome assembly for a cell to separate into successful daughter cells. There is still a significant unknown to the whole divisome with interacting proteins which may play a role which have yet to be discovered. YibQ, a currently labelled divergent polysaccharide deacetylase domain-containing protein which removes N-linked acetyl groups from cell wall polysaccharides (Serres et al., 2001). YibQ was a potential candidate for further study in the context of an EnvC interacting partner or as a part of the divisome machinery (**Figure 29**).

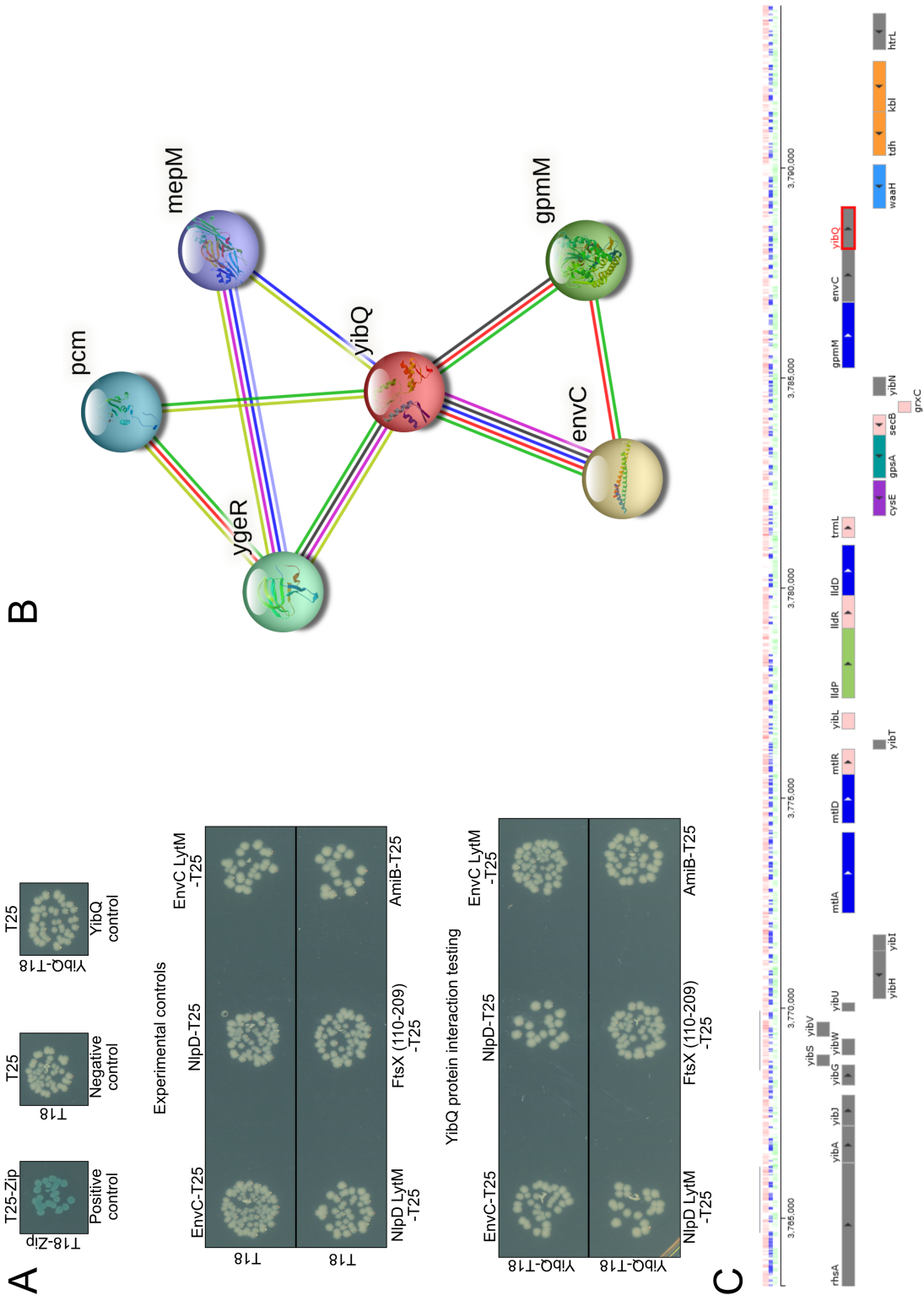


**Figure 29: YibQ lacks interactions with divisive components.** (A) Bacterial two-hybrid probing YibQ interactions with components of the divisiveome. This bacterial two-hybrid was all performed on the same plate (B) STRING analysis of potential YibQ interactors (Colour codes are standard STRING analysis) (C) Genetic positioning of YibQ in the *E. coli* genome. STRING line colours: Red = Indicates presence of gene fusion evidence, Green = Gene neighbourhood evidence, Blue = Gene co-occurrence evidence, purple = experimentally determined, yellow = Textmining evidence, light blue = Curated database evidence, black = Co-expression evidence.

Firstly, the gene encoding YibQ was found to be neighbouring EnvC in the *E. coli* genome and strongly suggested to interact with EnvC via STRING interaction analysis (**Figure 29B/C**) along with ActS (formerly ygeR). The bioinformatics suggest a function relating to EnvC and ActS, and in turn, amidase regulation. To test this theory, the divisome related bacterial two-hybrid library that has been constructed in the research group was suitable for investigating if YibQ interacts with any of the key divisome components. After a thorough investigation using both T18 fragment fusions attached at either the N- or C- terminus of YibQ (only one orientation shown in **Figure 29A**), the assay suggests the YibQ does not interact with EnvC nor NlpD (or in the LytM only forms) nor AmiB nor FtsX periplasmic domain (**Figure 29A**). Although an expression experiment and an SDS-PAGE gel would prove the expression of the YibQ-T18 fusions, the B2H assay reports that YibQ is not an interacting partner of EnvC or other divisome components. Further B2H testing against other divisome components, including ActS would be prudent to explore all options however at this time YibQ is still an unknown protein with no known confirmed interacting partners, nor its function.

### 3.3.4 NlpI is a potential scaffold protein for the divisome

It has been previously reported by (Banzhaf et al., 2020) that EnvC interacts with a scaffold protein, NlpI along with multiple classes of peptidoglycan peptidoglycan cleaving enzymes. To further investigate the interactions of EnvC with NlpI and other components of the divisome, bioinformatic and experimental approaches were used.

To provide context, a figure sourced from (Banzhaf et al., 2020) showed that an immobilised NlpI affinity chromatography highlighted a high number of potential interacting proteins including FtsX, AmiA, AmiC and EnvC (**Figure 30A**). The paper concludes NlpI as an outer membrane peptidoglycan peptidoglycan cleaving enzymes adaptor protein.

STRING interaction analysis (**Figure 30B/C**) suggests possible interactions with genetically neighbouring proteins deadD and pnp (RNA degradation) and prc (protease for PBP3). The protease prc is reported to use NlpI to chaperone proteins which have been targeted for degradation, NlpI scaffolds for PG multi-enzyme complexes. Like many bioinformatic techniques, STRING analysis can be limited by analysis at only the genetic or text-mining level and can highlight interactions in homologous systems but not the species you are investigating bioinformatic data can always be supported with clear experimental data. STRING is however good for choosing or predicting possible interactions between proteins that can be investigated experimentally. In the context of the divisome, NlpI is reported to bind both amidases and their respective regulators. To further investigate the interactions of NlpI with EnvC and other components of the divisome more closely, a bacterial two-hybrid analysis was performed (**Figure 31**)



To begin, the controls required as a part of the bacterial two-hybrid experiment indicate any false positives or false negatives (**Figure 31C**). Interestingly, one construct, T18-NlpI, with the T18 fragment on the N-terminus of NlpI produced a false positive on the negative control. This may suggest that NlpI itself is a 'sticky' protein which may well result in T18-NlpI molecules interacting with each other and creating a false positive interaction. Nevertheless, the other orientations using T18/T25 fragments had intact positive and negative controls which were used in the experiments. NlpI was tested for interactions against amidase regulators EnvC and NlpD in their full and LytM variants (**Figure 31B**) along with all three division-associated amidases, the division protein FtsX and lastly, a control, FtsA (**Figure 31A**) which resides in the cytoplasm in which NlpI should not interact, being a protein targeted to the periplasm. Interestingly, NlpI interacted with both amidase regulators in all forms along with FtsX and weakly with FtsA, however, no interaction was detected with AmiA, AmiB or AmiC in this experiment. It would appear that NlpI does interact with proteins associated with amidase regulation, including the ABC transporter protein FtsX, supporting the idea that NlpI is a scaffold protein for other protein-protein interactions. As all three amidases did not interact with NlpI, the experiment may not detect a direct interaction here, however an indirect interact may still occur if NlpI interacts with both amidase regulators and FtsX. The weak interaction with the cytoplasmic FtsA further suggests that NlpI has a wide range of interactors and recognises a range of protein domains, supporting the idea that NlpI is a 'sticky' protein. Overall, the bacterial two-hybrid experiment suggests NlpI is a scaffold protein for divisome components and may help facilitate interactions between amidase regulators and their targets with NlpI's ability to bind multiple types of protein folds as shown by a weak interaction with FtsA.

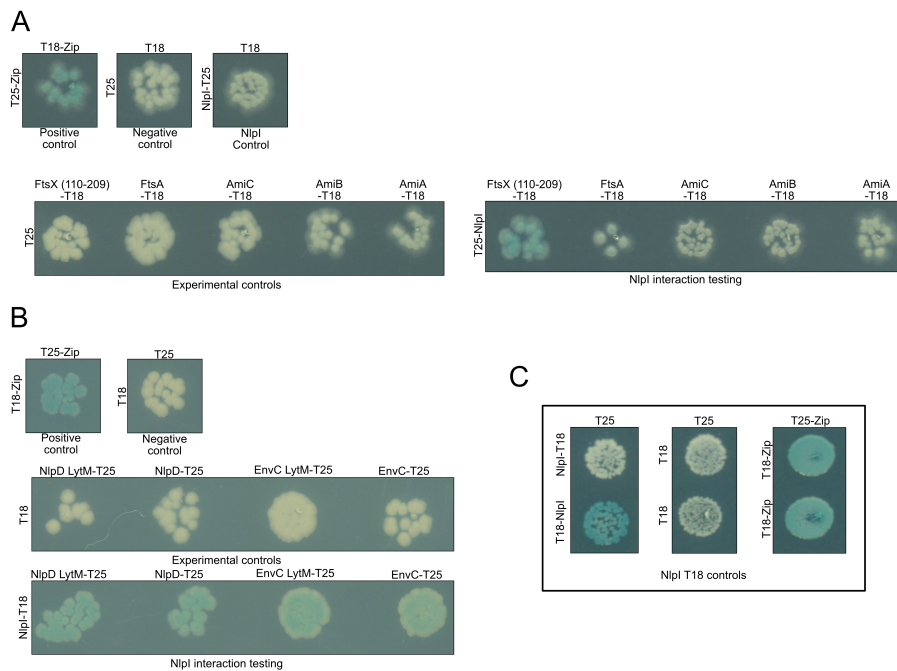


**Figure 31: NlpI as a potential scaffold for divisome components** (A) Bacterial two-hybrid probing NlpD interactions with periplasmic amidases, FtsX periplasmic domain and cytoplasmic based FtsA. (B) Bacterial two-hybrid probing NlpD interactions with amidase regulators and their respective LytM domains.(C) T18 controls for NlpI constructs performed by Dr Jonathan Cook. For each part of this figure, a new bacterial two-hybrid is performed on separate plates.

### 3.4 Discussion

This chapter further investigated the interactions of EnvC in the context of the divisome. The binding interface between EnvC and FtsX was probed moving to the interactions between EnvC and its targets, AmiA and AmiB with a set of bacterial two-hybrid analysis on the amidase system and on amidase binding mutants of the EnvC LytM domain itself. Variants of EnvC were also co-purified with AmiA to solidify the self-regulation mechanism present in the full EnvC protein. Lastly, potential EnvC interacting partners were investigated, including YibQ and NlpI.

Via bacterial two-hybrid analysis, in FtsX, the X-lobe and two key residues (Y114E and F152E) were identified to be essential in the interaction between FtsX periplasmic domain and EnvC. Due to the asymmetric 2-to-1 ratio interaction between FtsX and EnvC, it is interesting that single point mutations are sufficient to significantly hinder the interaction of FtsX in two molecules on two interaction sites with EnvC. It is worth noting however that colleagues in the group did show both the X-lobe and residues (Y114E and F152E) mutants in FtsX did prevent FtsEX from functioning properly *in vivo* (J. Cook et al., 2020). The bacterial two-hybrid experiment did however raise questions on how the interaction with FtsX with EnvC changes during ATP binding and hydrolysis in FtsE, a structure of the active form of FtsEX bound to EnvC would highlight the changes in the FtsX:EnvC interface.

Transitioning to EnvC itself and its interaction with AmiA and AmiB, this chapter highlighted a number of key mechanistic systems present in EnvC. Using a bacterial two-hybrid analysis and co-purification of truncated EnvC variants, EnvC was further supported to contain a restraining helix over the amidase binding groove present in the LytM domain, as reported in (J. Cook et al., 2020). Only when the restraining arm is removed does EnvC interact with AmiA or AmiB, and this is suspected to be the case of NlpD with AmiC although no structural information on NlpD is available.

The mutagenesis and bacterial two-hybrid of the LytM domain to probe AmiB interactions generally agreed with previous literature (Peters et al., 2013b). In general, the LytM mutants which did not activate the AmiB in (Peters et al., 2013b) also did not interact in the bacterial two-hybrid, however, two mutants, V324E and K321A which were previously shown to activate AmiA and AmiB, do not interact in the bacterial two-hybrid. Firstly, further controls, including an expression trial is

needed for the bacterial two-hybrid LytM mutant constructs to check proper folding and expression, secondly, these LytM mutants *in vivo* may react differently with no T18 fragment fused to the protein with other proteins aiding in the interactions in the periplasm, where the bacterial two-hybrid is only used in the cytoplasm. Lastly, the bacterial two-hybrid may be insufficiently sensitive enough to detect interactions of any of the LytM mutations however the constructs could still be able to activate AmiA or AmiB *in vivo*. This could be measured by the use of a *in vitro* peptidoglycan dye release assay using Remazol Brilliant blue labelled peptidoglycan. A simple experiment shown in (Zhou et al., 1988) where these LytM mutants could be incubated with AmiA or AmiB and compared to wild type to measure the increase in dye released over time, to measure amidase activation by mutated LytM domains.

The divisome is a complex set of protein machinery with numerous interactions and other proteins, undiscovered may be involved in the activity of FtsEX and EnvC in the periplasmic amidase regulatory pathway. Although the work performed in this chapter is preliminary, indications of potential interacting partners of the divisome were further understood. As currently labelled divergent polysaccharide deacetylase domain-containing protein (which removes N-linked acetyl groups from cell wall polysaccharides (Serres et al., 2001)) in *E. coli*, YibQ was a genetic neighbour to EnvC however based upon bacterial two-hybrid analysis, YibQ did not interact with any amidase regulators, amidases nor FtsX. The T18 fragment was added to either the N- or C-terminus to increase chances of detecting an interaction. Another control of an expression trial would be useful to determine if the YibQ-T18 constructs express and fold properly to eliminate this doubt. This chapter therefore suggests YibQ is not involved in the FtsEX:EnvC pathway by direct interaction. Perhaps due to the hypothesised function of YibQ is the answer why it does not interact with divisome proteins. The function of deacetylation on polysaccharides such as peptidoglycan is varied including resistance to environmental factors or antimicrobial peptides (Andreou et al., 2018). Perhaps that YibQ is part of a different system to the divisome, a system to react to environmental stresses and act accordingly. Further experiments including perhaps a high throughput binding assay would be useful to detect any interacting proteins of YibQ and then further investigations into any positive interactors would be effective as this is still a very unknown protein.

NlpI was another candidate to investigate interactions in the divisome and the Ft-

sEX:EnvC pathway. In (Banzhaf et al., 2020), NlpI was suggested as a scaffold adaptor protein for peptidoglycan cleaving enzymes and was shown to interact with a huge variety of proteins, including FtsX, EnvC, AmiA, AmiB and AmiC using immobilised NlpI affinity chromatography. Based on this chapter's bacterial two-hybrid experiments however, NlpI was found to only interact with EnvC and NlpD (both full and LytM only variants), FtsX and oddly FtsA. There was no direct protein-protein interaction detected on AmiA, AmiB or AmiC with NlpI. It was stipulated however that the bacterial two-hybrid experiment may have been unable to detect interactions between NlpI and AmiA/B/C nor that in-direct interactions of NlpI with division-associated amidases would also be undetectable using this technique. Perhaps NlpI cannot interact with the amidases directly but this requires further evidence such as a co-purification of NlpI and the amidases. The weak interaction with FtsA, which is present in the cytoplasm naturally, not the periplasm where NlpI is targeted to, poses a question if NlpI is able to bind non-specifically to a wide range of motifs and domains, irrelevant of their function. This would further suggest that NlpI is a scaffold protein for multiple types of proteins with a wide range of functions, with the function of NlpI to bring these interacting proteins in proximity to each other in the periplasm. This could be the case with EnvC and the amidases, facilitated with NlpI. Further work would be required to establish direct interactions between NlpI and individual binding partners, which may include co-expression and purification, bacterial two-hybrid analysis using constructs with point mutations in NlpI to break the interactions with interacting partners. To find further divisome based interactors of NlpI, bioinformatic techniques such as co-folding NlpI with potential partners to assess the likelihood of interaction or if there are any homologs of NlpI in other bacterial systems that have been explored.

As mentioned in the introduction, there are other LytM:amidase systems present in other bacterial species and even in *E. coli*. ActS was suggested to also interact with all three periplasmic amidases under cellular stress (Gurnani Serrano et al., 2021). Due to the presence of another LytM domain, ActS LytM domain interacts with AmiA during a co-purification, and upon sequence analysis, holds multiple similarities in the LytM domain with EnvC and NlpD. Although suggested to mainly function during lipopolysaccharide depletion stress, further experiments including a divisome focused bacterial two-hybrid screen would be useful to test *in vivo* interactions with other amidases and divisome components along with the LytM only

and full ActS constructs to test if a similar phenotype is found to EnvC and NlpD. A crystal structure of the ActS LytM domain would be prudent as a structural example of regulator activated amidase. Interestingly however, the co-purifications of the *E. coli* homolog EnvC LytM domains with AmiA from four other bacterial species showing homology in amidase binding sites in EnvC and amidase binding sites in a sequence alignment with *E. coli* EnvC, provides a glimpse that the FtsEX:EnvC:AmiA/B regulatory system is present in many other bacterial species. Again however, further similar evidence to this chapter for these other systems would be crucial for this claim.

This chapter advances our understanding of the interaction between EnvC, its self-inhibition mechanism and its interacting partners.

Due to the conserved nature of bacterial cell division, all evidence collected in *E. coli* may provide a starting model for other bacterial systems. Aside from being a critical part of the bacterial life cycle which should be understood, the function of EnvC in relation to FtsEX and periplasmic amidases is a step closer to identifying new antibiotic targets and strategies. The regulation of the essential process of septal peptidoglycan hydrolysis, which the function is conserved in bacteria, deregulation would provide a mechanism to create susceptibility in current antibiotic resistant strains.

Further research into the FtsEX:EnvC:AmiA/B pathway as a part of the greater divisome is required, there are multiple protein candidates now which are being discovered and may be involved in this highly regulated pathway which require further investigation. In terms of structural understanding, the work in this chapter provides a foundation to expand into the whole FtsEX:EnvC:AmiA/B complex, where the FtsEX transmembrane and ATPase domains remain to be solved, along with the active form of EnvC bound to an active amidase, all key structures in understanding the conformational changes cascading throughout this pathway.

## 4 Knockout characterisation of the FtsEX:EnvC:Amidase pathway

### 4.1 Abstract

The collection of proteins which facilitate division in bacteria is called the divisome. There are multiple components in the *E. coli* divisome each with varying unique structures and functions. One complex set of proteins involved is the FtsEX:EnvC:AmiA/B pathway which regulates amidase activity during septal peptidoglycan hydrolysis during the late stages of cell division. In this chapter, the importance of each component is explored via genomic knockout characterisation under varying environmentally stressful environments. It is found that both FtsEX and EnvC are both key in maintaining proper outer membrane permeability and envelope integrity under low osmotic and detergent conditions. The same is said for the amidases although only when two or more of the three *E. coli* amidases; AmiA, AmiB and AmiC are knocked out. This claim is further supported by sensitivities to vancomycin and detergent conditions and growth curves under similar conditions. Finally after microscopy analysis, the FtsEX, EnvC and the redundant division-associated amidase system, a  $\Delta amiab$  knockout strains show moderate chaining phenotypes from improper daughter cell separation, with the triple amidase knockout;  $\Delta amiabc$ , showing complete inability to separate daughter cells. Overall, this characterisation explores a redundant amidase system with two key regulating proteins required for proper hydrolysis of septal peptidoglycan with resulting cell separation. This highlights potential antibiotic targets to sensitise bacteria to previously ineffective treatments.

## 4.2 Introduction

The importance of the FtsEX:EnvC:AmiA/B pathway has already been deduced heavily in the literature to evidence the function of this pathway to regulate periplasmic amidases during cell division. This system is responsible for regulating the hydrolysis of septal peptidoglycan via amidases which is a required event for proper cell separation at the final stages of cell division (Du et al., 2016; Levin & Janakiraman, 2021). As reinforced in (J. Cook et al., 2020), the activity of FtsEX is important for resistance to detergent, low osmolarity and antibiotic conditions. The roles of the three amidases in *E. coli*, AmiA, AmiB and AmiC have been studied to find that without all three, an extreme chaining phenotype is produced, however cells containing at least one amidase appear to minimise the chaining phenotype, enough to hydrolyse the septal peptidoglycan (Heidrich et al., 2001; Uehara et al., 2010). FtsEX has also been shown to display this chaining phenotype (J. Cook et al., 2020).

There are gaps in the literature however, each component in the FtsEX:EnvC:AmiA/B pathway has different functions in cell division but also in cell viability. It is currently unknown the effect of lacking specific components of this pathway under different cell stresses and how these components affect the stability of the cell. The aim of this chapter is to characterise *E. coli* knockouts of the FtsEX:EnvC:AmiA/B to further the understanding of each component's role in cell division and the cell's ability to survive environmental stresses.

## 4.3 Results

### 4.3.1 Generating divisome *E. coli* double ( $\Delta amiab$ ) and triple ( $\Delta amiabc$ ) division-associated knockouts

To characterise the FtsEX:EnvC:AmiA/B pathway, a collection of *E. coli* mutants was collated. The majority of the mutants were purchased from the keio collection (Gene Bridges) (Baba et al., 2006) (**Table 2**). To probe the role of the individual amidases involved in cell division, double ( $\Delta amiab$ ) and triple ( $\Delta amiabc$ ) knockouts were made in this project in the same background as the purchased keio collection (BW25113). It is important to highlight that the strategy to have all knockouts in the same BW25113 background in this chapter allowed comparison of any other keio collection in the same background. The phenotypes shown are the result of these cells lacking the indicated gene and not a difference in genotypes. To further validate the keio collection mutants, we sequenced the regions of mutation to ensure a kanamycin gene is present at the correct location. To ensure there were no unwanted mutations within the genome, these keio knockouts would need to be whole genome sequenced in the future but have not been within this study. It is also worth noting that JC7 (**Table 2**), the strain used in this chapter lacking *FtsEX* was kindly created in-group by Dr Jonathan Cook within the same background (BW25113) as it was unavailable from the keio collection.

The method to make the  $\Delta amiab$  and  $\Delta amiabc$  knockouts are standard to the kit and protocol used from Gene Bridges (**Figure 32A**). The workflow involves removing the kanomycin resistance (Kan) cassette from the  $\Delta amiA$  single amidase keio knockout strain using a flippase plasmid. Using another Kan cassette flanked by homologous overhangs to the genomic location of AmiB, the RED/ET recombination flips out AmiB and adds in the Kan cassette. For the  $\Delta amiabc$  mutant, the whole process is repeated leaving a single FRT site on both AmiA and AmiB genomic regions with a kan cassette present at the site where *AmiC* was.

Aside from Sanger sequencing which was performed as a final check for successful removal of amidase genes, specific PCR experiments were periodically performed to check the  $\Delta amiab$  and  $\Delta amiabc$  knockout validity (**Figure 32B/C**). Using a combination of primers which external to the amidase genes and a *kan* specific primer, the  $\Delta amiab$  and  $\Delta amiabc$  knockouts were confirmed correct at all three

amidase sites in the BW25113 genome using PCR and sequencing. The end goal was successful to create  $\Delta amiab$  and  $\Delta amiabc$  knockout strains to investigate the effect of lacking two or three division associated amidases on *E. coli* cells and any phenotypes this creates.

**A**

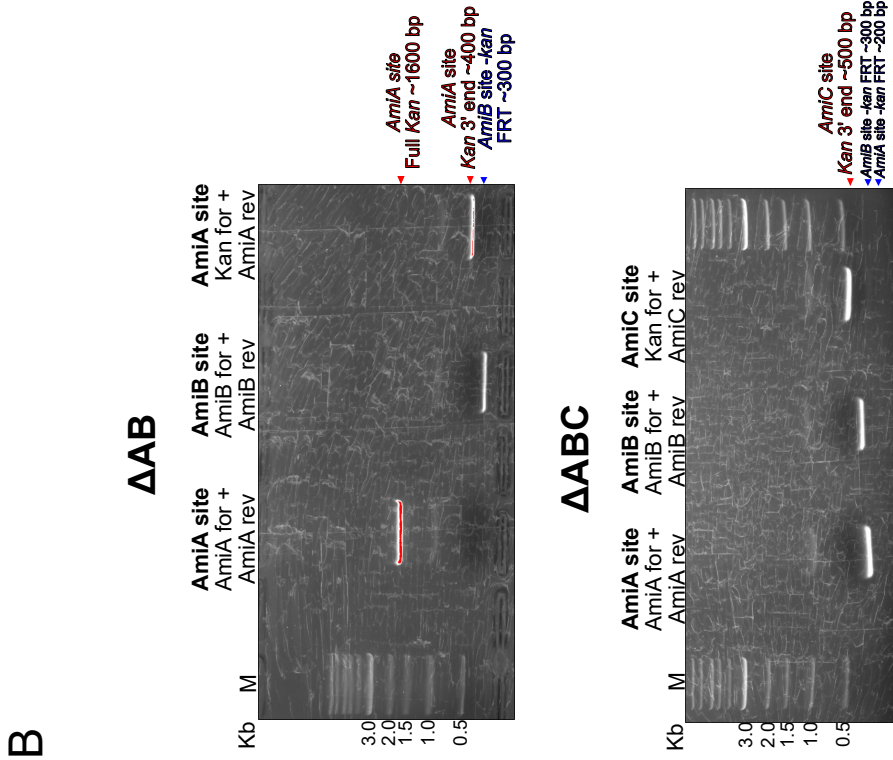
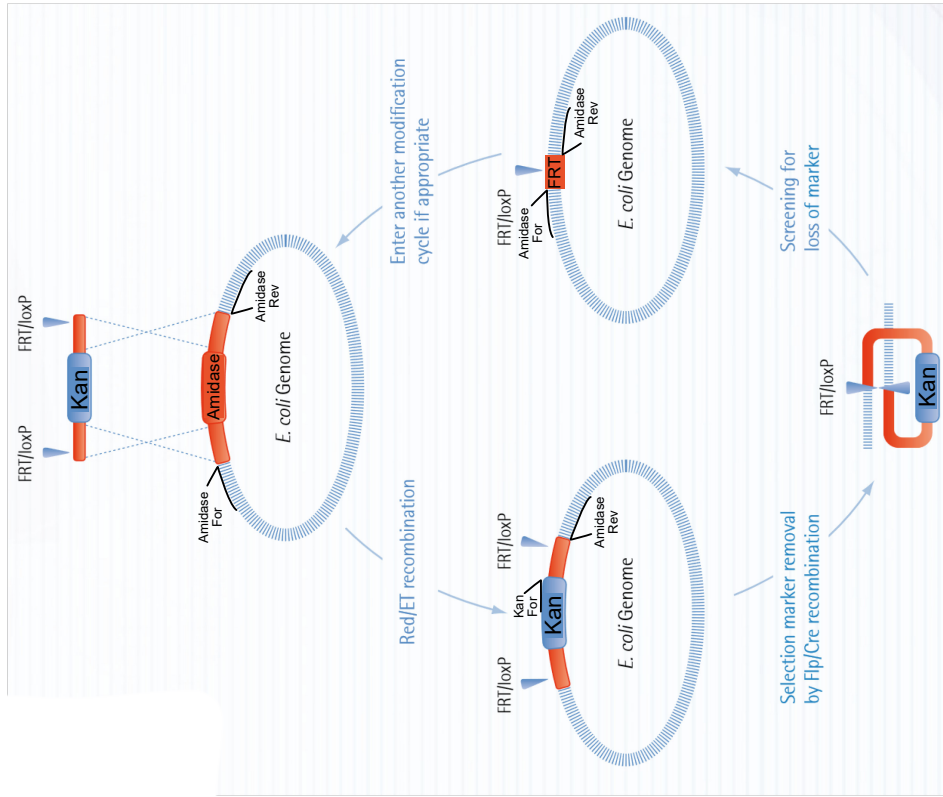


**Figure 32: Generating ( $\Delta amiab$ ) and  $\Delta amiabc$  amidase knockouts (A)** A brief overview on the Red/ET Recombination system from Gene Bridges. The primers labelled show the positioning in respect to the amidase genes. Diagram sourced and adapted from Red/ET Recombination Gene Bridges handbook (B) Confirming the ( $\Delta amiab$ ) amidase knockout, the size of the kan cassette at the AmiA size is the correct size and confirmed by kan specific primers with an external AmiA primer. The AmiB site only has FRT remaining from the removal of a previous kan cassette. (C) Confirming the  $\Delta amiabc$  amidase knockout, both the AmiA and AmiB sites lack the original genes with only a single FRT site remaining. The AmiC site is confirmed to contain a kan cassette at the location of the original AmiC gene, confirmed by the external AmiC primer.

### 4.3.2 FtsEX:EnvC pathway is essential for survival under low osmolarity and detergent conditions

In the literature and in (J. Cook et al., 2020), the effect of removing FtsEX and/or its functions were probed under low osmolarity and detergent conditions which produced interesting phenotypes produced by FtsEX knockout strains. Using the collection of knockouts within the FtsEX:EnvC:AmiA/B pathway, an investigation was undertaken to detect phenotypes during growth under stressful environments.

The knockout collection were subjected to LB standard conditions, low osmolarity (Lbon50 = No salt, 2-fold dilution of LB, half nutrients of LB, **Section 2.3.1**) and detergent (0.1 % SDS in LB **Section 2.3.1**) conditions during a 24 hour growth at 37°C. Each knockout was complemented by their respective proteins on a plasmid as a control. To further evidence any phenotypes produced, the same experiment was performed as a serial dilution assay on low osmolarity and detergent conditions spot plates to determine any differences between liquid and agar growth. For further reference of liquid or agar growth experiments further in this thesis, growth in LB is used as an viability assay, growth in Lbon50 is a measure of a cell's ability to survive osmotic and reduced nutrient pressures to test envelope integrity, usually used to determine any defects in peptidoglycan integrity. Lbon50 (1/2 diluted LB with no salt) to show the clearest phenotypes when the knockout strains are subjected to low osmotic pressure combined with a reduced nutrient condition. Lastly, growth in LB with detergent is a measure of outer membrane integrity and permeability. These conditions help determine defects in the membrane caused as a result of genomic knockouts and to determine if the knockout strains are resistant to stressful environments.

Starting with the single amidase knockouts, all three amidases behave similar to the wild-type BW25113 strain under all three conditions on the agar spot plates with little effect of low osmolarity and detergent conditions (**Figure 33 A/B**). A similar story in liquid growth occurs also (**Figure 34**), with little difference between the BW25113 strain and the single amidase knockouts with the exception of  $\Delta amiA$  and  $\Delta amiC$  under detergent conditions appears to have a reduced peak turbidity which is rescued when the respective proteins are reintroduced. Interestingly, this phenotype is not present in  $\Delta amiB$ , suggesting a previously mentioned redundancy in the amidase system.

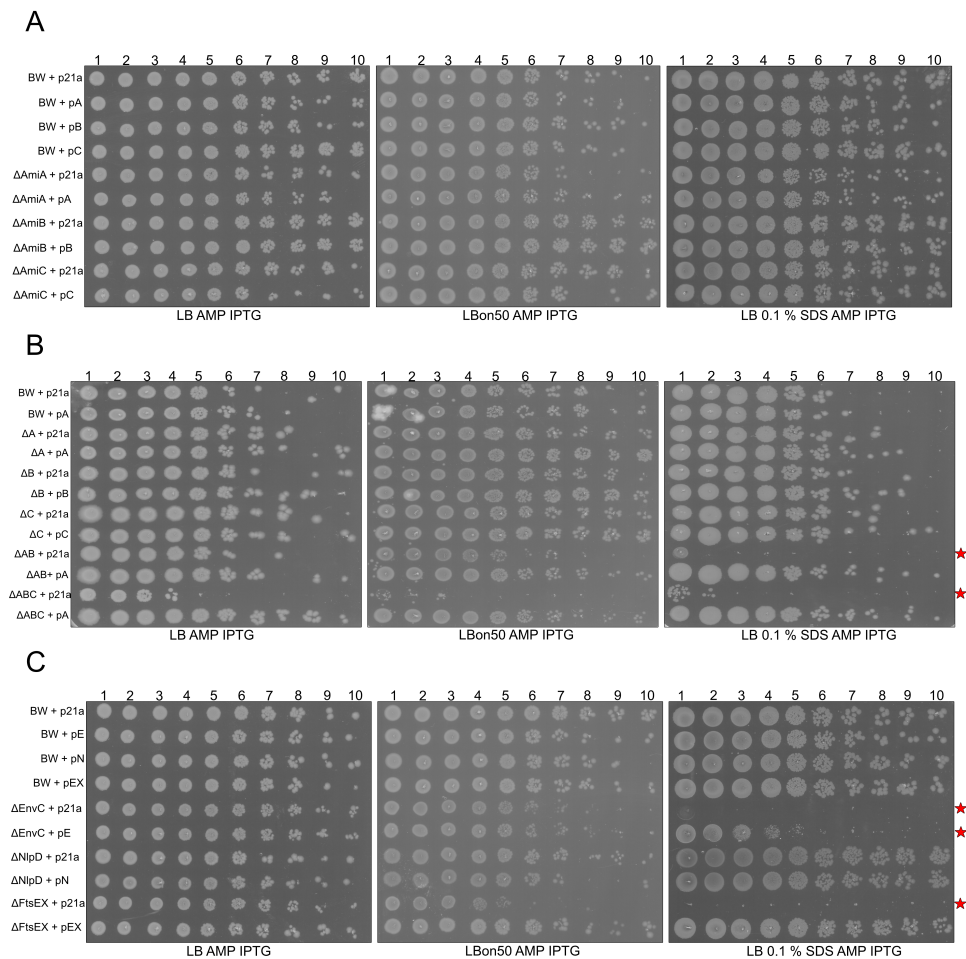


**Figure 33: FtsEX:EnvC pathway susceptibility to agar low osmolarity and detergent conditions.** Each dilution is a 10-fold. (A) Single amidase knockout screen, complemented with pET21a containing their respective genes. BW25113 is a control and expressed with all three amidases individually as a control. (B) Single, double ( $\Delta amiab$ ) and triple ( $\Delta amiabc$ ) amidase screen, complemented with their respective protein or AmiA only in the case of the double ( $\Delta amiab$ ) and triple ( $\Delta amiabc$ ) knockouts. (C) Regulator screen, complemented with their respective protein. BW25113 is expressed with all three amidases and both amidase regulators individually as a control. p21a = empty pET21a vector. pA = pET21a containing *amia*, pB = pET21a containing *amib*, pC = pET21a containing *amic*, pE = pET21a containing *envc*, pEX = pET21a containing *ftsEX*. All pET21a plasmids containing genes were all full versions of the genes containing their native signal sequences. This experiment had three technical repeat plates per condition per a total of three biological repeats. Plate images were modified to greyscale for clarity. Starred lanes indicate notable phenotypes.

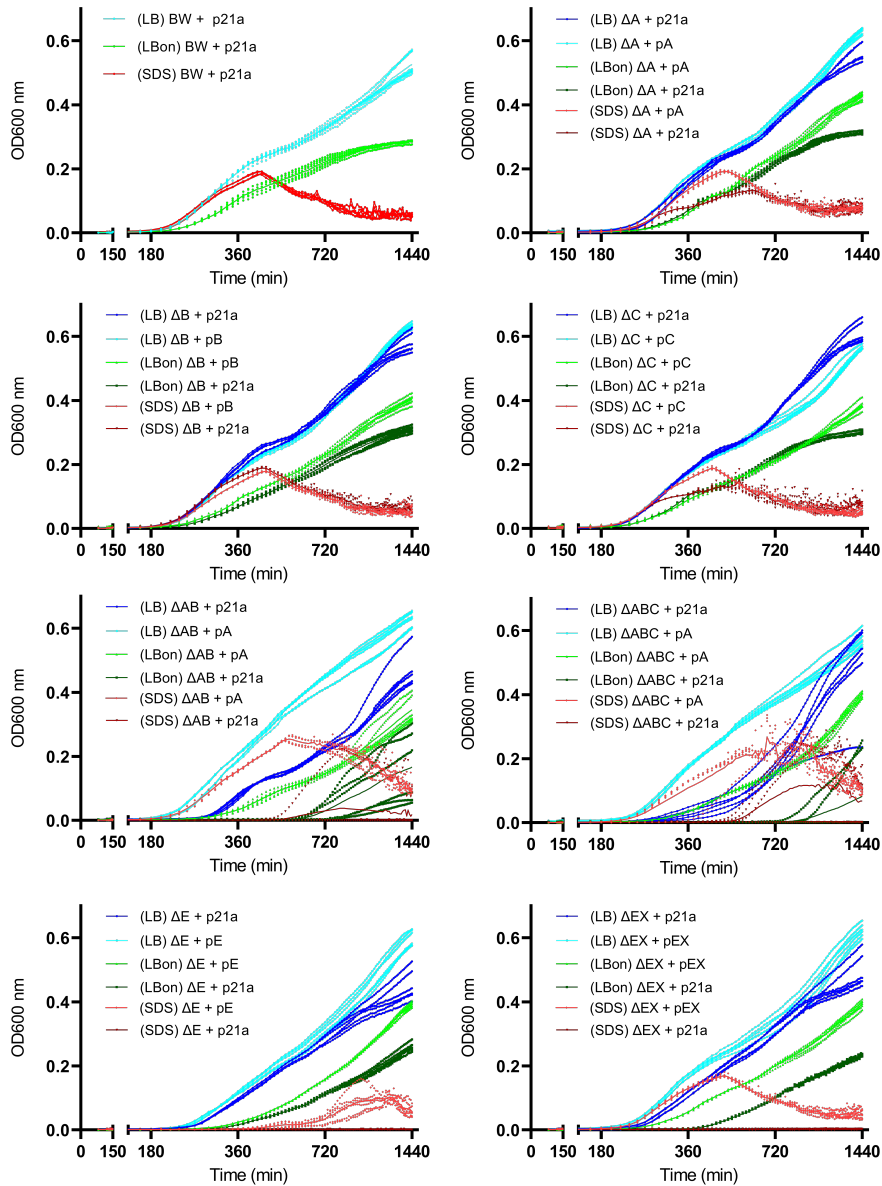


**Figure 34: FtsEX:EnvC pathway susceptibility to agar low osmolarity and detergent conditions under liquid growth.** Each replicate is plotted and a median line is fitted to each condition. Colours are used for each condition; Blue = LB, Green = Lbon50 (Low osmolarity) and Red = 0.1 % SDS (detergent). Culturing starts at 0.001 OD<sub>600</sub> and grown at 37°C for 24 hours with mild shaking with readings after every 15 minutes.

First of all, it is worth noting the unique growth curve results, as these differ from a standard bacterial growth curve. As seen in **Figure 34**, none of the cultures reach a stationary phase, which is likely down to the shaking incubation time. Due to limitations in the spectrophotometer used to incubate and measure the readings for the growth curves, it was only able to shake every 15 minutes for 30 seconds. This likely limited the bacterial growth and not allow sufficient oxygen to reach all growing cells. Secondly, the growth in SDS can be erratic as there appears to be a threshold growth  $OD_{600}$  until bacteria begins to lyse which can increase  $OD_{600}$  as a side effect. There is also appears to be stochastic mechanism in detergent growth where sometimes cultures will not grow and sometimes they will depending if the initial bacterial inoculation survives. This trend appeared in all sensitive knockouts and their three technical repeats per the three biological repeats performed.

The  $\Delta amiab$  and  $\Delta amiabc$  amidase knockouts present stronger phenotypes under all three conditions compared to their single knockout counterparts. Under agar growth conditions (**Figure 33 B**), only the  $\Delta amiabc$  knockout struggles to grow on LB only to 4 dilutions whereas the  $\Delta amiab$  strain grows to about 8 dilutions. Under low osmolarity conditions, a similar pattern appears with the  $\Delta amiab$  strain growing to 7 dilutions, a mild phenotype compared to the BW strain however the  $\Delta amiabc$  knockout only grows to the 3rd dilution, showing a strong susceptibility to low osmolarity conditions. The detergent conditions have both  $\Delta amiab$  and  $\Delta amiabc$  knockouts strongly susceptible to detergent stress. Both knockouts were rescued by AmiA under all three conditions, suggesting AmiA alone is sufficient to restore intrinsic detergent and low osmolarity condition resistances.

The phenotypes of both  $\Delta amiab$  and  $\Delta amiabc$  knockouts under liquid growth is more stochastic in nature (**Figure 34**). Both the  $\Delta amiab$  and  $\Delta amiabc$  strains have a longer lag phase and reduced gradient exponential phase and reduced maximum turbidity compared to the BW strain but is completely rescued again by AmiA. The low osmolarity conditions exaggerate the same phenotype with both  $\Delta amiab$  and  $\Delta amiabc$  knockouts generally only growing around 720 minutes but again completely restored by AmiA. Lastly, under detergent conditions, both  $\Delta amiab$  and  $\Delta amiabc$  knockouts will barely grow above 0.1  $OD_{600}$  after an extended lag phase however the detergent resistance is restored after AmiA is introduced. As indicated by the agar spot plates, both the ( $\Delta amiab$ ) and  $\Delta amiabc$  knockout amidase strains have a severe susceptibility to low osmolarity and detergent conditions (with the  $\Delta amiab$  strain surviving slightly improved under low osmolarity conditions) where

presumably majority of the cells are killed however the introduction of only AmiA is sufficient to restore intrinsic resistance to these conditions.

In agreement with (J. Cook et al., 2020),  $\Delta envc$  and  $\Delta ftsex$  knockouts only presented phenotypes under low osmolarity and detergent conditions. On the agar spot plates, both knockouts grew like the BW wild type on LB, however  $\Delta ftsex$  had reduced growth on low osmolarity conditions and was rescued by *FtsEX* to wild type levels. EnvC had a mild growth hindrance on the low osmolarity plate however was only weakly rescued when EnvC was complemented back in the cell. Interestingly, under detergent conditions both knockouts do not grow (barring a few tiny colonies on the *EnvC* knockout on the first dilution), the *FtsEX* knockout is completely restored to wild type levels upon *FtsEX* expression however again, EnvC expression only mildly restores the  $\Delta envc$  knockout to half the wild type levels. As a control, EnvC expressed in the BW25113 wild-strain does not have any effect. The same story is told in the growth curves. Normal growth under LB conditions, increased lag-phase, exponential phase and peak turbidity in both  $\Delta envc$  and  $\Delta ftsex$  knockouts, but again both rescued by their respective proteins. The detergent conditions again show an extreme sensitivity without *envc* or *ftsex*, but the  $\Delta envc$  knockout is only rescued weakly by EnvC whereas  $\Delta ftsex$  is restored to wild-type levels upon expression of *FtsEX*. It would appear that EnvC expressed by a plasmid into the periplasm produces an imperfect complementation which was also seen in (J. Cook et al., 2020), which is not uncommon in complementation experiments.

It is worth noting  $\Delta nlpd$  was initially investigated for a phenotype via the spot plates, however, no obvious phenotype was observed and the focus on this thesis is the *FtsEX:EnvC:AmiA/B* pathway, therefore the knockout was not further investigated to manage workloads.

Overall, the single amidase knockouts ( $\Delta amiA$ ,  $\Delta amiB$  and  $\Delta amiC$ ) individually do not affect the low osmolarity or detergent resistances of the cell, however, upon the removal of at least two or more amidases ( $\Delta amiab$  and  $\Delta amiabc$ ), cells become susceptible to these stressful environments but can be rescued by only one amidase, AmiA. The regulators, EnvC and *FtsEX*, while not key in standard growth conditions, exhibit key importance in the cell's resistance to detergent and less so in low osmolarity conditions. EnvC is not sufficient to fully rescue  $\Delta envc$  knockout under low and osmolarity and detergent conditions.

### **4.3.3 Cell wall permeability is a symptom of knockouts in the FtsEX:EnvC pathway**

To further characterise the effect of these divisome mutants on the stability and permeability of the cell wall, Minimal inhibitory concentration experiments were performed using the Gram-positive antibiotic, vancomycin (**Section 4.3.3**) and the detergent, Sodium dodecyl sulfate (SDS) (**Figure 36 MICs**). Vancomycin is a particularly useful antibiotic to determine whether any divisome knockout strains have defective outer membranes as vancomycin has a large molecular weight (1,449.3 g/mol) and cannot pass through outer membrane porins, therefore, any effect seen is a possible sign that the outer membrane permeability is defective. This is the same case for detergent conditions, with any sensitivity seen, is a indication of issues with outer membrane integrity.

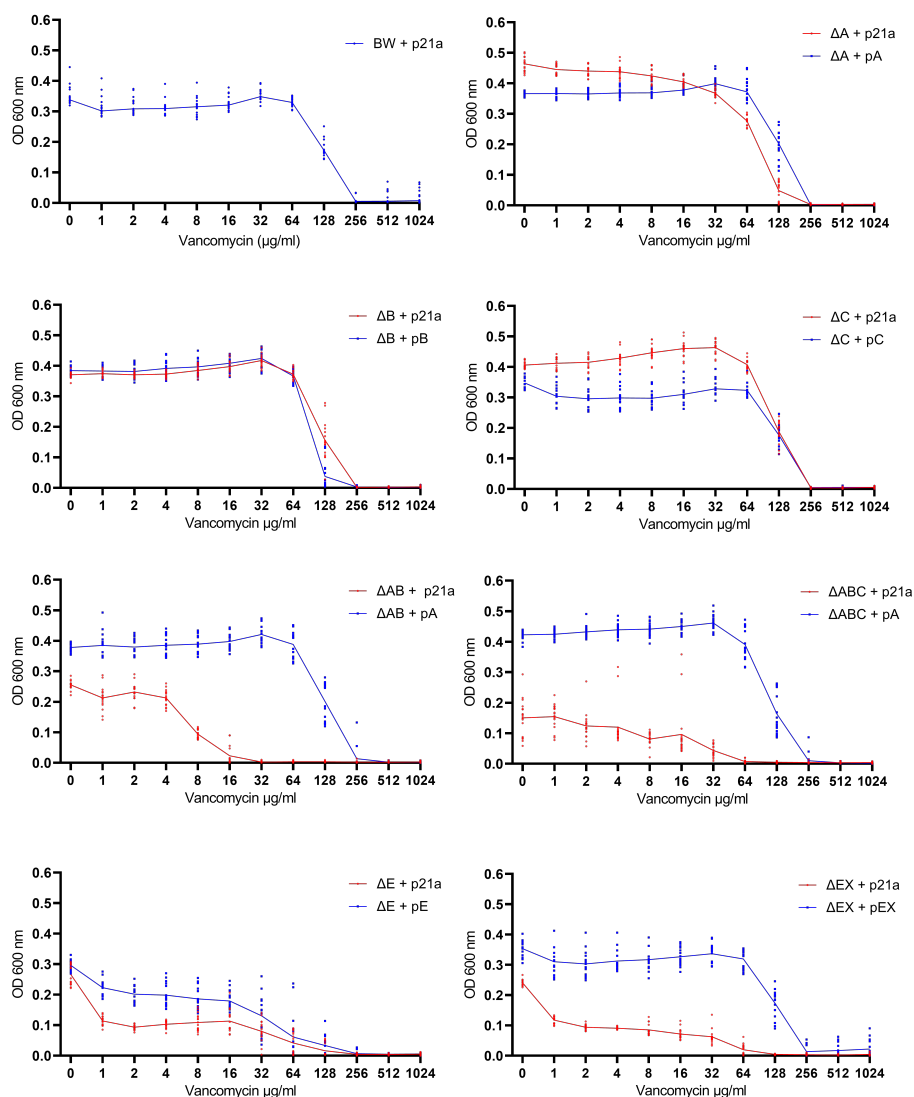


**Figure 35: FtsEX:EnvC:AmiA/B pathway knockouts are susceptible to Vancomycin.** Minimal inhibitory concentration experiments with all replicates presented. Turbidity of cells within different concentration of vancomycin after 18 hours at 37°C. The median line is mapped on sixteen repeats. Complemented cells with pET21a with respective genes (blue) and deficient cells with pET21a (red). Method reference 2.5.4.

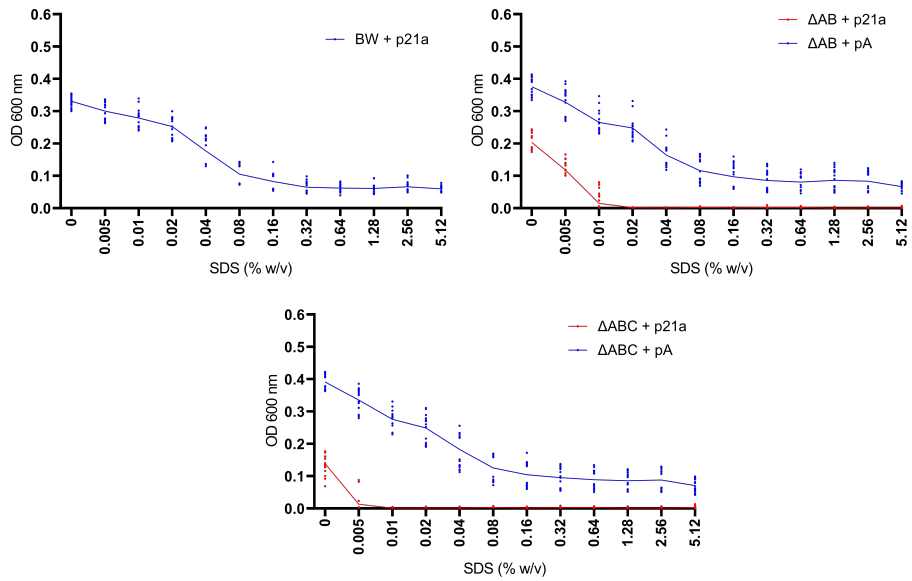


**Figure 36: ( $\Delta amiab$ ) and  $\Delta amiabc$  amidase knockouts are susceptible to detergent.** Minimal inhibitory concentration experiments with all replicates presented. Turbidity of cells within different concentration of SDS after 18 hours at 37°C. The median line is mapped on sixteen repeats. Complemented cells (blue) and deficient cells with pET21a (red). Method reference 2.5.4

Although having the same MIC as the wild-type at 256  $\mu\text{g/ml}$  vancomycin, the single amidase knockouts ( $\Delta\text{amiA}$ ,  $\Delta\text{amiB}$  and  $\Delta\text{amiC}$ ) do exhibit increased turbidities at lower concentrations of vancomycin. Both  $\Delta\text{amiA}$  and  $\Delta\text{amiC}$  knockouts growing better without expression of their respective proteins at lower concentrations of vancomycin, perhaps the plasmid expression of AmiA or AmiC causes cells a high energy cost or inappropriate levels of amidase are produced, causing some unwanted peptidoglycan hydrolysis. Another hypothesis is the expression of AmiA or AmiC via the pET21a vector may affect other bacterial systems outside the control of this experiment, reducing normal cellular growth speed. The  $\Delta\text{amiB}$  knockout, has no change in resistance to vancomycin with or without AmiB expressed.

The  $\Delta\text{amiab}$  and  $\Delta\text{amiabc}$  amidase knockouts show a strong sensitivity to vancomycin but are completely rescued by AmiA alone, similar to the previous experiments in this chapter. Interestingly, the MIC for  $\Delta\text{amiab}$  is 32  $\mu\text{g/ml}$  but for  $\Delta\text{amiabc}$  is higher at 64  $\mu\text{g/ml}$ . It is worth noting however that the  $\Delta\text{amiabc}$  struggles to grow above 0.2  $\text{OD}_{600}$  and is more stochastic in nature with a number of replicates growing up to 0.4  $\text{OD}_{600}$ . It could be perhaps that without all three amidases, cells are lysing under antibiotic pressure and can cause an increase in  $\text{OD}_{600}$  as the debris reaches the bottom of the growth wells. Compared to the wild-type however, both  $\Delta\text{amiab}$  and  $\Delta\text{amiabc}$  knockouts indicate a sensitivity to vancomycin, suggesting the antibiotic is able to cross the outer membrane in these knockouts, allowing vancomycin to inhibit peptidoglycan biosynthesis. Further evidencing an unstable peptidoglycan and a weakened integrity of the outer membrane, SDS MICs of both the  $\Delta\text{amiab}$  and  $\Delta\text{amiabc}$  knockouts confirm a strong sensitivity to detergent (**Figure 36**) with the MIC of the  $\Delta\text{amiab}$  strain at 0.02 % SDS and at 0.01 % SDS for the  $\Delta\text{amiabc}$  strain where the wild-type continues to survive at 5.12 % SDS. To sum up, the knockout strains  $\Delta\text{amiab}$  and  $\Delta\text{amiabc}$ , show reduced cell membrane integrity and sensitivity to antibiotic and detergent stresses.

Lastly, the regulator knockouts  $\Delta\text{envC}$  and  $\Delta\text{ftsEX}$  appear to have a mild sensitivity to vancomycin. EnvC-deficient cells produce low peak turbidities under vancomycin conditions however still keep the same MIC at 256  $\mu\text{g/ml}$  compared to wild-type. Adding EnvC expression only mildly increases peak growth of the EnvC-deficient cells, in line with the previous experiments in this chapter of EnvC only mildly rescuing the EnvC-deficient cells. FtsEX-deficient cells on the other

hand have significantly reduced growth under vancomycin conditions and has a 2-fold reduced MIC compared to wild-type. Again, like the previous experiments, FtsEX expression to these cells completely rescues the cells back to wild-type levels including the MIC value. Therefore cells lacking FtsEX has a greater negative effect on the permeability of the outer membrane with EnvC only weakly affecting the outer membrane permeability.

Overall, the MICs align with the previous experiments where the single amidase knockouts show little effect on the cell permeability and integrity however the  $\Delta amiab$ ,  $\Delta amiabc$  strain,  $\Delta envc$  and  $\Delta ftsex$  all exhibit sensitivities to vancomycin, indicating possible cell membrane permeability and a lack of cell stability.

#### **4.3.4 Proper cell separation is a key function of the FtsEX:EnvC pathway**

As previously described in the literature and in (J. Cook et al., 2020), cells lacking or containing defective FtsEX produce a chaining phenotype, presumably caused by a lack of amidase regulation to hydrolyse the final septal peptidoglycan during bacterial cell division along with a negative effect on FtsEX's other functions like promoting FtsA activity in recruiting downstream division components. In multiple studies (Heidrich et al., 2001; Mueller & Levin, 2020; Uehara et al., 2010), it is known that  $\Delta amiabc$  amidase mutants also produce a chaining phenotype, however a direct comparison of all the FtsEX:EnvC:AmiA/B knockouts and complemented has not been performed in conjunction with the previous experiments. Here the knockout collection is visualised under phase-contrast with their respective complementing proteins (**Figure 37**, **Figure 38**).

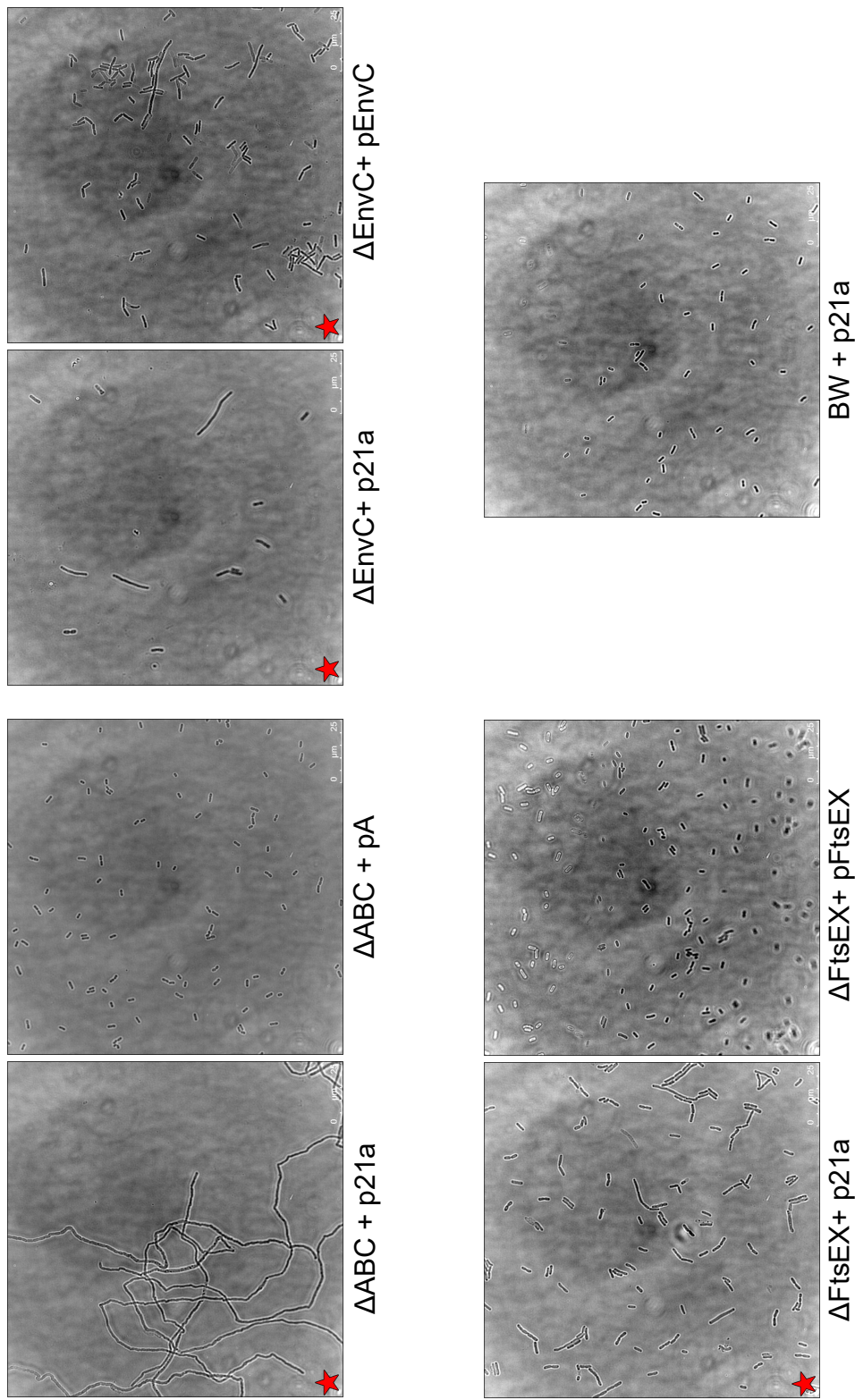


**Figure 37: FtsEX:EnvC:AmiA/B pathway knockouts produce varying chaining phenotypes.** Knockouts were transformed with either pET21a or complemented with their respective gene present on pET21a, *amia* only however for the  $\Delta amiab$  and  $\Delta amiabc$  amidase knockouts. Images were taken at 100x magnification with phase contrast imaging. Scale bars are located in the bottom right corner of each image. At least 10 locations of each slide were examined to ensure images are representative of the cellular population. This experiment had two complete biological repeats. p21a = empty pET21a vector, pAmiA = pET21a containing *amia*, pAmiB = pET21a containing *amiB*, pAmiC = pET21a containing *amiC*, pEnvC = pET21a containing *envc*, pFtsEX = pET21a containing *ftsEX*. All pET21a plasmids containing genes were all full versions of the genes containing their native signal sequences. Starred images indicate notable chaining phenotypes. Images were selected to represent the majority of cells seen during the experiments. Images were adjusted by colour inversion and scaled by contrast to provide clarity.

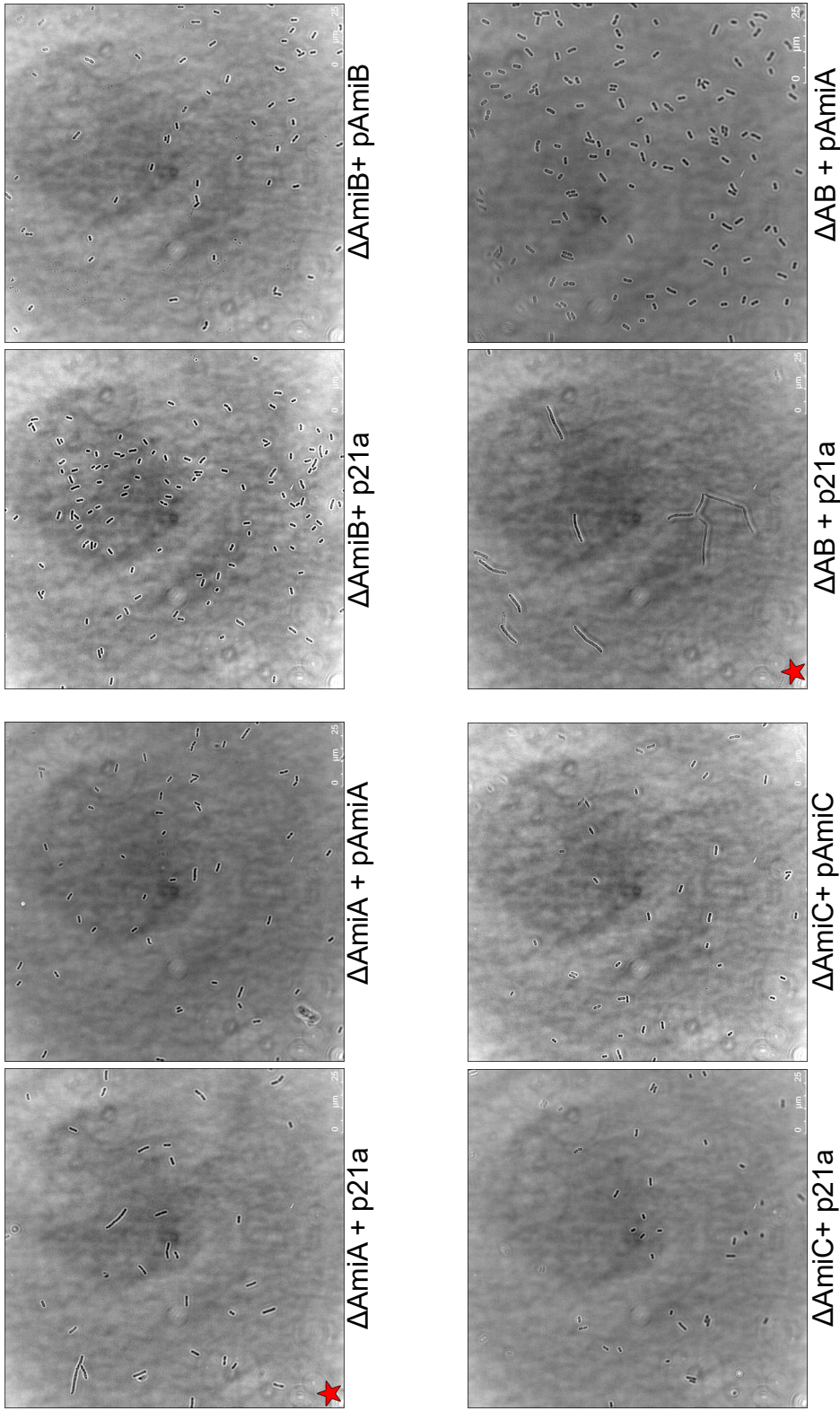


**Figure 38: Amidase knockouts produce varying chaining phenotypes.** Knockouts were transformed with either pET21a or complemented with their respective gene present on pET21a, *amia* only however for the  $\Delta amiab$  and  $\Delta amiac$  amidase knockouts. Images were taken at 100x magnification with phase contrast imaging. Scale bars are located in the bottom right corner of each image. At least 10 locations of each slide were examined to ensure images are representative of the cellular population. This experiment had two complete biological repeats. Starred images indicate notable chaining phenotypes. p21a = empty pET21a vector, pAmiA = pET21a containing *amia*, pAmiB = pET21a containing *amib*, pAmiC = pET21a containing *amc*, pEnvC = pET21a containing *envc*, pFtsEX = pET21a containing *ftsEX*. All pET21a plasmids containing genes were all full versions of the genes containing their native signal sequences. Images were selected to represent the majority of cells seen during the experiments. Images were adjusted by colour inversion and scaled by contrast to provide clarity.

It is worth noting that this experiment is a qualitative observation of knockout cells to see whether there is consistent chaining. It is to see whether chaining is present and if it is noticeably different by observation between the knockouts.

Starting with the single amidase knockouts,  $\Delta amiA$  is the only one exhibiting a phenotype where there are multiple short chained cells within all imaging sites of the slides imaged, notable when compared to the wild-type. This surprisingly is not present in the  $\Delta amib$  and  $\Delta amic$  amidase knockouts. AmiA rescues the weak chaining phenotype in  $\Delta amia$ , however it does suggest that AmiA has a more prominent role in keeping septal peptidoglycan hydrolysed during cell division compared to AmiB and AmiC, perhaps due to the differences in localisation or the fact AmiA is missing a targeting domain which AmiB and AmiC contain.

Unsurprisingly, the  $\Delta amiab$  and  $\Delta amiabc$  amidase knockouts produce a chaining phenotype. The  $\Delta amiab$  amidase knockout contains generally only short chained cells, with some cells showing partially separated ends, suggesting the cells are unable to complete the final separation of daughter cells, possibly due to residue septal peptidoglycan. This chaining phenotype is complemented completely by the expression of AmiA only. The  $\Delta amiabc$  amidase knockout exhibits an extreme chaining phenotype, with all cells joined together in a 'spaghetti' like fashion, again with cells showing partially separated poles from the next adjoining cell. Without all three division-associated amidases known in cell division (AmiA, AmiB and AmiC), the majority of the septal peptidoglycan is likely still intact, stuck throughout the chained cells, keeping them together. Only the expression of AmiA however is sufficient to rescue this phenotype back to wild-type like cells. The differences between the  $\Delta amiab$  and  $\Delta amiabc$  knockouts in previous experiments could be further explained by the chaining phenotypes.

The chaining phenotypes of the *EnvC*- and *FtsEX*-deficient cells are more unusual. Cells lacking *EnvC* show a chaining phenotype with a mixture of multi bacterium chains and other with only two cells attached together, presumably, stuck at the end of bacterial cell division with still intact septal peptidoglycan keeping the cells together. When complemented with a plasmid containing *EnvC* however, these cells do not clearly present like wild-type cells, they appear mildly more individual however the chaining remains, which is in line with the previous experiments where *EnvC* expression only weakly complements the phenotypes displayed in  $\Delta envc$ . Cells lacking *ftsEX* are more clear cut with an obvious chaining phenotype.

Upon the expression of FtsEX however, the cells are restored back to wild-type morphologies.

## 4.4 Discussion

The individual affects and roles of the FtsEX:EnvC:AmiA/B pathway were investigated in this chapter. Using a variety of microbiology techniques, a collection of divisome knockouts were studied for their phenotype on a number of environmental conditions.

The individual roles of each component in this amidase regulation pathway by analysing the effect of their absence on cell growth, membrane integrity and permeability, resistance to detergent and low osmolarity conditions and cell morphology. In line with the literature, the three division-associated periplasmic amidases (AmiA, AmiB and AmiC) in *E. coli*, appear to have a redundant role in hydrolysing septal peptidoglycan although with little to no phenotypes presenting in the single amidase knockouts. AmiA however does appear to have an effect on cell morphology and resistance to detergent, perhaps due to its more distributed expression across the periplasm (and lack of targeting domain) (Bernhardt & de Boer, 2003) although this would require further evidence of AmiA distribution throughout the cell cycle. As extensively shown in the literature and agreed with in this thesis,  $\Delta amiab$  and  $\Delta amiabc$  show that removing cell-division amidases, the ability of cells to separate and hydrolyse septal peptidoglycan becomes more defective with each amidase removed.

To further evidence the redundancy of these amidases, further double mutations should be created ( $\Delta amiAC$  and  $\Delta amiBC$ ) with all combinations of the three amidases complementing these knockouts in the same experiments to detect any differences of only one of the three amidases hydrolysing septal peptidoglycan. Although these knockout strains have been shown before in the literature (Heidrich et al., 2001), they have not been subjected to the experiments in this chapter. Furthermore, the  $\Delta amiab$  and  $\Delta amiabc$  strains used in this chapter should be complemented with AmiB and AmiC to compare if they can rescue the phenotypes shown in these cells like AmiA has used in this chapter. This chapter has shown differences in the three division-associated amidases in terms of function, and would be important to further investigate if there is a difference in function during cell division to explain why there are three amidases in *E. coli*. As a set, the three division-associated amidases in *E. coli* are essential for proper cell separation by hydrolysing septal peptidoglycan, without them, cells become sensitive to deter-

gent and Gram-positive antibiotics due to permeable membranes and a chaining phenotypes.

The type VII ABC transporter, FtsEX, has been further evidenced to have a key importance in regulating periplasmic amidases during cell division. As shown previously in (J. Cook et al., 2020), FtsEX-deficient and non-functional FtsEX cells were susceptible to low osmolarity conditions, detergent, Gram-positive antibiotics and produced chained cells. It is key to revisit that all experimental strains used in this chapter used the same background of BW25113 which can have an effect on the phenotypes seen. In (J. Cook et al., 2020), the MR10 strain (*LacZ* deficient derivative of *E. coli* strain MG1655) which lacked *FtsEX* was more susceptible to vancomycin than found in the BW25113 strain (JC7, **Table 2**) lacking *FtsEX*. It is therefore important to mention that the genetic background of the *E. coli* or other species can also be determinate in the phenotypes witnessed of divisome mutants on cell envelope integrity and sensitives to different stressful environments. It would be worth exploring the phenotypes of the same knockouts in other genetic backgrounds to determine the genotypes which produce more extreme phenotypes that may indicate further interactions or pathways that interact with the divisome. The idea behind this would be could these phenotypes shown in this chapter be created in other bacterial species, indicating some conservation the amidase regulation pathway.

The amidase regulator, EnvC, however has not been deeply characterised before in the literature aside from LytM amidase binding mutations and some knockout viability analysis (Peters et al., 2013b). EnvC-deficient cells presented similar phenotypes to  $\Delta$ *ftsEX* in terms of chaining, susceptibility to detergents, Gram-positive antibiotics and low osmolarity conditions. Unlike the other divisome knockouts however, EnvC complementation via a pET21a plasmid (containing *envC*) only mildly rescued EnvC-deficient phenotypes across all assays in this chapter. Interestingly, an overexpression of EnvC has been shown to produce irregular and swollen cells (Hara et al., 2002), however this study suggested it was the activity of the C-terminus hydrolytic activity which has since been proven inactive by (J. Cook et al., 2020), therefore exaggerated activation of AmiA and AmiB is more likely to be the cause. The BW25113 strain however lacks the genotype for overexpression (**Table 2**) and control expression of EnvC via pET21a did not appear to produce any notable phenotype in the growth curve, spot plate and MIC experiments. This could just be the result of an imperfect complementation due to a

plasmid gene expression pathway which produces inappropriate levels of EnvC in the periplasm that causes a dysregulation of other regulation systems during cell division. It is worth noting however as although the native signal sequences of the genes were used to localise proteins where they are targeted to go, further controls would be prudent to check proper protein localisation. An experiment for this could be fluorescence microscopy with cells expressing fluorescence tagged genes used in this chapter and confirm that all proteins reached the periplasm and the division septum.

Further study would be required to assess if expression level affects EnvC activity on the cell's ability to regulate periplasmic amidases during cell division.

To summarise, each component of the FtsEX:EnvC:AmiA/B pathway has been characterised whether cells deficient in these proteins cause cellular instability, membrane barrier permeability, chaining morphology, growth defects, sensitivity to detergent and Gram-positive antibiotics.

This chapter is another step forward in understanding the fundamentals of *E. coli* cell division and amidase regulation which can be applied to multiple other species and systems. This work can provide a foundation to perform further mutational and structural analysis on these components to assess key functional residues and interactions. The understanding that without specific components of this pathway, cells become susceptible to detergents and Gram-positive antibiotics may provide alternative targets for new treatments of Gram-negative bacterial infections.

## **5 Structure of *E. coli* amidase, AmiA**

### **5.1 Abstract**

The structure of *E. coli* division amidases have been a topic of interest due to their importance in hydrolysing septal peptidoglycan during the final stages of bacterial cell division. Here is presented a 2.35 angstrom resolution crystal structure of *E. coli* type 3 periplasmic amidase, AmiA. The structure further solidifies the hypothesis of a self-regulation mechanism of a blocking helix positioned over an active site containing a zinc co-factor. A previously unmodeled feature in other related type 3 amidase structures, a deemed interaction helix has been identified to potentially interact with the AmiA regulator, EnvC due to the presence of unusual hydrophobic solvent facing residues in this helix. AmiA would be a suitable model for other amidase systems due to its small length, simplicity and high conservation in active site residues and core amidase fold residues.

## 5.2 Introduction

The cell division amidases in *E. coli* are essential in hydrolysing septal peptidoglycan during the end stages of bacterial cell division. In *E. coli*, there are three N-acetylmuramoyl-L-alanine type 3 *E. coli* periplasmic amidases used in division; AmiA, AmiB and AmiC (Du & Lutkenhaus, 2017; Levin & Janakiraman, 2021). These amidases are regulated by EnvC (for AmiA and AmiB) and NlpD (AmiC) by direct interaction causing a currently undetermined structural mechanism to activate the amidases during cell division. It has been suggested that these amidases are self-regulated by a blocking helix which prevents the zinc based active site interacting with peptidoglycan (Rocaboy et al., 2013) and interaction with the respective regulator exposes the active site. The molecular mechanism however of how this occurs is currently undetermined; what conformational change occurs in the amidases during regulator interaction? Where and how does this interaction take place in both proteins? Are there other conformational changes in the amidase aside from the removal of the blocking helix from the active site? The answers to these questions are currently unknown.

The structure of *E. coli* AmiC was the first type 3 amidase to be solved presenting an AMIN domain, thought to bind peptidoglycan and promote proper localisation to the division site, a linker domain and a catalytic domain with a zinc active site blocked by a blocking helix (Rocaboy et al., 2013). A orthologue of the *E. coli* AmiB from *Bartonella henselae* Houston 1 was also solved, although only showing the catalytic domain (D. C. Yang et al., 2012b). This further evidenced a blocking helix covering conserved zinc-binding residues for an active site, also indicating conservation in domain folding of this catalytic domain to AmiC (Rocaboy et al., 2013). Lastly, the smallest of the three amidases, AmiA has not been structurally determined to test whether this potential type 3 amidase follows the same self-regulation and conservation to that of the other *E. coli* amidases.

## 5.3 Results

### 5.3.1 Generating *E. coli* AmiA crystals and X-ray diffraction

The first stages of obtaining a crystal structure of *E. coli* AmiA is by protein expression and purification, crystallisation trials and x-ray diffraction. Fortunately, the successful expression and purification of TB1034 (pET21A, AmiA-His) was relatively simple for his-tagged AmiA due to its exceptional expression. Using purification methods detailed in Section 2.6, AmiA-His was successfully purified (**Figure 39A**). It is worth noting the purification shown by SDS-PAGE in **Figure 39A** does appear low purity with multiple other contaminating proteins present, there was however an overabundance of AmiA present (nearly 70 mg/ml in the final stock) which was sufficient to override the other proteins and successfully crystallise AmiA. Using a higher concentration of imidazole in washes in the immobilised metal affinity purification did produce significantly lower concentrations of AmiA but purer, however this was often insufficient concentrations of AmiA to setup crystal trials.

Crystallisation trials were setup using the sitting drop vapour diffusion method at RT. Diffraction quality crystals were obtained in the structure screen 1+2 screen (Molecular dimensions) in condition A7/C5/C6 in a 96-well plate (**Table 3**). Crystals appeared after 2 weeks and grew to diffraction size after another 2 weeks (**Figure 39B**). These crystals were collected by loop and immersed in 20 % glycerol by Dr Allister Crow, packaged appropriately to send to Diamond Light Source in Oxford for X-ray diffraction analysis, X-ray diffractor controlled remotely by Dr Allister Crow and Tyler Baverstock during data collection. There was successful diffraction crystals at the resolution of 2.35 angstroms (**Figure 39C**).

**Table 3: AmiA crystallisation conditions**

<b>Crystal Screen</b>	<b>Position</b>	<b>Condition</b>	<b>Reference</b>
Structure Screen 1 + 2	A7	2 M Ammonium acetate, 0.1 M sodium citrate, 30 % PEG 4000, pH 5.6	Molecular Dimensions
Structure Screen 1 + 2	C5	1.4 M Sodium citrate tribasic dihydrate, 0.1 M sodium HEPES, pH 7.5	Molecular Dimensions
Structure Screen 1 + 2	C6	2 M Ammonium sulphate, 0.1 M sodium HEPES, 2 % PEG 400, pH 7.5	Molecular Dimensions

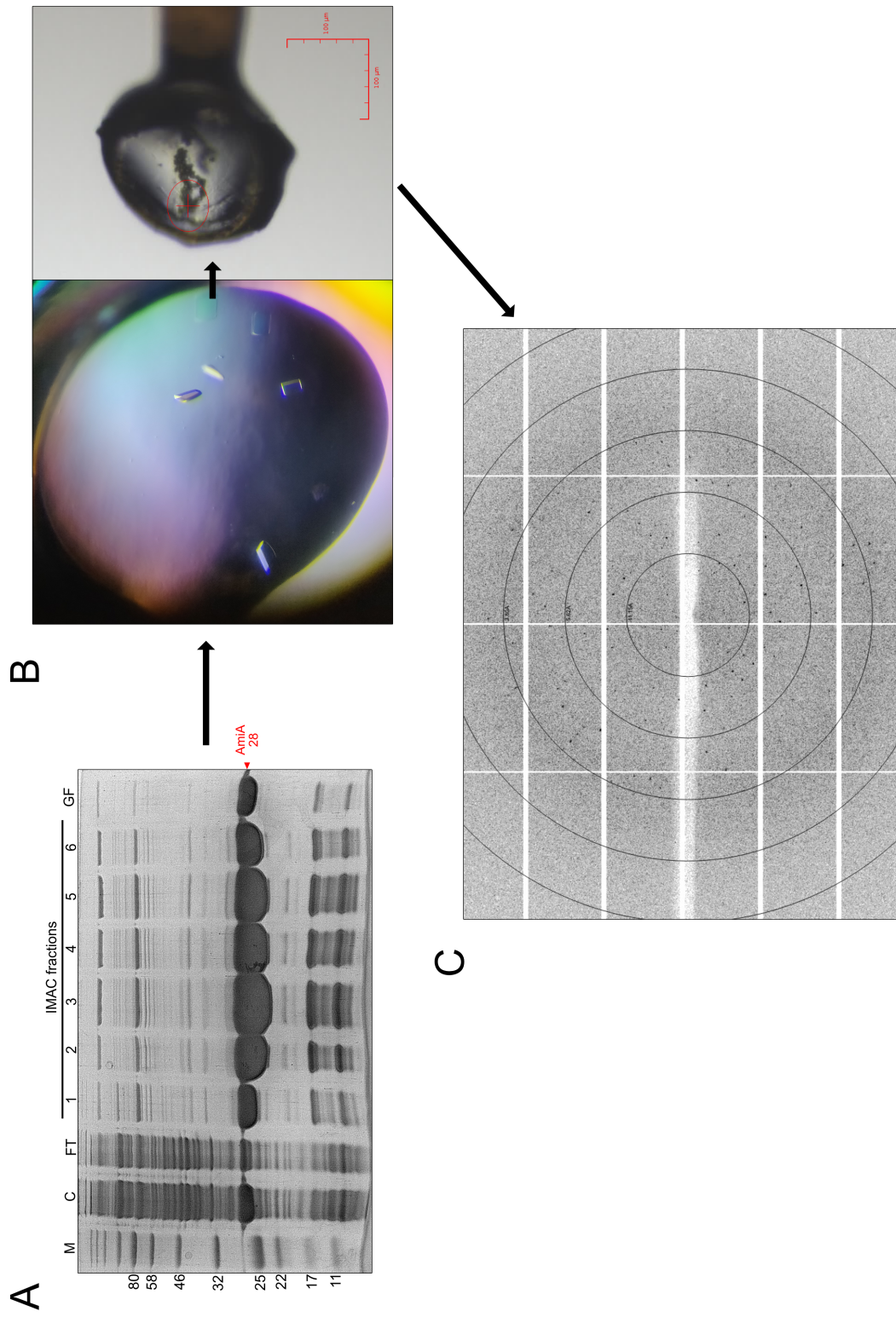


**Figure 39: AmiA from purification to diffraction pattern.** (A) Purification gel of AmiA. C = Crude extract, FT = Flow-through, IMAC = immobilised metal affinity chromatography. (B) Left = Growing crystals of AmiA in 1.4 M Sodium citrate tribasic dihydrate, 0.1 M sodium HEPES, pH 7.5 condition. Right = Crystal present in loop during remote operation at Oxford synchrotron. (C) Snapshot of diffraction pattern of a successfully diffracting AmiA crystal.

### 5.3.2 AmiA is a typical N-acetylmuramoyl-L-alanine type 3 *E. coli* periplasmic amidase

Initial processing including space group determination, scaling and merging were performed on the Diamond synchrotron server. Phases were determined by molecular displacement using a similar structure, PDB:5emi by using Phaser (McCoy et al., 2007). Phases were improved using solvent flattening and histogram matching using Parrot (Thain & Livny, 2005). Automated model building was performed in Buccaneer (Winn et al., 2011) to improve residue refinement. Models were completed using alternating rounds of model re-building via Coot (Emsley et al., 2010) and refinement via Refmac (Murshudov et al., 1997). Tools in Coot (Emsley et al., 2010) were used to assess geometry and Rampage (Lovell et al., 2003) to assess the distribution of backbone angles in the Ramachandran plot. Coordinates and structure factors have been deposited at the protein data bank. Further analysis of the structure used Pymol (LLC, 2023). Due to unwell-defined electron density, there are 7 missing residues at the extreme end of the C-terminus. As the AmiA structure has two molecules in the asymmetric unit, it is noted that in Chain B residues 178-192 are smeared in the electron density however has been built based on chain A which contained better electron density. . The presence of zinc was confirmed using X-ray fluorescence and calculation of anomalous difference maps.

The crystal structure of *E. coli* AmiA was determined by X-ray crystallography of successfully diffracting crystals to a 2.35 angstrom resolution. Each asymmetric unit contains two AmiA molecules. The full set of diffraction and refinement statistics are presented in **Table 4**. The structure of AmiA (**Figure 40A**) shows a typical N-acetylmuramoyl-L-alanine type 3 *E. coli* periplasmic amidase catalytic domain fold containing a layer of six-beta sheets and six alpha helices. AmiA contains three areas of interest; a blocking helix, an interaction helix and an active site containing zinc-binding residues. The active site contains a set of zinc-binding residues all bound to a single zinc atom (**Figure 40B, orange**); His 65, Glu80, His133, Asp135, Glu 167 and a nearby non-zinc binding potential active site residue, Glu242 . This active site however is blocked by a helix termed the 'blocking helix' (**Figure 40A, red**) (residues 151-177) which would be assumed to prevent peptidoglycan binding, a system of self-regulation as seen in AmiB and AmiC previously (Rocaboy et al., 2013; D. C. Yang et al., 2012b).

Another feature of note is an unusual helix adjacent to the blocking helix, which is oddly departed from the main amidase fold with a set of hydrophobic residues protruding outwardly into solvent (**Figure 40C, yellow**); Leu184, Leu185, Val188, Leu189, Leu192. Interestingly, during model building, this helix showed disparity between the two molecules of the asymmetrical unit in terms of positioning and electron density, where the helix in the molecule presented in (**Figure 40A**) was well defined but the other molecule lacked consistent electron density. This suggests this is a mobile element, previously uncaptured by other *E. coli* or ortholog amidase structures. This helix is termed the 'interaction helix' as it has the potential to be an interaction site for a number of reasons; It is positioned away from the rest of the main amidase catalytic fold, it has an unusual set of solvent-facing hydrophobic residues on its surface and appears to be mobile in nature upon closer inspection of the electron density map which could mean it is stabilised by the interaction of another protein.

In summary, AmiA is the simplest form of *E. coli* type 3 amidase structurally solved containing only the catalytic domain however highlighting a self-regulation system over the zinc-based active site and a potential mobile helix possibly important for EnvC interaction.

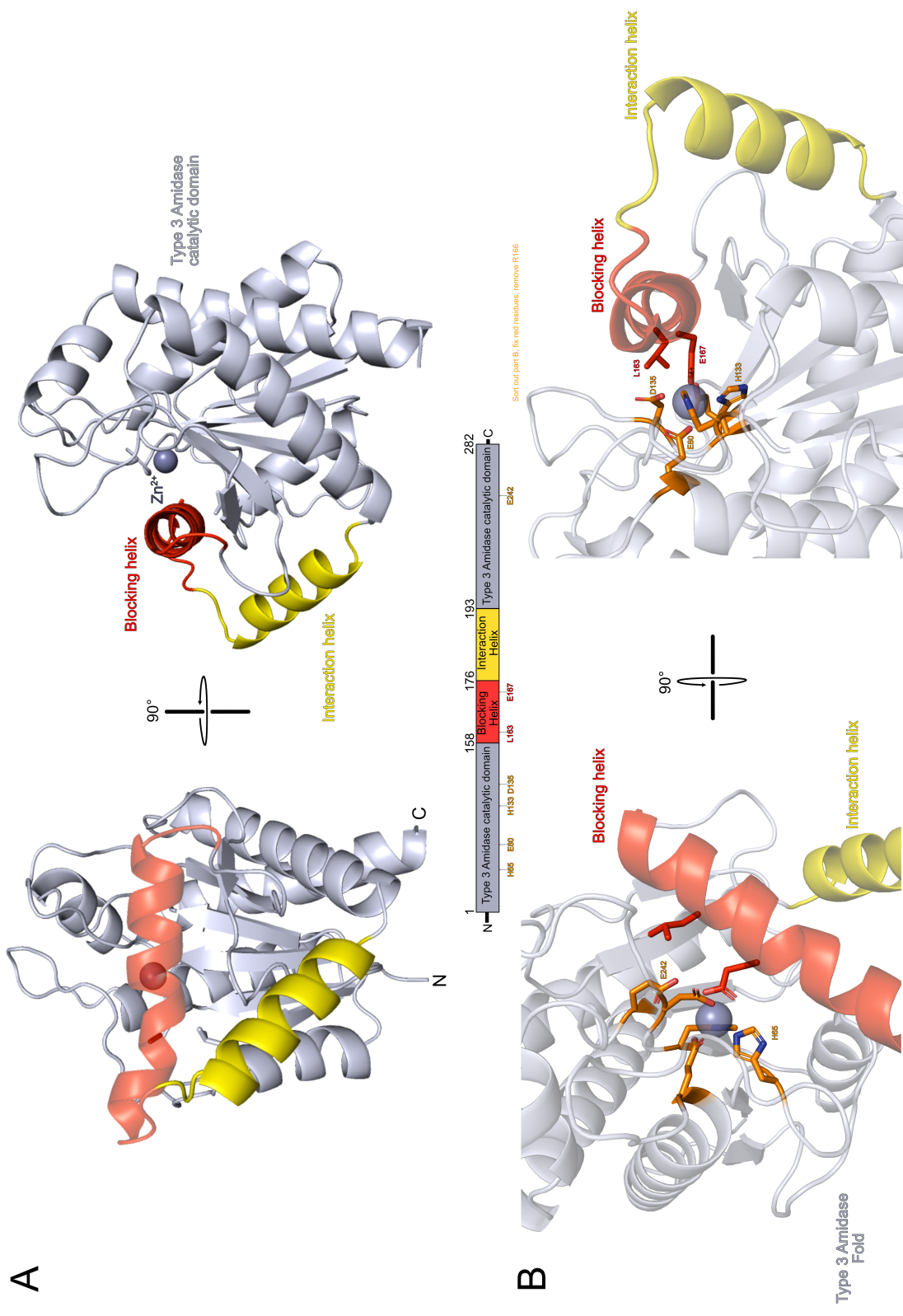


**Figure 40: AmiA is the catalytic domain of N-acetylmuramoyl-L-alanine type 3 *E. coli* periplasmic amidases.** (A) Complete structure of *E. coli* amidase AmiA rotated by 90 degrees on a vertical axis. (B) AmiA direct zinc binding residues (orange) and potentially key blocking helix interaction residues (red). Structure rotated by 90 degrees on a horizontal axis.

**Table 4: Data collection and refinement statistics.** \* = Values in parentheses indicate the highest resolution bin, † = Refinement statistics are from Refmac, ‡ = Ramachandran statistics as reported by Rampage.

	<b>AmiA 8C20</b>
<b>Data Collection</b>	
Beam line	Diamond I04-1
Wavelength (Å)	0.97950
<b>Crystal parameters</b>	
Space group	P 2 21 21
Unit cell dimensions (Å)	59.5, 73.9, 115.6
Unit cell angles (°)	90, 90, 90
<b>Reflection data*</b>	
Resolution range (Å)	59.51-2.35 (2.43-2.35)
Unique reflections	21,955 (2,121)
Rpim	0.050 (0.506)
I/σ(I)	10.4 (1.5)
CC½	0.999 (0.662)
Completeness (%)	100 (100)
Multiplicity	12.6 (12.1)
Wilson B (Å <sup>2</sup> )	51
<b>Refinement†</b>	
Resolution (Å)	59.60 - 2.35
Number of reflections	20,819
Roverall	0.177
Rfree	0.236
Rms (bond lengths) (Å)	0.007
Rms (bond angles) (°)	1.43
<b>Model B-factors</b>	
Proteins (Å <sup>2</sup> )	50, 60
Zn (Å <sup>2</sup> )	42, 43
Waters (Å <sup>2</sup> )	43
<b>Ramachandran statistics‡</b>	
Favoured (%)	97.6
Allowed (%)	2.4
Outlier (%)	0

### 5.3.3 AmiA interaction helix is highly mobile

To further investigate the hypothesis of the interaction helix being a mobile element in the AmiA structure, a B-factor analysis was performed on the AmiA structure (**Figure 41**). Overall, represented by blue and purple, the main internal beta sheets and majority of the main amidase catalytic domain fold generally contains low b-factors, including the active site and the zinc atom, indicating low motion. Shown by light blue and green, the main area of high B-factor is the linking set of residues between the blocking and interaction helices. Combined with the smeared electron density (during model building) of one of the AmiA molecules in the asymmetric unit and the high B-factors, this is likely a very mobile set of residues with high thermal motion. There is clearly flexibility between the two helices suggesting that the interaction helix is responsible for the movement of the blocking helix during the activation of AmiA during the interaction with EnvC. Where the two helices move to or how the structural rearrangement occurs is explored later.

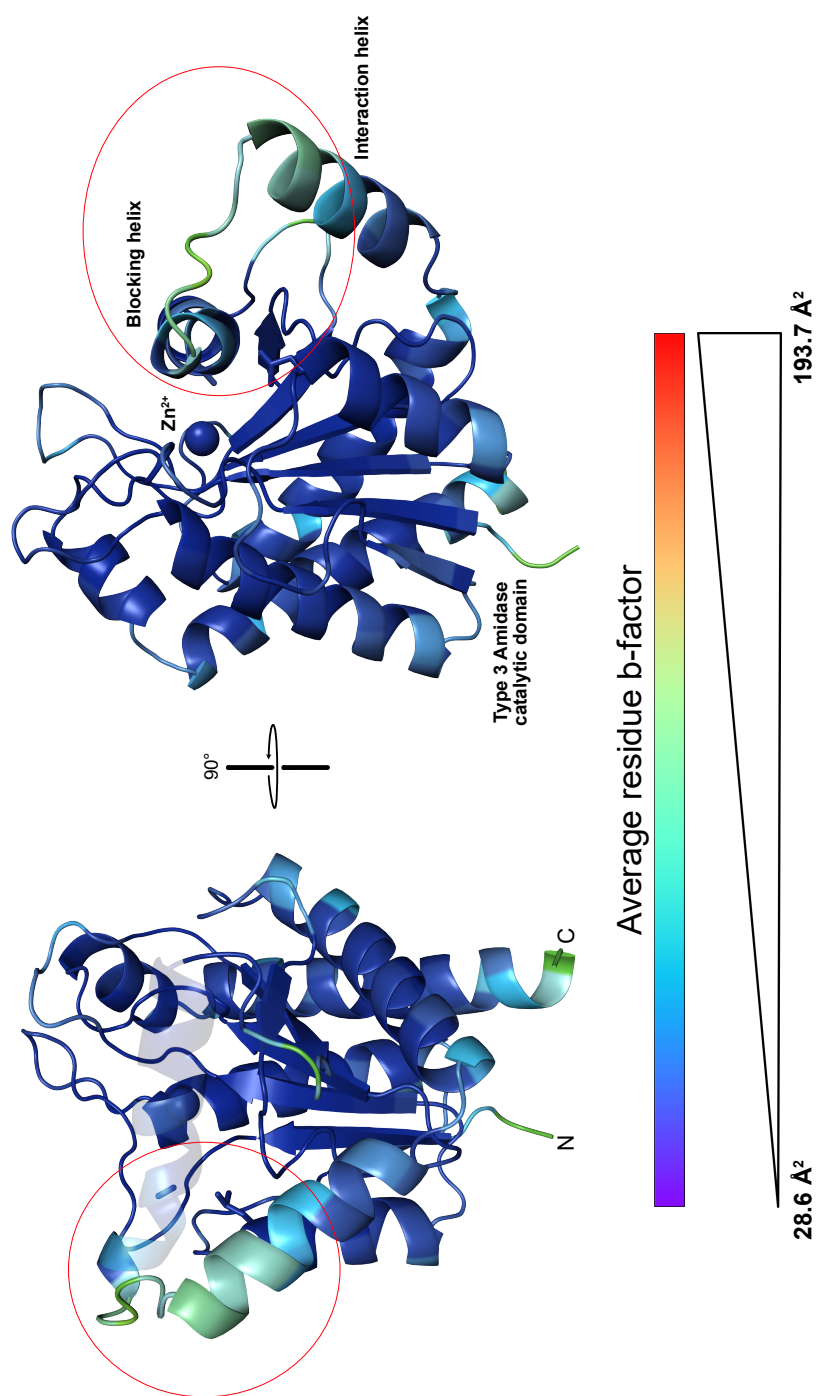


**Figure 41: AmiA has a flexible set of helices suggesting a self-regulatory mechanism.** AmiA is coloured based on residue B-factors with a scale representing high B-factor (red) and low (blue/purple). Areas of interest and mobility are indicated by the red circles. The AmiA structure is rotated 90 degrees along a vertical axis. B-factor colours based on Pymol analysis

### 5.3.4 AmiA contains high internal and active site conservation

As a comparison between AmiA and other published amidases, a standard settings Conserf analysis (Ashkenazy et al., 2016) was performed to detect conservation throughout the AmiA structure (**Figure 42**). The ConSurf server is a bioinformatics tool for estimating the evolutionary conservation of amino/nucleic acid positions in a protein/DNA/RNA molecule based on the phylogenetic relations between homologous sequences (Ashkenazy et al., 2016). The degree to which an amino (or nucleic) acid position is evolutionary conserved (i.e., its evolutionary rate) is strongly dependent on its structural and functional importance (Ashkenazy et al., 2016).

Overall, highlighted by purple areas, the internal structure of AmiA are very conserved whereas the external facing residues and helices appear generally variable and unique, shown by more green coloured areas (**Figure 42A**). A sequence view (**Figure 42B**) shows that all of the previously mentioned zinc-binding and active site residues (His 65, Glu80, His133, Asp135, Glu 167 and a non-zinc binding active site Glu242) are strongly conserved (highlighted by orange boxes) along with the key residues in the interaction helix (Leu184, Leu185, Val188, Leu189, Leu192) all exhibiting weaker but still present conservation. In comparison to the other helices in the structure, the interaction helix is the only one with conservation of the solvent facing residues, further indicating the requirement for these residues for an interaction, presumably, EnvC. These external interaction helix residues will be revisited later with further investigations. The residues linking the blocking and interaction helices however (residues 176-184) are variable with little conservation, perhaps due to their high mobility and B-factor.



### 5.3.5 AmiA contains a Zinc ion, essential for function

As described in other type 3 or type 3-like amidases such as *E. coli* AmiC and *Clostridioides difficile* CwlD respectively both contain a zinc atom that is essential for their function with specific and conserved zinc-binding residues. To confirm the presence of zinc in the AmiA protein, an X-ray edge scan was performed (**Figure 43A**) with an example of a theoretical zinc edge scan for reference (**Figure 43B**) and an anomalous scattering map constructed (**Figure 43C**)

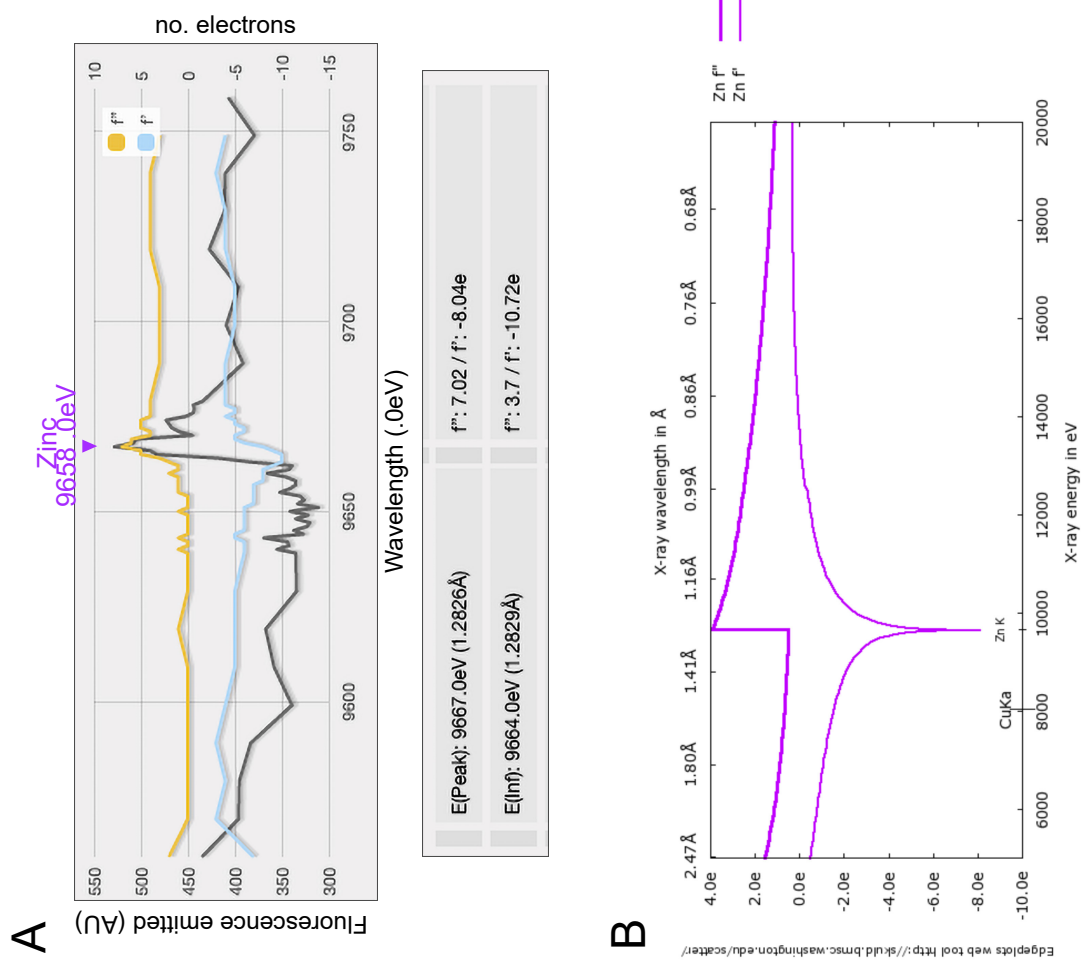


**Figure 43: A zinc ion is present in the AmiA active site.** (A) Top: X-ray fluorescence edge scan; black line = Raw X-ray fluorescence measurement obtained on the beam line (no units), blue line =  $f'$  anomalous scattering factor and yellow line =  $f''$  anomalous scattering factor. Both derived from the fluorescence data and are measured in units of electrons. Bottom: Readings of emission, resolution, electrons from the peak and inflections of the atomic scattering factor shown in the graph above. (B) Anomalous scattering map indicating zinc binding residues in AmiA, red = residues based in blocking helix, orange = active site residues. Map calculated from a reading the wavelength of 0.9795.0eV with a Zinc sigma level of 8.8.

The adsorption edge was measured by **Figure 43A** at approximately 9667 eV, consistent with the presence of zinc in comparison to **Figure 43B**. It is worth noting that experimental error and structural environment of the zinc may cause a peak shift slightly away from the theoretical value. Using the anomalous scattering map in **Figure 43C**, the zinc atom was identified present in the active site with a sigma level of 8.8 at the wavelength of 0.9795 Å and surrounded by zinc-binding residues, further evidencing the presence and the positioning of the zinc atom in the active site of AmiA. Although an anomalous scattering map reading below and near 9658.6 eV would further solidify the presence of a zinc in the structure.

### 5.3.6 AmiA has a conserved catalytic domain found in other type 3 amidases in *E. coli*

AmiA is one of three N-acetylmuramoyl-L-alanine type 3 *E. coli* periplasmic amidases used in cell division all of which hold striking similarity in their catalytic domain folds and conserved zinc-binding residues (**Figure 44**). As there is no solved structure of *E. coli* AmiB, a orthologue structure of only the catalytic domain from *Bartonella henselae str. Houston-1* was used instead. Upon visual inspection of all three amidases secondary structures, the blocking helix identified in AmiA is present in AmiB and AmiC also, which suggests a conserved self-regulatory mechanism present in cell division amidases, perhaps due to the importance of amidase activity regulation during division.

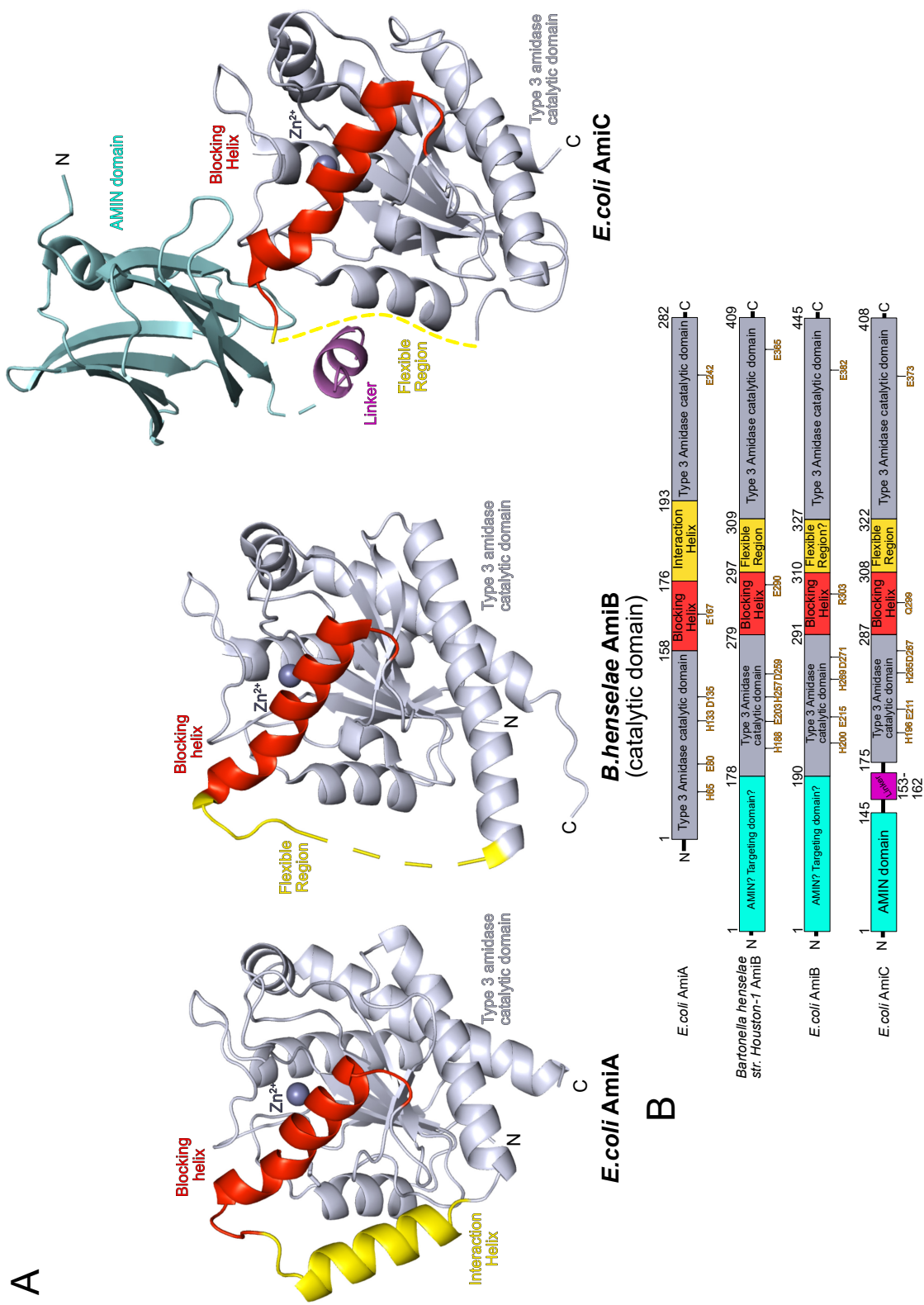


**Figure 44: Type 3 amidases have a significant level of structural conservation** (A) Annotated resolved structures of (left to right) *E. coli* AmiA, *E. coli* AmiB orthologue from *Bartonella henselae* Houston 1 (catalytic domain only) (D. C. Yang et al., 2012b) and *E. coli* AmiC (Rocabay et al., 2013). (B) Domain diagram of *E. coli* type 3 amidases and the *E. coli* AmiB orthologue from *Bartonella henselae* Houston 1. Zinc-binding residues (orange) As there is no structural information from *E. coli* AmiB, an alignment of the AmiB orthologue from *Bartonella henselae* Houston 1 was used to predict the zinc-binding residues.

Interestingly, only AmiA contains a resolved 'interaction helix' with AmiB and AmiC with unresolved 'clipped' regions perhaps, as a hypothesis, due to inconsistent electron density (Rocaboy et al., 2013; D. C. Yang et al., 2012b) but this would need to be confirmed by viewing the electron density maps of these other structures. What is known however, in the second molecule of the asymmetric unit of AmiA, the electron density map showed reduced electron density in the mobile interaction helix, with only the first molecule of the asymmetric unit of AmiA having clear electron density at the interaction helix. To be clear, there was sufficient electron density in the second molecule of the asymmetric unit of AmiA to build the interaction helix, with help of the first molecule model as a reference.

AmiA is the smallest of the three amidases with only containing the catalytic domain of which AmiB and AmiC also contain but with an additional domain with varying functions. In AmiC, it was deduced that the additional domain, called the AMIN domain, is required for AmiC localisation to the division site and can bind peptidoglycan (Rocaboy et al., 2013), whereas AmiB is thought to require this extra domain for targeting to the division site however this is unevidenced (D. C. Yang et al., 2012b). Clearly only the catalytic domain is required for function as AmiA lacks any other domain, although this may explain subtle differences in the localisation of AmiA to the other amidases in *E. coli* previously described (Bernhardt & De Boer, 2004) Lastly, the zinc-binding residues between the three amidases are strongly conserved with the only difference being the residue which binds to zinc from the blocking helix (**Figure 42B, orange**) which is consistent with the Conserf conservation analysis (Ashkenazy et al., 2016) of AmiA in **Figure 42**.

A sequence alignment of the three *E. coli* division amidases (**Figure 45**) correlates the conservation found in the solved structures (**Figure 44**). There is complete conservation of the active site zinc-binding residues across all three amidases (**Figure 45, orange**). The blocking helix is also generally conserved (**Figure 45, red**), perhaps due to the conservation in the active site. There are arrays of conservation also in the main catalytic domain amidase fold stemming from the zinc-binding residues into the internal six-beta sheets. The three amidases do target the same full septal peptidoglycan chain and cleave the amide bonds, however their localisation may differ. In AmiB and AmiC, there is a lack of conservation of the AMIN/targeting domain, perhaps due to the specific targeting of these amidases to different regulators. Lastly, the interaction/flexible helix shows moderate conservation, unsurprisingly, AmiC shows the most differences compared to AmiA and AmiB, again, supporting the idea this is specific to regulator interaction, evidenced by stronger similarity between AmiA and AmiB over AmiC.



### AMIN / Targeting domain

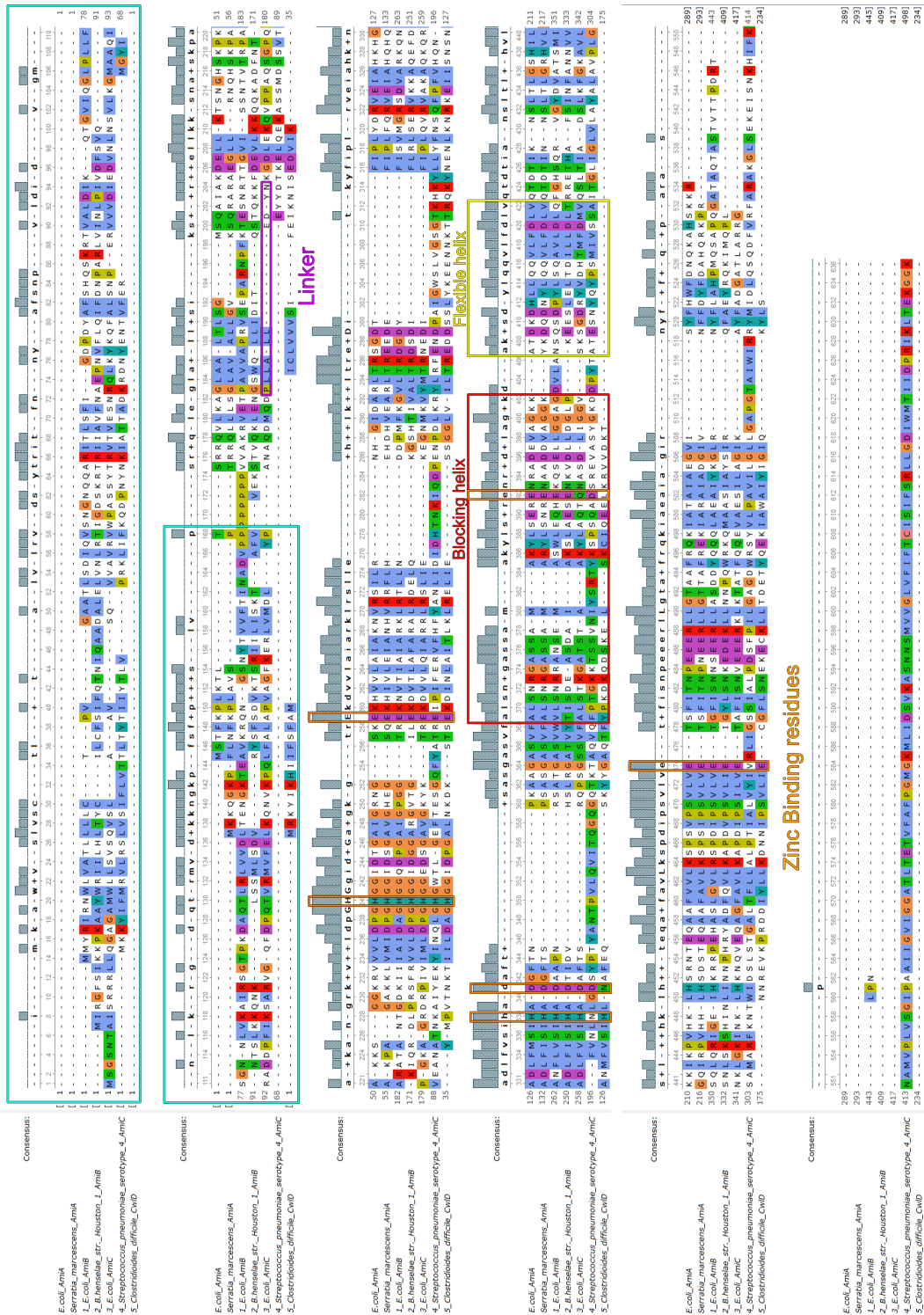


**Figure 46: The catalytic domain of type 3 amidases has strongly conserved regions. Clustal omega (Sievers et al., 2011) sequence alignment of a range of bacterial species' type 3 amidases. Key residues highlighted. Alignment image produced using UGENE (Okonechnikov et al., 2012) and colours based on ClustalX (Sievers et al., 2011) residue colouring.**

Branching out to other type 3 amidases in other bacterial systems, as the previous ConSurf analysis (**Figure 42**) revealed, the conservation found in only the *E. coli* proteins (**Figure 45**) tends to hold true for other species (**Figure 46**). Starting with the zinc-binding residues (**Figures 45 and 46, orange**), these are completely conserved across all species and all three *E. coli* amidases; AmiA, AmiB and AmiC. Again, across all amidases aligned, the beta-sheets stemmed from the zinc-binding residues are generally conserved with strong similarity. Moving onto the blocking (**Figures 45 and 46, red**) and interaction helices (**Figures 45 and 46, yellow**), aside from CwlD, which according to its structure (Alves Feliciano et al., 2021), does not appear to have a blocking nor interaction helices, the blocking helix is very similar in all amidases across the species along with the C-terminus end of the interaction helix, although the N-terminal end of this helix has significant difference across the amidases and species. Lastly, the AMIN/targeting domains have some similarity across AmiBs and AmiCs along with different species however there is significant differences towards to N-terminal end, assuming due to variation in signal sequences. Overall there appears to be different ways but conserved to regulate type 3 amidases with *E. coli* and other species using a blocking helix to self-regulate and an interaction helix as a regulator interaction site for activation with other species such as *Clostridioides difficile* using zinc-binding stabilisation to self-regulate. The catalytic domain fold is conserved across species however the mode of regulation is not always the same.

## 5.4 Discussion

This chapter was the presentation and interpretation of the solved crystal structure of the *E. coli* amidase, AmiA. This is the first instance of an *E. coli* amidase with a fully modelled catalytic domain, exposing some key features of the structure; a blocking helix (which blocks access of the active site to peptidoglycan), an interaction helix (which is predicted to interact with EnvC during amidase activation) and the zinc based active site. By comparison with other amidases, it is strongly suggested that the removal of the blocking helix via the flexible interaction helix is the self-regulation mechanism present in the type 3 amidases in *E. coli*. AmiA is the smallest and simplest of the *E. coli* amidases and when compared to amidases present in other bacterial species, there is strong conservation in the zinc-binding residues, the core beta sheets of the catalytic domains and some conservation in the blocking and interaction helices. This structure further solidifies the conserved structure and self-regulation system of amidases and is a suitable model for other amidase systems.

Upon the successful solving of the *E. coli* amidase AmiA, it is further confirmed the presence of a self-regulatory system. As seen in *E. coli* AmiC (Rocaboy et al., 2013) also, the presence of a blocking helix over the active site prevents amidase function, which therefore the removal of this helix from the active site is the cause of activation. As not previously seen, the solving of the interaction helix indicates a possible interaction between this helix and the AmiA regulator EnvC due to the presence of oddly hydrophobic solvent facing residues. The removal of the blocking helix concurs with previous literature such as *E. coli* AmiC (Rocaboy et al., 2013) and AmiB orthologues (D. C. Yang et al., 2012b) as a mechanism of amidase self-regulation when not bound to their respective regulators. Although the solving of the interaction helix further evidences this helix is important in the activation of AmiA, another solved structure of AmiA in its active form, perhaps bound to EnvC would be required to solidify this hypothesis of the mechanism of regulation of AmiA by the interaction with EnvC. Furthermore, evidencing that AmiA is active without the blocking helix would also be crucial to confirming the active form of AmiA.

Due to the high b-factors present in the interaction helix, this is the first instance of this feature being successfully modelled in an *E. coli* amidase. This provided

a unique opportunity to visualise the hydrophobic solvent facing residues present in this helix as a potentially interacting region with EnvC, specifically the LytM domain. The most noteworthy residues in the interaction helix include; Leu184, Leu185, Val188, Leu189, Leu192. These are the hydrophobic residues that by observation appear the most protruded into the environment, which would suggest they could be critical in interaction with EnvC, which would need to be investigated, in the next chapter.

These residues appeared the most protruded into the solvent environment, presumably waiting for the interaction with another protein. This is the first instance of a more precise prediction to where in the *E.coli* amidases, a regulator may interact. In (Rocaboy et al., 2013) with NlpD (LytM domain) suggested to interact with AmiC in the catalytic domain, which bares strong conservation and similarity to the AmiA molecule. However their equivalent 'interaction' helix was disordered in the AmiC structure so it is unknown where in the catalytic domain NlpD interacts with AmiC. Without further experiments such as a solved complex of AmiA bound to EnvC or with a bacterial two-hybrid investigating the interaction between AmiA and LytM with AmiA interaction helix mutants, the residues predicted to interact with EnvC are are hypothetical.

As previous studies have mentioned numerously (Alves Feliciano et al., 2021; Rocaboy et al., 2013; D. C. Yang et al., 2012b), the type 3 amidase uses a zinc co-factor present in the active site, required for function. In AmiA, a zinc co-factor was confirmed using anomalous scattering experiments although further wavelengths read for the anomalous scattering maps would completely solidify the location of zinc in the AmiA structure. Nevertheless, a zinc atom is present in the active site of AmiA with conserved zinc-binding residues in the active site and the blocking helix. In the blocking helix, Glu 167 positions the blocking helix over the active site, with residues His 65, Glu80, His133, Asp135 all directly binding to the zinc atom. Although another residue, Glu 242, although too far to interact directly with the zinc atom (4.6 angstroms), appears key in the interactions with the other active site residues. These active site residues are heavily conserved and are present in both the *E. coli* AmiC (Rocaboy et al., 2013) and orthologue *Bartonella henselae* (D. C. Yang et al., 2012b) AmiB and in multiple other amidases in other bacterial species (Figures 42 and 46). Further experiments *in vivo* and *in vitro* would be key to assess the importance of each identified active site residue in AmiA, such experiments could include peptidoglycan hydrolysis activity assays

or complementation of the  $\Delta amiabc$  amidase knockouts using active site AmiA mutants.

In summary, the work performed in this chapter is a part of fundamental bacterial biology in the regulation of an essential stage of bacterial cell division. Due to the simplicity of AmiA, it could be used as a structural model for other type 3 amidases in other bacterial species. With the successful modelling of the interaction helix, this is the first stage of structurally determining how *E. coli* amidases are regulated by the interaction with their regulators, and how activation occurs at an atomic level. Knowing the structure of a core amidase like AmiA, this could be a target of antibiotics due to their importance in the end stages of bacterial cell division, impairing the cells during infection treatment.

## **6 Mutational analysis of the *E. coli* periplasmic amidase, AmiA**

### **6.1 Abstract**

The regulation of periplasmic amidases during the late stages of cell division is an essential process to maintain cellular stability and to perform proper hydrolysis on septal peptidoglycan during daughter cell separation. One such *E. coli* amidase, AmiA is structurally self-regulated by a blocking helix over the active site, with only the interaction with its regulator, EnvC does AmiA become active and able to bind peptidoglycan. In this chapter, the mechanism by which EnvC causes the removal of the AmiA blocking helix from the active site is investigated through extensive mutagenesis. To evidence the mechanism, bacterial two-hybrid analysis confirms a number of essential residues required in AmiA to interact with EnvC in a previously explored interaction helix. Investigation into the key residues keeping the blocking helix over the active site results in two essential residues present in AmiA for this function. To probe the importance of the active site residues in AmiA, a stable constitutively active AmiA is created and shown to function *in vivo* which allowed the beginning of the mutation of the active site to detect the essential residues required for function. Overall, this is a significant step forward in structural biology for a generally conserved system that could apply to multiple other bacterial species.

## 6.2 Introduction

The cell division amidases in *E. coli* are essential in hydrolysing septal peptidoglycan during the end stages of bacterial cell division. In *E. coli*, there are three N-acetylmuramoyl-L-alanine type 3 *E. coli* periplasmic amidases used in division; AmiA, AmiB and AmiC (Du & Lutkenhaus, 2017; Levin & Janakiraman, 2021). These amidases are regulated by EnvC (for AmiA and AmiB) and NlpD (AmiC) by direct interaction causing a currently undetermined structural mechanism to activate the amidases during cell division. It is suggested that these amidases are self-regulated by a blocking helix which prevents the zinc based active site interacting with peptidoglycan (Rocaboy et al., 2013) and interaction with the respective regulator exposes the active site.

There is currently only one solved structure of an activated amidase bound to its respective regulator; CwID bound to its regulator, GerS from *Clostridioides difficile* (Alves Feliciano et al., 2021). Although this amidase strongly resembles type 3 amidases, this structure shows a different regulatory amidase system to that proposed for the amidases in *E. coli*. In *Clostridioides difficile*, CwID is regulated by an unstable zinc-binding residues when absent to GerS, however when GerS is bound to CwID, this stabilises binding of zinc-binding residues to the zinc co-factor in the CwID active site (Alves Feliciano et al., 2021). The function of this amidase regulator system is for a spore-specific peptidoglycan modification muramic- $\Delta$ -lactam (MAL) which contrasts to *E. coli* peptidoglycan side chain specific hydrolase activity of AmiA, AmiB and AmiC (Vermassen et al., 2019). The structural mechanism by which *E. coli* amidases are regulated is currently hypothesised by the removal of the blocking helix over the zinc-binding active site (Rocaboy et al., 2013; D. C. Yang et al., 2012b) however how the interaction of regulator to amidase causes this structural conformational change is currently unknown.

An important structure used in this chapter, a 3.4 angstrom structure of the AmiB enzymatic domain from *Citrobacter rodentium* bound to the cognate LytM activation domain of EnvC (**Figure 47** PDB: 8COJ). As seen in the *E. coli* AmiA structure (**Figure 40**), there is a main catalytic domain fold containing an active site housing a zinc co-factor. Here, the interaction helix of *C. rodentium* AmiB forms into an elongated back helix and interacts with EnvC LytM domain, like hypothesised in the *E. coli* AmiA structure. There is no blocking helix in the AmiB

structure, perhaps it was unable to be resolved due to the relatively high resolution, a check on the electron density map would be required. This structure is an insight into the activation mechanism that may occur in *E. coli* and can be used to predict a mechanism and the key residues involved.

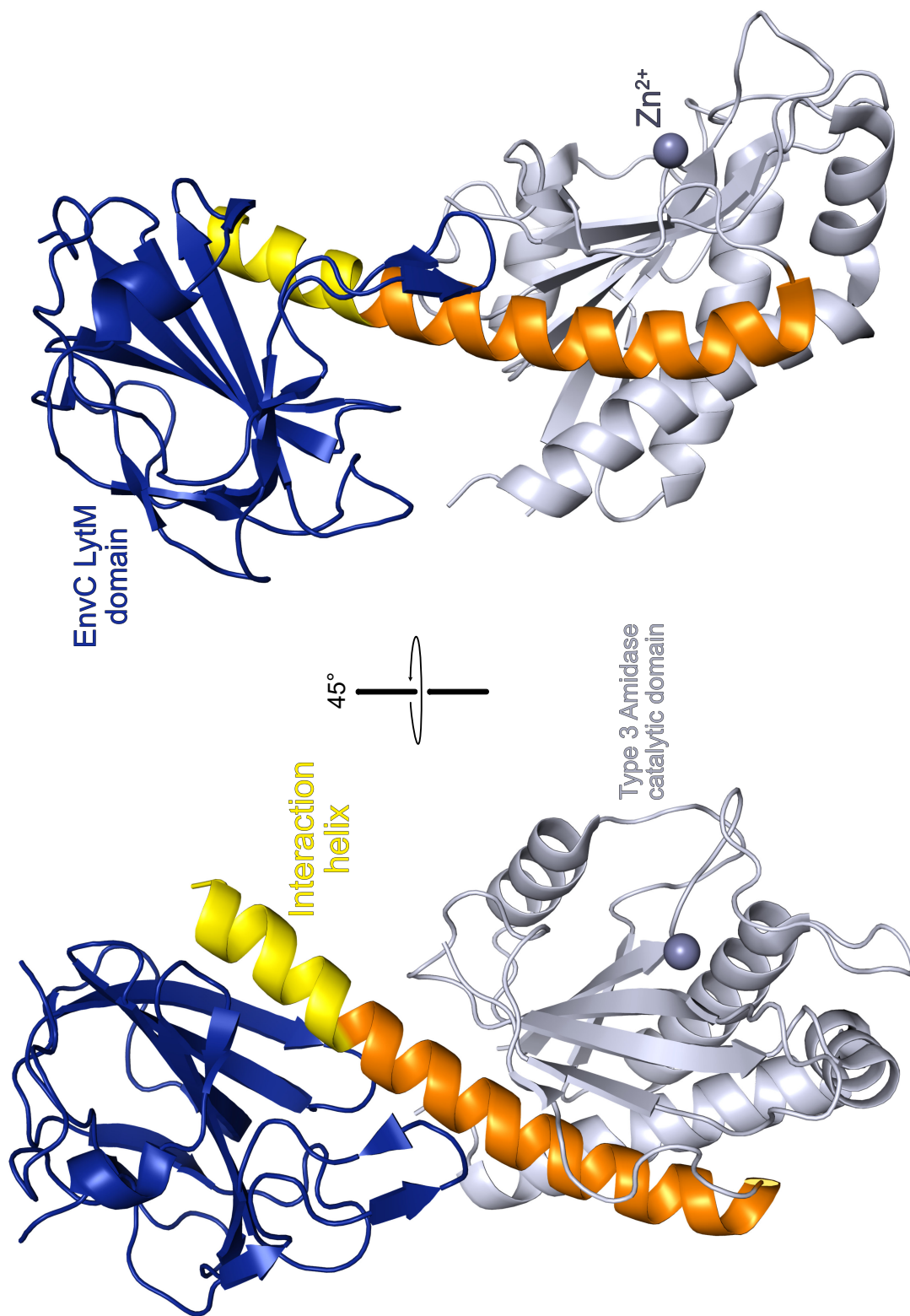


**Figure 47: Structure of an activated amidase bound regulator complex** This is a 3.35 angstrom structure of AmiB catalytic domain from *C. rodentium* bound to its cognate regulator, EnvC LytM domain. The zinc active site and interaction helix of AmiB bound to EnvC LytM domain are highlighted. PDB = 8COJ. This is unpublished data from the Crow Group at the University of Warwick, credit to Dr Allister Crow and Dr Jonathan Cook.

## 6.3 Results

### 6.3.1 AmiA is activated by direct interaction with EnvC

The structural conformational changes required for AmiA to become active has only been hypothesised by the removal of the blocking helix to allow peptidoglyan to bind to the zinc based active site.

Here presented is a model of AmiA activation bound to EnvC LytM domain (**Figure 48**). The model is based on an unpublished experimental structure of an *E. coli* homolog *Citrobacter rodentium* truncated AmiB bound to its cognate EnvC LytM domain. This structure (**Figure 47**) was determined by colleagues in the Crow lab (deposited in the protein databank 8C0J). The model was constructed using the 8C0J as a template structure in the SWISS model web based program (A. Waterhouse et al., 2018) with a target sequence using *E. coli* EnvC LytM domain sequence instead of *C. rodentium* EnvC LytM domain sequence in 8C0J with the *E. coli* AmiA sequence instead of the truncated *C. rodentium* AmiB sequence used in 8C0J. The hope is that as the type 3 amidase catalytic domain folds are consistently conserved as shown in the consurf analysis of AmiA (Ashkenazy et al., 2016), replacing the *C. rodentium* sequence with AmiB should produce a useful model.

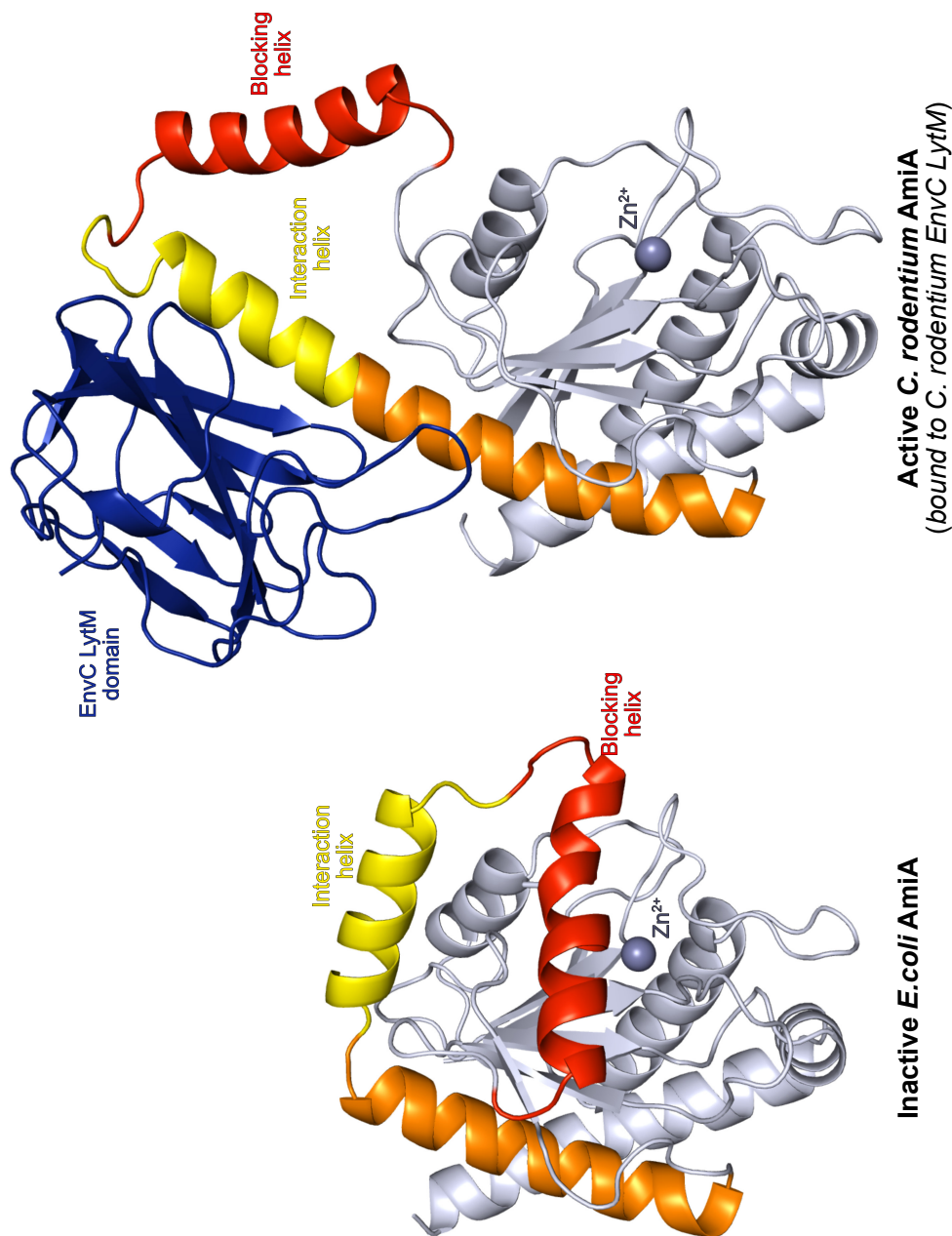


**Figure 48: EnvC LytM interaction causes a conformational change in AmiA, exposing the active site.** Left = Annotated *E. coli* AmiA structure. Right = Theoretical model for the *E. coli* AmiA/EnvC LytM interaction based on an unpublished experimental structure of truncated *C. rodentium* AmiB bound to cognate EnvC LytM solved in the Crow lab (PDB = 8C0J). Model created using SWISS model web service (A. Waterhouse et al., 2018).

The activated form of AmiA indicates the translation of the blocking helix (**Figure 48**, red) away from the active site, exposing the zinc-binding residues ready for peptidoglycan interactions. Interestingly, the interaction helix (**Figure 48**, yellow) that was previously predicted to interact with EnvC does translate to interact with the LytM domain while forming an extended alpha helix with the highlighted adjacent helix (**Figure 48**, orange). It is curious however that the blocking helix is moved a distance away from the main structure (approximately 10 angstroms from the interaction helix) with no interactions to the rest of the structure. Perhaps there is another part of EnvC which may interact with this blocking helix to further stabilise the active form of AmiA, or likely that the active form of AmiA is unstable compared to the active conformation which it reverts back to upon dissociation from EnvC.

### **6.3.2 AmiA interaction with EnvC is dependent on a set of hydrophobic residues in the interaction helix**

Investigating the interaction of the interaction helix of AmiA with the LytM domain from EnvC, a bacterial two-hybrid experiment probed the essential residues to this interaction (**Figure 49**). Based on the AmiA:EnvC LytM model (**Figure 48**), the hydrophobic residues which appear to be the most strongly involved in the interaction with the LytM domain are the same residues originally predicted off the AmiA structure; Leu184, Leu185, Val188, Leu189, Leu192 (**Figure 49A**). Surprisingly however, upon individually and doubly mutation of all five EnvC interaction residues, all mutations attempted break the interaction with EnvC. This would suggest that even small mutations of leucine to an alanine are sufficient to break or significantly hinder the interaction of the interaction helix of AmiA with the LytM domain, to the point that interaction is not detected via this technique. The interaction between AmiA and EnvC could therefore be deemed very specific with all five of these residues key in interaction and leading to proper regulation of AmiA.



It is worth noting however the bacterial two-hybrid shown in (**Figure 49B**) was later repeated by Dr Jonathan Cook in the same research group and AmiA mutants L184K and L189K did in-fact show weak interaction with EnvC LytM domain after 4-6 days. Although this is outside the normal bacterial two-hybrid experimental period of 3 days (controls remained correct), it may show these mutants while strongly affect the interaction between AmiA and EnvC, still means AmiA could be activated, albeit weakly.

Due to the surprise of all interaction helix residue mutations breaking interaction with EnvC, a control expression trials of all mutation bacterial two-hybrid constructs was performed in *E. coli* C43 cells to ensure the mutation was not preventing proper folding of AmiA (**Figure 50**). Fortunately, all soluble protein extracts after cell lysis exhibited proteins bands of all AmiA mutants on the SDS PAGE analysis which (**Figure 50**) indicates proper folding and expression of the contracts present consistent with the wild-type AmiA bound to a T18 fragment. Expression of the AmiA mutants and locating them within the soluble protein extract of the cells shows proteins have folded properly and not been placed in inclusion bodies with incorrectly folded aggregated proteins. As all the AmiA-T18 fusion proteins are well-expressed and stable, it does suggest the mutations that block interactions in the bacterial 2-hybrid experiment disrupt the interaction without impairing the proteins ability to fold.

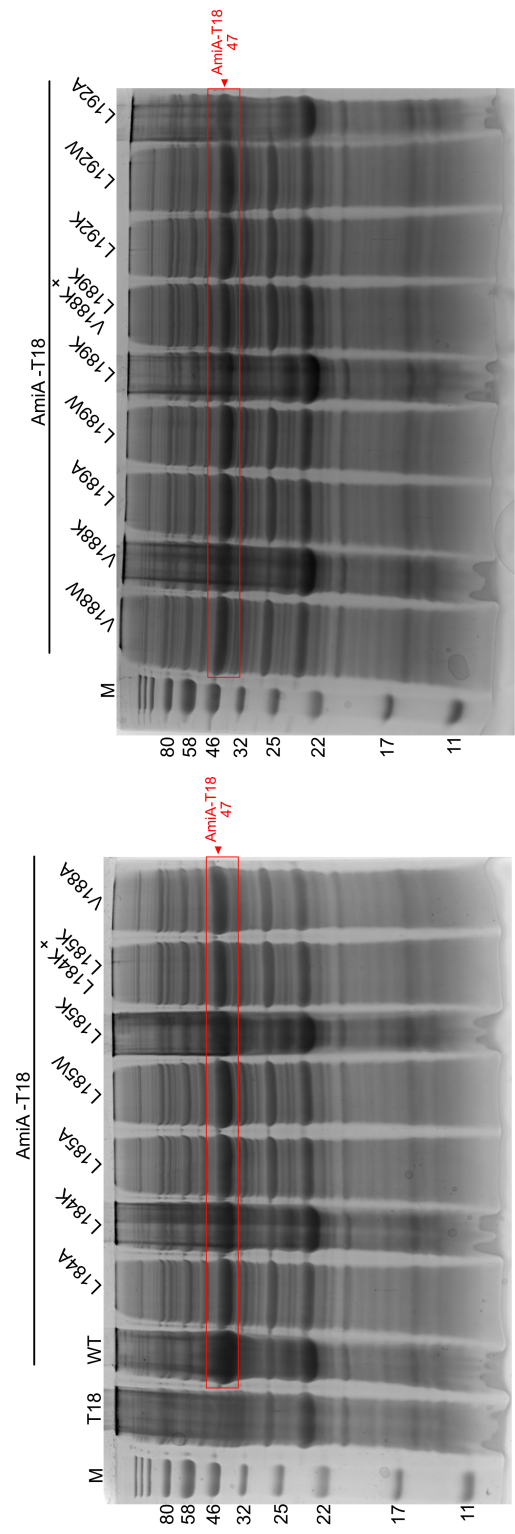


**Figure 50:** AmiA interaction helix mutants express properly. SDS-PAGE analysis of the crude expressions of AmiA-T18 constructs from Figure 49 in C43 *E. coli* cell line.

### 6.3.3 The blocking helix is essential to AmiA self-regulation

As the AmiA model bound to EnvC LytM highlights that the translation of the blocking helix away from the active site is essential in the activation of AmiA, further investigation into the key residues keeping the active site bound to the active site was performed. Firstly, to check if AmiA is active without the blocking and interaction helices, exposing the active site, multiple large deletions were constructed to remove these helices to produce a constitutively active AmiA with the most successful mutation structurally highlighted (**Figure 51A**). Additionally, upon closer inspection of the AmiA structure, two residues in the blocking helix were identified to be potentially important in positioning the blocking helix over the active site; Leu163 and Glu167 (**Figure 51B, red**). A series of point mutation constructs were created to measure the importance of these two residues in the self-regulation of AmiA. (**Section 8**)

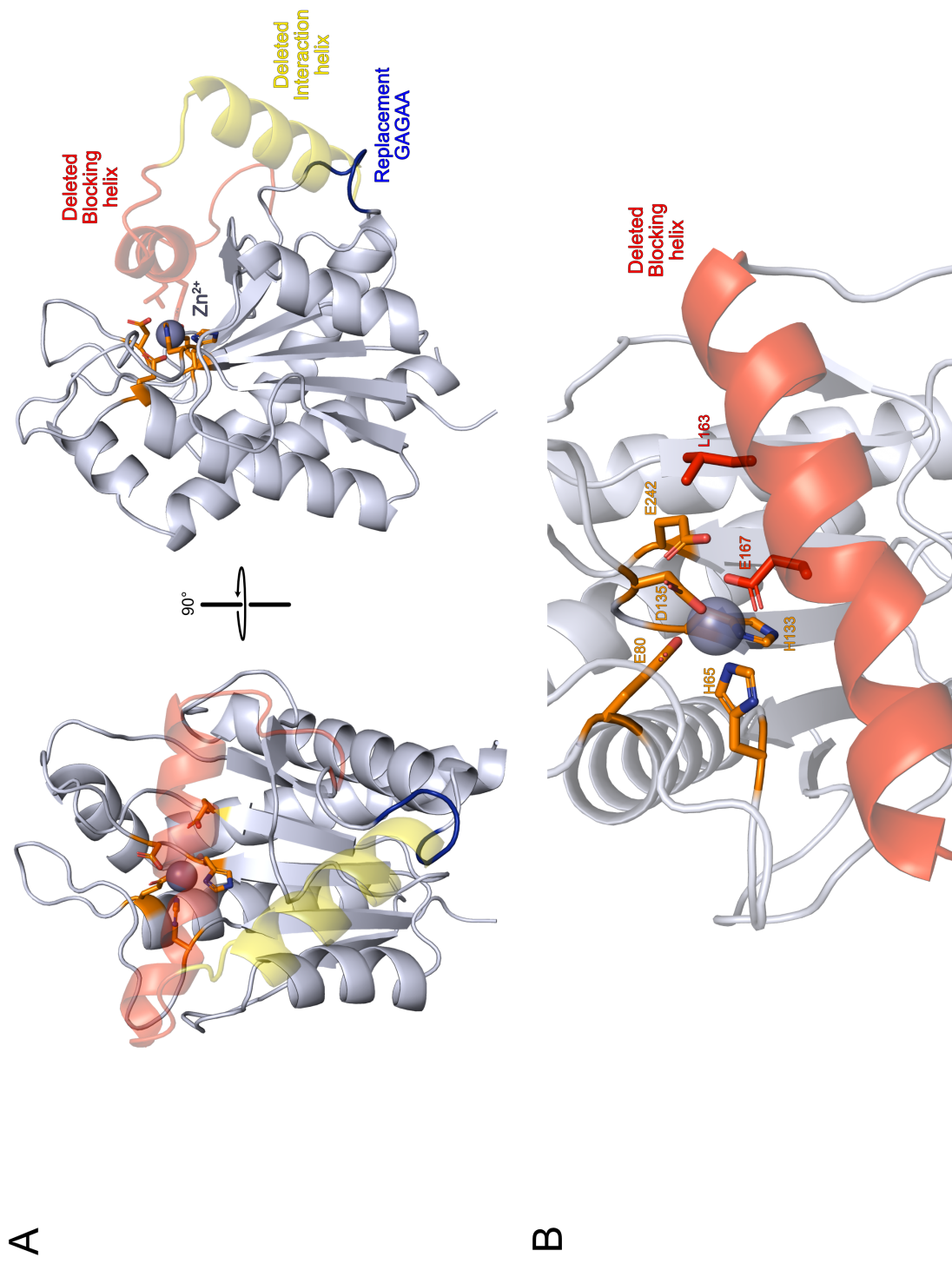
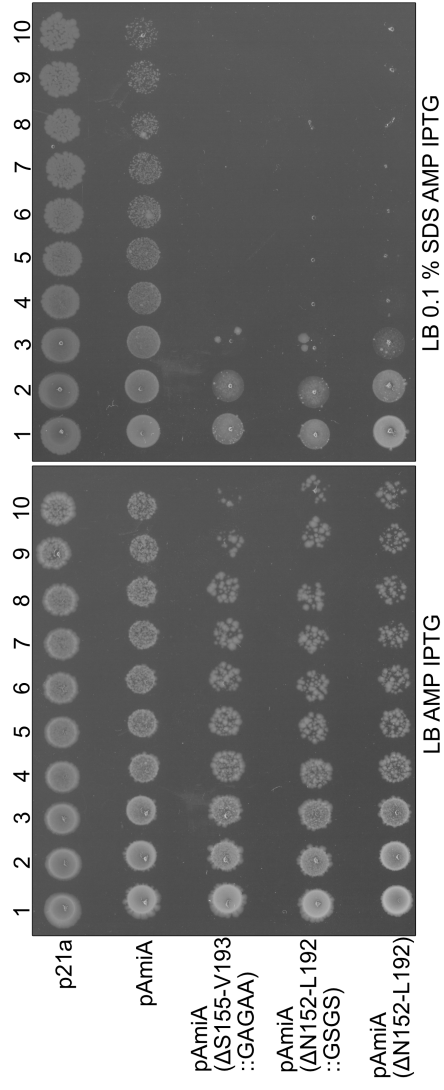


**Figure 51: Removal of the blocking and interaction helices produces a constitutively active AmiA.** (A) Constitutively active AmiA ( $\Delta$ S155-V193::GAGAA) modelled of the AmiA structure with SWISS model (A. Waterhouse et al., 2018). The original blocking and interaction helices from the WT structure are added for reference. (B) Key zinc binding residues and blocking helix interaction residues in AmiA active site. Orange = Zinc-binding / Active site residues, Red = Blocking helix residues to have suspected importance in active site regulation.

To assess the activity of the constitutively active AmiA variants and the blocking helix mutations, a periplasmic overexpression of the constructs was performed in *E. coli* C43 cells and then cells are subjected to detergent and low osmolarity conditions (**Figure 52**). When wild-type AmiA is over-expressed in the periplasm, there is no effect notable on the cell viability under all three conditions. All three constitutively active AmiA constructs have no effect on *E. coli* under standard growth conditions however under detergent, cells are strongly sensitive and cannot survive beyond three dilutions (**Figure 52A**). This would suggest that peptidoglycan is being uncontrollably hydrolysed by constitutively active AmiA and making cells unable to withstand detergent attack due to reduced stability. The construct displayed in (**Figure 51A**) and shown in (**Figure 52A**) to have replaced the blocking and interaction helices with GAGAA, is chosen to be an active control for future experiments due to its marginally greatest effect on cellular viability under detergent conditions compared to the other two active variants.

A



B

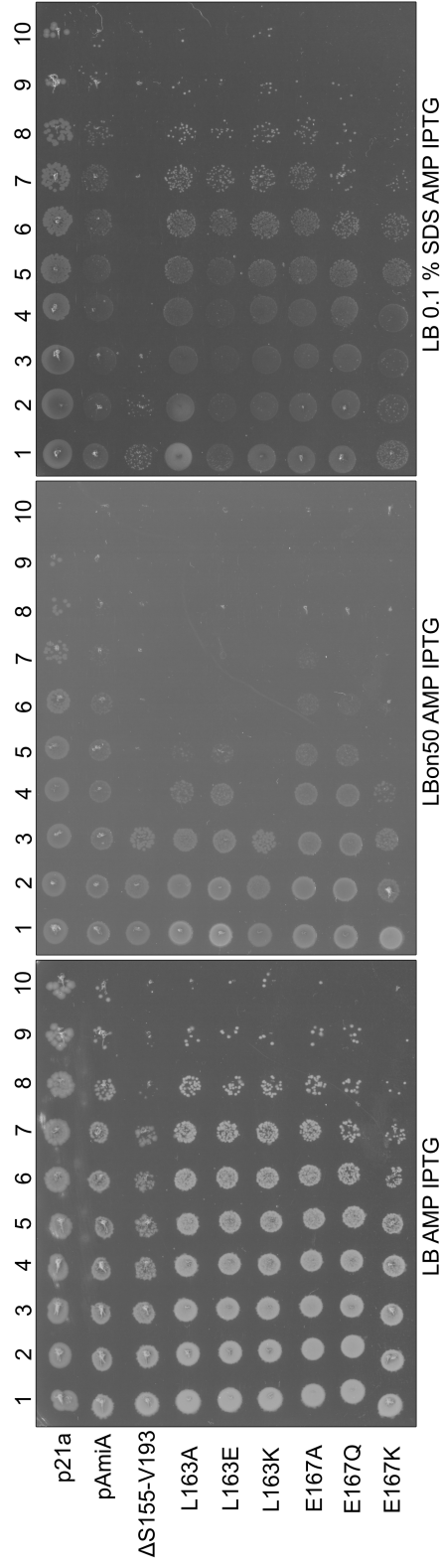


**Figure 52: AmiA is constitutively active without the blocking helix.** (A) Serial dilution spot plates of *E. coli* C43 over-expression of *AmiA* variants lacking the blocking and interaction helices. (B) Serial dilution spot plates of *E. coli* C43 over-expression of *AmiA* blocking helix mutants. Plate images were modified to greyscale for clarity.

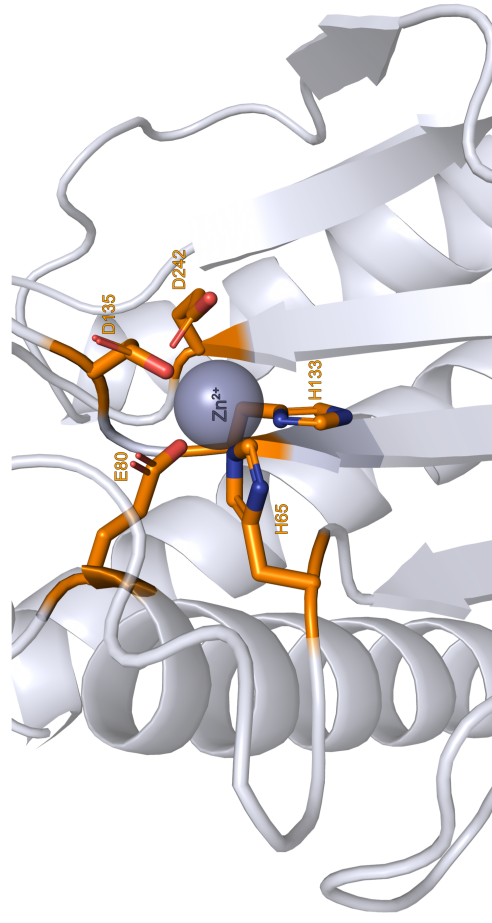
When the blocking helix AmiA mutants are over-expressed in the periplasm, varying AmiA activities are observed (**Figure 52B**). As expected, all blocking helix mutants has little to no effect under standard growth conditions with the constitutively active AmiA having a mild negative effect on cell growth at the highest dilution under standard growth conditions. The same phenotypes are highlighted under detergent conditions with constitutively active AmiA significantly hindered to only grow to dilution two and the blocking helix mutants showing little effect except L163E and E167K which show a mild effect on cell viability at higher dilutions. Interestingly, in low osmolarity conditions, the blocking helix mutations show significant reduced growth phenotypes. Mutations L163E and E167K both produce similar phenotypes to the constitutively active AmiA under low osmolarity conditions. The other mutations to note are L163E, L163A and E167Q all have reduced growth compared to the control and wild-type AmiA. Overall, the mutations of L163K and E167K were the closest to produce phenotypes of the constitutively active AmiA, highlighting the change from a hydrophobic or a negative charge respectively to a positive charge is sufficient to remove the blocking helix, preventing AmiA self-regulation to begin hydrolysing peptidoglycan uncontrollably leading to sensitivity to low osmolarity pressures.

### 6.3.4 AmiA active site and Zinc-binding residues are essential for function

The creation of a stable and functioning constitutively active AmiA construct allows an investigation of the zinc-binding residues of the active site of AmiA (**Figure 53**). The active site of AmiA as shown previously is strongly conserved across *E. coli* and other type 3 amidases in other bacterial systems. In *E. coli* AmiA, there are five active site residues in AmiA (excluding the blocking helix); His 65, Glu80, His133, Asp135 (zinc-binding) and Glu 242 (non-zinc binding) (**Figure 53A, orange**). To assess the importance of each residue in the AmiA active site, each residue was mutated into an alanine in the constitutively active AmiA construct and overexpressed in *E. coli* C43 under detergent and low osmolarity conditions (**Figure 53B**).

It is worth noting in some repeats the over-expression of wild-type AmiA has a very weak effect on cell growth in all conditions, which perhaps is the result of non-native activation of AmiA, a side-effect of AmiA over-expression. Under low osmolarity conditions, all five residues show little to no effect on cell viability compared to both p21a and wild-type controls, however under detergent conditions, three mutations; H65A, E80A and H133A all produce similar growths to the p21a and wild-type controls whereas D135A and E242A while grow one dilution better than the constitutively active AmiA, still have reduced growth compared to the controls. Any extra growth over the constitutively active AmiA indicates a deflection in AmiA activity, suggesting peptidoglycan is not being as efficiently hydrolysed compared to constitutively active AmiA, allowing cells to be more resistant to low osmolarity and detergent conditions. Any of these active site mutants will greatly affect the ability of the active site to bind zinc, suggesting a question that are the remaining active site residues sufficient to bind zinc alone, although they do still show weak activity, so it is possible there is some remaining activity. It is worth noting however, that other pathways may be affected by an constitutively active AmiA with this effect on the phenotype seen in this chapter is unknown. *in vitro* activity assays talked about in previous chapters (such as Remazol Brilliant blue dyed peptidoglycan (Zhou et al., 1988)) would be effective in determining if the constitutively active AmiA is in fact active independently. Overall this highlights that all the zinc-binding residues are potentially important in AmiA activity, although H65, E80 and H133 are suggested here to have a greater impact of their absence from the active site compared to D135 and E242.

A



B

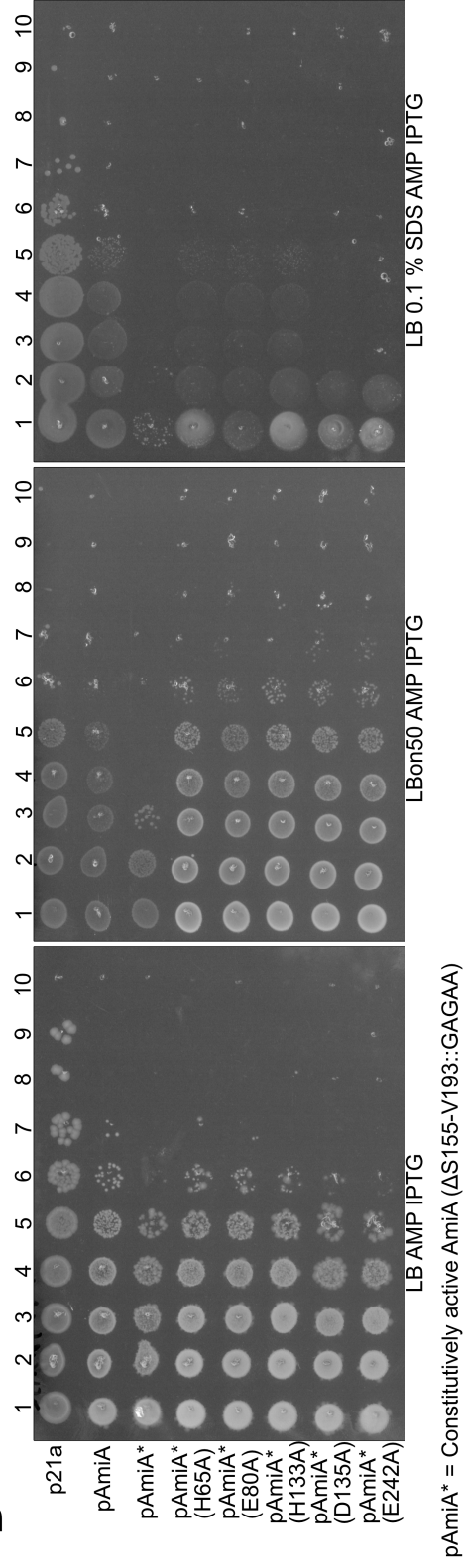


**Figure 53: AmiA zinc-binding residues are important for function.** (A) Zinc-binding residues in constitutively active AmiA lacking blocking and interaction helices. (B) Serial dilution spot plates of *E. coli* C43 cells over-expression of AmiA zinc-binding residues. Plate images were modified to greyscale for clarity.

## 6.4 Discussion

This chapter is a step forward into understanding the structural regulation of type 3 amidases. A proposed mechanism of the structural arrangement in AmiA that occurs upon EnvC LytM binding highlighted the residues involved in the interaction helix with the LytM domain. The residues interacting from AmiA to the LytM were all found to be essential in proper binding along with two residues in the blocking helix, L163 and E167 were crucial in maintaining the blocking helix positioning. Lastly, the five active site residues were identified and shown to all be important in AmiA activity, with H65, E80 H133, D135 and E242 all suggested to be important to the function of AmiA.

By the use of both the AmiA bound LytM model and the AmiA structure, residues key in the AmiA:LytM interaction and the amidase active site were identified. Firstly, via the AmiA bound LytM model inspection and bacterial two-hybrid analysis, unexpectedly, five residues were found to be essential in AmiA to interact with EnvC LytM domain; Leu184, Leu185, Val188, Leu189, Leu192 which was predicted in the AmiA only structure due to the solvent facing hydrophobic residues.

The mechanism of AmiA can be hypothesised with this new structural information. As described previously in (J. Cook et al., 2020), during bacterial cell division, FtsEX is recruited to the septum in which then EnvC binds to ftsX periplasmic domain. There is a self-regulation helix in EnvC to prevent AmiA (or AmiB) binding. FtsE binds to ATP and causes a conformational change in FtsEX and EnvC, which causes the regulation helix of EnvC to move into the heptad pairs forming a dual helix backbone, exposing the LytM amidase interaction groove. AmiA is present in the periplasm with the blocking helix preventing binding to peptidoglycan and the interaction helix unbound. AmiA can bind to the LytM domain of EnvC upon exposure of the amidase interaction groove of the LytM domain. Upon binding, interaction helix interacts with LytM domain of EnvC producing an extended alpha helix in AmiA causing the blocking helix to be removed from the active site, allowing peptidoglycan to interact, allowing AmiA to hydrolyse the amide bond linking the glycan strand with the peptide stem (MurNAc-(L-)A1A). When FtsE hydrolyses the bound ATP, another conformational change occurs throughout FtsEX, EnvC and AmiA. As the signal cascade reaches EnvC, the restraining helix blocks the LytM amidase binding groove, causing AmiA to dissociate. The AmiA

blocking helix will again interact with the zinc in the active site for stabilisation causing the interaction helix to move towards the active site. This is an example of a system which has at least two self-regulating proteins but also a signal cascade produced by the binding and hydrolysis of ATP in FtsE.

Further experiments using a constitutively active AmiA and blocking helix mutants further explain the requirement for a self-regulation system for AmiA. The periplasmic over-expression experiments were key in assessing if AmiA was active in an constitutively active form of which highlighted that without regulation, AmiA or other amidases could cause cells to have uncontrolled peptidoglycan hydrolysis however these experiments may also show that AmiA could be affecting other protein or membrane components in the periplasm unknown to us. Experimental data for the activity of *in vitro* of the most stable constitutively active AmiA variant could be important to assess whether it only targets peptidoglycan or perhaps other targets, even proteins, further evidencing the importance of self-regulation. This can be applied to the blocking helix mutations as well, although the periplasmic over-expression experiments did highlight that L163 and E167 in the blocking helix are crucial in maintaining positioning over the active site.

Expansion experiments would be useful to fully explore this interaction as the bacterial two-hybrid can miss weakly or delayed binding proteins, *in vitro* experiments such as thermoscale thermophoresis could be used to support the current claims. Additionally, although the model of AmiA bound to EnvC LytM was based of a high percentage similarity structure of *E. coli* AmiB (catalytic domain only) bound to LytM, a structure of active and inactive AmiA bound to a full length EnvC, or even a trio of AmiA bound to EnvC bound to FtsEX would solidify the conformational changes that is hypothesises to cascade throughout these proteins to activate AmiA.

In terms of the zinc-binding residues, unsurprisingly, the residues are found conserved previously however this is the first instance in which the active site residues were assessed in a constitutively active AmiA *in vivo*. All five of the active site residues were found to be important for function with H65, E80 and H133 to reduce AmiA activity the most when mutated, although further experimentation is required to support this. Further investigation into the active site could involve *in vitro* peptidoglycan hydrolysis assays of the active site mutant constructs with rates of activity would be key in comparing the importance of each residue to deter-

mine the minimum required for function. A comparison between AmiB and AmiC could be curious also to see whether those amidases produce the same phenotype as constitutively active AmiA with zinc-binding mutants.

In summary, the work performed in this chapter provides a significant insight into the structural regulation of the periplasmic amidase AmiA. AmiA is self-regulated upon the use of key zinc-binding and interacting residues in the blocking helix with the interaction helix specialising in the interaction with EnvC LytM domain. The interaction of EnvC with AmiA is essential to the activation of AmiA, allowing the active site to bind to peptidoglycan, however it has been shown without the blocking and interaction helices, AmiA can be a detriment to the cells under environmental stresses.

The structural regulation mechanism proposed in this chapter could be applied to multiple other systems as type 3 amidases are conserved throughout multiple bacterial species although this maybe one of many regulation systems of amidase activity during cell division. It should be highlighted however that with the knowledge that constitutively active AmiA cause a significant negative effect on cell wall stability and resistance to external pressures, AmiA or other amidases could be a target of antibiotics to cause uncontrolled hydrolysis of peptidoglycan, leaving bacteria susceptible to other treatments. Nevertheless this is a positive movement as a fundamental part of bacterial cell division and structural biology.

## 7 Final Discussion

This thesis is a collection of data investigating the FtsEX:EnvC:AmiA/B pathway. The aim of the thesis was to investigate the structural regulation of type 3 amidases in *E. coli* cell division (**Figure 54**). The work was split into four chapters; one, investigating the interactions of EnvC, two, finding phenotypes of divisome knockouts, three, solving and analysing the *E. coli* type 3 amidase AmiA and finally, four, a mutational analysis of the activation mechanism of AmiA. Overall, this thesis has made a contribution into the understanding of type 3 cell division amidase regulation, a fundamental biological process.

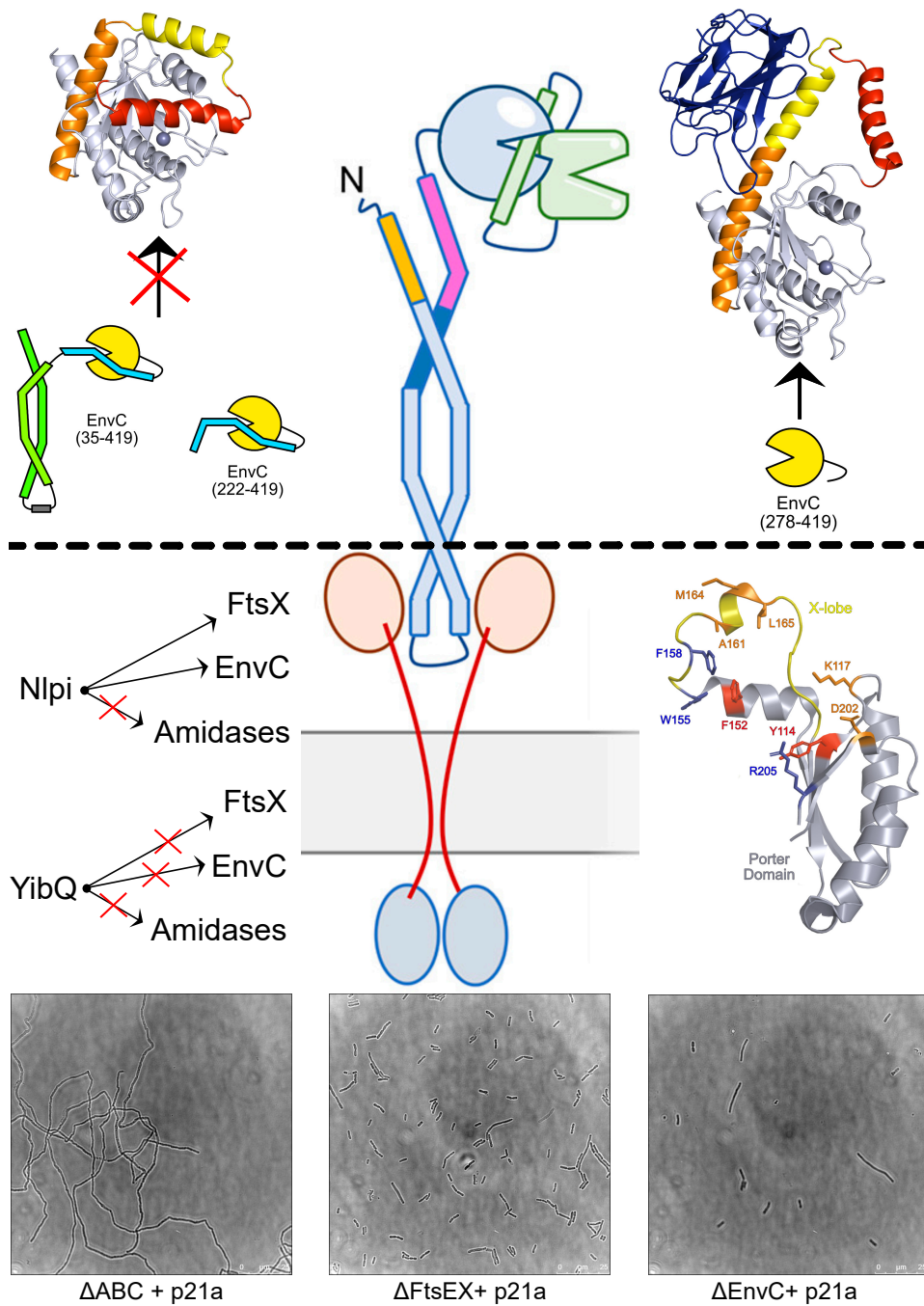


**Figure 54: The FtsEX:EnvC:AmiA pathway is controlled by numerous interactions;** The central diagram of FtsEX bound to EnvC bound to AmiA was sourced from (J. Cook et al., 2020). (Top half) Top left: AmiA structure showing two EnvC variants that will not interact with AmiA. Top right: The LytM domain of EnvC that will interact with AmiA showing the AmiA bound to EnvC LytM model. (Bottom half) Bottom left: Indicates the key detected interactions of Nlpi and YibQ in this thesis, crosses mean no detected interaction. Bottom right: FtsX porter domain from **Figure 23** with colours equalling the ability of residue mutants to break the FtsX:EnvC interaction in a bacterial-two-hybrid screen. (Red = Strongly, Orange = weakly, Blue = None). Bottom middle: Phase contrast microscopy at x100 magnification of  $\Delta abc$ ,  $\Delta ftsex$  and  $\Delta envc$  transformed with an empty pET21a vector. Image scales are found on the bottom right of each microscope image.

The FtsEX:EnvC:AmiA/B is an essential and highly regulated pathway with multiple regulatory mechanisms working together to maintain proper hydrolysis of septal peptidoglycan during *E. coli* bacterial cell division. The interaction between FtsEX and EnvC is required for the ATPase activity of FtsE to cause a signal transduction through FtsX into EnvC to remove the restraining arm of the EnvC LytM domain to expose the amidase binding groove in the LytM domain.

The amidase regulator EnvC is a crucial part of the FtsEX:EnvC:AmiA/B pathway. An inactive LytM containing protein that is shown to only interact with AmiA and AmiB when lacking a restraining arm over the amidase binding groove (**Figure 54**). The interaction with AmiA and AmiB is mediated by a 2:1 interaction with FtsEX in an asymmetric binding interface (**Figure 54**). Combined with other research in (J. Cook et al., 2020), the current theory of EnvC regulation is dependent on the ATP binding and hydrolysis of FtsEX. FtsEX binding of ATP causes conformational changes in FtsEX and EnvC allowing AmiA or AmiB to bind with the removal of the restraining helix from the amidase binding groove of the LytM domain. The interaction of AmiA/AmiB to EnvC has been suggested by data in this thesis to cause a conformational change in the amidase removing a blocking helix from the zinc active site, allowing amidase activity to occur. ATP hydrolysis in FtsEX causes another mechanotransmission signal to reach EnvC causing another conformational change, resulting in the dissociation of the amidase and restoring the restraining arm over the amidase binding groove in the LytM domain. Interestingly, as a comparison to another documented FtsEX system in *Streptococcus pneumoniae* (Briggs et al., 2021), EnvC is replaced by PcsB which is an active peptidoglycan hydrolase hypothesised to be regulated by FtsEX. Further study into other divisome architectures like in *S. pneumoniae* and *E. coli* would be a prominent step into understanding cell division across all bacterial species.

EnvC is part of a larger divisome network with other potential interacting partners. Nlpi as shown by (Banzhaf et al., 2020) and in this (**Figure 54**) does interact with EnvC, FtsX and NlpD, further supporting Nlpi as a scaffold protein, aiding proteins in interactions in the periplasm. A gene neighbour however, YibQ was not detected to interact with EnvC in this thesis by bacterial-two-hybrid analysis (**Figure 54**). The sole function of EnvC to activate AmiA and AmiB however cannot be understated with  $\Delta envc$  cells exhibiting chaining phenotypes along with defected cell integrity and permeability (**Figure 54**), indicating septal peptidoglycan hydrolysis by AmiA and AmiC is key for proper daughter cell separation.

As a part of a larger system, EnvC regulates amidase activity during cell division. When removed from the genome, *envc*, *ftsex* and *amiabc* all show extensive chaining phenotypes (**Figure 54**) with defects in cell integrity and permeability, displayed by sensitivities in detergent, low osmotic pressure and vancomycin environments. As a potential future research point, it is fascinating that causing defects in septal peptidoglycan hydrolysis results in membrane permeability to Gram-positive antibiotics, like vancomycin, which in a wild-type *E. coli* cell would be unaffected by using an intact peptidoglycan layer and outer membrane. If these key division proteins can be targeted (and are not present in human cells due to no peptidoglycan), it could open up potential use of previously ineffective antibiotics on weakened, permeable cells.

A hypothesis that is revisited often in this thesis, and in the literature, is the idea that the three division associated amidases *E. coli* are part of a redundant system. Shown in the knockout analysis in the thesis, single amidase knockouts have little to no effect on cell separation, integrity or permeability. AmiA, AmiB and AmiC while do contain conserved interior catalytic folds, there is still differences between them which elude to a slight difference in function. AmiC is regulated by NlpD which is localised to the outer membrane of the *E. coli* periplasm with AmiA and AmiB localised to EnvC on the inner membrane. The difference positioning may indicate different roles of each amidase at different sections of the septal peptidoglycan however why the requirement of two sets of amidases either side of peptidoglycan is required is unknown.

Another interesting topic of debate is the localisation of AmiA, AmiB and AmiC. As AmiC (and assumed AmiB) localise to the division site (Bernhardt & de Boer, 2003) with AmiA currently hypothesised to weakly localise to the division site along with more distribution across the periplasm throughout the cell cycle. Based upon the knockout characterisation in this thesis, there are subtle differences between the single amidase knockout strains, which connect with the current differences observed.  $\Delta amiA$  for example was shown to have notable chaining phenotype with  $\Delta amiB$  and  $\Delta amiC$  appearing wild-type like. AmiA also does lack a targeting/AMIN domain which AmiB and AmiC have, which would agree with a difference in localisation shown in the literature. Perhaps the increased distribution across the periplasm in *E. coli*, AmiA has a more important role in hydrolysing peptidoglycan compared to AmiB and AmiC perhaps even outside of division, in other regulatory systems, like that shown in ActS (Gurnani Serrano et al., 2021)

with the cell under different environmental stresses. It is possible that the redundancy of AmiA, AmiB and AmiC could be a difference in function in response to various cell stresses such as cell division or a depletion of Muramic- $\delta$ -lactam (ActS pathway) that AmiB and AmiC respond to cell division either side of the periplasm and AmiA is more of a generalised amidase with functions varying around cell division but also other regulatory pathways, more so than AmiB and AmiC. To investigate this further, it would be prudent to use the amidase knockout strains and subject them to different environmental stresses or affect different key pathways in *E. coli* and rescue these cells with different amidases to measure a difference in complementation, if any.

The 2.35 Å crystal structure of AmiA is good standard model for the catalytic fold of a *N*-acetylmuramoyl-L-alanine type 3 periplasmic cell division associated amidase. The key features of the catalytic domain include a blocking helix over the zinc co-factor active site and a mobile interaction helix with environment facing hydrophobic residues, predicted to interact with EnvC. Based on consurf analysis (Ashkenazy et al., 2016), the core AmiA catalytic fold and the active site is strongly conserved with variation in the blocking and interaction helices. When compared to the structures of the ortholog of AmiB from *Bartonella henselae* Houston 1 (D. C. Yang et al., 2012b) and *E. coli* AmiC (Rocaboy et al., 2013), key similarities and differences are observed. The self-regulation system of a blocking helix over a zinc active site is present in all three amidases adjacent to a mobile region which AmiB and AmiC structures were unable to solve. The main difference between AmiA to AmiB and AmiC is the presence of an AMIN domain, thought to be relevant in localisation and septum targeting, as mentioned previously, posing a potential difference in localisation of AmiA to the other amidases. The core folds and active site residues are consistently conserved in other bacterial systems also such as *Serratia marcescens*, *S. pneumoniae* and *Clostridoides difficile* as shown in this thesis. AmiA could be used as the simplest model of a *N*-acetylmuramoyl-L-alanine type 3 amidase to use on other bacterial species.

It is curious the diversity of amidase regulation in different bacterial systems. As presented here, the three amidases, AmiA, AmiB and AmiC are hypothesised to be regulated by a blocking helix over the active site, and only by the interaction with their respective regulator does the active site become available to bind peptidoglycan by the removal of the blocking helix elsewhere. Previously mentioned, ClwD bound to GerS (Alves Feliciano et al., 2021) features a type 3 like amidase from

*C. difficile* in which the amidase, CwID is self-regulated by being unable to stably bind the zinc co-factor without the interaction of the regulator, GerS, of which allows CwID to bind zinc in the active site stably. The amidase itself does not contain a blocking helix like in *E. coli* and potentially multiple other bacterial species. It is curious how many structural mechanisms there are currently unknown to regulate the potentially destructive activity of amidases like that shown in this project with a constitutively active AmiA. As previously mentioned, if amidases were able to be targeted by an antibiotic, this could create cells sensitive to other treatments or stressful environments, something that could be tested further based on this project.

The activation of AmiA is by the interaction of EnvC. Although only a model was used in this thesis based on a homolog *C. rodentium* AmiB bound to a cognate EnvC LytM structure from the Crow group, it is enough to provide insight into the activation mechanism of AmiA. As predicted, AmiA interacts with the EnvC LytM domain via the interaction helix containing hydrophobic residues which face into EnvC. This interface is easily broken by mutation, shown by bacterial-two-hybrid analysis, showing a very specific interaction is required between AmiA and EnvC. AmiA is activated by EnvC by the translation of the interaction helix towards EnvC forming an elongated helix at the back of AmiA. This moves the blocking helix away from the active site, exposing it, ready for activity. This is further supported by the creation of a constitutively active AmiA by the deletion of the blocking and interaction helices. Although only shown to negatively affect growth under low osmolarity and detergent conditions, expression of this active AmiA is potentially hydrolysing peptidoglycan in the periplasm (and perhaps negatively affecting other bacterial systems unknown), rendering cells sensitive to external pressures. Further experimentation using *in vitro* peptidoglycan degradation assays with this constitutively active AmiA would be required to confirm that it is in fact active and stable. This does however highlight an idea that if the LytM domain could be replicated with a small peptide that is able to cross the outer membrane, it could inappropriately activate AmiA and AmiB to hydrolyse peptidoglycan, rendering cells sensitive to external pressures. This could be a method to use to weaken bacterial cells before antibiotic treatment, however this would require extensive research.

An expansion of this field of work could appear as a further investigation of the AmiC activation pathway, exploration of other amidase regulation systems and a more medical route, the investigation of inappropriate activation of the division-associated amidases.

Firstly, the AmiC interaction and activation with NlpD while is known, the structural mechanism by which this occurs is currently unknown. It would be curious to find if the NlpD activation of AmiC is similar to the activation of AmiA or AmiB with EnvC as explored in this thesis, it would appear to be a similar mechanism of the removal of the blocking helix, however where on the AmiC structure NlpD would bind and activate AmiC, is unknown. An exploration of interaction partners of NlpD would also be useful to measure if this relates, if at all, to the activation mechanism of FtsEX on EnvC via ATP binding and hydrolysis.

Secondly, as eluded to by NlpI (Banzhaf et al., 2020) and ActS (Gurnani Serano et al., 2021), there are other proteins which interact with AmiA, AmiB and AmiC. Whether these interactions are in terms of activation, regulation or to promote other protein-protein interactions, further investigation of other binding partners of these amidases would hopefully highlight differences between the three amidases or highlight other regulation pathways which alter the activity of the amidases due to other environmental stress or stimuli. Adding to the interaction list of these division-associated amidases would provide a greater picture of the true inter-workings of the periplasm, a fundamental, and potentially conserved region of Gram-negative bacteria. . In conclusion, there are still a significant selection of questions and research routes to explore in this area of research in division-associated amidases, both fundamental biology but also potential medical applications.

## References

- Aarsman, M. E. G., Piette, A., Fraipont, C., Vinkenvleugel, T. M. F., Nguyen-Distèche, M., & den Blaauwen, T. (2005). Maturation of the Escherichia coli divisome occurs in two steps [eprint: <https://onlinelibrary.wiley.com/doi/pdf/10.1111/j.1365-2958.2005.04502.x>]. *Molecular Microbiology*, *55*(6), 1631–1645. <https://doi.org/10.1111/j.1365-2958.2005.04502.x>
- Addinall, S. G., Cao, C., & Lutkenhaus, J. (1997). FtsN, a late recruit to the septum in Escherichia coli. *Molecular Microbiology*, *25*(2), 303–309. <https://doi.org/10.1046/j.1365-2958.1997.4641833.x>
- Alcorlo, M., Straume, D., Lutkenhaus, J., Håvarstein, L. S., & Hermoso, J. A. (2020). Structural Characterization of the Essential Cell Division Protein FtsE and Its Interaction with FtsX in Streptococcus pneumoniae. *mBio*, *11*(5), e01488–20. <https://doi.org/10.1128/mBio.01488-20>
- Alcorlo, M., Dik, D. A., De Benedetti, S., Mahasanan, K. V., Lee, M., Domínguez-Gil, T., Heseck, D., Lastochkin, E., López, D., Boggess, B., Mobashery, S., & Hermoso, J. A. (2019). Structural basis of denuded glycan recognition by SPOR domains in bacterial cell division [Number: 1 Publisher: Nature Publishing Group]. *Nature Communications*, *10*(1), 5567. <https://doi.org/10.1038/s41467-019-13354-4>
- Alcorlo, M., Martínez-Caballero, S., Molina, R., & Hermoso, J. A. (2017). Carbohydrate recognition and lysis by bacterial peptidoglycan hydrolases. *Current Opinion in Structural Biology*, *44*, 87–100. <https://doi.org/10.1016/j.sbi.2017.01.001>
- Alves Feliciano, C., Eckenroth, B. E., Diaz, O. R., Doublíé, S., & Shen, A. (2021). A lipoprotein allosterically activates the CwID amidase during Clostridioides difficile spore formation. *PLoS Genetics*, *17*(9), e1009791. <https://doi.org/10.1371/journal.pgen.1009791>
- Anderson, D. E., Gueiros-Filho, F. J., & Erickson, H. P. (2004). Assembly Dynamics of FtsZ Rings in Bacillus subtilis and Escherichia coli and Effects of FtsZ-Regulating Proteins [Publisher: American Society for Microbiology]. *Journal of Bacteriology*, *186*(17), 5775–5781. <https://doi.org/10.1128/JB.186.17.5775-5781.2004>
- Andreou, A., Giastas, P., Christoforides, E., & Eliopoulos, E. E. (2018). Structural and Evolutionary Insights within the Polysaccharide Deacetylase Gene

- Family of Bacillus anthracis and Bacillus cereus. *Genes*, 9(8), 386. <https://doi.org/10.3390/genes9080386>
- Arends, S. J. R., Kustus, R. J., & Weiss, D. S. (2009). ATP-Binding Site Lesions in FtsE Impair Cell Division. *Journal of Bacteriology*, 191(12), 3772–3784. <https://doi.org/10.1128/JB.00179-09>
- Ashkenazy, H., Abadi, S., Martz, E., Chay, O., Mayrose, I., Pupko, T., & Ben-Tal, N. (2016). ConSurf 2016: An improved methodology to estimate and visualize evolutionary conservation in macromolecules. *Nucleic Acids Research*, 44(W1), W344–W350. <https://doi.org/10.1093/nar/gkw408>
- Attaibi, M., & den Blaauwen, T. (2022). An Updated Model of the Divisome: Regulation of the Septal Peptidoglycan Synthesis Machinery by the Divisome. *International Journal of Molecular Sciences*, 23(7), 3537. <https://doi.org/10.3390/ijms23073537>
- Aussel, L., Barre, F. X., Aroyo, M., Stasiak, A., Stasiak, A. Z., & Sherratt, D. (2002). FtsK Is a DNA motor protein that activates chromosome dimer resolution by switching the catalytic state of the XerC and XerD recombinases. *Cell*, 108(2), 195–205. [https://doi.org/10.1016/s0092-8674\(02\)00624-4](https://doi.org/10.1016/s0092-8674(02)00624-4)
- Baba, T., Ara, T., Hasegawa, M., Takai, Y., Okumura, Y., Baba, M., Datsenko, K. A., Tomita, M., Wanner, B. L., & Mori, H. (2006). Construction of Escherichia coli K-12 in-frame, single-gene knockout mutants: The Keio collection. *Molecular Systems Biology*, 2, 2006.0008. <https://doi.org/10.1038/msb4100050>
- Bailey, M. W., Bisicchia, P., Warren, B. T., Sherratt, D. J., & Männik, J. (2014). Evidence for Divisome Localization Mechanisms Independent of the Min System and SlmA in Escherichia coli [Publisher: Public Library of Science]. *PLOS Genetics*, 10(8), e1004504. <https://doi.org/10.1371/journal.pgen.1004504>
- Balakrishnan, S., Kamisetty, H., Carbonell, J. G., Lee, S.-I., & Langmead, C. J. (2011). Learning generative models for protein fold families [eprint: <https://onlinelibrary.wiley.com/>]. *Proteins: Structure, Function, and Bioinformatics*, 79(4), 1061–1078. <https://doi.org/10.1002/prot.22934>
- Banzhaf, M., Yau, H. C., Verheul, J., Lodge, A., Kritikos, G., Mateus, A., Cordier, B., Hov, A. K., Stein, F., Wartel, M., Pazos, M., Solovyova, A. S., Breukink, E., van Teeffelen, S., Savitski, M. M., den Blaauwen, T., Typas, A., & Vollmer, W. (2020). Outer membrane lipoprotein NlpI scaffolds pepti-

- doglycan hydrolases within multi-enzyme complexes in *Escherichia coli*. *The EMBO Journal*, 39(5), e102246. <https://doi.org/10.15252/emj.2019102246>
- Baranova, N., Radler, P., Hernández-Rocamora, V. M., Alfonso, C., López-Peigrín, M., Rivas, G., Vollmer, W., & Loose, M. (2020). Diffusion and capture permits dynamic coupling between treadmilling FtsZ filaments and cell division proteins [Number: 3 Publisher: Nature Publishing Group]. *Nature Microbiology*, 5(3), 407–417. <https://doi.org/10.1038/s41564-019-0657-5>
- Barre, F. X., Aroyo, M., Colloms, S. D., Helfrich, A., Cornet, F., & Sherratt, D. J. (2000). FtsK functions in the processing of a Holliday junction intermediate during bacterial chromosome segregation. *Genes & Development*, 14(23), 2976–2988. <https://doi.org/10.1101/gad.188700>
- Begg, K. J., Hatfull, G. F., & Donachie, W. D. (1980). Identification of new genes in a cell envelope-cell division gene cluster of *Escherichia coli*: Cell division gene ftsQ [Publisher: American Society for Microbiology]. *Journal of Bacteriology*, 144(1), 435–437. <https://doi.org/10.1128/jb.144.1.435-437.1980>
- Bei, W., Luo, Q., Shi, H., Zhou, H., Zhou, M., Zhang, X., & Huang, Y. (2022). Cryo-EM structures of LolCDE reveal the molecular mechanism of bacterial lipoprotein sorting in *Escherichia coli* [Publisher: Public Library of Science]. *PLOS Biology*, 20(10), e3001823. <https://doi.org/10.1371/journal.pbio.3001823>
- Benchling. (2022). Editor · Benchling. Retrieved February 11, 2022, from <https://benchling.com/editor>
- Bernard, C. S., Sadasivam, M., Shiomi, D., & Margolin, W. (2007). An altered FtsA can compensate for the loss of essential cell division protein FtsN in *Escherichia coli* [eprint: <https://onlinelibrary.wiley.com/doi/pdf/10.1111/j.1365-2958.2007.05738.x>]. *Molecular Microbiology*, 64(5), 1289–1305. <https://doi.org/10.1111/j.1365-2958.2007.05738.x>
- Bernhardt, T. G., & De Boer, P. A. J. (2004). Screening for synthetic lethal mutants in *Escherichia coli* and identification of EnvC (YibP) as a periplasmic septal ring factor with murein hydrolase activity [eprint: <https://onlinelibrary.wiley.com/doi/pdf/10.1111/j.1365-2958.2004.04063.x>]. *Molecular Microbiology*, 52(5), 1255–1269. <https://doi.org/10.1111/j.1365-2958.2004.04063.x>
- Bernhardt, T. G., & de Boer, P. A. J. (2003). The *Escherichia coli* amidase AmiC is a periplasmic septal ring component exported via the twin-arginine trans-

- port pathway. *Molecular microbiology*, 48(5), 1171–1182. Retrieved December 1, 2022, from <https://www.ncbi.nlm.nih.gov/pmc/articles/PMC4428285/>
- Bertani, G. (1951). Studies on lysogenesis. I. The mode of phage liberation by lysogenic *Escherichia coli*. *Journal of Bacteriology*, 62(3), 293–300. <https://doi.org/10.1128/jb.62.3.293-300.1951>
- Bertsche, U., Kast, T., Wolf, B., Fraipont, C., Aarsman, M. E. G., Kannenberg, K., Von Rechenberg, M., Nguyen-Distèche, M., Den Blaauwen, T., Höltje, J.-V., & Vollmer, W. (2006). Interaction between two murein (peptidoglycan) synthases, PBP3 and PBP1B, in *Escherichia coli* [eprint: <https://onlinelibrary.wiley.com/doi/pdf/10.1111/j.1365-2958.2006.05280.x>]. *Molecular Microbiology*, 61(3), 675–690. <https://doi.org/10.1111/j.1365-2958.2006.05280.x>
- Bigot, S., Corre, J., Louarn, J.-M., Cornet, F., & Barre, F.-X. (2004). FtsK activities in Xer recombination, DNA mobilization and cell division involve overlapping and separate domains of the protein. *Molecular Microbiology*, 54(4), 876–886. <https://doi.org/10.1111/j.1365-2958.2004.04335.x>
- Biolabs, N. E. (2022). New England Biolabs (UK) Ltd - /. Retrieved February 11, 2022, from <https://www.neb.uk.com/>
- Bishop, R. E., Gibbons, H. S., Guina, T., Trent, M. S., Miller, S. I., & Raetz, C. R. (2000). Transfer of palmitate from phospholipids to lipid A in outer membranes of gram-negative bacteria. *The EMBO journal*, 19(19), 5071–5080. <https://doi.org/10.1093/emboj/19.19.5071>
- Bisson-Filho, A. W., Hsu, Y.-P., Squyres, G. R., Kuru, E., Wu, F., Jukes, C., Sun, Y., Dekker, C., Holden, S., VanNieuwenhze, M. S., Brun, Y. V., & Garner, E. C. (2017). Treadmilling by FtsZ filaments drives peptidoglycan synthesis and bacterial cell division [Publisher: American Association for the Advancement of Science]. *Science*, 355(6326), 739–743. <https://doi.org/10.1126/science.aak9973>
- Boer, P. A. J. d., Crossley, R. E., & Rothfield, L. I. (1989). A division inhibitor and a topological specificity factor coded for by the minicell locus determine proper placement of the division septum in *E. coli* [Publisher: Elsevier]. *Cell*, 56(4), 641–649. [https://doi.org/10.1016/0092-8674\(89\)90586-2](https://doi.org/10.1016/0092-8674(89)90586-2)
- Bonis, M., Ecobichon, C., Guadagnini, S., Prévost, M.-C., & Boneca, I. G. (2010). A M23B family metallopeptidase of *Helicobacter pylori* required for cell shape, pole formation and virulence [eprint: <https://onlinelibrary.wiley.com/doi/pdf/10.1111/j.1365->

- 2958.2010.07383.x]. *Molecular Microbiology*, 78(4), 809–819. <https://doi.org/10.1111/j.1365-2958.2010.07383.x>
- Boyle, D. S., Grant, D., Draper, G. C., & Donachie, W. D. (2000). All major regions of FtsK are required for resolution of chromosome dimers. *Journal of Bacteriology*, 182(14), 4124–4127. <https://doi.org/10.1128/JB.182.14.4124-4127.2000>
- Briggs, N. S., Bruce, K. E., Naskar, S., Winkler, M. E., & Roper, D. I. (2021). The Pneumococcal Divisome: Dynamic Control of *Streptococcus pneumoniae* Cell Division. *Frontiers in Microbiology*, 12, 737396. <https://doi.org/10.3389/fmicb.2021.737396>
- Browder, H. P., Zygmunt, W. A., Young, J. R., & Tavormina, P. A. (1965). Lysostaphin: Enzymatic mode of action. *Biochemical and Biophysical Research Communications*, 19(3), 383–389. [https://doi.org/10.1016/0006-291X\(65\)90473-0](https://doi.org/10.1016/0006-291X(65)90473-0)
- Brown, A. R., Gordon, R. A., Hyland, S. N., Siegrist, M. S., & Grimes, C. L. (2020). Chemical Biology Tools for Examining the Bacterial Cell Wall [Publisher: Elsevier]. *Cell Chemical Biology*, 27(8), 1052–1062. <https://doi.org/10.1016/j.chembiol.2020.07.024>
- Buddelmeijer, N., & Beckwith, J. (2004). A complex of the *Escherichia coli* cell division proteins FtsL, FtsB and FtsQ forms independently of its localization to the septal region [eprint: <https://onlinelibrary.wiley.com/doi/pdf/10.1111/j.1365-2958.2004.04044.x>]. *Molecular Microbiology*, 52(5), 1315–1327. <https://doi.org/10.1111/j.1365-2958.2004.04044.x>
- Busiek, K. K., Eraso, J. M., Wang, Y., & Margolin, W. (2012). The Early Divisome Protein FtsA Interacts Directly through Its Ic Subdomain with the Cytoplasmic Domain of the Late Divisome Protein FtsN [Publisher: American Society for Microbiology]. *Journal of Bacteriology*, 194(8), 1989–2000. <https://doi.org/10.1128/JB.06683-11>
- Buske, P. J., & Levin, P. A. (2012). Extreme C Terminus of Bacterial Cytoskeletal Protein FtsZ Plays Fundamental Role in Assembly Independent of Modulatory Proteins \* [Publisher: Elsevier]. *Journal of Biological Chemistry*, 287(14), 10945–10957. <https://doi.org/10.1074/jbc.M111.330324>
- Buss, J., Coltharp, C., Huang, T., Pohlmeier, C., Wang, S.-C., Hatem, C., & Xiao, J. (2013). In vivo organization of the FtsZ-ring by ZapA and ZapB revealed by quantitative super-resolution microscopy [eprint: <https://onlinelibrary.wiley.com/doi/pdf/10.1111>

- Molecular Microbiology*, 89(6), 1099–1120. <https://doi.org/10.1111/mmi.12331>
- Buss, J. A., Peters, N. T., Xiao, J., & Bernhardt, T. G. (2017). ZapA and ZapB form an FtsZ-independent structure at midcell [eprint: <https://onlinelibrary.wiley.com/doi/pdf/10.1111/mmi.13655>]. *Molecular Microbiology*, 104(4), 652–663. <https://doi.org/10.1111/mmi.13655>
- Büttner, F. M., Faulhaber, K., Forchhammer, K., Maldener, I., & Stehle, T. (2016). Enabling cell-cell communication via nanopore formation: Structure, function and localization of the unique cell wall amidase AmiC2 of *Nostoc punctiforme*. *The FEBS journal*, 283(7), 1336–1350. <https://doi.org/10.1111/febs.13673>
- Büttner, F. M., Zoll, S., Nega, M., Götz, F., & Stehle, T. (2014). Structure-Function Analysis of *Staphylococcus aureus* Amidase Reveals the Determinants of Peptidoglycan Recognition and Cleavage \* [Publisher: Elsevier]. *Journal of Biological Chemistry*, 289(16), 11083–11094. <https://doi.org/10.1074/jbc.M114.557306>
- Carrasco-López, C., Rojas-Altuve, A., Zhang, W., Heseck, D., Lee, M., Barbe, S., André, I., Ferrer, P., Silva-Martin, N., Castro, G. R., Martínez-Ripoll, M., Mobashery, S., & Hermoso, J. A. (2011). Crystal Structures of Bacterial Peptidoglycan Amidase AmpD and an Unprecedented Activation Mechanism \* [Publisher: Elsevier]. *Journal of Biological Chemistry*, 286(36), 31714–31722. <https://doi.org/10.1074/jbc.M111.264366>
- Chen, J. C., & Beckwith, J. (2001). FtsQ, FtsL and FtsI require FtsK, but not FtsN, for co-localization with FtsZ during *Escherichia coli* cell division. *Molecular Microbiology*, 42(2), 395–413. <https://doi.org/10.1046/j.1365-2958.2001.02640.x>
- Chen, Y., & Erickson, H. P. (2005). Rapid in Vitro Assembly Dynamics and Subunit Turnover of FtsZ Demonstrated by Fluorescence Resonance Energy Transfer \* [Publisher: Elsevier]. *Journal of Biological Chemistry*, 280(23), 22549–22554. <https://doi.org/10.1074/jbc.M500895200>
- Cohen, D. N., Sham, Y. Y., Haugstad, G. D., Xiang, Y., Rossmann, M. G., Anderson, D. L., & Popham, D. L. (2009). Shared catalysis in virus entry and bacterial cell wall depolymerization. *Journal of Molecular Biology*, 387(3), 607–618. <https://doi.org/10.1016/j.jmb.2009.02.001>
- Coltharp, C., Buss, J., Plumer, T. M., & Xiao, J. (2016). Defining the rate-limiting processes of bacterial cytokinesis [Company: National Academy of Sci-

- ences Distributor: National Academy of Sciences Institution: National Academy of Sciences Label: National Academy of Sciences Publisher: Proceedings of the National Academy of Sciences]. *Proceedings of the National Academy of Sciences*, *113*(8), E1044–E1053. <https://doi.org/10.1073/pnas.1514296113>
- Conti, J., Viola, M. G., & Camberg, J. L. (2018). FtsA reshapes membrane architecture and remodels the Z-ring in *Escherichia coli* [eprint: <https://onlinelibrary.wiley.com/doi/pdf/10.1111/mmi.13902>]. *Molecular Microbiology*, *107*(4), 558–576. <https://doi.org/10.1111/mmi.13902>
- Cook, J., Baverstock, T. C., McAndrew, M. B. L., Stansfeld, P. J., Roper, D. I., & Crow, A. (2020). Insights into bacterial cell division from a structure of EnvC bound to the FtsX periplasmic domain [Publisher: Proceedings of the National Academy of Sciences]. *Proceedings of the National Academy of Sciences*, *117*(45), 28355–28365. <https://doi.org/10.1073/pnas.2017134117>
- Cook, W. R., de Boer, P. A. J., & Rothfield, L. I. (1989). Differentiation of the Bacterial Cell Division Site. In G. H. Bourne, K. W. Jeon, & M. Friedlander (Eds.), *International Review of Cytology* (pp. 1–31). Academic Press. [https://doi.org/10.1016/S0074-7696\(08\)60871-2](https://doi.org/10.1016/S0074-7696(08)60871-2)
- Corbin, B. D., Geissler, B., Sadasivam, M., & Margolin, W. (2004). Z-Ring-Independent Interaction between a Subdomain of FtsA and Late Septation Proteins as Revealed by a Polar Recruitment Assay. *Journal of Bacteriology*, *186*(22), 7736–7744. <https://doi.org/10.1128/JB.186.22.7736-7744.2004>
- Corbin, B. D., Wang, Y., Beuria, T. K., & Margolin, W. (2007). Interaction between cell division proteins FtsE and FtsZ. *Journal of Bacteriology*, *189*(8), 3026–3035. <https://doi.org/10.1128/JB.01581-06>
- Crawford, M. A., Lowe, D. E., Fisher, D. J., Stibitz, S., Plaut, R. D., Beaber, J. W., Zemansky, J., Mehrad, B., Glomski, I. J., Strieter, R. M., & Hughes, M. A. (2011). Identification of the bacterial protein FtsX as a unique target of chemokine-mediated antimicrobial activity against *Bacillus anthracis*. *Proceedings of the National Academy of Sciences of the United States of America*, *108*(41), 17159–17164. <https://doi.org/10.1073/pnas.1108495108>
- Crickmore, N., & Salmond, G. P. (1992). Genetic and physical clarification of the *Escherichia coli* genetic map in the 76.5-minute essential gene cluster

- ter containing heat shock and cell division genes. *Journal of Bacteriology*, *174*(23), 7880. <https://doi.org/10.1128/jb.174.23.7880.1992>
- Crow, A., Greene, N. P., Kaplan, E., & Koronakis, V. (2017). Structure and mechanotransmission mechanism of the MacB ABC transporter superfamily [Publisher: Proceedings of the National Academy of Sciences]. *Proceedings of the National Academy of Sciences*, *114*(47), 12572–12577. <https://doi.org/10.1073/pnas.1712153114>
- Dai, K., & Lutkenhaus, J. (1992). The proper ratio of FtsZ to FtsA is required for cell division to occur in *Escherichia coli* [Publisher: American Society for Microbiology]. *Journal of Bacteriology*, *174*(19), 6145–6151. <https://doi.org/10.1128/jb.174.19.6145-6151.1992>
- Dai, K., Xu, Y., & Lutkenhaus, J. (1993). Cloning and characterization of ftsN, an essential cell division gene in *Escherichia coli* isolated as a multicopy suppressor of ftsA12(Ts). *Journal of Bacteriology*, *175*(12), 3790–3797. <https://doi.org/10.1128/jb.175.12.3790-3797.1993>
- Daley, D. O., Rapp, M., Granseth, E., Melén, K., Drew, D., & von Heijne, G. (2005). Global topology analysis of the *Escherichia coli* inner membrane proteome. *Science (New York, N.Y.)*, *308*(5726), 1321–1323. <https://doi.org/10.1126/science.1109730>
- Datsenko, K. A., & Wanner, B. L. (2000). One-step inactivation of chromosomal genes in *Escherichia coli* K-12 using PCR products. *Proceedings of the National Academy of Sciences of the United States of America*, *97*(12), 6640–6645. <https://doi.org/10.1073/pnas.120163297>
- Dawson, R. J. P., & Locher, K. P. (2006). Structure of a bacterial multidrug ABC transporter [Number: 7108 Publisher: Nature Publishing Group]. *Nature*, *443*(7108), 180–185. <https://doi.org/10.1038/nature05155>
- de Boer, P. A. (2010). Advances in understanding *E. coli* cell fission. *Current Opinion in Microbiology*, *13*(6), 730–737. <https://doi.org/10.1016/j.mib.2010.09.015>
- Di Lallo, G., Fagioli, M., Barionovi, D., Ghelardini, P., & Paolozzi, L. (2003). Use of a two-hybrid assay to study the assembly of a complex multicomponent protein machinery: Bacterial septosome differentiation. *Microbiology (Reading, England)*, *149*(Pt 12), 3353–3359. <https://doi.org/10.1099/mic.0.26580-0>
- Domínguez-Cuevas, P., Porcelli, I., Daniel, R. A., & Errington, J. (2013). Differentiated roles for MreB-actin isologues and autolytic enzymes in *Bacillus*

- subtilis morphogenesis. *Molecular Microbiology*, 89(6), 1084–1098. <https://doi.org/10.1111/mmi.12335>
- Du, S., Henke, W., Pichoff, S., & Lutkenhaus, J. (2019). How FtsEX localizes to the Z ring and interacts with FtsA to regulate cell division. *Molecular microbiology*, 112(3), 881–895. <https://doi.org/10.1111/mmi.14324>
- Du, S., & Lutkenhaus, J. (2017). Assembly and Activation of the Escherichia coli Divisome. *Molecular microbiology*, 105(2), 177–187. <https://doi.org/10.1111/mmi.13696>
- Du, S., & Lutkenhaus, J. (2019). At the Heart of Bacterial Cytokinesis: The Z Ring [Publisher: Elsevier]. *Trends in Microbiology*, 27(9), 781–791. <https://doi.org/10.1016/j.tim.2019.04.011>
- Du, S., Pichoff, S., Kruse, K., & Lutkenhaus, J. (2018). FtsZ filaments have the opposite kinetic polarity of microtubules [Publisher: Proceedings of the National Academy of Sciences]. *Proceedings of the National Academy of Sciences*, 115(42), 10768–10773. <https://doi.org/10.1073/pnas.1811919115>
- Du, S., Pichoff, S., & Lutkenhaus, J. (2016). FtsEX acts on FtsA to regulate divisome assembly and activity. *Proceedings of the National Academy of Sciences of the United States of America*, 113(34), E5052–5061. <https://doi.org/10.1073/pnas.1606656113>
- Dubarry, N., Possoz, C., & Barre, F.-X. (2010). Multiple regions along the Escherichia coli FtsK protein are implicated in cell division [eprint: <https://onlinelibrary.wiley.com/doi/10.1111/j.1365-2958.2010.07412.x>]. *Molecular Microbiology*, 78(5), 1088–1100. <https://doi.org/10.1111/j.1365-2958.2010.07412.x>
- D’Ulisse, V., Fagioli, M., Ghelardini, P., & Paolozzi, L. (2007). Three functional subdomains of the Escherichia coli FtsQ protein are involved in its interaction with the other division proteins. *Microbiology (Reading, England)*, 153(Pt 1), 124–138. <https://doi.org/10.1099/mic.0.2006/000265-0>
- Duncan, T. R., Yahashiri, A., Arends, S. J. R., Popham, D. L., & Weiss, D. S. (2013). Identification of SPOR Domain Amino Acids Important for Septal Localization, Peptidoglycan Binding, and a Disulfide Bond in the Cell Division Protein FtsN [Publisher: American Society for Microbiology]. *Journal of Bacteriology*, 195(23), 5308–5315. <https://doi.org/10.1128/JB.00911-13>
- Durand-Heredia, J., Rivkin, E., Fan, G., Morales, J., & Janakiraman, A. (2012). Identification of ZapD as a Cell Division Factor That Promotes the Assembly of FtsZ in Escherichia coli [Publisher: American Society for Mi-

- crobiology]. *Journal of Bacteriology*, *194*(12), 3189–3198. <https://doi.org/10.1128/JB.00176-12>
- Durand-Heredia, J. M., Yu, H. H., De Carlo, S., Lesser, C. F., & Janakiraman, A. (2011). Identification and Characterization of ZapC, a Stabilizer of the FtsZ Ring in *Escherichia coli* [Publisher: American Society for Microbiology]. *Journal of Bacteriology*, *193*(6), 1405–1413. <https://doi.org/10.1128/JB.01258-10>
- Egan, A. J. F., Errington, J., & Vollmer, W. (2020). Regulation of peptidoglycan synthesis and remodelling [Number: 8 Publisher: Nature Publishing Group]. *Nature Reviews Microbiology*, *18*(8), 446–460. <https://doi.org/10.1038/s41579-020-0366-3>
- Egan, A. J. F., Jean, N. L., Koumoutsis, A., Bougault, C. M., Biboy, J., Sassine, J., Solovyova, A. S., Breukink, E., Typas, A., Vollmer, W., & Simorre, J.-P. (2014). Outer-membrane lipoprotein LpoB spans the periplasm to stimulate the peptidoglycan synthase PBP1B [Publisher: Proceedings of the National Academy of Sciences]. *Proceedings of the National Academy of Sciences*, *111*(22), 8197–8202. <https://doi.org/10.1073/pnas.1400376111>
- Emsley, P., Lohkamp, B., Scott, W. G., & Cowtan, K. (2010). Features and development of Coot. *Acta Crystallographica. Section D, Biological Crystallography*, *66*(Pt 4), 486–501. <https://doi.org/10.1107/S0907444910007493>
- Erickson, H. P., Anderson, D. E., & Osawa, M. (2010). FtsZ in Bacterial Cytokinesis: Cytoskeleton and Force Generator All in One [Publisher: American Society for Microbiology]. *Microbiology and Molecular Biology Reviews*, *74*(4), 504–528. <https://doi.org/10.1128/MMBR.00021-10>
- Euromedex. (2022). LIFE SCIENCE PRODUCTS – Euromedex, a world of solutions for a world of health. Retrieved February 11, 2022, from <https://web.euromedex.com/en/life-science-products/>
- Fenton, M., McAuliffe, O., O’Mahony, J., & Coffey, A. (2010). Recombinant bacteriophage lysins as antibacterials [Publisher: Taylor & Francis eprint: <https://doi.org/10.4161/bbug.1.1.9818>]. *Bioengineered Bugs*, *1*(1), 9–16. <https://doi.org/10.4161/bbug.1.1.9818>
- Finn, R. D., Tate, J., Mistry, J., Coghill, P. C., Sammut, S. J., Hotz, H.-R., Ceric, G., Forslund, K., Eddy, S. R., Sonnhammer, E. L. L., & Bateman, A. (2008). The Pfam protein families database. *Nucleic Acids Research*, *36*(Database issue), D281–D288. <https://doi.org/10.1093/nar/gkm960>

- Firczuk, M., & Bochtler, M. (2007). Folds and activities of peptidoglycan amidases [eprint: <https://onlinelibrary.wiley.com/doi/pdf/10.1111/j.1574-6976.2007.00084.x>]. *FEMS Microbiology Reviews*, 31(6), 676–691. <https://doi.org/10.1111/j.1574-6976.2007.00084.x>
- Firczuk, M., Mucha, A., & Bochtler, M. (2005). Crystal structures of active LytM. *Journal of Molecular Biology*, 354(3), 578–590. <https://doi.org/10.1016/j.jmb.2005.09.082>
- Fusinita van den Ent & Löwe, J. (2000). Crystal structure of the cell division protein FtsA from *Thermotoga maritima* [Publisher: John Wiley & Sons, Ltd]. *The EMBO Journal*, 19(20), 5300–5307. <https://doi.org/10.1093/emboj/19.20.5300>
- Garcia, P., Garcia, E., Ronda, C., Lopez, R., & Tomasz, A. (1983). A phage-associated murein hydrolase in *Streptococcus pneumoniae* infected with bacteriophage Dp-1. *Journal of General Microbiology*, 129(2), 489–497. <https://doi.org/10.1099/00221287-129-2-489>
- Garde, S., Chodiseti, P. K., & Reddy, M. (2021). Peptidoglycan: Structure, Synthesis, and Regulation [Publisher: American Society for Microbiology]. *EcoSal Plus*, 9(2). <https://doi.org/10.1128/ecosalplus.ESP-0010-2020>
- Gardner, K. A. J. A., Moore, D. A., & Erickson, H. P. (2013). The C-terminal linker of *Escherichia coli* FtsZ functions as an intrinsically disordered peptide [eprint: <https://onlinelibrary.wiley.com/doi/pdf/10.1111/mmi.12279>]. *Molecular Microbiology*, 89(2), 264–275. <https://doi.org/10.1111/mmi.12279>
- Geissler, B., & Margolin, W. (2005). Evidence for functional overlap among multiple bacterial cell division proteins: Compensating for the loss of FtsK. *Molecular Microbiology*, 58(2), 596–612. <https://doi.org/10.1111/j.1365-2958.2005.04858.x>
- Gennity, J. M., & Inouye, M. (1991). The protein sequence responsible for lipoprotein membrane localization in *Escherichia coli* exhibits remarkable specificity. *The Journal of Biological Chemistry*, 266(25), 16458–16464.
- Gerding, M. A., Liu, B., Bendezú, F. O., Hale, C. A., Bernhardt, T. G., & de Boer, P. A. J. (2009). Self-Enhanced Accumulation of FtsN at Division Sites and Roles for Other Proteins with a SPOR Domain (DamX, DedD, and RlpA) in *Escherichia coli* Cell Constriction [Publisher: American Society for Microbiology]. *Journal of Bacteriology*, 191(24), 7383–7401. <https://doi.org/10.1128/JB.00811-09>

- Gerding, M. A., Ogata, Y., Pecora, N. D., Niki, H., & De Boer, P. A. J. (2007). The trans-envelope Tol–Pal complex is part of the cell division machinery and required for proper outer-membrane invagination during cell constriction in *E. coli* [eprint: <https://onlinelibrary.wiley.com/doi/pdf/10.1111/j.1365-2958.2006.05571.x>]. *Molecular Microbiology*, *63*(4), 1008–1025. <https://doi.org/10.1111/j.1365-2958.2006.05571.x>
- Ghigo, J.-M., Weiss, D. S., Chen, J. C., Yarrow, J. C., & Beckwith, J. (1999). Localization of FtsL to the *Escherichia coli* septal ring [eprint: <https://onlinelibrary.wiley.com/doi/pdf/10.1111/j.1365-2958.1999.01213.x>]. *Molecular Microbiology*, *31*(2), 725–737. <https://doi.org/10.1046/j.1365-2958.1999.01213.x>
- Gibbs, T. W., Gill, D. R., & Salmond, G. P. (1992). Localised mutagenesis of the fts YEX operon: Conditionally lethal missense substitutions in the FtsE cell division protein of *Escherichia coli* are similar to those found in the cystic fibrosis transmembrane conductance regulator protein (CFTR) of human patients. *Molecular & general genetics: MGG*, *234*(1), 121–128. <https://doi.org/10.1007/BF00272353>
- Gill, D. R., Hatfull, G. F., & Salmond, G. P. (1986). A new cell division operon in *Escherichia coli*. *Molecular & general genetics: MGG*, *205*(1), 134–145. <https://doi.org/10.1007/BF02428043>
- Gilmore, M. E., Bandyopadhyay, D., Dean, A. M., Linnstaedt, S. D., & Popham, D. L. (2004). Production of Muramic -Lactam in *Bacillus subtilis* Spore Peptidoglycan. *Journal of Bacteriology*, *186*(1), 80–89. <https://doi.org/10.1128/JB.186.1.80-89.2004>
- Goehring, N. W., & Beckwith, J. (2005). Diverse Paths to Midcell: Assembly of the Bacterial Cell Division Machinery [Publisher: Elsevier]. *Current Biology*, *15*(13), R514–R526. <https://doi.org/10.1016/j.cub.2005.06.038>
- Goehring, N. W., Gonzalez, M. D., & Beckwith, J. (2006). Premature targeting of cell division proteins to midcell reveals hierarchies of protein interactions involved in divisome assembly [eprint: <https://onlinelibrary.wiley.com/doi/pdf/10.1111/j.1365-2958.2006.05206.x>]. *Molecular Microbiology*, *61*(1), 33–45. <https://doi.org/10.1111/j.1365-2958.2006.05206.x>
- Goehring, N. W., Robichon, C., & Beckwith, J. (2007). Role for the Nonessential N Terminus of FtsN in Divisome Assembly [Publisher: American Society for Microbiology]. *Journal of Bacteriology*, *189*(2), 646–649. <https://doi.org/10.1128/JB.00992-06>

- Goley, E. D., Comolli, L. R., Fero, K. E., Downing, K. H., & Shapiro, L. (2010). DipM links peptidoglycan remodelling to outer membrane organization in *Caulobacter* [eprint: <https://onlinelibrary.wiley.com/doi/pdf/10.1111/j.1365-2958.2010.07222.x>]. *Molecular Microbiology*, *77*(1), 56–73. <https://doi.org/10.1111/j.1365-2958.2010.07222.x>
- Gonzalez, M. D., Akbay, E. A., Boyd, D., & Beckwith, J. (2010). Multiple Interaction Domains in FtsL, a Protein Component of the Widely Conserved Bacterial FtsLBQ Cell Division Complex [Publisher: American Society for Microbiology]. *Journal of Bacteriology*, *192*(11), 2757–2768. <https://doi.org/10.1128/JB.01609-09>
- Gray, A. N., Egan, A. J., van't Veer, I. L., Verheul, J., Colavin, A., Koumoutsis, A., Biboy, J., Altelaar, A. F. M., Damen, M. J., Huang, K. C., Simorre, J.-P., Breukink, E., den Blaauwen, T., Typas, A., Gross, C. A., & Vollmer, W. (2015). Coordination of peptidoglycan synthesis and outer membrane constriction during *Escherichia coli* cell division (G. Storz, Ed.) [Publisher: eLife Sciences Publications, Ltd]. *eLife*, *4*, e07118. <https://doi.org/10.7554/eLife.07118>
- Greene, N. P., Kaplan, E., Crow, A., & Koronakis, V. (2018). Antibiotic Resistance Mediated by the MacB ABC Transporter Family: A Structural and Functional Perspective. *Frontiers in Microbiology*, *9*. <https://doi.org/10.3389/fmicb.2018.00950>
- Gurnani Serrano, C. K., Winkle, M., Martorana, A. M., Biboy, J., Morè, N., Moynihan, P., Banzhaf, M., Vollmer, W., & Polissi, A. (2021). ActS activates peptidoglycan amidases during outer membrane stress in *Escherichia coli*. *Molecular Microbiology*, *116*(1), 329–342. <https://doi.org/10.1111/mmi.14712>
- Haeusser, D. P., & Margolin, W. (2016). Splitsville: Structural and functional insights into the dynamic bacterial Z ring [Number: 5 Publisher: Nature Publishing Group]. *Nature Reviews Microbiology*, *14*(5), 305–319. <https://doi.org/10.1038/nrmicro.2016.26>
- Hale, C. A., & Boer, P. A. J. d. (1997). Direct Binding of FtsZ to ZipA, an Essential Component of the Septal Ring Structure That Mediates Cell Division in *E. coli* [Publisher: Elsevier]. *Cell*, *88*(2), 175–185. [https://doi.org/10.1016/S0092-8674\(00\)81838-3](https://doi.org/10.1016/S0092-8674(00)81838-3)
- Hale, C. A., & de Boer, P. A. J. (1999). Recruitment of ZipA to the Septal Ring of *Escherichia coli* Is Dependent on FtsZ and Independent of FtsA [Pub-

- lisher: American Society for Microbiology]. *Journal of Bacteriology*, *181*(1), 167–176. <https://doi.org/10.1128/JB.181.1.167-176.1999>
- Hale, C. A., Rhee, A. C., & de Boer, P. A. J. (2000). ZipA-Induced Bundling of FtsZ Polymers Mediated by an Interaction between C-Terminal Domains [Publisher: American Society for Microbiology]. *Journal of Bacteriology*, *182*(18), 5153–5166. <https://doi.org/10.1128/JB.182.18.5153-5166.2000>
- Hale, C. A., Shiomi, D., Liu, B., Bernhardt, T. G., Margolin, W., Niki, H., & de Boer, P. A. J. (2011). Identification of *Escherichia coli* ZapC (YcbW) as a Component of the Division Apparatus That Binds and Bundles FtsZ Polymers [Publisher: American Society for Microbiology]. *Journal of Bacteriology*, *193*(6), 1393–1404. <https://doi.org/10.1128/JB.01245-10>
- Hanahan, D. (1983). Studies on transformation of *Escherichia coli* with plasmids. *Journal of Molecular Biology*, *166*(4), 557–580. [https://doi.org/10.1016/s0022-2836\(83\)80284-8](https://doi.org/10.1016/s0022-2836(83)80284-8)
- Haney, S. A., Glasfeld, E., Hale, C., Keeney, D., He, Z., & Boer, P. d. (2001). Genetic Analysis of the *Escherichia coli* FtsZ-ZipA Interaction in the Yeast Two-hybrid System: CHARACTERIZATION OF FtsZ RESIDUES ESSENTIAL FOR THE INTERACTIONS WITH ZipA AND WITH FtsA \* 210 [Publisher: Elsevier]. *Journal of Biological Chemistry*, *276*(15), 11980–11987. <https://doi.org/10.1074/jbc.M009810200>
- Hara, H., Narita, S., Karibian, D., Park, J. T., Yamamoto, Y., & Nishimura, Y. (2002). Identification and characterization of the *Escherichia coli* envC gene encoding a periplasmic coiled-coil protein with putative peptidase activity. *FEMS Microbiology Letters*, *212*(2), 229–236. <https://doi.org/10.1111/j.1574-6968.2002.tb11271.x>
- Heidrich, C., Templin, M. F., Ursinus, A., Merdanovic, M., Berger, J., Schwarz, H., De Pedro, M. A., & Höltje, J.-V. (2001). Involvement of N-acetylmuramyl-l-alanine amidases in cell separation and antibiotic-induced autolysis of *Escherichia coli* [eprint: <https://onlinelibrary.wiley.com/doi/pdf/10.1046/j.1365-2958.2001.02499.x>]. *Molecular Microbiology*, *41*(1), 167–178. <https://doi.org/10.1046/j.1365-2958.2001.02499.x>
- Heidrich, C., Ursinus, A., Berger, J., Schwarz, H., & Höltje, J.-V. (2002). Effects of Multiple Deletions of Murein Hydrolases on Viability, Septum Cleavage, and Sensitivity to Large Toxic Molecules in *Escherichia coli*. *Journal of Bacteriology*, *184*(22), 6093–6099. <https://doi.org/10.1128/JB.184.22.6093-6099.2002>

- Heijenoort, J. v. (2001). Formation of the glycan chains in the synthesis of bacterial peptidoglycan. *Glycobiology*, *11*(3), 25R–36R. <https://doi.org/10.1093/glycob/11.3.25R>
- Herricks, J. R., Nguyen, D., & Margolin, W. (2014). A thermosensitive defect in the ATP binding pocket of FtsA can be suppressed by allosteric changes in the dimer interface [Publisher: John Wiley & Sons, Ltd]. *Molecular Microbiology*, *94*(3), 713–727. <https://doi.org/10.1111/mmi.12790>
- Hillmann, F., Argentini, M., & Buddelmeijer, N. (2011). Kinetics and phospholipid specificity of apolipoprotein N-acyltransferase. *The Journal of Biological Chemistry*, *286*(32), 27936–27946. <https://doi.org/10.1074/jbc.M111.243519>
- Hollenstein, K., Frei, D. C., & Locher, K. P. (2007). Structure of an ABC transporter in complex with its binding protein [Number: 7132 Publisher: Nature Publishing Group]. *Nature*, *446*(7132), 213–216. <https://doi.org/10.1038/nature05626>
- Höltje, J.-V. (1995). From growth to autolysis: The murein hydrolases in *Escherichia coli*. *Archives of Microbiology*, *164*(4), 243–254. <https://doi.org/10.1007/BF02529958>
- Höltje, J.-V., Kopp, U., Ursinus, A., & Wiedemann, B. (1994). The negative regulator of  $\beta$ -lactamase induction AmpD is a N-acetyl-anhydromuramyl-L-alanine amidase. *FEMS Microbiology Letters*, *122*(1-2), 159–164. <https://doi.org/10.1111/j.1574-6968.1994.tb07159.x>
- Huang, K.-H., Durand-Heredia, J., & Janakiraman, A. (2013). FtsZ Ring Stability: Of Bundles, Tubules, Crosslinks, and Curves [Publisher: American Society for Microbiology]. *Journal of Bacteriology*, *195*(9), 1859–1868. <https://doi.org/10.1128/JB.02157-12>
- Huang, K.-H., Mychack, A., Tchorzewski, L., & Janakiraman, A. (2016). Characterization of the FtsZ C-Terminal Variable (CTV) Region in Z-Ring Assembly and Interaction with the Z-Ring Stabilizer ZapD in *E. coli* Cytokinesis [Publisher: Public Library of Science]. *PLOS ONE*, *11*(4), e0153337. <https://doi.org/10.1371/journal.pone.0153337>
- J, M., T, M., I, A., Cm, D., & Cp, M. (2012). Structure of the basal components of a bacterial transporter [Publisher: Proc Natl Acad Sci U S A]. *Proceedings of the National Academy of Sciences of the United States of America*, *109*(14). <https://doi.org/10.1073/pnas.1120113109>

- Jean, N. L., Rutherford, T. J., & Löwe, J. (2020). FtsK in motion reveals its mechanism for double-stranded DNA translocation [Publisher: Proceedings of the National Academy of Sciences]. *Proceedings of the National Academy of Sciences*, *117*(25), 14202–14208. <https://doi.org/10.1073/pnas.2001324117>
- Jumper, J., Evans, R., Pritzel, A., Green, T., Figurnov, M., Ronneberger, O., Tunyasuvunakool, K., Bates, R., Žídek, A., Potapenko, A., Bridgland, A., Meyer, C., Kohl, S. A. A., Ballard, A. J., Cowie, A., Romera-Paredes, B., Nikolov, S., Jain, R., Adler, J., ... Hassabis, D. (2021). Highly accurate protein structure prediction with AlphaFold [Number: 7873 Publisher: Nature Publishing Group]. *Nature*, *596*(7873), 583–589. <https://doi.org/10.1038/s41586-021-03819-2>
- Kamisetty, H., Ovchinnikov, S., & Baker, D. (2013). Assessing the utility of coevolution-based residue–residue contact predictions in a sequence- and structure-rich era [Publisher: Proceedings of the National Academy of Sciences]. *Proceedings of the National Academy of Sciences*, *110*(39), 15674–15679. <https://doi.org/10.1073/pnas.1314045110>
- Kaplan, E., Greene, N. P., Crow, A., & Koronakis, V. (2018). Insights into bacterial lipoprotein trafficking from a structure of LolA bound to the LolC periplasmic domain. *Proceedings of the National Academy of Sciences of the United States of America*, *115*(31), E7389–E7397. <https://doi.org/10.1073/pnas.1806822115>
- Karimova, G., Dautin, N., & Ladant, D. (2005). Interaction network among *Escherichia coli* membrane proteins involved in cell division as revealed by bacterial two-hybrid analysis. *Journal of Bacteriology*, *187*(7), 2233–2243. <https://doi.org/10.1128/JB.187.7.2233-2243.2005>
- Käshammer, L., Ent, F. v. d., Jeffery, M., Jean, N. L., Hale, V. L., & Löwe, J. (2022). Divisome core complex in bacterial cell division revealed by cryo-EM [Pages: 2022.11.21.517367 Section: New Results]. <https://doi.org/10.1101/2022.11.21.517367>
- Kerff, F., Petrella, S., Mercier, F., Sauvage, E., Herman, R., Pennartz, A., Zervosen, A., Luxen, A., Frère, J.-M., Joris, B., & Charlier, P. (2010). Specific Structural Features of the N-Acetylmuramoyl-l-Alanine Amidase AmiD from *Escherichia coli* and Mechanistic Implications for Enzymes of This Family. *Journal of Molecular Biology*, *397*(1), 249–259. <https://doi.org/10.1016/j.jmb.2009.12.038>

- Knowles, T. J., Scott-Tucker, A., Overduin, M., & Henderson, I. R. (2009). Membrane protein architects: The role of the BAM complex in outer membrane protein assembly. *Nature Reviews. Microbiology*, 7(3), 206–214. <https://doi.org/10.1038/nrmicro2069>
- Korkhov, V. M., Mireku, S. A., & Locher, K. P. (2012). Structure of AMP-PNP-bound vitamin B12 transporter BtuCD–F [Number: 7420 Publisher: Nature Publishing Group]. *Nature*, 490(7420), 367–372. <https://doi.org/10.1038/nature11442>
- Korndörfer, I. P., Danzer, J., Schmelcher, M., Zimmer, M., Skerra, A., & Loessner, M. J. (2006). The crystal structure of the bacteriophage PSA endolysin reveals a unique fold responsible for specific recognition of *Listeria* cell walls. *Journal of Molecular Biology*, 364(4), 678–689. <https://doi.org/10.1016/j.jmb.2006.08.069>
- Kovacs-Simon, A., Titball, R. W., & Michell, S. L. (2011). Lipoproteins of bacterial pathogens. *Infection and Immunity*, 79(2), 548–561. <https://doi.org/10.1128/IAI.00682-10>
- Krupka, M., Rowlett, V. W., Morado, D., Vitrac, H., Schoenemann, K., Liu, J., & Margolin, W. (2017). *Escherichia coli* FtsA forms lipid-bound minirings that antagonize lateral interactions between FtsZ protofilaments [Number: 1 Publisher: Nature Publishing Group]. *Nature Communications*, 8(1), 15957. <https://doi.org/10.1038/ncomms15957>
- Lee, J.-Y., Kinch, L. N., Borek, D. M., Wang, J., Wang, J., Urbatsch, I. L., Xie, X.-S., Grishin, N. V., Cohen, J. C., Otwinowski, Z., Hobbs, H. H., & Rosenbaum, D. M. (2016). Crystal structure of the human sterol transporter ABCG5/ABCG8 [Number: 7604 Publisher: Nature Publishing Group]. *Nature*, 533(7604), 561–564. <https://doi.org/10.1038/nature17666>
- Lee, M., Artola-Recolons, C., Carrasco-López, C., Martínez-Caballero, S., Heseck, D., Spink, E., Lastochkin, E., Zhang, W., Hellman, L. M., Boggess, B., Hermoso, J. A., & Mobashery, S. (2013). Cell-Wall Remodeling by the Zinc-Protease AmpDh3 from *Pseudomonas aeruginosa* [Publisher: American Chemical Society]. *Journal of the American Chemical Society*, 135(34), 12604–12607. <https://doi.org/10.1021/ja407445x>
- Leeuw, E. D., Graham, B., Phillips, G. J., Hagen-Jongman, C. M. T., Oudega, B., & Luirink, J. (1999). Molecular characterization of *Escherichia coli* FtsE and FtsX. *Molecular Microbiology*, 31(3), 983–993. <https://doi.org/10.1046/j.1365-2958.1999.01245.x>

- Levdikov, V. M., Blagova, E. V., McFeat, A., Fogg, M. J., Wilson, K. S., & Wilkinson, A. J. (2012). Structure of components of an intercellular channel complex in sporulating *Bacillus subtilis*. *Proceedings of the National Academy of Sciences of the United States of America*, *109*(14), 5441–5445. <https://doi.org/10.1073/pnas.1120087109>
- Levin, P. A., & Janakiraman, A. (2021). Localization, Assembly, and Activation of the *Escherichia coli* Cell Division Machinery. *EcoSal Plus*, *9*(2), eESP00222021. <https://doi.org/10.1128/ecosalplus.ESP-0022-2021>
- Liepinsh, E., Génèreux, C., Dehareng, D., Joris, B., & Otting, G. (2003). NMR Structure of *Citrobacter freundii* AmpD, Comparison with Bacteriophage T7 Lysozyme and Homology with PGRP Domains. *Journal of Molecular Biology*, *327*(4), 833–842. [https://doi.org/10.1016/S0022-2836\(03\)00185-2](https://doi.org/10.1016/S0022-2836(03)00185-2)
- Liu, B., Hale, C. A., Persons, L., Phillips-Mason, P. J., & de Boer, P. A. J. (2019). Roles of the DedD Protein in *Escherichia coli* Cell Constriction [Publisher: American Society for Microbiology]. *Journal of Bacteriology*, *201*(8), e00698–18. <https://doi.org/10.1128/JB.00698-18>
- Liu, B., Persons, L., Lee, L., & de Boer, P. A. J. (2015). Roles for both FtsA and the FtsBLQ subcomplex in FtsN-stimulated cell constriction in *Escherichia coli* [eprint: <https://onlinelibrary.wiley.com/doi/pdf/10.1111/mmi.12906>]. *Molecular Microbiology*, *95*(6), 945–970. <https://doi.org/10.1111/mmi.12906>
- Liu, Z., Mukherjee, A., & Lutkenhaus, J. (1999). Recruitment of ZipA to the division site by interaction with FtsZ [eprint: <https://onlinelibrary.wiley.com/doi/pdf/10.1046/j.1365-2958.1999.01322.x>]. *Molecular Microbiology*, *31*(6), 1853–1861. <https://doi.org/10.1046/j.1365-2958.1999.01322.x>
- LLC. (2023). The PyMOL Molecular Graphics System. Retrieved February 28, 2023, from <https://pymol.org/2/#page-top>
- Locher, K. P. (2016). Mechanistic diversity in ATP-binding cassette (ABC) transporters. *Nature Structural & Molecular Biology*, *23*(6), 487–493. <https://doi.org/10.1038/nsmb.3216>
- Loose, M., & Mitchison, T. J. (2014). The bacterial cell division proteins FtsA and FtsZ self-organize into dynamic cytoskeletal patterns [Number: 1 Publisher: Nature Publishing Group]. *Nature Cell Biology*, *16*(1), 38–46. <https://doi.org/10.1038/ncb2885>

- Lopez, R. (1981). Bacteriophages of *Streptococcus pneumoniae*. *Reviews of Infectious Diseases*, 3(2), 212–223. <https://doi.org/10.1093/clinids/3.2.212>
- Lorenz, C., Dougherty, T. J., & Lory, S. (2016). Transcriptional Responses of *Escherichia coli* to a Small-Molecule Inhibitor of LolCDE, an Essential Component of the Lipoprotein Transport Pathway. *Journal of Bacteriology*, 198(23), 3162–3175. <https://doi.org/10.1128/JB.00502-16>
- Lovell, S. C., Davis, I. W., Arendall, W. B., de Bakker, P. I. W., Word, J. M., Prisant, M. G., Richardson, J. S., & Richardson, D. C. (2003). Structure validation by Calpha geometry: Phi,psi and Cbeta deviation. *Proteins*, 50(3), 437–450. <https://doi.org/10.1002/prot.10286>
- Löwe, J., & Amos, L. A. (1998). Crystal structure of the bacterial cell-division protein FtsZ. *Nature*, 391(6663), 203–206. <https://doi.org/10.1038/34472>
- Lu, J. Z., Fujiwara, T., Komatsuzawa, H., Sugai, M., & Sakon, J. (2006). Cell wall-targeting domain of glycylglycine endopeptidase distinguishes among peptidoglycan cross-bridges. *The Journal of Biological Chemistry*, 281(1), 549–558. <https://doi.org/10.1074/jbc.M509691200>
- Luo, Q., Yang, X., Yu, S., Shi, H., Wang, K., Xiao, L., Zhu, G., Sun, C., Li, T., Li, D., Zhang, X., Zhou, M., & Huang, Y. (2017). Structural basis for lipopolysaccharide extraction by ABC transporter LptB2FG [Number: 5 Publisher: Nature Publishing Group]. *Nature Structural & Molecular Biology*, 24(5), 469–474. <https://doi.org/10.1038/nsmb.3399>
- Lutkenhaus, J. (2009). Min Oscillation in Bacteria. In M. Maroto & N. A. M. Monk (Eds.), *Cellular Oscillatory Mechanisms* (pp. 49–61). Springer. [https://doi.org/10.1007/978-0-387-09794-7\\_4](https://doi.org/10.1007/978-0-387-09794-7_4)
- Ma, X., & Margolin, W. (1999). Genetic and Functional Analyses of the Conserved C-Terminal Core Domain of *Escherichia coli* FtsZ [Publisher: American Society for Microbiology]. *Journal of Bacteriology*, 181(24), 7531–7544. <https://doi.org/10.1128/JB.181.24.7531-7544.1999>
- Malinverni, J. C., & Silhavy, T. J. (2009). An ABC transport system that maintains lipid asymmetry in the gram-negative outer membrane. *Proceedings of the National Academy of Sciences of the United States of America*, 106(19), 8009–8014. <https://doi.org/10.1073/pnas.0903229106>
- Männik, J., Walker, B. E., & Männik, J. (2018). Cell cycle-dependent regulation of FtsZ in *Escherichia coli* in slow growth conditions [eprint: <https://onlinelibrary.wiley.com/doi/pdf/10.1111/mmi.14135>]. *Molecular Microbiology*, 110(6), 1030–1044. <https://doi.org/10.1111/mmi.14135>

- Mao, G., Zhao, Y., Kang, X., Li, Z., Zhang, Y., Wang, X., Sun, F., Sankaran, K., & Zhang, X. C. (2016). Crystal structure of E. coli lipoprotein diacylglyceryl transferase. *Nature Communications*, 7, 10198. <https://doi.org/10.1038/ncomms10198>
- Marteyn, B. S., Karimova, G., Fenton, A. K., Gazi, A. D., West, N., Touqui, L., Prevost, M.-C., Betton, J.-M., Poyraz, O., Ladant, D., Gerdes, K., Sansonetti, P. J., & Tang, C. M. (2014). ZapE Is a Novel Cell Division Protein Interacting with FtsZ and Modulating the Z-Ring Dynamics [Publisher: American Society for Microbiology]. *mBio*, 5(2), e00022–14. <https://doi.org/10.1128/mBio.00022-14>
- Martínez-Caballero, S., Lee, M., Artola-Recolons, C., Carrasco-López, C., Heseck, D., Spink, E., Lastochkin, E., Zhang, W., Hellman, L. M., Boggess, B., Mobashery, S., & Hermoso, J. A. (2013). Reaction Products and the X-ray Structure of AmpDh2, a Virulence Determinant of *Pseudomonas aeruginosa* [Publisher: American Chemical Society]. *Journal of the American Chemical Society*, 135(28), 10318–10321. <https://doi.org/10.1021/ja405464b>
- Massey, T. H., Aussel, L., Barre, F.-X., & Sherratt, D. J. (2004). Asymmetric activation of Xer site-specific recombination by FtsK. *EMBO reports*, 5(4), 399–404. <https://doi.org/10.1038/sj.embor.7400116>
- Massey, T. H., Mercogliano, C. P., Yates, J., Sherratt, D. J., & Löwe, J. (2006). Double-Stranded DNA Translocation: Structure and Mechanism of Hexameric FtsK [Publisher: Elsevier]. *Molecular Cell*, 23(4), 457–469. <https://doi.org/10.1016/j.molcel.2006.06.019>
- Masuda, K., Matsuyama, S.-i., & Tokuda, H. (2002). Elucidation of the function of lipoprotein-sorting signals that determine membrane localization. *Proceedings of the National Academy of Sciences of the United States of America*, 99(11), 7390–7395. <https://doi.org/10.1073/pnas.112085599>
- Matsuyama, S. i., Yokota, N., & Tokuda, H. (1997). A novel outer membrane lipoprotein, LolB (HemM), involved in the LolA (p20)-dependent localization of lipoproteins to the outer membrane of *Escherichia coli*. *The EMBO journal*, 16(23), 6947–6955. <https://doi.org/10.1093/emboj/16.23.6947>
- Mavrici, D., Marakalala, M. J., Holton, J. M., Prigozhin, D. M., Gee, C. L., Zhang, Y. J., Rubin, E. J., & Alber, T. (2014). Mycobacterium tuberculosis FtsX extracellular domain activates the peptidoglycan hydrolase, RipC. *Pro-*

- ceedings of the National Academy of Sciences of the United States of America*, 111(22), 8037–8042. <https://doi.org/10.1073/pnas.1321812111>
- May, K. L., & Grabowicz, M. (2018). The bacterial outer membrane is an evolving antibiotic barrier [Publisher: National Academy of Sciences Section: Commentary]. *Proceedings of the National Academy of Sciences*, 115(36), 8852–8854. <https://doi.org/10.1073/pnas.1812779115>
- Mayer, M. J., Garefalaki, V., Spoerl, R., Narbad, A., & Meijers, R. (2011). Structure-based modification of a *Clostridium difficile*-targeting endolysin affects activity and host range. *Journal of Bacteriology*, 193(19), 5477–5486. <https://doi.org/10.1128/JB.00439-11>
- McCausland, J. W., Yang, X., Squyres, G. R., Lyu, Z., Bruce, K. E., Lamanna, M. M., Söderström, B., Garner, E. C., Winkler, M. E., Xiao, J., & Liu, J. (2021). Treadmilling FtsZ polymers drive the directional movement of sPG-synthesis enzymes via a Brownian ratchet mechanism [Number: 1 Publisher: Nature Publishing Group]. *Nature Communications*, 12(1), 609. <https://doi.org/10.1038/s41467-020-20873-y>
- McCoy, A. J., Grosse-Kunstleve, R. W., Adams, P. D., Winn, M. D., Storoni, L. C., & Read, R. J. (2007). Phaser crystallographic software [Number: 4 Publisher: International Union of Crystallography]. *Journal of Applied Crystallography*, 40(4), 658–674. <https://doi.org/10.1107/S0021889807021206>
- McLeod, S. M., Fleming, P. R., MacCormack, K., McLaughlin, R. E., Whiteaker, J. D., Narita, S.-I., Mori, M., Tokuda, H., & Miller, A. A. (2015). Small-molecule inhibitors of gram-negative lipoprotein trafficking discovered by phenotypic screening. *Journal of Bacteriology*, 197(6), 1075–1082. <https://doi.org/10.1128/JB.02352-14>
- Meeske, A. J., Sham, L.-T., Kimsey, H., Koo, B.-M., Gross, C. A., Bernhardt, T. G., & Rudner, D. Z. (2015). MurJ and a novel lipid II flippase are required for cell wall biogenesis in *Bacillus subtilis*. *Proceedings of the National Academy of Sciences of the United States of America*, 112(20), 6437–6442. <https://doi.org/10.1073/pnas.1504967112>
- Meisner, J., Llopis, P. M., Sham, L.-T., Garner, E., Bernhardt, T. G., & Rudner, D. Z. (2013). FtsEX is required for CwlO peptidoglycan hydrolase activity during cell wall elongation in *Bacillus subtilis*. *Molecular microbiology*, 89(6), 1069–1083. <https://doi.org/10.1111/mmi.12330>
- Meisner, J., & Moran, C. P. (2011). A LytM domain dictates the localization of proteins to the mother cell-forespore interface during bacterial endospore

- formation. *Journal of Bacteriology*, *193*(3), 591–598. <https://doi.org/10.1128/JB.01270-10>
- Möll, A., Dörr, T., Alvarez, L., Chao, M. C., Davis, B. M., Cava, F., & Waldor, M. K. (2014). Cell Separation in *Vibrio cholerae* Is Mediated by a Single Amidase Whose Action Is Modulated by Two Nonredundant Activators. *Journal of Bacteriology*, *196*(22), 3937–3948. <https://doi.org/10.1128/JB.02094-14>
- Möll, A., Schlimpert, S., Briegel, A., Jensen, G. J., & Thanbichler, M. (2010). DipM, a new factor required for peptidoglycan remodelling during cell division in *Caulobacter crescentus* [eprint: <https://onlinelibrary.wiley.com/doi/pdf/10.1111/j.1365-2958.2010.07224.x>]. *Molecular Microbiology*, *77*(1), 90–107. <https://doi.org/10.1111/j.1365-2958.2010.07224.x>
- Monteiro, J. M., Pereira, A. R., Reichmann, N. T., Saraiva, B. M., Fernandes, P. B., Veiga, H., Tavares, A. C., Santos, M., Ferreira, M. T., Macário, V., VanNieuwenhze, M. S., Filipe, S. R., & Pinho, M. G. (2018). Peptidoglycan synthesis drives an FtsZ-treadmilling-independent step of cytokinesis [Number: 7693 Publisher: Nature Publishing Group]. *Nature*, *554*(7693), 528–532. <https://doi.org/10.1038/nature25506>
- Mori, H., & Ito, K. (2001). The Sec protein-translocation pathway. *Trends in Microbiology*, *9*(10), 494–500. [https://doi.org/10.1016/s0966-842x\(01\)02174-6](https://doi.org/10.1016/s0966-842x(01)02174-6)
- Mueller, E. A., & Levin, P. A. (2020). Bacterial Cell Wall Quality Control during Environmental Stress [Publisher: American Society for Microbiology]. *mBio*, *11*(5), e02456–20. <https://doi.org/10.1128/mBio.02456-20>
- Murshudov, G. N., Vagin, A. A., & Dodson, E. J. (1997). Refinement of macromolecular structures by the maximum-likelihood method. *Acta Crystallographica. Section D, Biological Crystallography*, *53*(Pt 3), 240–255. <https://doi.org/10.1107/S09074444996012255>
- Nakada, S., Sakakura, M., Takahashi, H., Okuda, S., Tokuda, H., & Shimada, I. (2009). Structural investigation of the interaction between LolA and LolB using NMR. *The Journal of Biological Chemistry*, *284*(36), 24634–24643. <https://doi.org/10.1074/jbc.M109.001149>
- Nanninga, N. (1991). Cell division and peptidoglycan assembly in *Escherichia coli* [eprint: <https://onlinelibrary.wiley.com/doi/pdf/10.1111/j.1365-2958.1991.tb00751.x>]. *Molecular Microbiology*, *5*(4), 791–795. <https://doi.org/10.1111/j.1365-2958.1991.tb00751.x>

- Narita, S.-I., Matsuyama, S.-I., & Tokuda, H. (2004). Lipoprotein trafficking in *Escherichia coli*. *Archives of Microbiology*, *182*(1), 1–6. <https://doi.org/10.1007/s00203-004-0682-4>
- Narita, S.-i., Tanaka, K., Matsuyama, S.-i., & Tokuda, H. (2002). Disruption of lolCDE, encoding an ATP-binding cassette transporter, is lethal for *Escherichia coli* and prevents release of lipoproteins from the inner membrane. *Journal of Bacteriology*, *184*(5), 1417–1422. <https://doi.org/10.1128/JB.184.5.1417-1422.2002>
- Narita, S.-I., & Tokuda, H. (2017). Bacterial lipoproteins; biogenesis, sorting and quality control. *Biochimica Et Biophysica Acta. Molecular and Cell Biology of Lipids*, *1862*(11), 1414–1423. <https://doi.org/10.1016/j.bbalip.2016.11.009>
- Nayar, A. S., Dougherty, T. J., Ferguson, K. E., Granger, B. A., McWilliams, L., Stacey, C., Leach, L. J., Narita, S.-i., Tokuda, H., Miller, A. A., Brown, D. G., & McLeod, S. M. (2015). Novel Antibacterial Targets and Compounds Revealed by a High-Throughput Cell Wall Reporter Assay. *Journal of Bacteriology*, *197*(10), 1726–1734. <https://doi.org/10.1128/JB.02552-14>
- Nickerson, N. N., Jao, C. C., Xu, Y., Quinn, J., Skippington, E., Alexander, M. K., Miu, A., Skelton, N., Hankins, J. V., Lopez, M. S., Koth, C. M., Rutherford, S., & Nishiyama, M. (2018). A Novel Inhibitor of the LolCDE ABC Transporter Essential for Lipoprotein Trafficking in Gram-Negative Bacteria. *Antimicrobial Agents and Chemotherapy*, *62*(4), e02151–17. <https://doi.org/10.1128/AAC.02151-17>
- Okada, U., Yamashita, E., Neuberger, A., Morimoto, M., van Veen, H. W., & Murakami, S. (2017). Crystal structure of tripartite-type ABC transporter MacB from *Acinetobacter baumannii*. *Nature Communications*, *8*, 1336. <https://doi.org/10.1038/s41467-017-01399-2>
- Okonechnikov, K., Golosova, O., Fursov, M., & the UGENE team. (2012). Unipro UGENE: A unified bioinformatics toolkit. *Bioinformatics*, *28*(8), 1166–1167. <https://doi.org/10.1093/bioinformatics/bts091>
- Okuda, S., & Tokuda, H. (2009). Model of mouth-to-mouth transfer of bacterial lipoproteins through inner membrane LolC, periplasmic LolA, and outer membrane LolB. *Proceedings of the National Academy of Sciences of the United States of America*, *106*(14), 5877–5882. <https://doi.org/10.1073/pnas.0900896106>

- Ortiz, C., Natale, P., Cueto, L., & Vicente, M. (2016). The keepers of the ring: Regulators of FtsZ assembly. *FEMS Microbiology Reviews*, *40*(1), 57–67. <https://doi.org/10.1093/femsre/fuv040>
- Ovchinnikov, S., Kamisetty, H., & Baker, D. (2014). Robust and accurate prediction of residue–residue interactions across protein interfaces using evolutionary information (B. Roux, Ed.) [Publisher: eLife Sciences Publications, Ltd]. *eLife*, *3*, e02030. <https://doi.org/10.7554/eLife.02030>
- Park, K.-T., Du, S., & Lutkenhaus, J. (2020). Essential Role for FtsL in Activation of Septal Peptidoglycan Synthesis [Publisher: American Society for Microbiology]. *mBio*, *11*(6), e03012–20. <https://doi.org/10.1128/mBio.03012-20>
- Pazos, M., Natale, P., Margolin, W., & Vicente, M. (2013). Interactions among the early Escherichia coli divisome proteins revealed by bimolecular fluorescence complementation [eprint: <https://onlinelibrary.wiley.com/doi/pdf/10.1111/1462-2920.12225>]. *Environmental Microbiology*, *15*(12), 3282–3291. <https://doi.org/10.1111/1462-2920.12225>
- Pazos, M., Peters, K., Boes, A., Safaei, Y., Kenward, C., Caveney, N. A., Laguri, C., Breukink, E., Strynadka, N. C. J., Simorre, J.-P., Terrak, M., & Vollmer, W. (2020). SPOR Proteins Are Required for Functionality of Class A Penicillin-Binding Proteins in Escherichia coli [Publisher: American Society for Microbiology]. *mBio*, *11*(6), e02796–20. <https://doi.org/10.1128/mBio.02796-20>
- Pease, P. J., Levy, O., Cost, G. J., Gore, J., Ptacin, J. L., Sherratt, D., Bustamante, C., & Cozzarelli, N. R. (2005). Sequence-directed DNA translocation by purified FtsK. *Science (New York, N.Y.)*, *307*(5709), 586–590. <https://doi.org/10.1126/science.1104885>
- Pennartz, A., Génèreux, C., Parquet, C., Mengin-Lecreulx, D., & Joris, B. (2009). Substrate-Induced Inactivation of the Escherichia coli AmiD N-Acetylmuramoyl-l-Alanine Amidase Highlights a New Strategy To Inhibit This Class of Enzyme [Publisher: American Society for Microbiology]. *Antimicrobial Agents and Chemotherapy*, *53*(7), 2991–2997. <https://doi.org/10.1128/AAC.01520-07>
- Peters, N. T., Dinh, T., & Bernhardt, T. G. (2011). A Fail-Safe Mechanism in the Septal Ring Assembly Pathway Generated by the Sequential Recruitment of Cell Separation Amidases and Their Activators. *Journal of Bacteriology*, *193*(18), 4973–4983. <https://doi.org/10.1128/JB.00316-11>

- Peters, N. T., Morlot, C., Yang, D. C., Uehara, T., Vernet, T., & Bernhardt, T. G. (2013a). Structure–function analysis of the LytM domain of EnvC, an activator of cell wall remodelling at the Escherichia coli division site [eprint: <https://onlinelibrary.wiley.com/doi/pdf/10.1111/mmi.12304>]. *Molecular Microbiology*, 89(4), 690–701. <https://doi.org/10.1111/mmi.12304>
- Peters, N. T., Morlot, C., Yang, D. C., Uehara, T., Vernet, T., & Bernhardt, T. G. (2013b). Structure-function analysis of the LytM domain of EnvC, an activator of cell wall remodelling at the Escherichia coli division site. *Molecular Microbiology*, 89(4), 690–701. <https://doi.org/10.1111/mmi.12304>
- Petiti, M., Serrano, B., Faure, L., Lloubes, R., Mignot, T., & Duché, D. (2019). Tol Energy-Driven Localization of Pal and Anchoring to the Peptidoglycan Promote Outer-Membrane Constriction. *Journal of Molecular Biology*, 431(17), 3275–3288. <https://doi.org/10.1016/j.jmb.2019.05.039>
- Pichoff, S., Du, S., & Lutkenhaus, J. (2018). Disruption of divisome assembly rescued by FtsN-FtsA interaction in Escherichia coli. *Proceedings of the National Academy of Sciences of the United States of America*, 115(29), E6855–E6862. <https://doi.org/10.1073/pnas.1806450115>
- Pichoff, S., Du, S., & Lutkenhaus, J. (2019). Roles of FtsEX in cell division. *Research in microbiology*, 170(8), 374–380. <https://doi.org/10.1016/j.resmic.2019.07.003>
- Pichoff, S., & Lutkenhaus, J. (2002). Unique and overlapping roles for ZipA and FtsA in septal ring assembly in Escherichia coli [Publisher: John Wiley & Sons, Ltd]. *The EMBO Journal*, 21(4), 685–693. <https://doi.org/10.1093/emboj/21.4.685>
- Pichoff, S., Shen, B., Sullivan, B., & Lutkenhaus, J. (2012). FtsA mutants impaired for self-interaction bypass ZipA suggesting a model in which FtsA's self-interaction competes with its ability to recruit downstream division proteins. *Molecular microbiology*, 83(1), 151–167. <https://doi.org/10.1111/j.1365-2958.2011.07923.x>
- Poggio, S., Takacs, C. N., Vollmer, W., & Jacobs-Wagner, C. (2010). A protein critical for cell constriction in the Gram-negative bacterium Caulobacter crescentus localizes at the division site through its peptidoglycan-binding LysM domains [eprint: <https://onlinelibrary.wiley.com/doi/pdf/10.1111/j.1365-2958.2010.07223.x>]. *Molecular Microbiology*, 77(1), 74–89. <https://doi.org/10.1111/j.1365-2958.2010.07223.x>

- Priyadarshini, R., de Pedro, M. A., & Young, K. D. (2007). Role of Peptidoglycan Amidases in the Development and Morphology of the Division Septum in *Escherichia coli* [Publisher: American Society for Microbiology]. *Journal of Bacteriology*, *189*(14), 5334–5347. <https://doi.org/10.1128/JB.00415-07>
- Raetz, C. R. H., Reynolds, C. M., Trent, M. S., & Bishop, R. E. (2007). Lipid A modification systems in gram-negative bacteria. *Annual Review of Biochemistry*, *76*, 295–329. <https://doi.org/10.1146/annurev.biochem.76.010307.145803>
- RayChaudhuri, D. (1999). ZipA is a MAP–Tau homolog and is essential for structural integrity of the cytokinetic FtsZ ring during bacterial cell division [Publisher: John Wiley & Sons, Ltd]. *The EMBO Journal*, *18*(9), 2372–2383. <https://doi.org/10.1093/emboj/18.9.2372>
- Reddy, M. (2007). Role of FtsEX in cell division of *Escherichia coli*: Viability of ftsEX mutants is dependent on functional SufI or high osmotic strength. *Journal of Bacteriology*, *189*(1), 98–108. <https://doi.org/10.1128/JB.01347-06>
- Rees, D. C., Johnson, E., & Lewinson, O. (2009). ABC transporters: The power to change [Number: 3 Publisher: Nature Publishing Group]. *Nature Reviews Molecular Cell Biology*, *10*(3), 218–227. <https://doi.org/10.1038/nrm2646>
- Ricard, M., & Hirota, Y. (1973). Process of Cellular Division in *Escherichia coli*: Physiological Study on Thermosensitive Mutants Defective in Cell Division. *Journal of Bacteriology*, *116*(1), 314–322. Retrieved November 15, 2022, from <https://www.ncbi.nlm.nih.gov/pmc/articles/PMC246424/>
- Rigden, D. J., Jedrzejewski, M. J., & Galperin, M. Y. (2003). Amidase domains from bacterial and phage autolysins define a family of -d,l-glutamate-specific amidohydrolases [Publisher: Elsevier]. *Trends in Biochemical Sciences*, *28*(5), 230–234. [https://doi.org/10.1016/S0968-0004\(03\)00062-8](https://doi.org/10.1016/S0968-0004(03)00062-8)
- Rocaboy, M., Herman, R., Sauvage, E., Remaut, H., Moonens, K., Terrak, M., Charlier, P., & Kerff, F. (2013). The crystal structure of the cell division amidase AmiC reveals the fold of the AMIN domain, a new peptidoglycan binding domain [eprint: <https://onlinelibrary.wiley.com/doi/pdf/10.1111/mmi.12361>]. *Molecular Microbiology*, *90*(2), 267–277. <https://doi.org/10.1111/mmi.12361>
- Romberg, L., Simon, M., & Erickson, H. P. (2001). Polymerization of FtsZ, a Bacterial Homolog of Tubulin: IS ASSEMBLY COOPERATIVE? \* [Pub-

- lisher: Elsevier]. *Journal of Biological Chemistry*, 276(15), 11743–11753. <https://doi.org/10.1074/jbc.M009033200>
- Roseboom, W., Nazir, M. G., Meiresonne, N. Y., Mohammadi, T., Verheul, J., Buncherd, H., Bonvin, A. M. J. J., De Koning, L. J., De Koster, C. G., De Jong, L., & Den Blaauwen, T. (2018). Mapping the Contact Sites of the Escherichia coli Division-Initiating Proteins FtsZ and ZapA by BAMG Cross-Linking and Site-Directed Mutagenesis [Number: 10 Publisher: Multidisciplinary Digital Publishing Institute]. *International Journal of Molecular Sciences*, 19(10), 2928. <https://doi.org/10.3390/ijms19102928>
- Rowlett, V. W., Mallampalli, V. K. P. S., Karlstaedt, A., Dowhan, W., Taegtmeier, H., Margolin, W., & Vitrac, H. (2017). Impact of Membrane Phospholipid Alterations in Escherichia coli on Cellular Function and Bacterial Stress Adaptation. *Journal of Bacteriology*, 199(13), e00849–16. <https://doi.org/10.1128/JB.00849-16>
- Rowlett, V. W., & Margolin, W. (2015). The Min system and other nucleoid-independent regulators of Z ring positioning. *Frontiers in Microbiology*, 6, 478. <https://doi.org/10.3389/fmicb.2015.00478>
- Rowlett, V. W., & Margolin, W. (2013). The bacterial Min system [Publisher: Elsevier]. *Current Biology*, 23(13), R553–R556. <https://doi.org/10.1016/j.cub.2013.05.024>
- Rued, B. E., Alcorlo, M., Edmonds, K. A., Martínez-Caballero, S., Straume, D., Fu, Y., Bruce, K. E., Wu, H., Håvarstein, L. S., Hermoso, J. A., Winkler, M. E., & Giedroc, D. P. (2019). Structure of the Large Extracellular Loop of FtsX and Its Interaction with the Essential Peptidoglycan Hydrolase PcsB in Streptococcus pneumoniae. *mBio*, 10(1), e02622–18. <https://doi.org/10.1128/mBio.02622-18>
- Rueda, S., Vicente, M., & Mingorance, J. (2003). Concentration and Assembly of the Division Ring Proteins FtsZ, FtsA, and ZipA during the Escherichia coli Cell Cycle [Publisher: American Society for Microbiology]. *Journal of Bacteriology*, 185(11), 3344–3351. <https://doi.org/10.1128/JB.185.11.3344-3351.2003>
- Ruiz, N. (2008). Bioinformatics identification of MurJ (MviN) as the peptidoglycan lipid II flippase in Escherichia coli. *Proceedings of the National Academy of Sciences of the United States of America*, 105(40), 15553–15557. <https://doi.org/10.1073/pnas.0808352105>

- Saleh, O. A., Pérals, C., Barre, F.-X., & Allemand, J.-F. (2004). Fast, DNA-sequence independent translocation by FtsK in a single-molecule experiment. *The EMBO journal*, *23*(12), 2430–2439. <https://doi.org/10.1038/sj.emboj.7600242>
- Salmond, G. P., & Plakidou, S. (1984). Genetic analysis of essential genes in the ftsE region of the Escherichia coli genetic map and identification of a new cell division gene, ftsS. *Molecular & general genetics: MGG*, *197*(2), 304–308. <https://doi.org/10.1007/BF00330978>
- Sauvage, E., Derouaux, A., Fraipont, C., Joris, M., Herman, R., Rocaboy, M., Schloesser, M., Dumas, J., Kerff, F., Nguyen-Distèche, M., & Charlier, P. (2014). Crystal Structure of Penicillin-Binding Protein 3 (PBP3) from Escherichia coli. *PLoS ONE*, *9*(5), e98042. <https://doi.org/10.1371/journal.pone.0098042>
- Scheffers, D.-J., Robichon, C., Haan, G. J., den Blaauwen, T., Koningstein, G., van Bloois, E., Beckwith, J., & Luirink, J. (2007). Contribution of the FtsQ Transmembrane Segment to Localization to the Cell Division Site [Publisher: American Society for Microbiology]. *Journal of Bacteriology*, *189*(20), 7273–7280. <https://doi.org/10.1128/JB.00723-07>
- Schmidt, K. L., Peterson, N. D., Kustus, R. J., Wissel, M. C., Graham, B., Phillips, G. J., & Weiss, D. S. (2004). A predicted ABC transporter, FtsEX, is needed for cell division in Escherichia coli. *Journal of Bacteriology*, *186*(3), 785–793. <https://doi.org/10.1128/JB.186.3.785-793.2004>
- Schoenemann, K. M., Krupka, M., Rowlett, V. W., Distelhorst, S. L., Hu, B., & Margolin, W. (2018). Gain-of-function variants of FtsA form diverse oligomeric structures on lipids and enhance FtsZ protofilament bundling [eprint: <https://onlinelibrary.wiley.com/doi/pdf/10.1111/mmi.14069>]. *Molecular Microbiology*, *109*(5), 676–693. <https://doi.org/10.1111/mmi.14069>
- Schoenemann, K. M., Vega, D. E., & Margolin, W. (2020). Peptide Linkers within the Essential FtsZ Membrane Tethers ZipA and FtsA Are Nonessential for Cell Division [Publisher: American Society for Microbiology]. *Journal of Bacteriology*, *202*(6), e00720–19. <https://doi.org/10.1128/JB.00720-19>
- Schumacher, M. A., Ohashi, T., Corbin, L., & Erickson, H. P. (2020). High-resolution crystal structures of Escherichia coli FtsZ bound to GDP and GTP [Number: 2 Publisher: International Union of Crystallography]. *Acta Crystallographica Section F: Structural Biology Communications*, *76*(2), 94–102. <https://doi.org/10.1107/S2053230X20001132>

- Schumacher, M. A., Huang, K.-H., Zeng, W., & Janakiraman, A. (2017). Structure of the Z Ring-associated Protein, ZapD, Bound to the C-terminal Domain of the Tubulin-like Protein, FtsZ, Suggests Mechanism of Z Ring Stabilization through FtsZ Cross-linking \* [Publisher: Elsevier]. *Journal of Biological Chemistry*, 292(9), 3740–3750. <https://doi.org/10.1074/jbc.M116.773192>
- Serres, M. H., Gopal, S., Nahum, L. A., Liang, P., Gaasterland, T., & Riley, M. (2001). A functional update of the Escherichia coli K-12 genome. *Genome Biology*, 2(9), RESEARCH0035. <https://doi.org/10.1186/gb-2001-2-9-research0035>
- Seydel, A., Gounon, P., & Pugsley, A. P. (1999). Testing the '+2 rule' for lipoprotein sorting in the Escherichia coli cell envelope with a new genetic selection. *Molecular Microbiology*, 34(4), 810–821. <https://doi.org/10.1046/j.1365-2958.1999.01647.x>
- Sham, L.-T., Barendt, S. M., Kopecky, K. E., & Winkler, M. E. (2011). Essential PcsB putative peptidoglycan hydrolase interacts with the essential FtsXSpn cell division protein in Streptococcus pneumoniae D39. *Proceedings of the National Academy of Sciences of the United States of America*, 108(45), E1061–1069. <https://doi.org/10.1073/pnas.1108323108>
- Sham, L.-T., Butler, E. K., Lebar, M. D., Kahne, D., Bernhardt, T. G., & Ruiz, N. (2014). Bacterial cell wall. MurJ is the flippase of lipid-linked precursors for peptidoglycan biogenesis. *Science (New York, N.Y.)*, 345(6193), 220–222. <https://doi.org/10.1126/science.1254522>
- Sham, L.-T., Jensen, K. R., Bruce, K. E., & Winkler, M. E. (2013). Involvement of FtsE ATPase and FtsX Extracellular Loops 1 and 2 in FtsEX-PcsB Complex Function in Cell Division of Streptococcus pneumoniae D39. *mBio*, 4(4), e00431–13. <https://doi.org/10.1128/mBio.00431-13>
- Si, F., Treut, G. L., Sauls, J. T., Vadia, S., Levin, P. A., & Jun, S. (2019). Mechanistic Origin of Cell-Size Control and Homeostasis in Bacteria [Publisher: Elsevier]. *Current Biology*, 29(11), 1760–1770.e7. <https://doi.org/10.1016/j.cub.2019.04.062>
- Sievers, F., Wilm, A., Dineen, D., Gibson, T. J., Karplus, K., Li, W., Lopez, R., McWilliam, H., Remmert, M., Söding, J., Thompson, J. D., & Higgins, D. G. (2011). Fast, scalable generation of high-quality protein multiple sequence alignments using Clustal Omega [Publisher: John Wiley & Sons,

- Ltd]. *Molecular Systems Biology*, 7(1), 539. <https://doi.org/10.1038/msb.2011.75>
- Silhavy, T. J., Kahne, D., & Walker, S. (2010). The Bacterial Cell Envelope. *Cold Spring Harbor Perspectives in Biology*, 2(5), a000414. <https://doi.org/10.1101/cshperspect.a000414>
- Singh, H., Velamakanni, S., Deery, M. J., Howard, J., Wei, S. L., & van Veen, H. W. (2016). ATP-dependent substrate transport by the ABC transporter MsbA is proton-coupled [Number: 1 Publisher: Nature Publishing Group]. *Nature Communications*, 7(1), 12387. <https://doi.org/10.1038/ncomms12387>
- Singh, S. K., SaiSree, L., Amrutha, R. N., & Reddy, M. (2012). Three redundant murein endopeptidases catalyse an essential cleavage step in peptidoglycan synthesis of Escherichia coli K12 [eprint: <https://onlinelibrary.wiley.com/doi/pdf/10.1111/mmi.12058>]. *Molecular Microbiology*, 86(5), 1036–1051. <https://doi.org/10.1111/mmi.12058>
- Skoog, K., Söderström, B., Widengren, J., von Heijne, G., & Daley, D. O. (2012). Sequential Closure of the Cytoplasm and Then the Periplasm during Cell Division in Escherichia coli [Publisher: American Society for Microbiology]. *Journal of Bacteriology*, 194(3), 584–586. <https://doi.org/10.1128/JB.06091-11>
- Söderström, B., Chan, H., Shilling, P. J., Skoglund, U., & Daley, D. O. (2018). Spatial separation of FtsZ and FtsN during cell division [eprint: <https://onlinelibrary.wiley.com/doi/pdf/10.1111/mmi.13888>]. *Molecular Microbiology*, 107(3), 387–401. <https://doi.org/10.1111/mmi.13888>
- Söderström, B., & Daley, D. O. (2017). The bacterial divisome: More than a ring? *Current Genetics*, 63(2), 161–164. <https://doi.org/10.1007/s00294-016-0630-2>
- Söderström, B., Mirzadeh, K., Toddo, S., von Heijne, G., Skoglund, U., & Daley, D. O. (2016). Coordinated disassembly of the divisome complex in Escherichia coli [eprint: <https://onlinelibrary.wiley.com/doi/pdf/10.1111/mmi.13400>]. *Molecular Microbiology*, 101(3), 425–438. <https://doi.org/10.1111/mmi.13400>
- Söderström, B., Skoog, K., Blom, H., Weiss, D. S., von Heijne, G., & Daley, D. O. (2014). Disassembly of the divisome in Escherichia coli: Evidence that FtsZ dissociates before compartmentalization [eprint: <https://onlinelibrary.wiley.com/doi/pdf/10.1111/mmi.12534>]. *Molecular Microbiology*, 92(1), 1–9. <https://doi.org/10.1111/mmi.12534>

- Spratt, B. G. (1975). Distinct penicillin binding proteins involved in the division, elongation, and shape of *Escherichia coli* K12. [Publisher: Proceedings of the National Academy of Sciences]. *Proceedings of the National Academy of Sciences*, 72(8), 2999–3003. <https://doi.org/10.1073/pnas.72.8.2999>
- Sycuro, L. K., Pincus, Z., Gutierrez, K. D., Biboy, J., Stern, C. A., Vollmer, W., & Salama, N. R. (2010). Peptidoglycan crosslinking relaxation promotes *Helicobacter pylori*'s helical shape and stomach colonization. *Cell*, 141(5), 822–833. <https://doi.org/10.1016/j.cell.2010.03.046>
- Szczepaniak, J., Holmes, P., Rajasekar, K., Kaminska, R., Samsudin, F., Inns, P. G., Rassam, P., Khalid, S., Murray, S. M., Redfield, C., & Kleanthous, C. (2020). The lipoprotein Pal stabilises the bacterial outer membrane during constriction by a mobilisation-and-capture mechanism [Number: 1 Publisher: Nature Publishing Group]. *Nature Communications*, 11(1), 1305. <https://doi.org/10.1038/s41467-020-15083-5>
- Szczepaniak, J., Press, C., & Kleanthous, C. (2020). The multifarious roles of Tol-Pal in Gram-negative bacteria. *FEMS Microbiology Reviews*, 44(4), 490–506. <https://doi.org/10.1093/femsre/fuaa018>
- Szweda, P., Schielmann, M., Kotłowski, R., Gorczyca, G., Zalewska, M., & Milewski, S. (2012). Peptidoglycan hydrolases-potential weapons against *Staphylococcus aureus*. *Applied Microbiology and Biotechnology*, 96(5), 1157–1174. <https://doi.org/10.1007/s00253-012-4484-3>
- Szwedziak, P., Wang, Q., Freund, S. M., & Löwe, J. (2012). FtsA forms actin-like protofilaments [Publisher: John Wiley & Sons, Ltd]. *The EMBO Journal*, 31(10), 2249–2260. <https://doi.org/10.1038/emboj.2012.76>
- Taguchi, A., Welsh, M. A., Marmont, L. S., Lee, W., Sjodt, M., Kruse, A. C., Kahne, D., Bernhardt, T. G., & Walker, S. (2019). FtsW is a peptidoglycan polymerase that is functional only in complex with its cognate penicillin-binding protein [Number: 4 Publisher: Nature Publishing Group]. *Nature Microbiology*, 4(4), 587–594. <https://doi.org/10.1038/s41564-018-0345-x>
- Takeda, K., Miyatake, H., Yokota, N., Matsuyama, S.-i., Tokuda, H., & Miki, K. (2003). Crystal structures of bacterial lipoprotein localization factors, LolA and LolB. *The EMBO journal*, 22(13), 3199–3209. <https://doi.org/10.1093/emboj/cdg324>
- Tang, X., Chang, S., Luo, Q., Zhang, Z., Qiao, W., Xu, C., Zhang, C., Niu, Y., Yang, W., Wang, T., Zhang, Z., Zhu, X., Wei, X., Dong, C., Zhang, X., & Dong, H. (2019). Cryo-EM structures of lipopolysaccharide transporter

- LptB2FGC in lipopolysaccharide or AMP-PNP-bound states reveal its transport mechanism. *Nature Communications*, 10(1), 4175. <https://doi.org/10.1038/s41467-019-11977-1>
- Tang, X., Chang, S., Zhang, K., Luo, Q., Zhang, Z., Wang, T., Qiao, W., Wang, C., Shen, C., Zhang, Z., Zhu, X., Wei, X., Dong, C., Zhang, X., & Dong, H. (2021). Structural basis for bacterial lipoprotein relocation by the transporter LolCDE [Number: 4 Publisher: Nature Publishing Group]. *Nature Structural & Molecular Biology*, 28(4), 347–355. <https://doi.org/10.1038/s41594-021-00573-x>
- Taschner, P. E., Huls, P. G., Pas, E., & Woldringh, C. L. (1988). Division behavior and shape changes in isogenic ftsZ, ftsQ, ftsA, pbpB, and ftsE cell division mutants of Escherichia coli during temperature shift experiments. *Journal of Bacteriology*, 170(4), 1533–1540. <https://doi.org/10.1128/jb.170.4.1533-1540.1988>
- ter Beek, J., Guskov, A., & Slotboom, D. J. (2014). Structural diversity of ABC transporters. *Journal of General Physiology*, 143(4), 419–435. <https://doi.org/10.1085/jgp.201411164>
- Thain, D., & Livny, M. (2005). PARROT: AN APPLICATION ENVIRONMENT FOR DATA-INTENSIVE COMPUTING ((PREPRINT VERSION)). Retrieved February 28, 2023, from <https://www.semanticscholar.org/paper/PARROT%3A-AN-APPLICATION-ENVIRONMENT-FOR-COMPUTING-Thain-Livny/ac934b7ee086aa724403adfb256da7946383ad29>
- Tokuda, H., & Matsuyama, S.-i. (2004). Sorting of lipoproteins to the outer membrane in E. coli. *Biochimica et Biophysica Acta (BBA) - Molecular Cell Research*, 1693(1), 5–13. <https://doi.org/10.1016/j.bbamcr.2004.02.005>
- Tsang, M.-J., & Bernhardt, T. G. (2015). A role for the FtsQLB complex in cytokinetic ring activation revealed by an ftsL allele that accelerates division [eprint: <https://onlinelibrary.wiley.com/doi/pdf/10.1111/mmi.12905>]. *Molecular Microbiology*, 95(6), 925–944. <https://doi.org/10.1111/mmi.12905>
- Tsang, M.-J., Yakhnina, A. A., & Bernhardt, T. G. (2017). NlpD links cell wall remodeling and outer membrane invagination during cytokinesis in Escherichia coli [Publisher: Public Library of Science]. *PLOS Genetics*, 13(7), e1006888. <https://doi.org/10.1371/journal.pgen.1006888>
- Tsukahara, J., Mukaiyama, K., Okuda, S., Narita, S.-i., & Tokuda, H. (2009). Dissection of LolB function—lipoprotein binding, membrane targeting and in-

- corporation of lipoproteins into lipid bilayers. *The FEBS journal*, 276(16), 4496–4504. <https://doi.org/10.1111/j.1742-4658.2009.07156.x>
- Uehara, T., Dinh, T., & Bernhardt, T. G. (2009). LytM-domain factors are required for daughter cell separation and rapid ampicillin-induced lysis in *Escherichia coli*. *Journal of Bacteriology*, 191(16), 5094–5107. <https://doi.org/10.1128/JB.00505-09>
- Uehara, T., Parzych, K. R., Dinh, T., & Bernhardt, T. G. (2010). Daughter cell separation is controlled by cytokinetic ring-activated cell wall hydrolysis [Publisher: John Wiley & Sons, Ltd]. *The EMBO Journal*, 29(8), 1412–1422. <https://doi.org/10.1038/emboj.2010.36>
- Ursinus, A., van den Ent, F., Brechtel, S., de Pedro, M., Höltje, J.-V., Löwe, J., & Vollmer, W. (2004). Murein (Peptidoglycan) Binding Property of the Essential Cell Division Protein FtsN from *Escherichia coli* [Publisher: American Society for Microbiology]. *Journal of Bacteriology*, 186(20), 6728–6737. <https://doi.org/10.1128/JB.186.20.6728-6737.2004>
- Usenik, A., Renko, M., Mihelič, M., Lindič, N., Borišek, J., Perdih, A., Pretnar, G., Müller, U., & Turk, D. (2017). The CWB2 Cell Wall-Anchoring Module Is Revealed by the Crystal Structures of the *Clostridium difficile* Cell Wall Proteins Cwp8 and Cwp6. *Structure (London, England: 1993)*, 25(3), 514–521. <https://doi.org/10.1016/j.str.2016.12.018>
- van Heijenoort, J. (2011). Peptidoglycan hydrolases of *Escherichia coli*. *Microbiology and molecular biology reviews: MMBR*, 75(4), 636–663. <https://doi.org/10.1128/MMBR.00022-11>
- Vega, D. E., & Margolin, W. (2019). Direct Interaction between the Two Z Ring Membrane Anchors FtsA and ZipA [Publisher: American Society for Microbiology]. *Journal of Bacteriology*, 201(4), e00579–18. <https://doi.org/10.1128/JB.00579-18>
- Vermassen, A., Leroy, S., Talon, R., Provot, C., Popowska, M., & Desvaux, M. (2019). Cell Wall Hydrolases in Bacteria: Insight on the Diversity of Cell Wall Amidases, Glycosidases and Peptidases Toward Peptidoglycan. *Frontiers in Microbiology*, 10. Retrieved November 30, 2022, from <https://www.frontiersin.org/articles/10.3389/fmicb.2019.00331>
- Vischer, N. O. E., Verheul, J., Postma, M., van den Berg van Saparoea, B., Galli, E., Natale, P., Gerdes, K., Luirink, J., Vollmer, W., Vicente, M., & den Blaauwen, T. (2015). Cell age dependent concentration of *Escherichia coli* divisome proteins analyzed with ImageJ and ObjectJ. *Frontiers in Micro-*

- biology*, 6. Retrieved May 23, 2022, from <https://www.frontiersin.org/article/10.3389/fmicb.2015.00586>
- Vogeley, L., El Arnaout, T., Bailey, J., Stansfeld, P. J., Boland, C., & Caffrey, M. (2016). Structural basis of lipoprotein signal peptidase II action and inhibition by the antibiotic globomycin. *Science (New York, N.Y.)*, 351(6275), 876–880. <https://doi.org/10.1126/science.aad3747>
- Vollmer, W., Joris, B., Charlier, P., & Foster, S. (2008). Bacterial peptidoglycan (murein) hydrolases. *FEMS Microbiology Reviews*, 32(2), 259–286. <https://doi.org/10.1111/j.1574-6976.2007.00099.x>
- Wang, L., Khattar, M. K., Donachie, W. D., & Lutkenhaus, J. (1998). FtsI and FtsW are localized to the septum in *Escherichia coli*. *Journal of Bacteriology*, 180(11), 2810–2816. <https://doi.org/10.1128/JB.180.11.2810-2816.1998>
- Wang, L., & Lutkenhaus, J. (1998). FtsK is an essential cell division protein that is localized to the septum and induced as part of the SOS response [eprint: <https://onlinelibrary.wiley.com/doi/pdf/10.1046/j.1365-2958.1998.00958.x>]. *Molecular Microbiology*, 29(3), 731–740. <https://doi.org/10.1046/j.1365-2958.1998.00958.x>
- Wang, X., Possoz, C., & Sherratt, D. J. (2005). Dancing around the divisome: Asymmetric chromosome segregation in *Escherichia coli*. *Genes & Development*, 19(19), 2367–2377. <https://doi.org/10.1101/gad.345305>
- Waterhouse, A., Bertoni, M., Bienert, S., Studer, G., Tauriello, G., Gumienny, R., Heer, F. T., de Beer, T. A. P., Rempfer, C., Bordoli, L., Lepore, R., & Schwede, T. (2018). SWISS-MODEL: Homology modelling of protein structures and complexes. *Nucleic Acids Research*, 46(W1), W296–W303. <https://doi.org/10.1093/nar/gky427>
- Waterhouse, A. M., Procter, J. B., Martin, D. M. A., Clamp, M., & Barton, G. J. (2009). Jalview Version 2—a multiple sequence alignment editor and analysis workbench. *Bioinformatics*, 25(9), 1189–1191. <https://doi.org/10.1093/bioinformatics/btp033>
- Weart, R. B., & Levin, P. A. (2003). Growth Rate-Dependent Regulation of Medial FtsZ Ring Formation [Publisher: American Society for Microbiology]. *Journal of Bacteriology*, 185(9), 2826–2834. <https://doi.org/10.1128/JB.185.9.2826-2834.2003>
- Weiss, D. S. (2015). Last but not least: New insights into how FtsN triggers constriction during *Escherichia coli* cell division [eprint: <https://onlinelibrary.wiley.com/doi/pdf/10.1111>

- Molecular Microbiology*, 95(6), 903–909. <https://doi.org/10.1111/mmi.12925>
- Weiss, D. S., Chen, J. C., Ghigo, J.-M., Boyd, D., & Beckwith, J. (1999). Localization of FtsI (PBP3) to the Septal Ring Requires Its Membrane Anchor, the Z Ring, FtsA, FtsQ, and FtsL [Publisher: American Society for Microbiology]. *Journal of Bacteriology*, 181(2), 508–520. <https://doi.org/10.1128/JB.181.2.508-520.1999>
- Whitley, K. D., Jukes, C., Tregidgo, N., Karinou, E., Almada, P., Cesbron, Y., Henriques, R., Dekker, C., & Holden, S. (2021). FtsZ treadmilling is essential for Z-ring condensation and septal constriction initiation in *Bacillus subtilis* cell division [Number: 1 Publisher: Nature Publishing Group]. *Nature Communications*, 12(1), 2448. <https://doi.org/10.1038/s41467-021-22526-0>
- Wilkens, S. (2015). Structure and mechanism of ABC transporters. *F1000Prime Reports*, 7, 14. <https://doi.org/10.12703/P7-14>
- Winn, M. D., Ballard, C. C., Cowtan, K. D., Dodson, E. J., Emsley, P., Evans, P. R., Keegan, R. M., Krissinel, E. B., Leslie, A. G. W., McCoy, A., McNicholas, S. J., Murshudov, G. N., Pannu, N. S., Potterton, E. A., Powell, H. R., Read, R. J., Vagin, A., & Wilson, K. S. (2011). Overview of the CCP4 suite and current developments. *Acta Crystallographica. Section D, Biological Crystallography*, 67(Pt 4), 235–242. <https://doi.org/10.1107/S0907444910045749>
- Wissel, M. C., & Weiss, D. S. (2004). Genetic analysis of the cell division protein FtsI (PBP3): Amino acid substitutions that impair septal localization of FtsI and recruitment of FtsN. *Journal of Bacteriology*, 186(2), 490–502. <https://doi.org/10.1128/JB.186.2.490-502.2004>
- Woldringh, C. L., Mulder, E., Huls, P. G., & Vischer, N. (1991). Toporegulation of bacterial division according to the nucleoid occlusion model. *Research in Microbiology*, 142(2), 309–320. [https://doi.org/10.1016/0923-2508\(91\)90046-D](https://doi.org/10.1016/0923-2508(91)90046-D)
- Xu, K., Zhang, M., Zhao, Q., Yu, F., Guo, H., Wang, C., He, F., Ding, J., & Zhang, P. (2013). Crystal structure of a folate energy-coupling factor transporter from *Lactobacillus brevis* [Number: 7448 Publisher: Nature Publishing Group]. *Nature*, 497(7448), 268–271. <https://doi.org/10.1038/nature12046>
- Yahashiri, A., Jorgenson, M. A., & Weiss, D. S. (2015). Bacterial SPOR domains are recruited to septal peptidoglycan by binding to glycan strands that lack

- stem peptides [Publisher: Proceedings of the National Academy of Sciences]. *Proceedings of the National Academy of Sciences*, 112(36), 11347–11352. <https://doi.org/10.1073/pnas.1508536112>
- Yakhnina, A. A., McManus, H. R., & Bernhardt, T. G. (2015). The cell wall amidase AmiB is essential for *Pseudomonas aeruginosa* cell division, drug resistance, and viability. *Molecular microbiology*, 97(5), 957–973. <https://doi.org/10.1111/mmi.13077>
- Yakushi, T., Masuda, K., Narita, S., Matsuyama, S., & Tokuda, H. (2000). A new ABC transporter mediating the detachment of lipid-modified proteins from membranes. *Nature Cell Biology*, 2(4), 212–218. <https://doi.org/10.1038/35008635>
- Yamane, T., Koyama, Y., Nojiri, Y., Hikage, T., Akita, M., Suzuki, A., Shirai, T., Ise, F., Shida, T., & Sekiguchi, J. (2001). RCSB PDB - 1JWQ: Structure of the catalytic domain of CwlV, N-acetylmuramoyl-L-alanine amidase from *Bacillus (Paenibacillus) polymyxa* var. *colistinus*. Retrieved December 5, 2022, from <https://www.rcsb.org/structure/1JWQ>
- Yang, D. C., Peters, N. T., Parzych, K. R., Uehara, T., Markovski, M., & Bernhardt, T. G. (2011). An ATP-binding cassette transporter-like complex governs cell-wall hydrolysis at the bacterial cytokinetic ring [Publisher: Proceedings of the National Academy of Sciences]. *Proceedings of the National Academy of Sciences*, 108(45), E1052–E1060. <https://doi.org/10.1073/pnas.1107780108>
- Yang, D. C., Tan, K., Joachimiak, A., & Bernhardt, T. G. (2012a). A conformational switch controls cell wall-remodelling enzymes required for bacterial cell division [eprint: <https://onlinelibrary.wiley.com/doi/pdf/10.1111/j.1365-2958.2012.08138.x>]. *Molecular Microbiology*, 85(4), 768–781. <https://doi.org/10.1111/j.1365-2958.2012.08138.x>
- Yang, D. C., Tan, K., Joachimiak, A., & Bernhardt, T. G. (2012b). A conformational switch controls cell wall-remodelling enzymes required for bacterial cell division. *Molecular Microbiology*, 85(4), 768–781. <https://doi.org/10.1111/j.1365-2958.2012.08138.x>
- Yang, J.-C., Van Den Ent, F., Neuhaus, D., Brevier, J., & Löwe, J. (2004). Solution structure and domain architecture of the divisome protein FtsN [eprint: <https://onlinelibrary.wiley.com/doi/pdf/10.1111/j.1365-2958.2004.03991.x>]. *Molecular Microbiology*, 52(3), 651–660. <https://doi.org/10.1111/j.1365-2958.2004.03991.x>

- Yang, X., Lyu, Z., Miguel, A., McQuillen, R., Huang, K. C., & Xiao, J. (2017). GTPase activity–coupled treadmilling of the bacterial tubulin FtsZ organizes septal cell wall synthesis [Publisher: American Association for the Advancement of Science]. *Science*, *355*(6326), 744–747. <https://doi.org/10.1126/science.aak9995>
- Yang, X., McQuillen, R., Lyu, Z., Phillips-Mason, P., De La Cruz, A., McCausland, J. W., Liang, H., DeMeester, K. E., Santiago, C. C., Grimes, C. L., de Boer, P., & Xiao, J. (2021). A two-track model for the spatiotemporal coordination of bacterial septal cell wall synthesis revealed by single-molecule imaging of FtsW [Number: 5 Publisher: Nature Publishing Group]. *Nature Microbiology*, *6*(5), 584–593. <https://doi.org/10.1038/s41564-020-00853-0>
- Yu, X. C., Tran, A. H., Sun, Q., & Margolin, W. (1998). Localization of cell division protein FtsK to the Escherichia coli septum and identification of a potential N-terminal targeting domain. *Journal of Bacteriology*, *180*(5), 1296–1304. <https://doi.org/10.1128/JB.180.5.1296-1304.1998>
- Yu, X.-C., Weihe, E. K., & Margolin, W. (1998). Role of the C Terminus of FtsK in Escherichia coli Chromosome Segregation [Publisher: American Society for Microbiology]. *Journal of Bacteriology*, *180*(23), 6424–6428. <https://doi.org/10.1128/JB.180.23.6424-6428.1998>
- Zhang, R., Zhou, M., Bargassa, M., & Joachimiak, A. (2008). RCSB PDB - 3CZX: The crystal structure of the putative N-acetylmuramoyl-L-alanine amidase from Neisseria meningitidis. Retrieved December 1, 2022, from <https://www.rcsb.org/structure/3czx>
- Zhou, R., Chen, S., & Recsei, P. (1988). A dye release assay for determination of lysostaphin activity. *Analytical Biochemistry*, *171*(1), 141–144. [https://doi.org/10.1016/0003-2697\(88\)90134-0](https://doi.org/10.1016/0003-2697(88)90134-0)
- Zoll, S., Schlag, M., Shkumatov, A. V., Rautenberg, M., Svergun, D. I., Götz, F., & Stehle, T. (2012). Ligand-Binding Properties and Conformational Dynamics of Autolysin Repeat Domains in Staphylococcal Cell Wall Recognition [Publisher: American Society for Microbiology]. *Journal of Bacteriology*, *194*(15), 3789–3802. <https://doi.org/10.1128/JB.00331-12>

## 8 Appendix

**Table 5:** Plasmids used in this thesis

Clone no.	Vector	Contents	Tag	Figure	Ref
<b>Results Chapter One</b>					
<i>Base bacterial two-hybrid vectors</i>					
pkNT25	pkNT25	T25	no tag	<b>Figures 22 to 24, 26, 29, 31 and 49</b>	(Euromedex, 2022)
pkT25	pkT25	T25	no tag	<b>Figures 22 to 24, 26, 29, 31 and 49</b>	(Euromedex, 2022)
pUT18	pUT18	T18	no tag	<b>Figures 22 to 24, 26, 29, 31, 49 and 50</b>	(Euromedex, 2022)
pUT18C	pUT18C	T18	no tag	<b>Figures 22 to 24, 26, 29, 31, 49 and 50</b>	(Euromedex, 2022)
pKT25-zip	pKT25	Leucine Zip	-T25	<b>Figures 22 to 24, 26, 29, 31 and 49</b>	(Euromedex, 2022)
pUT18C-zip	pUT18C	Leucine Zip	T18-	<b>Figures 22 to 24, 26, 29, 31 and 49</b>	(Euromedex, 2022)
<i>Base expression vectors</i>					

Clone no.	Vector	Contents	Tag	Figure	Ref
pET21a	pET21a	None	None	Figures 33, 34, 36, 39, 52 and 53, Section 4.3.3, and ??	EMD Bio-sciences
pETDuet-1	pETDuet-1	None	No tag	Figures 24, 25 and 27	EMD Bio-sciences
<i>Bacterial two-Hybrid Experiments (EnvC and the FtsX periplasmic domain variants)</i>					
pJC6 125	pUT18	FtsX(110-209)	-T18	<b>Figures 23, 29 and 31</b>	Dr Jonathan Cook (J. Cook et al., 2020)
pJC6 124	pKNT25	EnvC(35-419)	-T25	<b>Figures 15, 25, 29 and 31</b>	Dr Jonathan Cook (J. Cook et al., 2020)
pJC6 194	pUT18	FtsX (110-209) $\Delta$ 145-171:GG (X-lobe deletion in FtsX periplasmic domain)	-T18	<b>Figure 23</b>	Dr Jonathan Cook (J. Cook et al., 2020)
pMiTB1001	pUT18	FtsX (110-209) (Y114A) (Interface variant in FtsX periplasmic domain)	-T18	<b>Figure 23</b>	Tyler Baverstock (J. Cook et al., 2020)
pMiTB1002	pUT18	FtsX (110-209) (Y114E) (Interface variant in FtsX periplasmic domain)	-T18	<b>Figure 23</b>	Tyler Baverstock (J. Cook et al., 2020)

<b>Clone no.</b>	<b>Vector</b>	<b>Contents</b>	<b>Tag</b>	<b>Figure</b>	<b>Ref</b>
pMiTB1003	pUT18	FtsX (110-209) (K117A) (Interface variant in FtsX periplasmic domain)	-T18	<b>Figure 23</b>	Tyler Baverstock (J. Cook et al., 2020)
pMiTB1004	pUT18	FtsX (110-209) (F152A) (Interface variant in FtsX periplasmic domain)	-T18	<b>Figure 23</b>	Tyler Baverstock (J. Cook et al., 2020)
pMiTB1005	pUT18	FtsX (110-209) (F152E) (Interface variant in FtsX periplasmic domain)	-T18	<b>Figure 23</b>	Tyler Baverstock (J. Cook et al., 2020)
pMiTB1006	pUT18	FtsX (110-209) (W155A) (Interface variant in FtsX periplasmic domain)	-T18	<b>Figure 23</b>	Tyler Baverstock (J. Cook et al., 2020)
pMiTB1007	pUT18	FtsX (110-209) (F158A) (Interface variant in FtsX periplasmic domain)	-T18	<b>Figure 23</b>	Tyler Baverstock (J. Cook et al., 2020)
pMiTB1008	pUT18	FtsX (110-209) (F158E) (Interface variant in FtsX periplasmic domain)	-T18	<b>Figure 23</b>	Tyler Baverstock (J. Cook et al., 2020)

<b>Clone no.</b>	<b>Vector</b>	<b>Contents</b>	<b>Tag</b>	<b>Figure</b>	<b>Ref</b>
pMiTB1009	pUT18	FtsX (110-209) (A161D) (Interface variant in FtsX periplasmic domain)	-T18	<b>Figure 23</b>	Tyler Baverstock (J. Cook et al., 2020)
pMiTB1010	pUT18	FtsX (110-209) (M164A) (Interface variant in FtsX periplasmic domain)	-T18	<b>Figure 23</b>	Tyler Baverstock (J. Cook et al., 2020)
pMiTB1011	pUT18	FtsX (110-209) (L165A) (Interface variant in FtsX periplasmic domain)	-T18	<b>Figure 23</b>	Tyler Baverstock (J. Cook et al., 2020)
pMiTB1012	pUT18	FtsX (110-209) (D202A) (Interface variant in FtsX periplasmic domain)	-T18	<b>Figure 23</b>	Tyler Baverstock (J. Cook et al., 2020)
pMiTB1013	pUT18	FtsX (110-209) (R205A) (Interface variant in FtsX periplasmic domain)	-T18	<b>Figure 23</b>	Tyler Baverstock (J. Cook et al., 2020)
<i>Bacterial two-Hybrid Experiments (Amidase and regulators)</i>					
pTB1011	pUT18	sol AmiA	-T18	<b>Figures 24, 31 and 49</b>	Tyler Baverstock (J. Cook et al., 2020)
pJC6 238	pUT18	sol AmiB	-T18	<b>Figures 24, 26 and 31</b>	Dr Jonathan Cook (J. Cook et al., 2020)

Clone no.	Vector	Contents	Tag	Figure	Ref
pTB1009	pUT18	sol AmiC	-T18	<b>Figures 24 and 31</b>	Tyler Baverstock (J. Cook et al., 2020)
pJC6 257	pKNT25	EnvC (278-419) (EnvC LytM domain)	-T25	<b>Figures 24, 29, 31 and 49</b>	Dr Jonathan Cook (J. Cook et al., 2020)
pTB1005	pKNT25	NlpD (27-379)	-T25	<b>Figures 24, 29, 31 and 49</b>	Tyler Baverstock (J. Cook et al., 2020)
pTB1010	pKNT25	NlpD (250-379) (NlpD LytM domain)	-T25	<b>Figures 24, 29, 31 and 49</b>	Tyler Baverstock (J. Cook et al., 2020)
<i>Co-expression and co-purification of amidases (AmiA and AmiB) with the EnvC LytM domain</i>					
pTB1016	petDUET1	EnvC (278-419) in first site, and AmiA (35-289) in the second	N-term His-tag on EnvC LytM domain and no tag on AmiA	<b>Figures 24 and 25</b>	Tyler Baverstock (J. Cook et al., 2020)
pJC6 278	petDUET1	EnvC (278-419) in first site, and AmiB (23-446) in the second	N-term His-tag on EnvC LytM domain and no tag on AmiB	<b>Figure 24</b>	Dr Jonathan Cook (J. Cook et al., 2020)
<i>Co-expression and co-purification of AmiA with the EnvC variants</i>					

Clone no.	Vector	Contents	Tag	Figure	Ref
pTB1022	petDUET1	EnvC (35-419) in the first site, and AmiA (35-289) in the second	N-term His-tag on EnvC and no tag on AmiA	<b>Figure 22</b>	Dr Jonathan Cook (J. Cook et al., 2020)
pTB1023	petDUET1	EnvC (222-419) in the first site, and AmiA (35-289) in the second	N-term His-tag on EnvC and no tag on AmiA	<b>Figure 22</b>	Dr Jonathan Cook (J. Cook et al., 2020)
<i>Bacterial two-hybrid experiments (EnvC LytM amidase binding mutants)</i>					
pJC6 253	pUT18C	EnvC(278-419)	T18-	<b>Figure 22</b>	Dr Jonathan Cook (J. Cook et al., 2020)
pJC6 249	pKNT25	EnvC (216-247)	-T25	<b>Figure 22</b>	Dr Jonathan Cook, this project
pJC6 243	pKNT25	sol AmiB	-T25	<b>Figure 26</b>	Dr Jonathan Cook (J. Cook et al., 2020)
pMiTB1014	pUT18C	EnvC (278-419) ( $\Delta$ 312-320)	T18-	<b>Figure 26</b>	Tyler Baverstock, this project
pMiTB1015	pUT18C	EnvC (278-419) (K321A)	T18-	<b>Figure 26</b>	Tyler Baverstock, this project
pMiTB1016	pUT18C	EnvC (278-419) (V324E)	T18-	<b>Figure 26</b>	Tyler Baverstock, this project

Clone no.	Vector	Contents	Tag	Figure	Ref
pMiTB1017	pUT18C	EnvC (278-419) (Y350A)	T18-	<b>Figure 26</b>	Tyler Baverstock, this project
pMiTB1018	pUT18C	EnvC (278-419) (V353A)	T18-	<b>Figure 26</b>	Tyler Baverstock, this project
pMiTB1019	pUT18C	EnvC (278-419) (E403A)	T18-	<b>Figure 26</b>	Tyler Baverstock, this project
pMiTB1020	pUT18C	EnvC (278-419) (E403R)	T18-	<b>Figure 26</b>	Tyler Baverstock, this project
pMiTB1021	pUT18C	EnvC (278-419) (R405H)	T18-	<b>Figure 26</b>	Tyler Baverstock, this project
<i>Co-expression and co-purification of homolog AmiA with EnvC LytM domain</i>					
pJC6 707	pETDUET1	YgeR (ActS) (114-251) in first site, and AmiA (23-446) in the second	N-term His-tag on EnvC LytM domain and no tag on AmiA	<b>Figure 27</b>	Dr Jonathan Cook, this project
pTB1051	pETDUET1	<i>Serratia marcescens</i> EnvC (302-444) in first site, and <i>Serratia marcescens</i> AmiA (43-293) in the second	N-term His-tag on EnvC LytM domain and no tag on AmiA	<b>Figure 27</b>	Tyler Baverstock, this project

Clone no.	Vector	Contents	Tag	Figure	Ref
pTB1052	pETDUET1	<i>Edwardsiella tarda</i> EnvC (308-450) in first site, and <i>Edwardsiella tarda</i> AmiA (40-290) in the second	N-term His-tag on EnvC LytM domain and no tag on AmiA	<b>Figure 27</b>	Tyler Baverstock, this project
pTB1053	pETDUET1	<i>Klebsiella pneumoniae</i> EnvC (281-423) in first site, and <i>Klebsiella pneumoniae</i> AmiA (36-290) in the second	N-term His-tag on EnvC LytM domain and no tag on AmiA	<b>Figure 27</b>	Tyler Baverstock, this project
pTB1054	pETDUET1	<i>Enterobacter chengduensis</i> EnvC (285-427) in first site, and <i>Enterobacter chengduensis</i> AmiA (36-291) in the second	N-term His-tag on EnvC LytM domain and no tag on AmiA	<b>Figure 27</b>	Tyler Baverstock, this project
<i>Bacterial two-hybrid experiments (YibQ interaction screen)</i>					
pJC6 123	pKNT25	FtsX (110-209)	-T25	<b>Figure 29</b>	Dr Jonathan Cook (J. Cook et al., 2020)
pTB1024	pUT18C	YibQ (24-319)	T18-	<b>Figure 29</b>	Tyler Baverstock, this project
pTB1036	pUT18	YibQ (24-319)	-T18	<b>Figure 29</b>	Tyler Baverstock, this project

Clone no.	Vector	Contents	Tag	Figure	Ref
<i>Bacterial two-hybrid experiments (NlpI interaction screen)</i>					
pJC6 291	pUT18C	FtsA (2-420)	T18-	<b>Figure 31</b>	Dr Jonathan Cook (J. Cook et al., 2020)
pTB1012	pUT18	NlpI (20-294)	-T18	<b>Figure 31</b>	Tyler Baverstock, this project
pTB1013	pUT18C	NlpI (20-294)	T18-	<b>Figure 31</b>	Tyler Baverstock, this project
pTB1014	pKNT25	NlpI (20-294)	T25-	<b>Figure 31</b>	Tyler Baverstock, this project
pTB1015	pKT25	NlpI (20-294)	-T25	<b>Figure 31</b>	Tyler Baverstock, this project
<b>Results Chapter Two</b>					
<i>Generating <math>\Delta</math>amiab and <math>\Delta</math>amiabc amidase knockouts</i>					
pRedET (tet)	pRedET	RedET recombination machinery	No tag	<b>Figure 32</b>	GENE BRIDGES
707-FLPe	707-FLPe	FLP (flippase)	No tag	<b>Figure 32</b>	GENE BRIDGES
<i>Disome Knockout Complementation plasmids</i>					
pTB1028	pET21a	Full AmiA (including signal sequence)	No tag	<b>Figures 33, 34 and 36, Section 4.3.3, and ??</b>	Tyler Baverstock, this project

Clone no.	Vector	Contents	Tag	Figure	Ref
pTB1029	pET21a	Full AmiB (including signal sequence)	No tag	Figures 33, 34 and 36, Section 4.3.3, and ??	Tyler Baverstock, this project
pTB1030	pET21a	Full AmiC (including signal sequence)	No tag	Figures 33, 34 and 36, Section 4.3.3, and ??	Tyler Baverstock, this project
pTB1031	pET21a	Full EnvC (including signal sequence)	No tag	Figures 33, 34 and 36, Section 4.3.3, and ??	Tyler Baverstock, this project
pTB1032	pET21a	Full NlpD (including signal sequence)	No tag	Figures 33, 34 and 36, Section 4.3.3, and ??	Tyler Baverstock, this project
pTB1033	pET21a	Full FtsEX (including signal sequence)	No tag	Figures 33, 34 and 36, Section 4.3.3, and ??	Tyler Baverstock, this project
<b>Results Chapter Three</b>					
<i>Expression and purification of AmiA</i>					

Clone no.	Vector	Contents	Tag	Figure	Ref
pTB1034	pET21a	AmiA (35-289)	C-term His-tag on AmiA	<b>Figure 39</b>	Tyler Baverstock, this project
<b>Results Chapter Four</b>					
<i>Bacterial two-hybrid experiments (AmiA EnvC LytM binding mutants)</i>					
pMiTB1022	pUT18C	AmiA (35-289) (L184A)	-T18	<b>Figures 49 and 50</b>	Tyler Baverstock, this project
pJC6 622	pUT18C	AmiA (35-289) (L184K)	-T18	<b>Figures 49 and 50</b>	Dr Jonathan Cook, this project
pMiTB1023	pUT18C	AmiA (35-289) (L185A)	-T18	<b>Figures 49 and 50</b>	Tyler Baverstock, this project
pMiTB1024	pUT18C	AmiA (35-289) (L185W)	-T18	<b>Figures 49 and 50</b>	Tyler Baverstock, this project
pJC6 624	pUT18C	AmiA (35-289) (L185K)	-T18	<b>Figures 49 and 50</b>	Dr Jonathan Cook, this project
pJC6 643	pUT18C	AmiA (35-289) (L184K + L185K)	-T18	<b>Figures 49 and 50</b>	Dr Jonathan Cook, this project
pMiTB1024	pUT18C	AmiA (35-289) (L185W)	-T18	<b>Figures 49 and 50</b>	Tyler Baverstock, this project
pMiTB1025	pUT18C	AmiA (35-289) (V188A)	-T18	<b>Figures 49 and 50</b>	Tyler Baverstock, this project

Clone no.	Vector	Contents	Tag	Figure	Ref
pMiTB1026	pUT18C	AmiA (35-289) (V188W)	-T18	<b>Figures 49 and 50</b>	Tyler Baverstock, this project
pJC6 627	pUT18C	AmiA (35-289) (V188K)	-T18	<b>Figures 49 and 50</b>	Dr Jonathan Cook, this project
pMiTB1027	pUT18C	AmiA (35-289) (L189A)	-T18	<b>Figures 49 and 50</b>	Tyler Baverstock, this project
pMiTB1028	pUT18C	AmiA (35-289) (L189W)	-T18	<b>Figures 49 and 50</b>	Tyler Baverstock, this project
pJC6 629	pUT18C	AmiA (35-289) (L189K)	-T18	<b>Figures 49 and 50</b>	Dr Jonathan Cook, this project
pJC6 672	pUT18C	AmiA (35-289) (V188K + L189K)	-T18	<b>Figures 49 and 50</b>	Dr Jonathan Cook, this project
pMiTB1029	pUT18C	AmiA (35-289) (L192A)	-T18	<b>Figures 49 and 50</b>	Tyler Baverstock, this project
pMiTB1030	pUT18C	AmiA (35-289) (L192W)	-T18	<b>Figures 49 and 50</b>	Tyler Baverstock, this project
pJC6 645	pUT18C	AmiA (35-289) (L192K)	-T18	<b>Figures 49 and 50</b>	Dr Jonathan Cook, this project
<i>Constitutively Active AmiA periplasmic overexpression</i>					

Clone no.	Vector	Contents	Tag	Figure	Ref
pTB1050	pET21a	Full AmiA (with signal sequence) ( $\Delta$ 155-193::GAGAA)	No tag	<b>Figures 51 to 53</b>	Tyler Baverstock, this project
pTB1055	pET21a	Full AmiA (with signal sequence) ( $\Delta$ 152-192::GSGS)	No tag	<b>Figures 52 and 53</b>	Tyler Baverstock, this project
pTB1056	pET21a	Full AmiA (with signal sequence) ( $\Delta$ 152-192)	No tag	<b>Figures 52 and 53</b>	Tyler Baverstock, this project
<i>AmiA Blocking helix mutants periplasmic overexpression</i>					
pJC6 687	pET21a	Full AmiA (L163A)	No tag	<b>Figure 52</b>	Dr Jonathan Cook, this project
pJC6 714	pET21a	Full AmiA (L163E)	No tag	<b>Figure 52</b>	Dr Jonathan Cook, this project
pJC6 716	pET21a	Full AmiA (L163K)	No tag	<b>Figure 52</b>	Dr Jonathan Cook, this project
pJC6 718	pET21a	Full AmiA (L167A)	No tag	<b>Figure 52</b>	Dr Jonathan Cook, this project
pJC6 709	pET21a	Full AmiA (L167Q)	No tag	<b>Figure 52</b>	Dr Jonathan Cook, this project

<b>Clone no.</b>	<b>Vector</b>	<b>Contents</b>	<b>Tag</b>	<b>Figure</b>	<b>Ref</b>
pJC6 689	pET21a	Full AmiA (L167K)	No tag	<b>Figure 52</b>	Dr Jonathan Cook, this project
<i>Constitutively Active AmiA active site mutants periplasmic overexpression</i>					
pMiTB1031	pET21a	Full AmiA (35-289) (( $\Delta$ 155-193::GAGAA, H65A)	No tag	<b>Figure 53</b>	Tyler Baverstock, this project
pMiTB1032	pET21a	Full AmiA (35-289) (( $\Delta$ 155-193::GAGAA, E80A)	No tag	<b>Figure 53</b>	Tyler Baverstock, this project
pMiTB1033	pET21a	Full AmiA (35-289) (( $\Delta$ 155-193::GAGAA, H133A)	No tag	<b>Figure 53</b>	Tyler Baverstock, this project
pMiTB1034	pET21a	Full AmiA (35-289) (( $\Delta$ 155-193::GAGAA, D135A)	No tag	<b>Figure 53</b>	Tyler Baverstock, this project
pMiTB1034	pET21a	Full AmiA (35-289) (( $\Delta$ 155-193::GAGAA, E242A)	No tag	<b>Figure 53</b>	Tyler Baverstock, this project
End of Table					